A STUDY OF SOME NON-COVALENT FUNCTIONAL GROUP-ARENE INTERACTIONS

A Thesis Presented by

Joëlle Moïse

In Partial Fulfilment of the Requirements for the Award of the Degree of

DOCTOR OF PHILOSOPHY OF THE
UNIVERSITY OF LONDON

Christopher Ingold Laboratories
Department of Chemistry
University College London
WC1H 0AJ   LONDON

UCL

February 2006

UMI Number: U593023

UMI U593023

ProQuest LLC
789 East Eisenhower Parkway
P.O. Box 1346
Ann Arbor, MI 48106-1346

ABSTRACT

This thesis describes an investigation of the weak non-covalent interactions between the π-system of an aromatic ring and various functional groups.

The first section comprises a review of the current literature on the through space aromatic ring interactions based on theoretical, biological and experimental chemistry and especially focuses on the π-interactions involving a functional group.

The second section describes the synthesis of a series of novel 9,10-propanoanthracenes, with a common framework, consisting of a rigid structure containing two independent aromatic systems and a flexible bridge. The central carbon atom of the bridge can be substituted with two different functional groups, which are held in close proximity to the centre of one of the aromatic rings. This gives rise to two possible conformers, whose population relies on the difference in the strength of the interactions between the aromatic ring and each substituent of the bridge, relative to the solvent being employed. The conformational equilibria of each derivative were studied by NMR spectroscopy using variable temperature techniques and solvents. The presumed equilibria under those two variables were compared in order to give some insight into the nature of the π interactions involved.

The thesis concludes with a formal account of the experimental procedures used, the compounds prepared and an appendix detailing theoretical data obtained by computational chemistry and crystal structures data.

DECLARATION

The research described in this thesis is, to the best of my knowledge, original except where due reference is made to other authors.

TABLE OF CONTENTS

ACKNOWLEDGEMENTS

A big gratitude must go to my friends from France, for having come to visit me (and London!) several times and for being present after all those years. Amongst them, a special thank goes to Yann and Caro, for having shared the experience of doing a PhD at the same time and coping with the same difficulties and doubts.

Most of all, I would like to thank my parents and my brother for, their frequent trips to London, for their love, understanding and endless support. I would not have been able to make it without them.

ABBREVIATIONS

ACh	Acetylcholine
AcOH	Acetyl acid
Ac_2O	Acetic anhydride
Arg	Arginine
Asn	Asparagine
Bn	Benzyl
b.p.	Boiling point
br	Broad
Bu	butyl
cat.	Catalytic
CI	Chemical ionization
d	Doublet
DAST	Diethylaminosulfur trifluoride
DIBAH	Di-*iso*-butylaluminum hydride
DME	Dimethoxyethane
DMSO	Dimethylsulfoxide
EI	Electronic impact
eq.	Molar equivalent(s)
Et	Ethyl
Et_2O	Diethyl ether
EtOAc	Ethyl acetate
EtOH	Ethanol
g	Gram(s)
Gln	Glutamine
h	Hour(s)
H_{ar}	Aromatic protons
His	Histidine
Hz	Hertz
i	*iso*

IR	Infrared
J	Coupling constant
LAH	Lithium aluminium hydride
lit.	Literature value
Lys	Lysine
m	Multiplet
M	unspecified metal
M^+	Molecular ion
Me	Methyl
$MeNO_2$	Nitromethane
MeOH	Methanol
min	Minute(s)
mL	Millilitre(s)
mol	Mole(s)
mmol	Millimole(s)
m.p.	Melting point
n	*neo*
NMR	Nuclear Magnetic Resonance
NOE	Nuclear Overhäuser Effect
P.E.	Petroleum ether
Ph	Phenyl
Phe	Phenylalanine
ppm	Parts per million
R	Unspecified carbon substituent
R_f	Retention factor
r.t.	Room temperature
s	Singlet
t	Triplet
t	*tert*
TBAF	Tetrabutylammonium fluoride
THF	Tetrahydrofuran

Tf	Trifluoromethylsulfonyl
TLC	Thin layer chromatography
TMS	Trimethylsilyl
Trp	Tryptophan
Ts	*para*-Toluenesulfonyl
TsOH	*para*-Toluenesulfonic acid (tosic acid)
Tys	Tyrosine
w	Weak
Δ	Reflux
δ_C	Carbon chemical shift in ppm
δ_H	Proton chemical shift in ppm
ν_{max}	Peak frequencies in infrared spectra
μL	Microlitre(s)
μmol	Micromole(s)

CHAPTER 1

INTRODUCTION

1.1 – Introduction

This thesis is concerned with the synthesis of a series of molecules, which, through dynamic NMR measurements, can function as conformational balances in order to probe the weak non-covalent interactions between an aromatic ring and various functional groups. It is therefore appropriate, in the present section, to discuss the nature of such non-covalent π-interactions and their relevance in molecular recognition and drug design. In addition, the theoretical approach to through space interactions involving an aromatic system will be elaborated.

Consequently, this introduction is divided into three parts. The first defines and examines some of the fundamental aspects of the interactions involving an aromatic ring and also provides a brief account of the most common π-interaction *viz.*, the arene-arene interaction, with emphasis being placed on their crucial role (in dictating of molecular geometry) in biological and synthetic systems. In order to better understand the behaviour of the aromatic system, the second part of this chapter provides an overview of the interactions between an arene and X-H (X = C, O, N), and a third part is concerned with the importance of cation-π interactions in biological systems.

1.2 – Interactions between aromatic rings

A vast number of both natural and synthetic molecules possess at least one aromatic ring moiety, and, in recent years, the ability of the ring to participate in non-covalent inter- and intramolecular interactions has become increasingly apparent. Studies have indicated the key role of these interactions in such diverse areas as protein folding, base pair stacking in DNA, host-guest binding, crystal engineering, drug-receptor interactions and other molecular recognition processes.[1] Consequently, the understanding of such interactions becomes crucial for the design of new efficient drugs and ligands, as well as for the development of new materials. Considerable research efforts have therefore been initiated in order to understand the behaviour of aromatic rings in π-stacking phenomena.

1.2.1 – The nature of π-π interactions

1.2.1.1 – Quadrupole moment

The quadrupole moment of an aromatic system, simply defined as the molecular charge distribution, is considered to be the most reliable theoretical basis for consideration of π-π interactions.[2] The quadrupole moments of several aromatic units were determined from studies of the electric field-gradient birefringence. The large negative value of the quadrupole moment of benzene (-33.3×10^{-40} C.m²) can be visualised using the familiar picture of delocalised negative charge above and below the plane of the six carbon atoms, and consequently, the positive charge is distributed around the edges (Figure 1). In hexafluorobenzene, the electron charge density is now contained in the plane of the carbon ring and the sign of the quadrupole moment changes to $+31.7\times10^{-40}$ C.m² due to the strong electronegativity of the fluorine atoms.
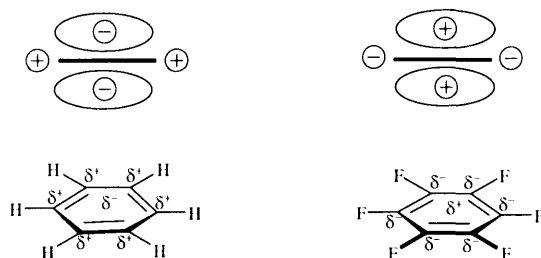
Figure 1 Schematic representation of the quadrupole moments of benzene and hexafluorobenzene

Interestingly, the quadrupole moment of 1,3,5-trifluorobenzene ($+3.1\times10^{-40}$ C.m²) is approximately the sum of the quadrupole moments of benzene and hexafluorobenzene, thus demonstrating the bond additivity of this molecular property.

1.2.1.2 – π-stacking geometry of benzene molecules

The benzene dimer has often been chosen as a model system for the investigation of π-π interactions and, in their early gas-phase studies, Klemperer and co-workers[3] found this dimer to be polar in its ground vibrational state. Its polarity was attributed to the presence of a permanent dipole. Since all geometries in which the planes of the two benzene molecules are parallel give a nonpolar dimer, these stacking possibilities were eliminated.

For a better understanding of the different arrangements of two aromatic rings in close proximity the following terms are chosen to describe the different geometries (Figure 2) and their stability will be discussed later in this chapter.

| planar sandwich
or
parallel-stacked
(a) | T-shaped
or
edge-to-face
(b) | parallel-displaced
or
offset-stacked
(c) |
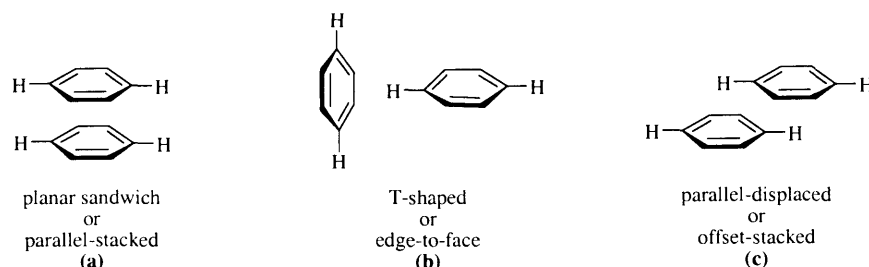
Figure 2 Proposed lowest energy geometries of the benzene dimer

Although early molecular modelling calculations predicted that porphyrin rings would have parallel-stacked structures, this contradicted experimental studies in which only the parallel-displaced arrangement was observed. In light of this, by considering the electrostatic charge distribution of the π-system, and envisaging the aromatic ring as a quadrupole, Hunter and Sanders[4] performed simple electrostatic calculations for the benzene dimers and developed a series of rules for a qualitative understanding of π-π interactions. They proposed a model of a π-system with an aromatic ring described as two regions of negatively charged π-electron density surrounding a positively charged σ-framework as depicted in Figure 3. Thus, T-shaped and parallel-displaced geometries were found to be the preferred arrangement.

T-shaped stacking   Parallel-displaced stacking
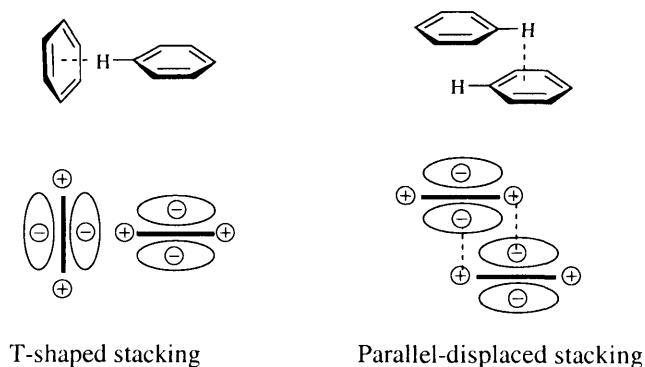
Figure 3 T-Shaped and parallel-displaced stacking of the benzene dimer indicated by the quadrupole moments of the benzene ring

These crucial insights lead to a qualitative understanding of π-π interactions and indicate that the interactions between two aromatic rings are predominantly controlled by π-π repulsions and π-σ attractions. As a consequence, these rules provide great power in molecular design.

Electrostatic and *ab initio* MO calculations[5] have shown that the three edge-to-face geometries **(a)**, **(d)** and **(f)** have potential minima but the differing computational approaches gave variant potential minima geometries to those depicted in Figure 4. For example, some of these variants can be obtained by simple rotation of the upper ring around its six-fold axis with respect to the lower ring. However in all cases, the geometries **(a)** and **(f)** exhibited the lowest energies (-9.2 to -10.0 kJ.mol^{-1})[5] and the calculated ring centre-to-centre distance in the T-shaped stacking arrangement **(a)** is 5.0-5.2 Å. Assuming that the ring radius and the C-H bond length in a molecule of benzene are 1.40 and 1.08 Å respectively, the distance between the proton of the upper ring and the lower aromatic centre is then 2.5-2.7 Å, and corresponds to an interacting H-to-ring centre perpendicular distance.
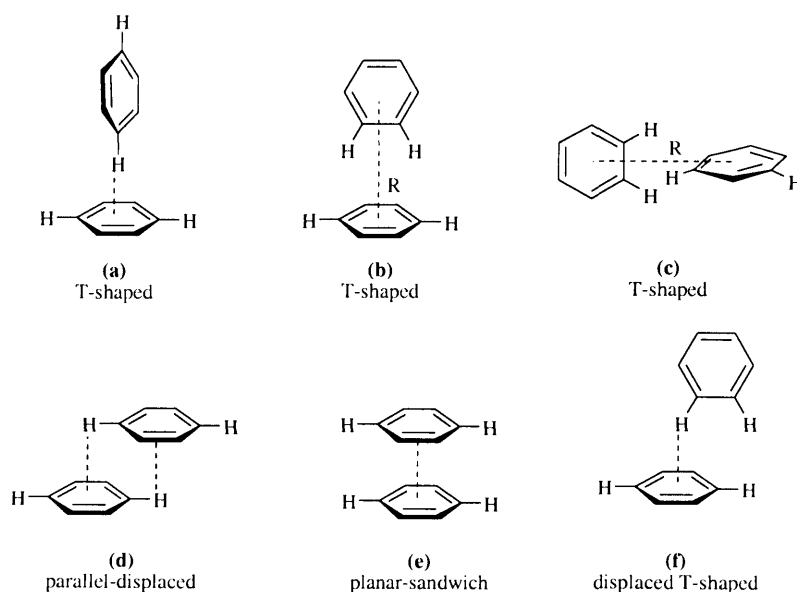
Figure 4 Representation of the possible geometries of the benzene dimer

Subsequent work by Hobza _et al._[6] supported these ideas and four potential minima were identified using high quality _ab initio_ calculations. The parallel-displaced stacking (**d**), the T-shaped (**a**) and the displaced T-shaped geometry (**f**) were all found to be very close with similar stabilisation energies (Figure 4 and Table 1).

	Interaction energy (kcal.mol⁻¹)	Interaction energy (kJ.mol⁻¹)	R (Å)
(a)	-1.893	-7.91	5.00
(b)	-1.658	-6.93	5.10
(c)	-0.682	-2.85	6.22
(d)	-1.978	-8.27	3.85
(e)	-0.853	-3.57	3.90
(f)	-1.921	-8.03	5.05

Table 1 Interaction energies for different geometries of the benzene dimer and distance R between the two aromatic centres[6]

This study found that the potential minimum for the stacking in structure (**b**) was considerably less than in the other three (**a**), (**d**) and (**f**). The extra stability of the T-shaped (**a**) was provided by an increased entropy distribution due to the free rotation of this structure. The calculated stabilisation enthalpy of the dimer (-10.0 kJ.mol⁻¹) agreed with that found from the bulk properties of benzene (-9.6 kJ.mol⁻¹) indicating that dispersion, and not electrostatic forces, was largely responsible for the attractive edge-to-face interactions, leading to the T-shaped arrangement. Additionally, the distance R in geometry (**a**) agreed with the experimental values obtained in solid benzene.

The crystalline form of a supramolecular system maximises the dispersion interactions and minimises the repulsion forces, thus bringing to light some information on the structures of molecular complexes and the nature of the non-covalent interactions between the binding partners in the solid state. Interestingly, only two of the most stable structures of the dimer, (**a**) and (**d**), are observed in solid benzene as well as in crystalline proteins showing a preference for the T-shaped arrangement, in which the distance between the ring centres is 5.025 Å.[7] Recently, ^{1}H NMR investigations of the dipolar coupling in liquid benzene[8] have provided some evidence for T-shaped stacking which was up to 2.93 kJ.mol⁻¹ (0.7 kcal.mol⁻¹) more stable than the parallel-sandwich structure.

In conclusion, theoretical and experimental studies, crystal structure data and measurements of gas phase complexes have all indicated that the T-shaped π-stacking arising from the quadrupole moment of the aromatic units is preferred.

1.2.2 – π-π interactions in organic molecules

1.2.2.1 – Aromatic-aromatic interactions in biological systems

Despite their weakness compared to other non-covalent interactions such as hydrogen bonding, π-π interactions play a vital role in the conformation of biological macromolecules, such as DNA or proteins, and also in biological molecular recognition. The important influence of these intramolecular edge-to-face interactions on self-assembly phenomena emerged and their abundance in proteins was initially shown in the early work of Burtley and Petsko[1a] who examined 34 high resolution three-dimensional protein structures. They demonstrated that, on average, 60% of aromatic side chains (Phe, Trp, Tyr) were involved in aromatic-aromatic interactions, with 80% of these interacting groups separated by seven or more amino acids. Additionally, the phenyl ring centroids were preferentially separated by a distance of between 4.5 and 7.0 Å, with a 90° dihedral angle being most common. Thus, the T-shaped structure was the most predominant type of π-π stacking in this complete survey based on distances and dihedral angle. The authors also suggested that the total contribution of π-π interactions was comparable to the free energy of protein folding. These results were confirmed by the analysis performed by Thornton[9] where the T-shaped arrangement was found most often in the 162 Phe-Phe interactions in proteins. In their investigation of 505 high resolution X-ray crystal structures of proteins, McGaughey *et al.*[10] found that the parallel-displaced structure was 2.1-4.2 kJ.mol^{-1} (0.5-1.0 kcal.mol^{-1}) more stable than a T-shaped structure for the full set of aromatic side chain amino acids. The competition between these two geometries was investigated by studies of preferential arrangement of aromatic amino acids in α-helices.[11] Indeed, the preferred structure of the aromatic pair was dependent on the distance of the two aromatic rings, their location in the protein, either in the core or on the surface, and on the nature of the investigated amino acids (Figure 5).

Phe 498

Trp 494
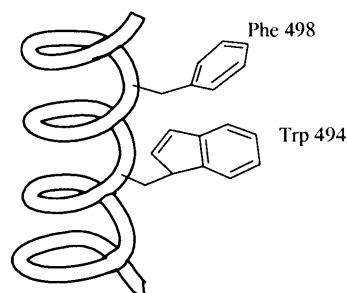
Figure 5 Example of interacting aromatic pair in *i* and *i+4* positions in α-helix
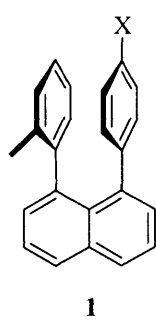
Interactions of phenylalanine in the *i* position of an α-helix with natural and unnatural aromatic groups in the *i*+4 position have stabilising effects of -0.4 to 3.3 kJ.mol^{-1} (-0.1 to -0.8 kcal.mol^{-1}), and the Phe-Phe interaction provides the greatest stability.[12] Additionally, π-π interactions have a crucial role in the stabilisation of the folded arrangement of proteins and, even in the core of the helix, the presence of phenylalanine and other aromatic side chains can increase the overall helicity by a factor of 2. These interactions are also critical for the 3D structure of double helical DNA by controlling the base-stacking interactions which determine the sequence-dependent structure and properties of DNA.[13] Using the model of aromatic-aromatic interactions described by Hunter,[14] calculations enable the reproduction of the experimental conformational preference of different DNA sequences.

1.2.2.2 – π-π Interactions in specifically designed synthetic organic molecules

Accurate studies on arene-arene interactions are far from trivial due to the complexity of molecular systems in which multiple intra- and intermolecular interactions contribute to the total stabilisation energy. Nevertheless, this research area of specifically designed molecules where the conformation depends on attractive or repulsive arene-arene interactions has expanded in the last decade.[15] From the large volume of work in this area to date, only a few relevant examples of molecular systems designed to study π-π interactions will be discussed.[16]

1.2.2.2.1 - Intramolecular non-covalent π-π interactions

As we have seen, attractive interactions between two aromatic rings with similar electron density will favour the T-shaped and parallel-displaced arrangements. Parallel stacking is an important arrangement both in the solid state and in solution especially when substituents on the rings can modify the electron density, for example when one of the aromatic systems becomes electron deficient whilst the other is electron rich. Accordingly, a series of 1,8-diarylnaphtalenes **1**[17] have been synthesised in order to establish the role of electron charge transfer in arene-arene interactions and their optimum orientation (Figure 6).

	X	$\Delta G^{\neq}$ (kJ.mol^{-1})
1a	OCH_3	58.2
1b	CH_3	60.2
1c	H	61.5
1d	Cl	64.9
1e	CO_2CH_3	70.7
1f	NO_2	72.4

Figure 6   Barrier to rotation $\Delta G^{\neq}$ (kJ.mol^{-1}) in $(CD_3)_2SO$ for substituted 1,8 diarylnaphtalene molecules **1**

Due to the enforced face-to-face arrangement of the two aryl substituents in 1,8-diarylnaphtalenes, it proved possible to measure the barrier to rotation of the aryl units. This barrier depended on the strength of the parallel-stacked interactions in the ground state, which was much larger when the substituent X was electron withdrawing. This study demonstrated that there was an increase in stability for the parallel-stacked structure of electron deficient rings relative to electron rich ones, agreeing well with the Hunter and Sandler rules described earlier (Section 2.1.2).[4]

Another interesting investigation of the parallel-stacked structure was performed by ^{1}H NMR experiments in $(CD_3)_2SO$ of the ester linked aromatic units **2-7**[18] which afforded linear or U-shaped conformations. Stabilisation of the folded conformation (U-shaped) depended on the formation of intramolecular interactions between the two planar aromatic

groups, and the nature and magnitude of these interactions were determined by ^{1}H NMR spectroscopy (Figures 7 and 8).
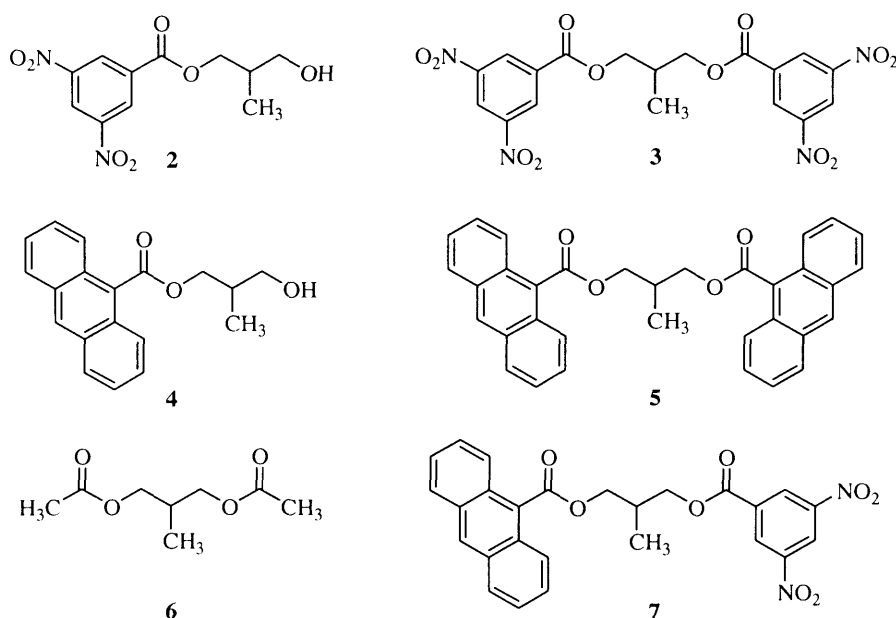
Figure 7 Compounds used to probe intramolecular aromatic interactions in benzene

The presence of a small substituent at the central carbon in **2-7** provided non equivalent geminal protons and NOE experiments enabled the distance between the two aromatic units to be calculated. Similarities in the chemical shifts of the aromatic protons and the vicinal spin coupling constants in the ^{1}H NMR spectra were observed for the monoester **2** and its symmetrical diester analogue **3**, which indicated that there was an absence of intramolecular interactions between the two aromatic systems in the diester **3**, and similarly in the esters **4** and **5**. Nevertheless, the ^{1}H NMR signals of the aromatic protons of the unsymmetrical diester **7** were shifted upfield indicating the formation of intramolecular interactions. However, the nature of the interactions responsible for the U-shaped conformation was not determined and thus, those interactions could be dispersion (van der Waals interactions), charge-transfer or quadrupolar controlled.
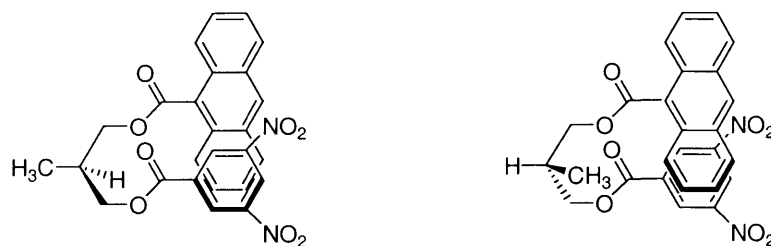
Figure 8   U-Shaped geometries of **7** stabilised by π-π interactions

If van der Waals interactions were the most important, the symmetrical anthracene derivative **5**, which has the largest van der Waals contacts, should have exhibited the greatest effect rather than the structure **7**. Furthermore, no charge-transfer bands were observed in the UV spectra. As the quadrupole moments of the aromatic units were of opposite sign, the electrostatic interactions between the dinitrophenyl and anthracene units are responsible for the stabilisation of the U-shaped conformation. Contrastingly, in the symmetrical esters **3** and **5,** the quadrupole interaction was repulsive, indicating the absence of intramolecular interactions.

Jennings _et al._[19] were the first to carry out detailed studies on the imine **10** in order to quantify attractive intramolecular edge-to-face interactions both in the solid state and in chloroform solution (Figure 9).

10
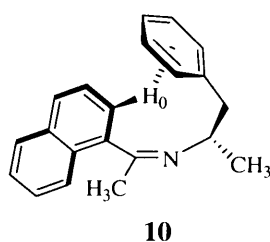
Figure 9   Edge-to-face interaction between the naphthalene unit and the benzene ring in the imine **10**

Although the ^{1}H NMR spectrum revealed an upfield shift of the naphtyl proton H_0, the X-ray structure indicated the formation of intramolecular edge-to-face stacking between H_0 and the benzyl ring. In this conformation, H_0 was projected into the aromatic face of the benzyl substituent at a close-contact perpendicular distance of 2.68 Å and offset by only 0.39 Å from the aromatic centre. The same group also synthesised and studied the preferred conformation of other flexible acyclic molecules **11**, whose structures were comparable to that of **10**.[16a,20] A similar stacking arrangement was observed both in solution and by X-ray

crystallography due to the formation of this intramolecular edge-to-face interaction (Figure 10).
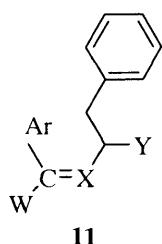
compd	Ar	W	X	Y
11a	1-naphthalene	$C(Me)_2OH$	N	Ph
11b	$2\text{-}BrC_6\text{-}H_4$	Me	N	Ph
11c	1-naphthalene	Et	N	Me
11d	$2\text{-}MeOC_6H_4$	Me	N-O	Ph
11e	$2\text{-}CF_3C_6H_4$	Me	N-O	H
11f	1-naphthalene	Me	N-O	CO_2Me
11g	1-naphthalene	Me	CH	Me

Figure 10   Structure of imines **11a-g** enable to form an edge-to-face interaction between the aromatic substituent and the benzene ring

X-ray crystal structures of the major atropisomers of **11c-f** showed that the hydrogen H_0 (on position 6 of the 2-substituted ring as depicted in Figure 9) projected into the aromatic face of the benzyl group at a perpendicular distance of 2.57-2.73 Å and were offset from the ring centre by 0.19-0.48 Å. Furthermore, the ^1H NMR signal of H_0 was found to be shifted upfield on cooling, thus demonstrating that the two conformational states **A** and **B** were in equilibrium at room temperature. On decreasing the temperature, the rate of conformational interconversion was reduced with conformer **A** being favoured (Figure 11).

Conformation A   Conformation B
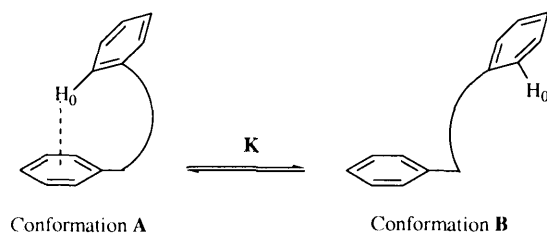
Figure 11   Conformation equilibrium between the folded conformation **A** and the stretched **B**

The stabilisation enthalpy of the folded conformer **A**, experimentally estimated to be up to -6.69 kJ.mol^{-1} (-1.6 kcal.mol^{-1}), is in agreement both with the experimental value in the benzene dimer and with theoretical calculations for the benzene dimer in the T-shaped structure (-6.3 to -8.2 kJ.mol^{-1}). In 1994, Wilcox and co-workers measured the equilibrium between the folded and the open conformation of **12** in order to estimate the strength of the edge-to-face interactions (Figure 12).[21]
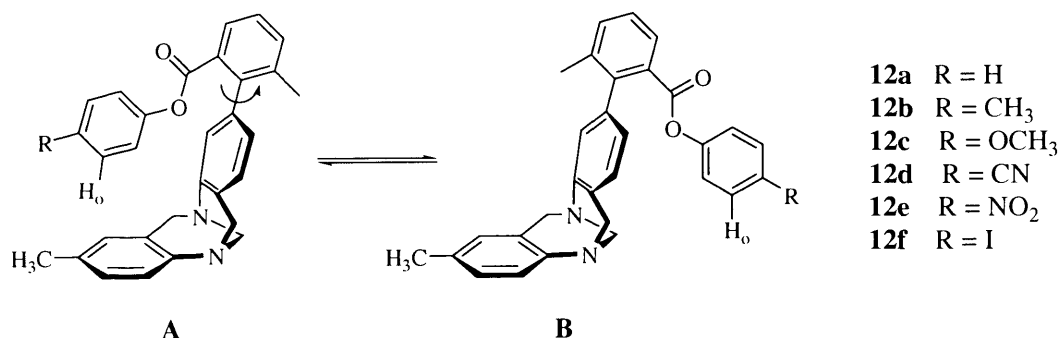
Figure 12   Molecular torsional balance **12a-f** described by Wilcox to quantify aromatic edge-to-face interactions. T-Shaped aromatic interactions are effective only in the folded conformation **A**

This novel system was described as a "molecular torsion balance" since the two limiting conformations **A** and **B** are separated by a considerable barrier to rotation, *ca.* >75 kJ.mol^{-1} (18 kcal.mol^{-1}). An X-ray diffraction study of **12e** and the observed upfield shift of the H$_0$ signal in the ^{1}H NMR proton spectrum confirmed stabilisation of conformation **A** by edge-to-face interactions. The folded conformation was therefore preferred by $\Delta G° = -1.67$ to -2.72 kJ.mol^{-1} (-0.4 to -0.65 kcal.mol^{-1}) depending on the nature of the substituent R. The highest stability was observed for compounds with electron deficient aromatic rings (**12d** and **12e**). The molecular torsion balance **13**[22] was also synthesised (Figure 13).
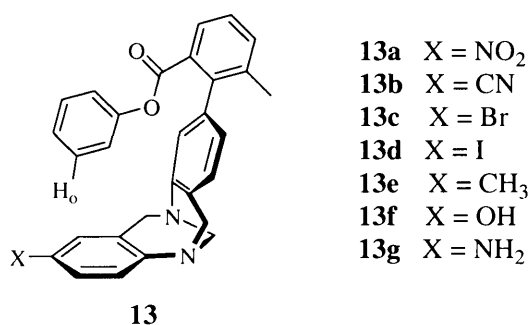
Figure 13 Molecular torsional balance **13** designed to study the substitution effects on the aromatic edge-to-face interactions

The magnitude of the energetic preference for the folded conformation was not affected by the electron withdrawing or electron donating character of the substituent. However, computational investigations[23] suggested that the preference for the folded conformation, which can arise from the attractive edge-to-face interactions may have been underestimated

by neglecting the effects of solvents, since solvation may shift the equilibrium in favour of the non-folded conformer.

1.2.2.2.2 – Intermolecular π-π interactions and organic host-guest complexes

The importance of non-covalent interactions in molecular association provides a suitable basis for developing organic host-guest complexes that illustrate particularly efficient and straightforward approaches to molecular recognition.[1c,24] Host-guest chemistry has attracted considerable interest in recent years and many synthetic receptors, such as cyclophanes (or molecular tweezers), have been designed to investigate the intermolecular π-stacking interactions between substrate and receptor. Complexation of a substituted naphthalene by a cyclophane was studied by Diederich and co-workers[25] in 1986, and an electron deficient guest exhibited favourable interactions with the receptor (Figure 14). In this complex, the cyclophane was envisaged to be an electron donor host and a more stable complex 14 was formed with an electron deficient guest.

14

X = CH$_2$OH, OH, NH$_2$, OCH$_3$, CH$_3$, OAc, CO$_2$CH$_3$, CO$_2$H, NO$_2$, CN
Y = CH$_2$OH, OH, NH$_2$, OCH$_3$, CH$_3$, CHO, NO$_2$, CN, CO$_2$H, NO$_2$, OAc
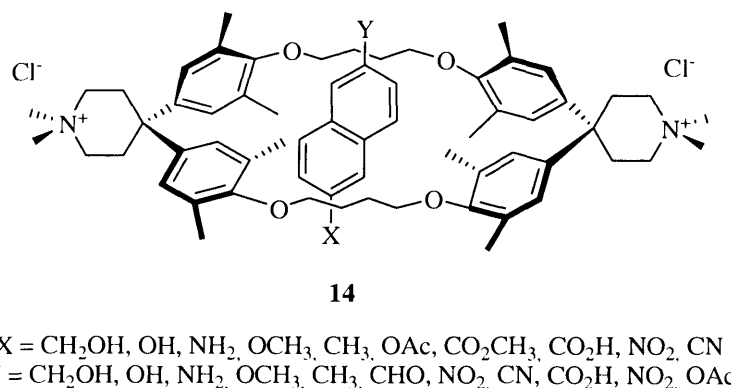
Figure 14 Average geometry of complexes formed between the cyclophane and the substrate

For the successful design of binding receptors in host-guest chemistry, the stereoelectronic complementarity between host and guest, as well as the preorganisation of the binding site prior to complexation,[26] are two crucial principles. Formation of a complex induced a shift of the signals of the naphthyl protons in the ^{1}H NMR spectrum and the more electron poor the substituents on the naphthyl ring, the deeper the guest could be accommodated in the cavity formed by the host. The stacking of the naphthalene in the host cavity gave rise to an

edge-to-face arrangement between the four aromatic rings of the receptor and the naphthyl protons and this emphasised the importance of polar contributions in π-π interactions.

Molecular recognition of ethyl adenine was investigated in an elegant fashion by Rebek *et al.*[27] who studied the binding affinity of receptor 15 towards a series of adenine derivatives. Ethyl adenine was hydrogen bonded to the imide group of the receptor with both Watson-Crick and Hoogsteen base-pairing, as illustrated in Figure 15.
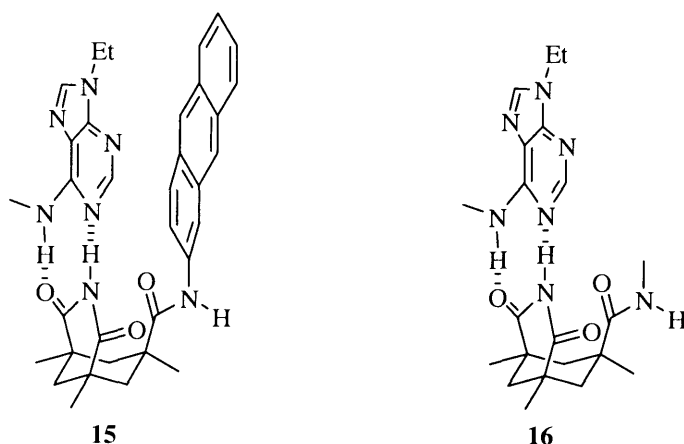
Figure 15 Complex receptor-adenine stabilised by hydrogen bond and π-π interactions

These ^{1}H NMR binding studies revealed a high association constant for complexation of adenine by the hosts (240 M^{-1}) whereas replacement of the anthracene unit by a methyl group led to a decrease in stability (75 M^{-1}). Stabilisation of the adenine substrate by the anthracene system was thus explained by the π-interactions between the adenine components and the anthracene unit, as well as by preorganisation which was induced by the rigidity of the host-guest couple.

Within the last twenty years, molecular tweezers have been subjected to extensive studies as a new molecular architecture for receptors. The rigid structure of 17, designed and synthesised by Zimmerman,[28] forced the chromophore substituents to be approximately 7 Å apart, ideal for a planar aromatic guest, such as 2,4,7-trinitrofluorenone 18 (Figure 16). This guest was chosen as it contained two significantly electron deficient aromatic rings which would demonstrate the importance of electronic properties in π-π interactions.

R = N⁺(Me)₃   **17a**
R = C(Me)₃   **17b**
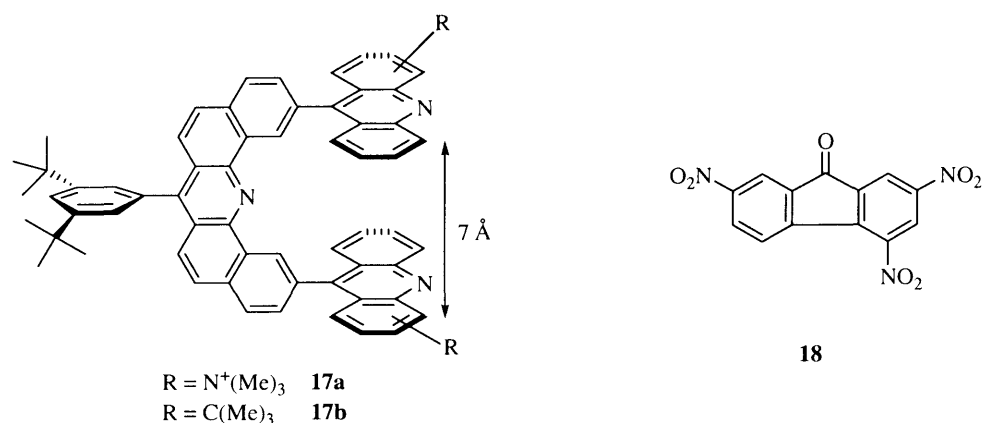
Figure 16 Zimmerman's molecular tweezer **17** and structure of a studied substrate **18**

Complexation studies, performed by ^{1}H NMR spectroscopy in chloroform revealed that the signals of the protons of **18** were shifted upfield, indicating the formation of the host-guest complex. It was observed that **18** was bound five times more strongly by the electron poor receptor **17a** than by the alkyl substituted analogue **17b** ($697 \ M^{-1}$ and $149 \ M^{-1}$ respectively). Consequently, the association constant increased on enriching the electron density of the receptor, confirming the importance of the stereoelectronic complementarity in the stabilisation of the host-guest complex by aromatic interactions.

Klärner and co-workers[29] have extensively studied molecular tweezers and clips as synthetic receptors beginning with the depicted structures because of their preorganised belt geometry (Figure 17).

19   **20**
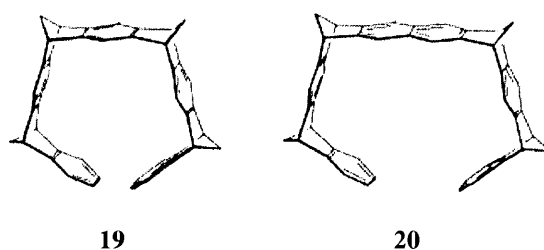
Figure 17 Structure of Tetramethylene-bridged Tweezers **19** and **20** used as receptor for aromatic substrates

However, bond angle distortions require little energy and, therefore, should induce a certain flexibility in these systems, allowing the receptor "arms" to be expanded and compressed during substrate complexation in a manner comparable to the working principle of mechanical tweezers. Furthermore, the size and shape of the receptor cavities can be

modulated by the number of spacer units incorporated. The potential surface both for the inside and the outside of the cavity of the receptor was calculated by various methods. All agreed that this potential was drastically more negative inside the tweezer cavity than outside. Therefore, complexation of the substrate occurred inside the cavity instead of above the central aromatic spacer unit.

The association constants K_a of tweezers **19** and **20** with the following series of substrates were consequently estimated by ^{1}H NMR spectroscopy in chloroform (Figure 18 and Table 2).
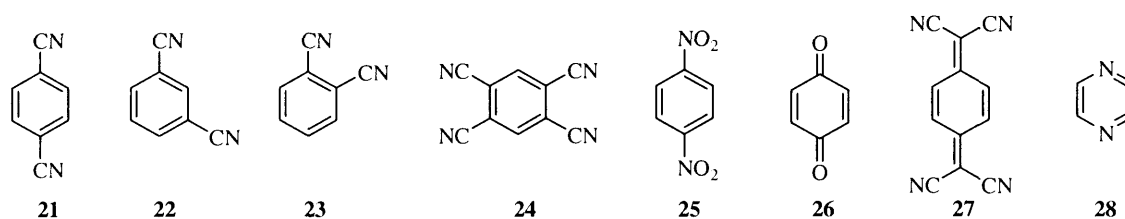
Figure 18   Series of substrates for the complexes with **19** and **20**

Substrates	K_a (M^{-1})	
	Receptor **19**	Receptor **20**
21	110	10
22	85	<1
23	40	<1
24	45	80
26	20	<1
27	n/a	1100
28	8	<1

Table 2   Association constants K_a (M^{-1}) of complexes with **19** and **20** as receptors at 21 °C. Because of the high stability of the complex **19-27**, association constants cannot be determined using the ^{1}H NMR method.

Examination of these results revealed that the complexes formed with receptor **19** show a stronger binding interaction than those formed with receptor **20**, thus agreeing with theoretical calculations.

19-27 complex   20-27 complex
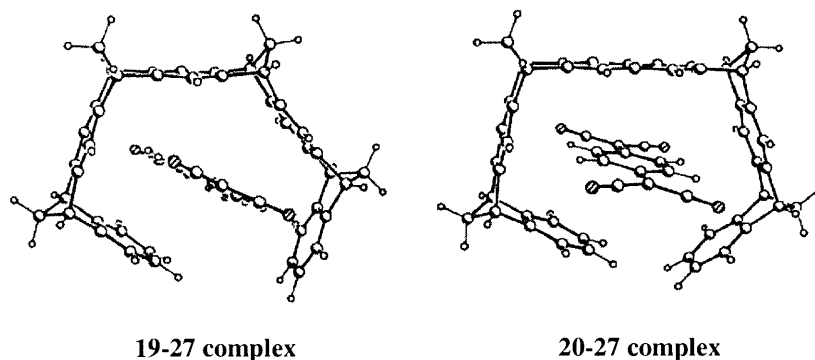
Figure 19   Diagrams for crystal structure determination of the complexes of the substrate **27** with both receptors **19** and **20**

The crystal structure of the **19-27** complex (Figure 19) exhibited three π-π stacking interactions which strongly stabilise the substrate in the receptor cavity. Indeed, the favoured stacking of the aromatic ring of **27** permitted the formation of two edge-to-face interactions with both receptor arms, as well as a parallel-displaced interaction with the aromatic system at the end of the molecule. Furthermore, the crystal structure of the **20-27** complex did not exhibit this arrangement and one only edge-to-face interaction was observed. Thus, the crucial importance of the geometric topology of the tweezers for the binding properties was confirmed in this study. The authors extended this investigation to a wider series of molecular tweezers and clips[30] and the crystal structure of the complex between the receptor **28** with **24** is shown in Figure 20.

28   28-24 complex
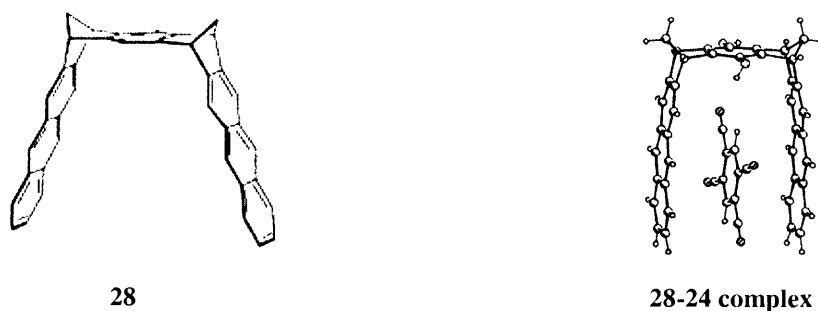
Figure 20   Structure of dimethylene-bridged clip **28** and single crystal structure of the complex between the receptor **28** and the substrate **24**

In this complex, the molecular plane of the substrate in the receptor cavity was almost parallel to the receptor arms (anthracene unit) and perfectly orthogonal to the central spacer

unit. ^{1}H NMR spectroscopy of the complex at high temperature showed a rotation of the substrate inside the cavity around an axis parallel to the central spacer unit. This molecular clip was an efficient receptor for electron-deficient neutral substrates, such as the nitrile **24**, due to the complementary nature of the electrostatic potential of the substrate to that inside the receptor cavities. Moreover, these results emphasise the two crucial principles for host design in molecular recognition, *viz.*, that both the shape and electrostatic potential must be complementary, and this leads to a rationalisation of complex formation of various aromatic hosts and cyclic peptides.[31]

Hunter and co-workers[32] have intensively studied π-π interactions using a double mutant cycle for measuring edge-to-face interactions (Figure 21).
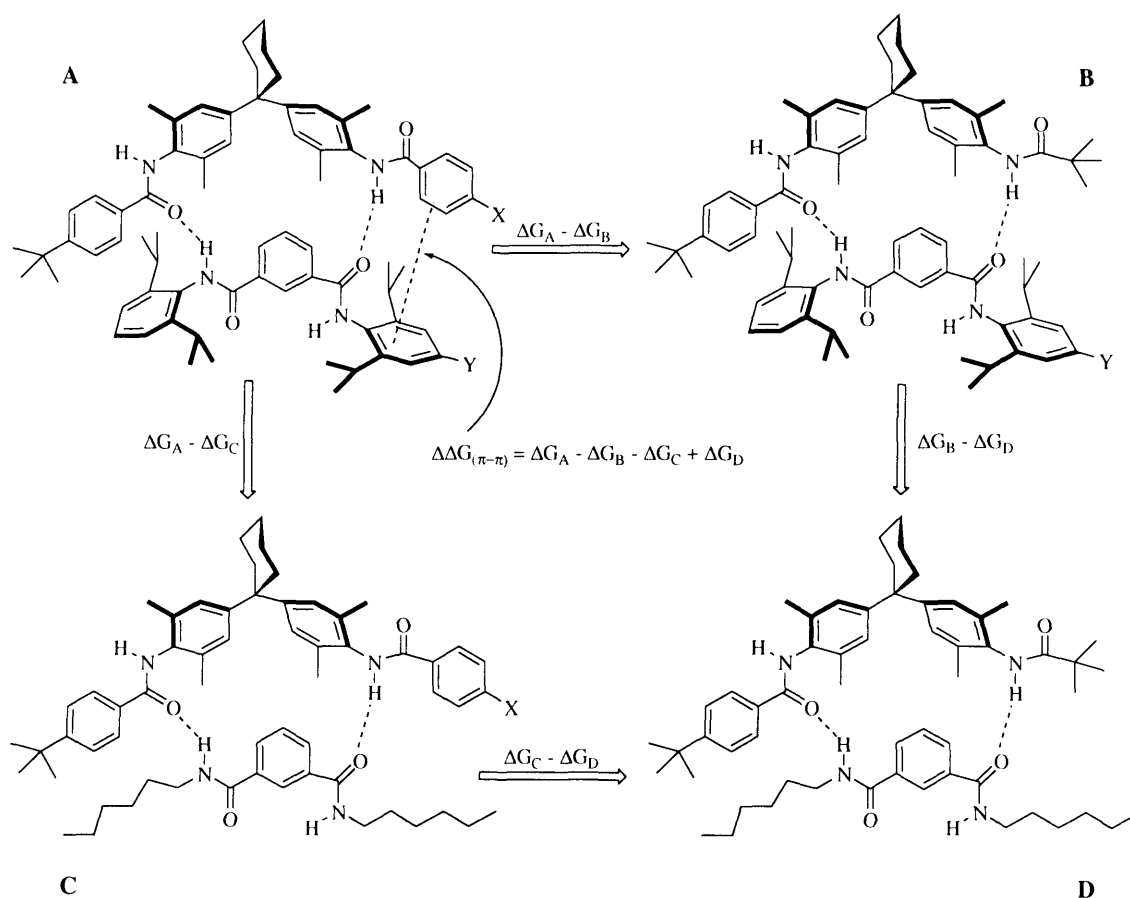
Figure 21   Chemical double mutant cycle to measure the magnitude (ΔΔG) of the terminal edge-to-face aromatic interaction in complex **A**

The X-ray crystal structure of complex **A** showed the presence of an edge-to-face interaction and removal of one or the other aromatic rings (**A** to **B** or **A** to **C**) resulted in the

loss of the π-π interaction, but also could affect the other contributing interactions, *e.g.* the hydrogen bonds. The double mutant **D** took into account these secondary changes such that the sum $\Delta\Delta G(\pi$-$\pi)$ represented only the energy of the edge-to-face interaction. Therefore, the authors argued that the difference of free energies of the non-substituted edge-to-face interaction would be -1.4 kJ.mol^{-1} and that changing the substituents X and Y would affect the free-energy relationship giving interaction energies ranging from +1.2 kJ.mol^{-1} to -4.6 kJ.mol^{-1}. Interestingly, the binding energy was related to the rigidity of the backbone and replacing the flexible diphenylcyclohexyl spacer unit by a diphenylnorbornane unit afforded a higher association constant since the guest was a better fit in the host cavity.[33] A decrease of the edge-to-face interaction energy was observed as a result. However, in a recent paper, Hunter has extended his work to three different double mutant cycles[34] in which the unsubstituted edge-to-face interaction was -1.4 kJ.mol^{-1}.

The binding strength between two π-systems was shown by Smithrud and Diederich[35] to be highly solvent dependent in a study of complexation of pyrene with cyclophane **29** (Figure 22).
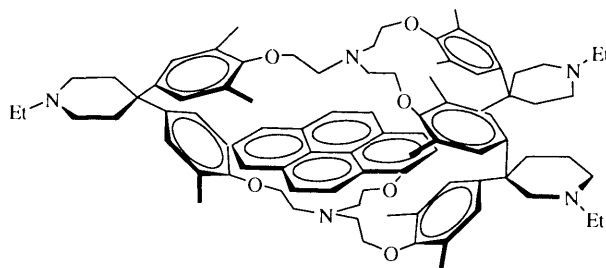
Figure 22 Complexation of the cyclophane **29** with pyrene

The association constant was determined in 18 solvents of different polarity and a linear relationship was obtained between the free energy of complex formation and the empirical polarity parameter $E_T(30)$ (Figure 23). The entire polarity scale showed that apolar host-guest complexation decreased from water (-$\Delta G°$ = 9.4 kcal.mol^{-1}) to non-aqueous polar protic solvents, to dipolar aprotic solvents and to apolar solvents like carbon disulfide (-$\Delta G°$ = 1.3 kcal.mol^{-1}).
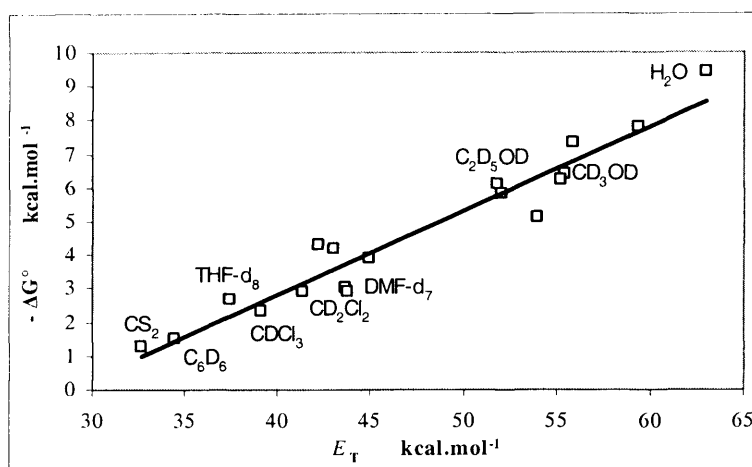
Figure 23   Dependence of the free energy of complexation of the cyclophane-pyrene complex, $-\Delta G°$ (kcal.mol^{-1}) on the polarity $E_T(30)$ (kcal.mol^{-1})

The authors argued that it was the solvent properties which induced almost exclusively the observed differences in the binding strengths. Solvent molecules with high cohesive interactions interacted more favourably with bulk solvent than with the free apolar surfaces of the receptor or pyrene molecules and therefore, free energy was gained upon the release of surface-solvating molecules to the bulk solvent during the complexation step. Thus, with the highest cohesive interaction and the lowest molecular polarisability, water was the best solvent for apolar binding.

All previous studies on intra- and intermolecular interactions involving two aromatic systems viewed an aromatic ring as a quadrupole, thus explaining the T-shaped and parallel-displaced stacking as the most stable geometries for the complexation of two similar aromatic rings. The importance of the participation of these interactions to the binding energies in host-guest complexes and in protein folding is now well-established but their exact role as well as their quantification in a general fashion has not yet been defined as the strength of the π-π interactions is dependent on many factors, for example steric accessibility, electron density of the ring and solvation.

1.3 – Interactions between an aromatic ring and a functional group

Although a prevalence of arene-arene interactions exists in the literature, other interactions involving an aromatic ring have been found in natural and synthetic molecules. As the aromatic ring can be envisaged as a "hydrogen bond acceptor"[1b] with its π-electron cloud sitting above and below the plane of the ring, its close proximity to electron deficient functionality, such as an acidic proton, can generate a weak hydrogen bond interaction. Consequently, based upon these facts, many researchers have investigated these weak interactions of a soft acid, such as C-H or X-H (X = N, O, etc.) with the π-system which was envisaged as a soft base.

1.3.1 – Hydrogen bonding to aromatic π systems

1.3.1.1 – The C-H/π hydrogen bonds

1.3.1.1.1 – Definition and physical properties

The concept of the C-H/π interaction was introduced by Nishio *et al.*,[36,37] and, over the last twenty years, the importance of this interaction in host-guest complexes and in the structure of proteins and nucleic acids has been highlighted. The C-H/π interaction belongs to the borderline region of hydrogen bonding but can be considered as such, inasmuch as some proton donor properties of the C-H bonds are involved in the interaction.[38] Although the enthalpy for a single unit of C-H/π interaction is approximately 2.1-4.2 kJ.mol^{-1} (0.5-1.0 kcal.mol^{-1}), which was smaller than the calculated energies of the "true" hydrogen bonds involving a π-system (8-12 kJ.mol^{-1}), this interaction is thought of as a weak hydrogen bond.[38] At the weakest limit, a hydrogen bond can hardly be distinguished from van der Waals interactions (dispersion interaction and exchange repulsion). However, the C-H/π hydrogen bond is entropically advantageous and many C-H groups may participate simultaneously in the interaction with a π-base without considerable loss of entropy.[39] Therefore, the total energetic contribution of the combined effect of such multiple interactions becomes significant such that the C-H/π interaction may be considered as one of the driving forces to constrain a peptide conformation formed between side chains in

close proximity and to direct the specific conformation in most proteins.[40] The most important stabilisation factor of the C-H/π interaction largely comes from the dispersion interaction, although electrostatic interactions also contribute to *ca.* 20% of the total energy of the interaction. Although not essential, electrostatic interactions, which are orientation dependent, determine the geometry of the C-H/π complex and, for example, the position of a molecule of methane in the most stable methane-benzene complex, which is above the aromatic plane with one hydrogen directed towards the centre of the ring with the C-H•••π angle approaching 180°.[40,41] Thus, the orientation of the C-H proton towards the aromatic ring affects the binding strength. However, the proportion of the electrostatic forces is dependent on the degree of hybridation of the carbon atom in the C-H bond. High level *ab initio* calculations estimated that this proportion increased from sp^3-CH through sp^2-CH to sp-CH. Consequently, the stronger the proton donating ability of the C-H bond the stronger was the stabilising effect (sp-CH > sp^2-CH > sp^3-CH > CHX_3 > CH_3X),[42] and, the C-H proton acidity affected the distance between the hydrogen atom and the π-plane following the same trend. Despite broad interests in the C-H/π interaction in many areas of chemistry and biology, very little is known about its physical origin, and knowledge of this interaction essentially arises from the understanding of crystal packing, host-guest complexation and conformational preference.

1.3.1.1.2 – *Intramolecular C-H/π interactions and conformation of organic compounds*

Initially, Wilcox and co-workers studied the conformational equilibrium of the torsional balances **12** and **13** (Figures 12 and 13, Chapter 1.2.2.2.1), in order to establish the π-stacking interactions between two aromatic rings. However, the replacement of the phenyl ester by an isopropyl ester in the flexible unit of the balance was also investigated in order to examine the strength of the aryl-alkyl interactions (Figure 24).[22] A series of methyl ester analogues were also prepared to act as a control of the C-H/π interactions as the C-H proton of the methyl ester would be too far from the target π-system and no stabilisation of the folded conformation by non-covalent interactions would be expected. Indeed, no preference for either state of the methyl ester has been observed.

30a	R = NO$_2$
30b	R = CN
30c	R = Br
30d	R = I
30e	R = CH$_3$
30f	R = OH
30g	R = NH$_2$
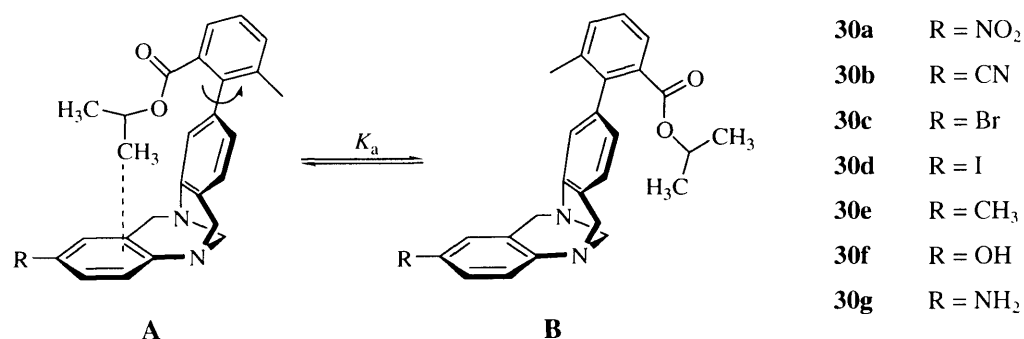
Figure 24 Conformational state for alkyl ester **30**

From Table 3, the folding energy $\Delta G°$ for the isopropyl esters is larger than that of their phenyl ester analogues indicating that dispersion forces are the driving forces for aromatic interactions, instead of electrostatic forces. Interestingly, the two isopropyl groups can generate more C-H/π interactions than a phenyl group and Nishio[43] argued that, even weak, co-occurring C-H/π interactions can stabilise a conformation more than the π-π interactions involving the phenyl group thus justifying the higher folding energies obtained for the isopropyl esters.

	$\Delta G°_{fold}$ (± 10%) Methyl ester kJ.mol^{-1} (kcal.mol^{-1})	$\Delta G°_{fold}$ (± 10%) isopropyl ester kJ.mol^{-1} (kcal.mol^{-1})	$\Delta G°_{fold}$ (± 10%) phenyl ester kJ.mol^{-1} (kcal.mol^{-1})
30a	0.46 (0.11)	-2.13 (-0.51)	-0.88 (-0.21)
30b	0.25 (0.06)	-2.67 (-0.64)	-1.25 (-0.30)
30c	-0.25 (-0.06)	-1.92 (-0.46)	-0.96 (-0.23)
30d	0.08 (0.02)	-2.26 (-0.54)	-1.09 (-0.26)
30e	-0.17 (-0.04)	-1.84 (-0.44)	-1.13 (-0.27)
30f	-0.12 (-0.03)	-1.96 (-0.47)	-0.96 (-0.23)
30g	-0.25 (-0.06)	-1.42 (-0.34)	-0.75 (-0.18)

Table 3 Folding energies $\Delta G°$ of methyl, isopropyl and phenyl esters (kJ.mol^{-1} and kcal.mol^{-1})

One year later, Nishio and co-workers published a study on the C-H/π interactions in peptides, using the crystal structure database.[44] Amongst the investigated compounds, 42% exhibited short C-H•••π distances, even shorter than the sum of van der Waals radii, indicating that aromatic interactions were involved. Moreover, the C-H hydrogen atom was positioned above the π-plane in order to participate in this interaction. The authors highlighted the importance of this interaction in maintaining the folded structure of peptides, leading to the specific 3D geometry of proteins and enzymes. Thus, the C-H/π interaction was responsible for peptide structure and its stability. Also from their investigations of the intramolecular C-H/π interactions in the crystal structures of organic compounds,[45] 29% of the studied molecules contained short C-H/π intramolecular distances (< 3.05 Å). Interestingly, the shortest distance for a 5-membered C-H/π interaction was *ca.* 2.63 Å with this distance increasing in larger-membered interactions. Formation of intramolecular hydrogen bonding is favoured in the 5- and 6-membered rings and this confirms the similarities between the C-H/π interactions and hydrogen bonding, indicating that the crystal structure is not only dependent on interactions such as hydrogen bonding or van der Waals interactions, but is also affected by the C-H/π interaction geometry. Consequently, the most stable geometry of procaterol hydrochloride hemihydrate **31** in solution exhibits a short distance between the isopropyl group and the aromatic ring (Figure 25).
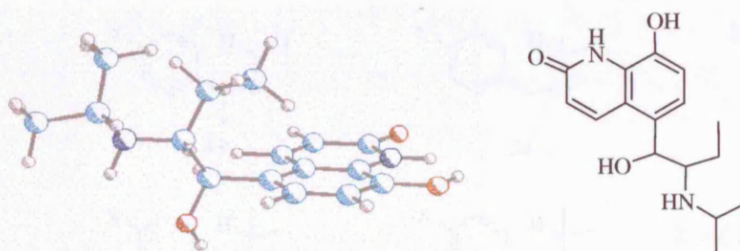
Figure 25 Structure of Procaterol hydrochloride hemihydrate **31** found in the crystal state and in solution where the isopropyl group resides above the aromatic ring and is stabilised by C-H/π interaction. (Dark blue) nitrogen atom, (red) oxygen atom, (light blue) carbon atom.

The conformation of benzyl formate **32** can be either folded or stretched[46] and the magnitude of the NOE enhancements can afford an estimation upon the conformational ratio (Figure 26).

Ratio of NOE
(folded/stretched) : 10%

Folded   **32**   Stretched
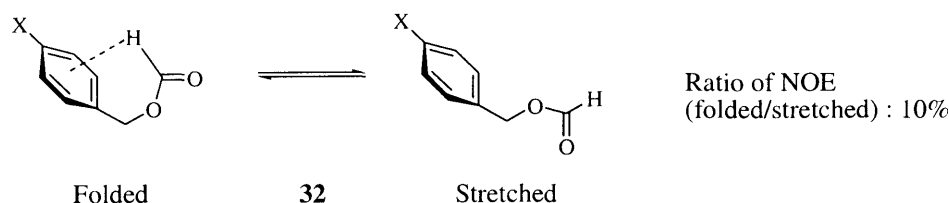
Figure 26 Conformational equilibria of benzyl formate **32**

NOE enhancement is dependent only on the distance between two nuclei, and is a powerful means to detect the through space proximity of two atoms, without consideration of their connectivity. Consequently, an increase in the ratio of the folded to the stretched conformer was reported after modifying the electron density of the aromatic ring by replacing a hydrogen atom by an electron donating substituent X, leading the authors to suggest that stabilisation of the C-H/π interaction occurred by partial transfer of charge from the π-orbital of the aromatic ring to the σ^*-orbital of the C-H bond.[47]

Similarly, NOE enhancements, combined with molecular mechanic calculations,[43,48] were used by Nishio in a study of a series of organic compounds capable of forming 5-membered C-H/π interactions (Figure 27).

32   **33**   **34**   **35**

36   **37**   **38**   X = CH$_3$O, CH$_3$, H, Cl, Br, CF$_3$, NO$_2$
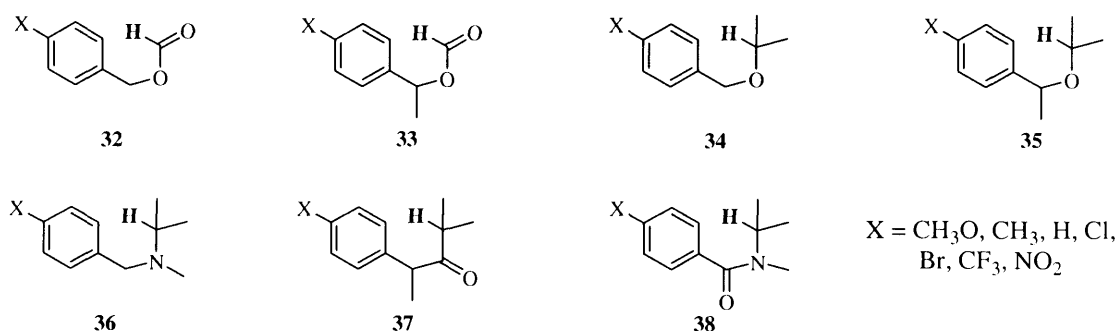
Figure 27 Benzylic derivatives in which a C-H/π interaction can occur between the aromatic ring and the proton, in bold style

The results obtained from the NOE experiments were also confirmed by upfield shifts in the ^{1}H NMR spectra of the signals of the donor C-H atoms in the folded conformation as this proton is expected to lie above the π-system and be subjected to the diamagnetic anisotropy of the aromatic ring. Substitution in the aromatic ring in a series of compounds was investigated in order to show the effects of the perturbation of the electron density of the aromatic ring on the strength of the C-H/π interaction. In the presence of "true" hydrogen bonding, an electron-donating substituent on the hydrogen acceptor should favour the interaction, and the results obtained in this study displayed this trend, therefore providing experimental support for the hydrogen-bond-like character of this interaction. The effects of the electronegativity of the proton of the C-H donor have also been highlighted and indeed, the acidity of the proton of the C-H donor increased with the electronegativity of the atom in position α (C=O < NMe < O). Acidity increased in the order **37** < **36** < **35** indicating that the more acidic the hydrogen atom, the stronger the C-H/π interaction. In amide **38**, the significant NOE enhancements indicated the stabilisation of the folded conformer. The flexibility of **38** enabled the isopropyl group to adopt a favourable position in order to participate in the C-H/π interactions as it can approach the aromatic system in the perpendicular plane, allowing the maximum overlap of the σ_{CH} and p_π orbitals. Another aspect of the C-H/π interaction is the effect of additional effects on the benzylic position. By comparison of the results obtained for **32** with that of **33**, and **34** with **35**, the electronic effect of the introduced methyl group was shown to be negligible, confirming the hydrogen-bond-like character of the C-H/π interaction.

Ab Initio MO calculations, performed two years ago by Nishio and co-workers[49] on substituted aromatics which were able to adopt a folded conformation stabilised by C-H/π interactions, failed in predicting the correct conformational equilibrium, thus highlighting the limits of the calculation methods. Indeed, it appears that the importance of the C-H/π interaction in the stabilisation of these model structures is neglected, and this emphasizes the need for a geometry prediction programmes to take into account the magnitude of this interaction.

1.3.1.1.3 – Crystal packing and C-H/π interactions in molecular recognition

The C-H/π interaction participates in stabilising the 3D structure of proteins[50] and host-guest complexation,[51] even if it does not act as the most predominant force.[52] Host-cavity inclusion has been investigated in the crystalline structures of numerous host-guest complexes, where one of the participating molecules contains at least one aromatic ring.[53] Interestingly, the conformation of many structures was maintained in solution, and the relative strength of the total participation of the C-H/π interactions in complex formation could be studied. As an example of the importance of this interaction in host-guest complexation, the tetramer **39**[54] has been designed as a multidentate host with a bowl-shaped cavity capable of multi hydrogen-bonding fixation of guests, such as simple alcohols.

R = (CH$_2$)$_{10}$CH$_3$

39

Complex with butan-1-ol
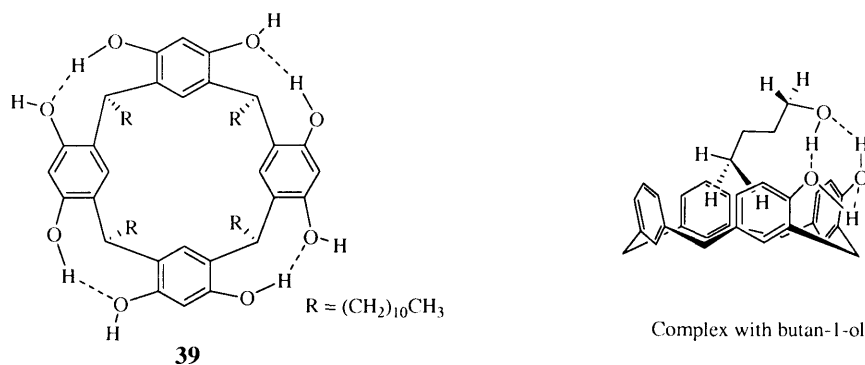
Figure 28   Structure of the calix[4]arene **39** and its complexation with butan-1-ol stabilised by the combination of hydrogen bonding and C-H/π interactions between the four aromatic rings of the receptor and the aliphatic chain of the alcohol.

Binding studies of **39** with several guests were investigated by NMR spectroscopy and the binding constants were observed to increase with the length of the guest chain in the order, ethanol < propanol < butanol, with branching, *i.e.* in the order, ethanol < *iso*-propanol < *tert*-butanol, highlighting the minor effects of steric hindrance. In essence, with a long aliphatic chain, the protons of the methyl groups can interact with the four aromatic rings in the host cavity and gave better stabilisation of the host-guest complex. The X-ray structure[55] of calix[4]arene **40** from acetone showed the presence of two molecules of acetone; one in the host cavity with a short distance between the protons

of the methyl groups and the centre of the π-systems, the other one outside, stabilised by a weak interaction with the nitrobenzyl group substituent on one ring of the host (Figure 29).
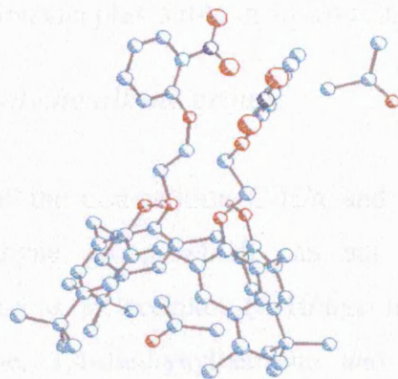
Figure 29   Structure of the calix[4]arene derivative **40** in complexation with 2 molecules of acetone. The methyl groups are directed onto the aromatic rings of the receptor. (Dark blue) nitrogen atom, (red) oxygen atom, (light blue) carbon atom

Evidence for intermolecular C-H/π interactions in biology has been given from the participation in the stabilisation of protein complexes,[56] and a relevant example is provided by the complex of D-galactose/D-glucose binding protein with β-D-glucose.[57] In this complex, the hexose ring is trapped between the aromatic side chains of Trp183 (on the β face) and Phe 16 (on the α face) at van der Waals distance.
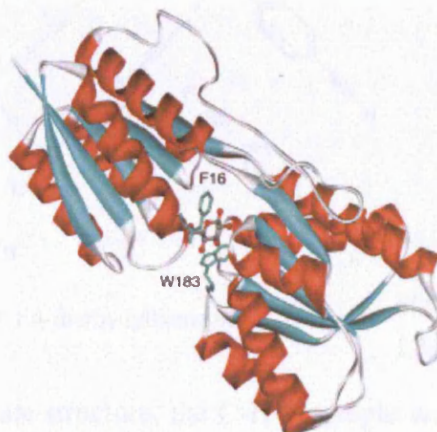
Figure 30   Complexation of β-D-glucose by the D-galactose/D-glucose binding protein

A highly important property of the C-H/π interaction is the ability to persist in polar protic media, such as water, due to the predominant participation of the dispersion force in the binding energy, whereas in polar organic solvents, binding is facilitated through effective

hydrogen bonding.[58] Coulombic forces and "true" hydrogen bonding, on the contrary, are not very effective in polar protic solvents.[36] Therefore, when considering biochemical processes, the C-H/π interaction can play a role in aqueous as well as in nonpolar media.

1.3.1.1.4 – Interactions involving alkyne groups

An interesting case study of the competition C-H/π and π-π interactions concerns the presence of a terminal ethyne group which can act as a hydrogen bond donor (C-H/π_{ar} interaction) and also as an acceptor (C-H/$\pi_{C\equiv C}$ interaction). The X-ray crystal structures of ethynylbenzene, 1,4-diethynylbenzene and 1,3,5-triethynylbenzene were determined by Boese and co-workers,[59] and, although having a similar core, these compounds gave different crystal packings. The geometry of 1,4-diethynylbenzene in the solid state was stabilised by T-shaped C-H/$\pi_{C\equiv C}$ interactions between two ethynyl groups and was the sole intermolecular interaction (Figure 31a).
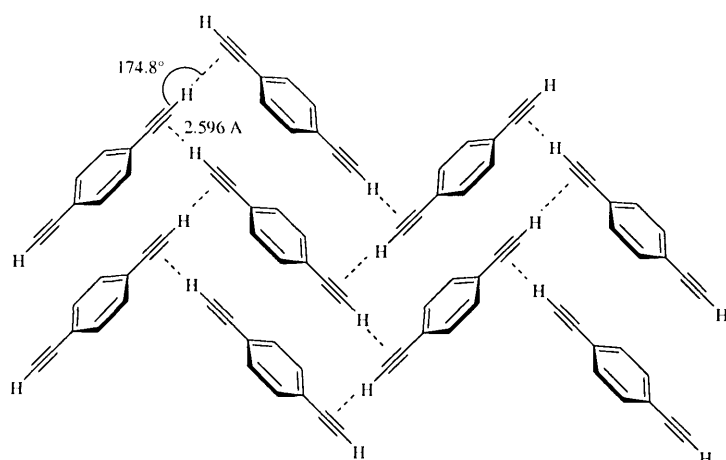
Figure 31a Packing structure of 1,4-diethynylbenzene
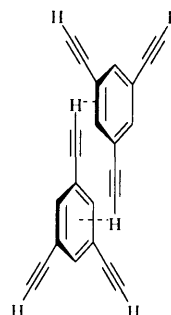
Figure 31b Packing structure of 1,3,5-triethynylbenzene

Remarkably in this solid state structure, the C-H•••π angle was approximately 180°, which has been found to be most favourable for the C-H/π interaction and the intermolecular distance was comparable to that of hydrogen bonding. However, the crystal packing of 1,3,5-triethynyl benzene did not show the same short contact interaction, and the dimer showed that the closest contact with the alkyne proton being just above the aromatic ring

(Figure 31b). Conversely, in the crystal stacking of ethynylbenzene, C-H/π_{ar} interactions were observed.
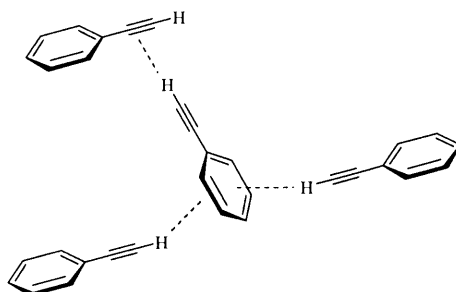
Figure 32 Interactions C-H/π_{ar} and C-H/ $\pi_{C\equiv C}$ present in the crystal structure of ethynylbenzene

Five molecules were found in the unit cell, with two and a half in the asymmetric unit, with half of the molecules being disordered. Two short contact distances were observed between the alkyne proton and the benzene ring, and a further intermolecular interaction involved the $\pi_{C\equiv C}$ system. The angles between the planes of the benzene rings lay between 80 and 90° and the shortest C-H/π distance was 2.82 Å, which is comparable to the distance between two benzene rings in the T-shaped conformation (2.76 Å). It is remarkable that ethynylbenzene melts at -45 °C, much lower than benzene itself, whereas the melting points of 1,4-diethynylbenzene and 1,3,5-triethynylbenzene are 97 and 104 °C respectively. This indicates that the crystal packing of ethynylbenzene is not as efficient as that of the benzene and demonstrates the weakness of the C-H/π interaction. The magnitude of the C-H/π interactions has been estimated by high level *ab initio* calculations[41] and the interaction energy for the acetylene-benzene complex was predicted to be -11.8 kJ.mol^{-1} (-2.83 kcal.mol^{-1}), a more negative value than the ethane-benzene complex (-7.61 kJ.mol^{-1}). This large negative value is the result of the large attractive electrostatic interaction in the acetylene-benzene complex and the most favourable geometry is T-shaped stacking between the acetylene and benzene, with a distance of 3.5 Å between the centre of the benzene ring and the carbon atom of the acetylene. This attractive force elongates the C-H bond of the acetylene to give a stronger interaction with the aromatic ring (Figure 33).[60]
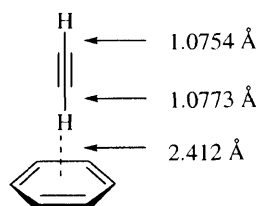
Figure 33 Optimised geometry of acetylene-benzene complex with bond distances
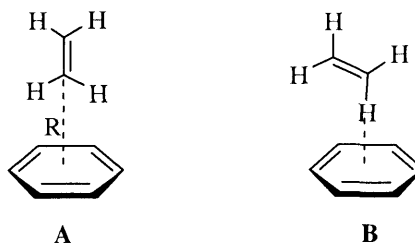
Figure 34 Two possible geometries for ethylene-benzene complex

In comparison, two stable geometries **A** and **B** have been found for the benzene-ethylene complex. In contrast to the acetylene-benzene complex, the T-shaped structure **A** was not the most stable and the calculated interaction energy of the complex **B** was less negative (-7.36 and -8.61 $kJ.mol^{-1}$ respectively). However, these electrostatic forces are responsible of the stabilisation of the ethylene-benzene complex, as with the acetylene-benzene complex, although the significant difference in interaction energies of the geometries **A** and **B** are due to their orientation dependency.

1.3.1.1.5 – C-H/π interactions in organic reactions

In addition to the prevalence for the C-H/π hydrogen bonding in biology and biochemical processes, the role of this interaction in the stereoselectivity of organic reactions has been increasingly studied. These reactions include Diels-Alder reactions where the interaction vindicates the formation of the *endo*-adduct,[61] catalytic enantioselective reactions,[62] photoreactions, chiral resolution[63] and transition metal complexes. Since an extensive review about the importance of this interaction in organic reactions has just been published,[64] a brief account on the most relevant reactions where the C-H/π interactions influence stereoselectivity, will be discussed in this section.

The coupling of 1,3-bis(bromomethyl)-7-*t*-butylpyrene **41** with a series of 1,3-bis(mercaptomethyl)benzenes **42** gave the *syn* adduct as the sole product when R = Me or Et, whereas the *anti* conformer was formed exclusively when R = F or OMe (Scheme 1).[65]
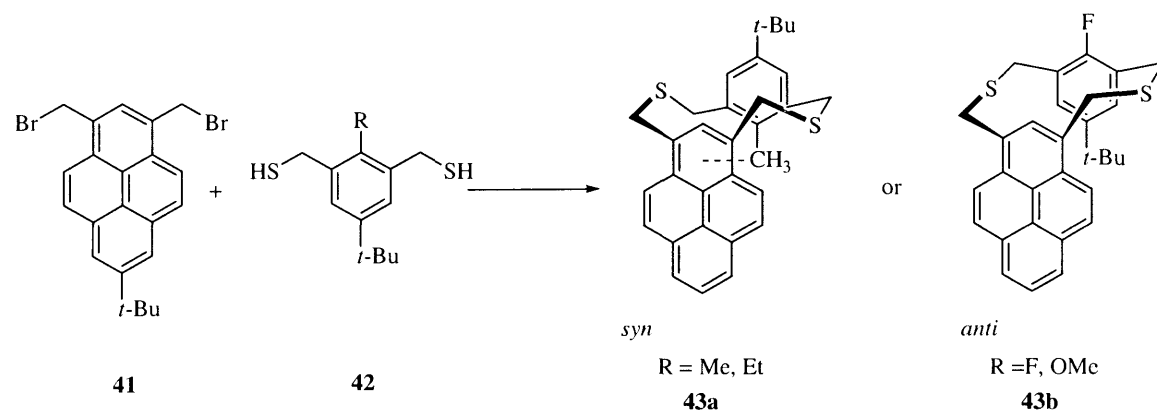
Scheme 1   Coupling   reactions   of   1,3-bis(bromomethyl)-7-*t*-butylpyrene   **41**   with 1,3-bis(mercaptomethyl)benzenes **42**

Interaction between the pyrene aromatic ring and the substituent Me or Et favoured the *syn* adduct as the exclusive product in terms of C-H/π hydrogen bonding, whereas the fluorine atom or the methoxy group led to a repulsive dipolar interaction with the pyrene ring, justifying the formation of the *anti* adduct as the sole product. Therefore, the selectivity of this reaction is based on a compromise between the attractive (C-H/π) and repulsive (electrostatic, steric) forces.

Nucleophilic addition to a series of ketones **44** has recently been studied by *ab initio* calculations[66] and stabilisation of the transition state geometry by C-H/π interactions vindicated the structure of the preferred product (Figure 35). The relative stability of the rotamers **44a** and **44b** was attributed to the formation of 5- or 6-membered C-H/π bonding (Figure 36).
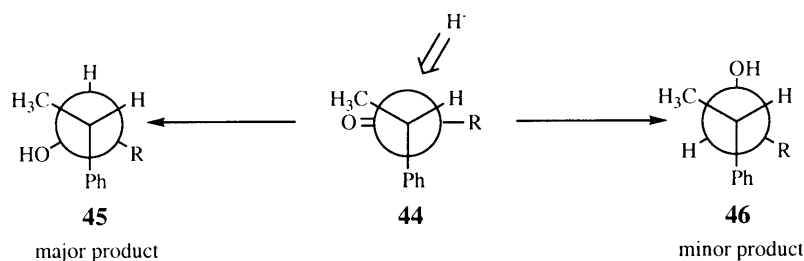
Figure 35 Suggested model for addition of nucleophiles to alkyl 1-phenylethyl ketones **44**
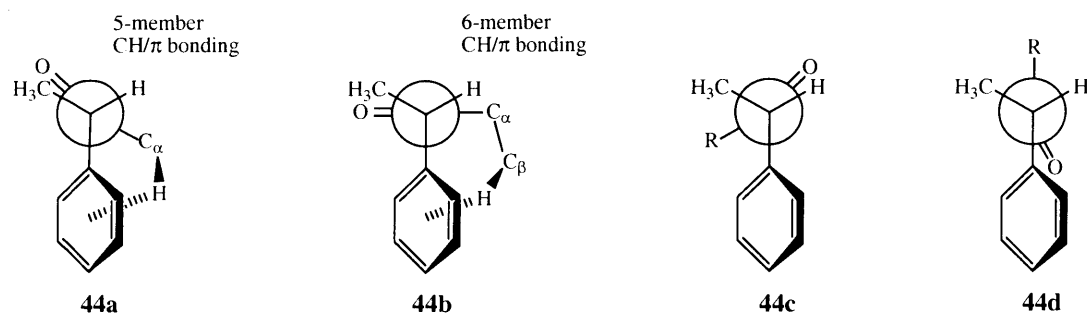
Figure 36 Possible rotamers of alkyl 1-phenylethyl ketones **44** and CH/π hydrogen bonds suggested for rotamers **44a** and **44b**

The abundance of rotamers **44a** and **44b** decreased from R = Me to R = Et and R = *i*-Pr while that of rotamer **44b** increased with the same substitution pattern. However, the rotamer **44d** has not been observed because of the unfavourable electrostatic interaction. The relative abundance of the four rotamers is shown in the Table 4.

R	44a	44b	44c	44d
CH_3	95.9	-	4.1	0.0
C_2H_5	94.3	2.6	3.1	0.0
i-C_3H_7	90.2	8.4	1.4	0.0
t-C_4H_9	-	100.0	0.0	0.0

Table 4 Rotameric abundance (%) of alkyl 1-phenylethyl ketones **44**

The approach of a nucleophile (LiH) to the prevalent conformer (**44b** when R = *t*-C_4H_9, all other cases **44a**) can take place more easily from the less-hindered side of the carbonyl π-face. Therefore, rotamers **44a** and **44b** would lead to the formation of **45** as the predominant product whereas nucleophilic addition to the rotamer **44c** would give a 1:1 mixture of **45** and **46**. Similarly, the origin of the diastereofacial selectivity for the

oxidation of sulfides **47** into sulfoxides **48** was studied by _ab initio_ calculations (Figure 37).[67]
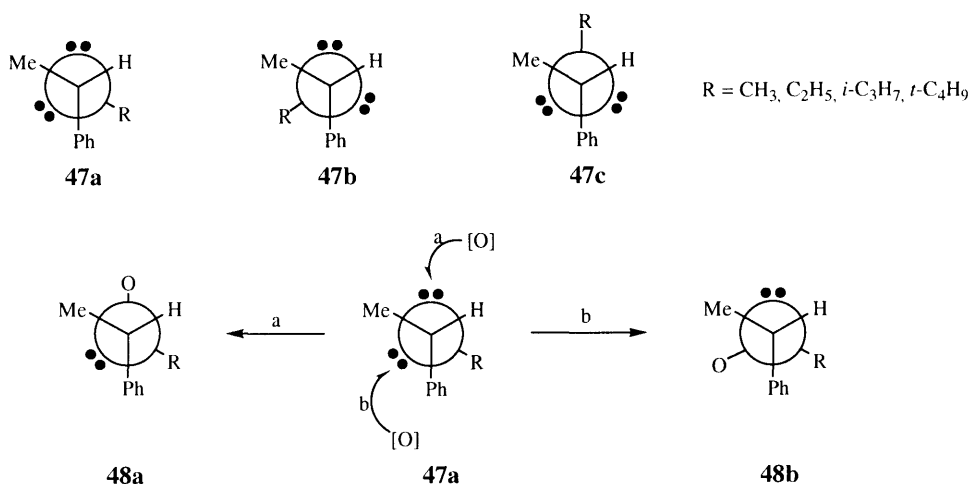
Figure 37 Diastereoselective oxidation of the sulfides **47** into the sulfoxides **48**

The relative abundance of rotamer **47a** was found to be predominant, and oxidation of this rotamer led to the two possible diastereoisomers **48a** and **48b**. A significant preference for the oxidation of the least hindered lone pair occurred, corresponding to the formation of diastereoisomer **47a**. The relative abundance of the rotamers of the sulfides **47** and ratio of the diastereoisomers **48a** and **48b** are reported in Table 5.

	Relative abundance			Product ratio
	47a	**47b**	**47c**	**48a/48b**
CH$_3$	87.9	6.6	5.5	3.1
C$_2$H$_5$	92.4	3.2	4.4	3.2
i-C$_3$H$_7$	95.1	2.3	2.6	3.6
t-C$_4$H$_9$	99.0	0.1	0.9	49.0

Table 5 Relative abundance of rotamers **47a**, **47b** and **47c** of 1-phenyl sulfides **47** and the observed diastereoisomeric ratio of the oxidation products **48a** and **48b**

The above results obtained for nucleophilic attack on the series of ketones **44** highlights the importance of the stabilisation of the transition state geometry by the C-H/π interaction leading to diastereofacial selection to provide the products.

Although the C-H/π interaction can be considered as one of the weakest types of hydrogen bonding, it may well become highly significant in terms of stabilisation after consideration of the additivity of a number of C-H/π interactions occurring in any system is taken into account. With a predominant role in biological, biochemical and chemical processes, this interaction plays a similar role to that of the classical hydrogen bond and must be considered in any molecular modelling programmes. Until now, the potential use of the C-H/π bonding interaction has barely been exploited despite the constant efforts of many research groups. Learning more about this interaction can be thought of as one of the most fascinating challenges in chemistry and biochemistry.

1.3.1.2 – X-H/π Hydrogen bonding involving a π-system as acceptor and an electronegative atom as donor

1.3.1.2.1 – X-H/π Hydrogen bonding in biological systems

Conventional hydrogen bonding interactions, *i.e.* X-H•••A, in which both X and A are very electronegative atoms, is well-established in playing a crucial role in the folding of proteins,[68] protein-ligand recognition, as well as in enzymatic activity.[69] However, weaker hydrogen bonding, and consequently "non-conventional" hydrogen bonding, also contributes a stabilising influence in structural biology. This "non-conventional" hydrogen bonding occurs between a donor X-H, in which X is either an oxygen or nitrogen atom, and the π-cloud of an aromatic system acting as a hydrogen bond acceptor. Each amino acid can be envisaged as a hydrogen bond donor and because of their side chains substituents, some can possess an additional donor centre (Lys, Arg, Asn, Gln, His) thus increasing the probability of N-H/π hydrogen bonding occurring. The first relevant example of N-H/π hydrogen bonding in proteins was shown in the X-ray structure of bovine pancreatic trypsin inhibitor (BPTI).[70] The two faces of the aromatic system of the tyrosine chain interact with two different N-H protons, one π-hydrogen bonding with the glycine amide and the other with asparagine. The short distances H•••π-centre were found to be 3.5 and 3.6 Å and the angles N-H•••π were 4° and 18° respectively. With an extensive study on the X-H/π interaction in 592 high-resolution protein crystal structures,[71] the distance between X and the centre of the aromatic system was estimated at *ca.* 3.4 – 3.8 Å with an X-H•••π angle at *ca.* 8 – 16°, corresponding to a T-shaped geometry. In 1986, the X-ray structure of the

hemoglobin protein complex with a ligand exhibited a similar N-H/π hydrogen bond with the N-H proton of the asparagine chain directed towards the centre of an aromatic ring of the drug.[72] Empirically calculated potential functions suggested that the amide-benzene hydrogen bond was approximately 12.5 kJ.mol^{-1} (3 kcal.mol^{-1}), with the nitrogen-benzene distance between 2.9 and 3.6 Å.[73] More recently, a great number of proteins presenting N-H/π interactions have been studied and recurrent patterns have been observed for side chain π-hydrogen bonds of peptides. Stabilisation of strand edges and helix termini can be governed by interactions between partners far apart in sequence[71] and X-H/π interactions can be envisaged as determining the secondary structure of proteins. Conversely, O-H/π interactions are less ubiquitous in proteins than the N-H analogue but can act in exactly the same manner. The lower number of O-H/π interactions may arise from the ability of the hydroxy group to rotate to find a partner for a conventional hydrogen bonding.[71] However, O-H/π interactions often occur in protein-water complexes and also contribute to the hydration energy.[74] Thus π-interaction with a molecule of water inside hydrophobic cavities may significantly contribute to the stability of the protein structure.[75] Although these interactions are weak alone, in combination, they can play a crucial role in structure stabilisation, drug recognition, DNA recognition or enzymatic action, comparable to conventional hydrogen bonding thus should be considered as a proper hydrogen bond in the determination of the 3D structure of proteins.

1.3.1.2.2 – Solvation of benzene. Physical properties of the X-H/π hydrogen bonding

In section 1.2.1.2, the complexation of two molecules of benzene was investigated in order to rationalise the π-π interactions and their more stable geometries, and consequently, replacing one molecule of benzene by a H-bonding molecule can permit the investigation of the stability of the X-H/benzene complexes and their optimised geometries. Some theoretical and experimental studies on the solvation of benzene with different X-H partners, have been reported.[76] Spectroscopic measurements of water-benzene and ammonia-benzene complexes revealed the position of the X-H donor to be above the benzene plane and indicating that benzene was acting as a proton acceptor.[77,78] There have been many relevant theoretical studies on the solvation of benzene,[78] however, Tsuzuki and his group published fundamental paper on the comparison of the O-H/π, N-H/π and C-H/π

interactions using high level *ab initio* calculations.[79] The geometries of ammonia-benzene, water-benzene and methane-benzene investigated[41] are depicted in Figure 38 and the calculated interaction energies of these geometries, as well as the intermolecular distance R, *i.e.* the distance X•••centre of the ring, are reported in Table 6.
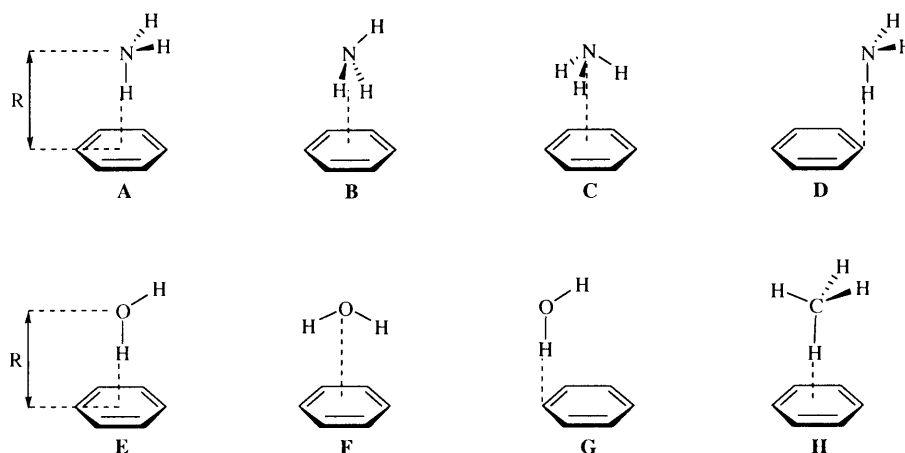
Figure 38 Possible geometries for ammonia-benzene and water-benzene complexes

	ammonia-benzene				water-benzene			methane-benzene
	A	**B**	**C**	**D**	**E**	**F**	**G**	**H**
E_{tot} (kcal.mol^{-1})	-2.22	-2.07	-1.72	-1.84	-3.02	-3.17	-2.77	-1.45
E_{tot} (kJ.mol^{-1})	-9.30	-8.65	-7.19	-7.69	-12.62	-13.25	-11.58	-6.06
R (Å)	3.6	3.6	3.6	3.6	3.4	3.4	3.4	3.8

Table 6 Total energy E_{tot} (kcal.mol^{-1} and kJ.mol^{-1}) of the different ammonia-benzene, water-benzene and methane-benzene complexes and the distance R (Å) between the centre of the benzene ring and the centre atom of the other molecule

The attraction between benzene and either ammonia or water is weaker than that for a conventional hydrogen bond and the interaction energy calculated for the ammonia-benzene complex was approximately 40% that of the hydrogen bond for the water dimer (30% for the methane-benzene complex). Although the monodentate complex **A** is more stable than the bi- and tridentate complexes **B** and **C**, the largest energy difference was only 2.09 kJ.mol^{-1}. Also, the stabilisation energies of these three complexes were similar and these facts could explain the different types of orientations found in the crystals.[80] The authors compared the X-H/π interactions with those of C-H/π system as the same forces govern these interactions: charge transfer was not essential for the attraction and orientation

of the X-H/π interactions and the electrostatic forces were mainly responsible for the magnitude of the total energy E_{tot}. Consequently the order of magnitude of the E_{tot} values agrees with the order of electronegativity of the proton-donating atoms (C < N < O).[77b] Furthermore, the dispersion interaction also plays an important role in the magnitude of the X-H/π interactions, as it does with the C-H/π interactions. In the calculated energies of the water-benzene and ammonia-benzene complexes with a long intermolecular interaction (> 4.0 Å), a substantial attraction of the two partners still persisted, confirming that the driving forces were not short-range interactions, such as charge transfer, but long-range (dispersion and electrostatic). The optimised minimum intermolecular distances for ammonia-benzene, water-benzene and methane-benzene complexes were calculated to be 3.4, 3.6 and 3.8 Å respectively. The difference in intermolecular interactions may arise from the difference in the van der Waals radii of the proton-donating atoms (O: 1.40 Å, N: 1.55 Å, C: 1.75 Å), and from the magnitude of the participating electrostatic forces. Furthermore, the calculated interaction energy of the ammonia-benzene complex in its most stable geometry (geometry **A**, E_{tot} = -9.30 kJ.mol^{-1}) agreed well with the experimental value (-10.20 kJ.mol^{-1}).[81] Under physiological conditions, the side chain of Lys is most often protonated and therefore the attractive interactions are cation/π bonding instead of N-H/π interactions and the properties of the ammonia-benzene complex are not valid anymore (vide infra).

The stabilisation energy of the formamide-benzene complex has been calculated up to be -17 kJ.mol^{-1} (-3 kcal.mol^{-1}) in the gas phase,[82] which is slightly stronger than a π-π interaction and two energetically similar conformations have been found for this complex: the parallel-stacking **A** and the T-shaped geometry **B**, in which an N-H/π interaction occurs (Figure 39).
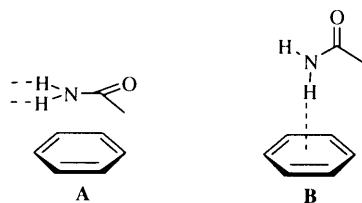
Figure 39   geometries of the formamide-benzene complex
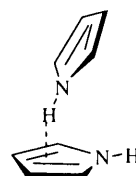
Figure 40   pyrrole dimer

The pyrrole dimer (Figure 40) displays a T-shaped geometry, with an angle of *ca.* 50° between the planes of the aromatic rings and an N-H/π interaction.[83]

The energetically attractive X-H/π hydrogen bond, where X = O, N or S, is weaker than a classical hydrogen bond but stronger than C-H/π bonding. Contraction of the X-H bond is often observed in the π-hydrogen bond and leads to a shift of the X-H stretch to a higher frequency in the IR spectrum. This feature has been described as an anti-hydrogen bond, since the opposite phenomenon, *i.e.* elongation of the X-H bond, is observed in the classical hydrogen bond, which has more recently been renamed as a blue-shifted hydrogen bond.[84]

In their investigation of the X-H/π hydrogen bond using the Cambridge Structural Database, Malone and co-workers found that the commonly depicted T-shaped geometry where the hydrogen is directed towards the centre of the aromatic ring is rarely adopted and that the preferred geometry involves one carbon of the aromatic ring.[80]

X-H/π interactions have also been investigated in crystal structures of 2- and 3-aminophenols Figure 41a and 41b).[85]
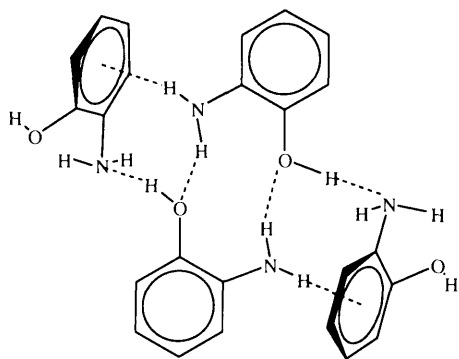
Figure 41a Interactions in the crystal structure of 2-aminophenol
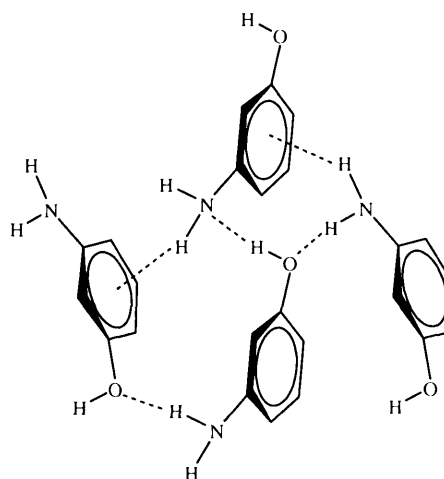
Figure 41b Interactions in the crystal structure of 3-aminophenol

These compounds show an N-H/π interaction and the hydroxy group is engaged in a stronger conventional hydrogen bond with the nitrogen atom as acceptor, agreeing with the rules of Etter[86] which state that the strongest possible hydrogen bond forms between the most powerful donor and acceptor available. Moreover, crystal structure of (S)-2,2,2-trifluoro-1-(9-anthryl)ethanol performed by Rzepa in 1991[87] exhibited two

interesting intermolecular O-H/π interactions which favoured the formation of a dimer in solid state whereas an intermolecular interaction between the hydroxy and the CF_3 groups was expected.[88] Although this interaction generated an unusual O-H•••π angle of 87°, the corresponding distance of 2.3 Å reinforced the presence of an hydrogen bond.

1.3.1.2.3 – X-H/π Hydrogen bond in designed synthetic receptors

Considering the abundance of "non conventional" hydrogen bonding in biological systems, its importance in the stabilisation of the 3D structure of proteins and the extensive number of systems designed to study π-π interactions, few examples of hydrogen bonding to a π-system have been investigated in host-guest recognition. The most relevant work has been reported by Hunter and co-workers with the complexation of a series of six-membered ring 1,4-dicarbonyl systems with cyclophane **49** (Figure 42).[89]
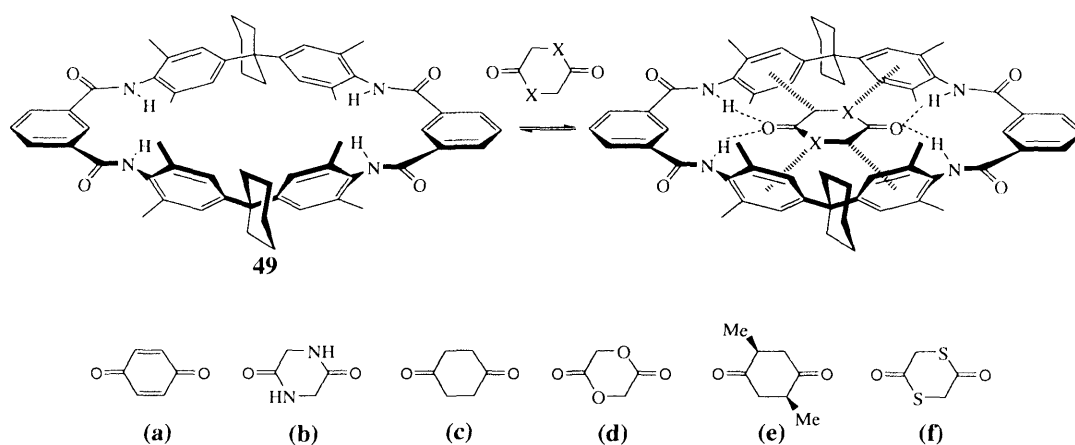
Figure 42   Inclusion complexation of cyclic 1,4-dicarbonyls by the macrocyclic tetramide receptor **49** and potential interactions stabilising the complex

substrate	Association constant (M^{-1})	$\Delta\delta$ complexation for amide NH of **49** (ppm)
(a)	$2.3 \pm 0.4 \times 10^2$	+1.1
(b)	$1.0 \pm 0.5 \times 10^6$	+1.5
(c)	$8.5 \pm 0.4 \times 10^2$	+1.2
(d)	$3.4 \pm 0.6 \times 10^2$	+0.8
(e)	$2.6 \pm 0.4 \times 10^2$	+0.8
(f)	$1.1 \pm 0.2 \times 10^2$	+0.8

Table 7   Association constant (M^{-1}) and ^1H NMR data for complexation by the cyclophane **49**

They studied the association constant of the complexation of **49** with the substrates **(a)-(f)** in chloroform using ^{1}H NMR and the results are reported in the Table 7. From these results, 1,4-cyclohexanedione **(c)** is bound to the receptor by hydrogen bonding between the two carbonyl groups and the four N-H protons, and a similar binding arrangement is observed for the complexation with substrates **(a)**, **(d)**, **(e)** and **(f)**. However, the complex of diamide **(b)** is stabilised by additional N-H/π hydrogen bonds and the crystal structure of this complex[90] clearly shows the N-H protons of **(b)** directed towards the aromatic ring of the cyclophane **49**. Interestingly, the binding forces within this complex are strong enough for it to persist in water $(0.7 \times 10^1 \ M^{-1})$.

The association constant, determined by ^{1}H NMR spectroscopy in chloroform, of the complex between the cyclophane receptor **50** and a serotonin mimic was $4.8 \pm 1.3 \times 10^3 \ M^{-1}$. Furthermore, the complexation induced a significant downfield shift in the signal of the N-H proton of the guest, *ca.* 5.46 ppm, supporting the formation of an N-H/π hydrogen bond between the N-H proton of the guest and the central aromatic ring of the anthracene unit. Because of the stabilising effect of the hydrogen bond between the hydroxy group of the guest and the receptor, the serotonin mimic was assumed to adopt a T-shaped structure towards the anthracene (Figure 43).

50   R = CO$_2$CH$_3$
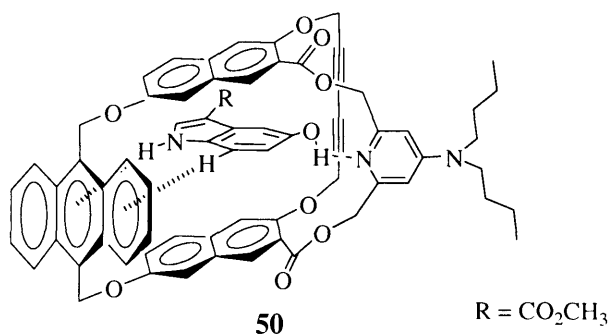
Figure 43   N-H/π interaction in the complex formed between the cyclophane receptor **50** with serotonin mimic

In order to provide some new insights into O-H/π interactions, Nishio *et al.* studied the conformation of alkyl benzyl alcohols **51**[91] for which the three stable rotamers depicted in Figure 44, can be considered to be stabilised by C-H/π and O-H/π interactions.

R = CH₃, C₂H₅, *i*-Pr, *t*-Bu
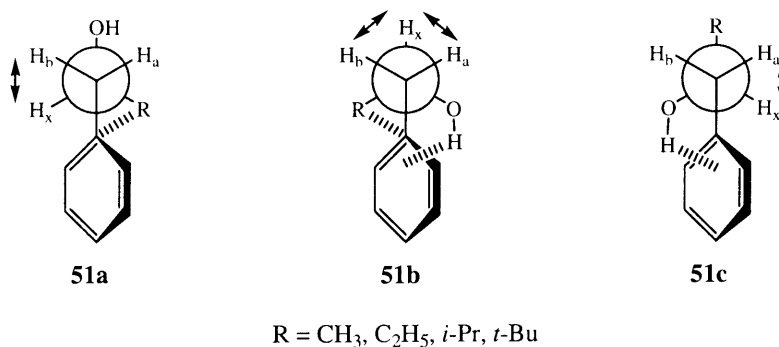
Figure 44   Most stable rotamers of **51** and possible interactions involved

In the rotamers **51a** and **51c**, only one intramolecular π-interaction can occur (C-H/π in **51a** and O-H/π in **51c**), whereas both can occur in rotamer **51b**, although the latter conformer shows two unfavourable H/H interactions. Table 8 shows the relative abundance of the three conformations of **51** estimated by *ab initio* calculations and also as determined by the ratio of NOE enhancements of the protons H_a and H_b when H_x was irradiated.

R	51a		51b		51c	
	Calculated	NMR	Calculated	NMR	Calculated	NMR
CH₃	19.7	25.3	29.0	18.1	51.3	56.6
C₂H₅	17.7	21.7	26.1	17.9	56.2	60.4
i-Pr	12.7	11.1	14.3	17.3	73.0	71.4
t-Bu	1.0	-	0.9	10.6	98.1	89.4

Table 8   Relative abundance (%) of the stable rotamers of **51** calculated by ab initio method and by ¹H NMR experiments

Similarities between the theoretical calculations and experimental results demonstrate the strength of the O-H/π *vs.* C-H/π interactions and the rotamer **51c** is always favoured. However, from the low ratio of rotamer **51b**, the authors argued that intramolecular π-interactions may not be strong enough to compensate for the steric repulsion between the vicinal C-H protons[92]. We believe that the significantly more bulky hydroxy and alkyl functionalities interacting with the phenyl ring led to a crowded conformation, thus

justifying the low ratio of the rotamer **51b**, to a greater extent than the repulsion between protons.

The crystal structures of biological and synthetic molecules, as well as a wide range of host-guest complexes have all given undeniable evidence for the existence of hydrogen bonding towards the aromatic ring, and calculations have provided a theoretical estimation of the binding strengths. From these theoretical values, X-H/π hydrogen bonding (X = O, NR) is weaker than a conventional hydrogen bond yet stronger than a C-H/π interaction. However, no experimental comparison of the relative strengths of O-H/π *vs.* N-H/π interactions has been reported to date.

1.4 – Cation/π interactions

1.4.1 – Cation/π interactions in biological structures

1.4.1.1 – Binding interaction in the side chains of proteins

As previously discussed, the amino groups of the side chain of proteins are often protonated under physiological conditions and can exhibit a stabilising cation/π interaction with an aromatic moiety in close proximity. To a first approximation, cation/π interactions can be considered as an ion-quadrupole interaction between a positively charged group, such as an ammonium cation, and the electron rich π-cloud of an aromatic ring.[93] In an ammonium-aromatic side-chain interaction, the methylene group directly adjacent to the positively charged group of Lys and Arg carries a substantial positive charge and thus contact between this CH_2 and the face of an aromatic is also a cation/π interaction. This geometric interaction is commonly observed in proteins[94] and may be driven either by a cation/π interaction between the CH_2 (δ+) and the π-cloud or by a hydrophobic effect. In an investigation of peptides[95] designed to study in-depth the behaviour of a cation towards an aromatic ring, it was established that the magnitude of the interaction was dependent on the orientation of the cationic and aromatic units and was comparable to a classical hydrogen bond. In an α-helix, the *i*, *i*+4 Trp-Lys pair provided no additional stability to the helix[96] while an *i*, *i*+4 Trp-Arg pair provided -1.7 kJ.mol^{-1} (-0.4 kcal.mol^{-1}).[97] However, the interaction energy of an *i*, *i*+4 Trp-His$^+$ pair was estimated to be -3.3 to 5.0 kJ.mol^{-1} (-0.8 to

-1.2 kcal.mol^{-1}),[98] whereas the neutral Trp-His pairing interaction was 0.4 kcal.mol^{-1} relative to solvation in water. Within proteins, a cation/π interaction can occur between Phe, Tyr or Trp and Lys, Arg or protonated His.[99] In water, their binding energies lie between -1.7 and -10.0 kJ.mol^{-1} (-0.4 and -2.4 kcal.mol^{-1}) but are lower than those predicted theoretically (-13.4 to -15.0 kJ.mol^{-1}).[100] For the aromatic residues, Trp is the most common π-system participating in these interactions with a remarkable 26% of all Trp residues involved in energetically significant cation/π interactions,[101] and theoretical studies have established that it can form the strongest interaction with a cation. Of the cationic amino acids, only Arg and Lys have been well-studied and cation/π interactions involving Arg are more likely to be formed. The difference in geometries between the aromatic ring and Arg or Lys may explain the predominance of Arg interactions. This amino acid preferentially interacts with a π-system in a stacked geometry, hence increasing the hydrophobic contribution but, the interaction between Lys and an aromatic ring does not involve this additional interaction (Figure 45). In many crystals structures,[93] the arginine-aromatic ring complex adopts predominantly the parallel geometry but a few examples shows both geometries, for example in lactoferrin.[102]

Parallel (stacking)	Perpendicular (Hydrogen bonding)	
		Arginine (Arg)
		Tryptophan (Trp)
		Histidine (His)
		Phenylalanine (Phe)
		Lysine (Lys)
		Tyrosine (Tyr)
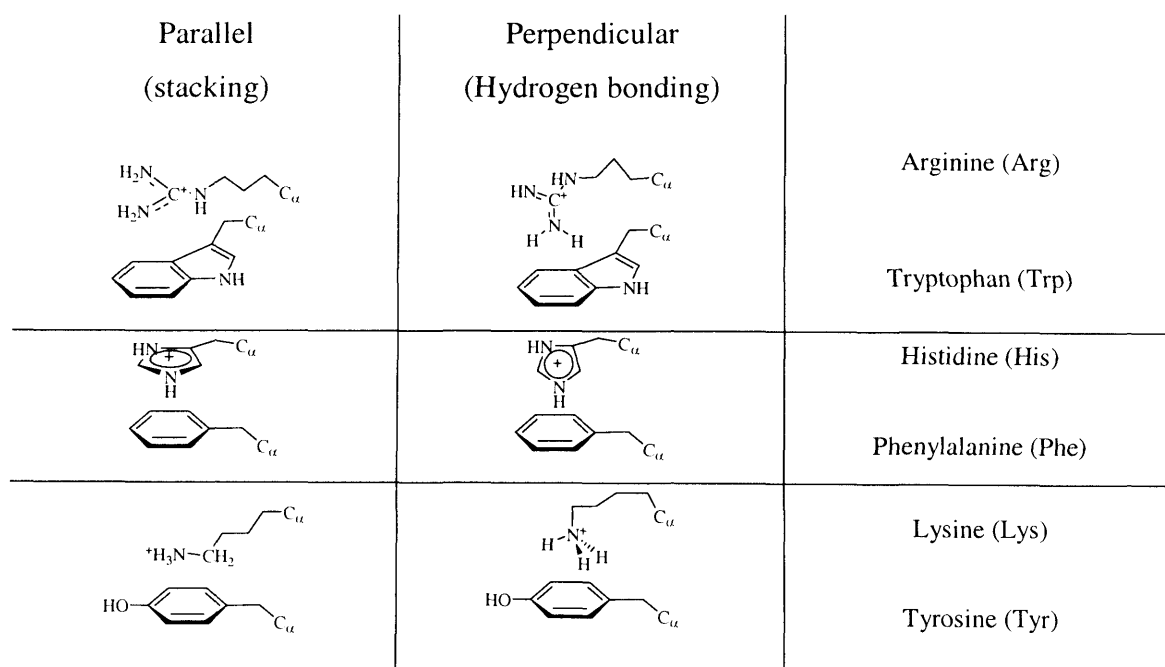
Figure 45 Parallel and T-shaped geometries for Side-chain amino acids involved in cation/π interactions

Interestingly, in the human growth hormone receptor extracellular domain[103] and in human prolactin receptor extracellular domain,[104] several aromatic and cationic side chains from different strands of the protein involving both Lys and Arg, interact to form an extended series of cation-π interactions. In the former example, parallel stacking is the geometry most commonly found and the cation/π interactions work in tandem within the molecule. A systematic study of 17 residue peptides[105] demonstrated that the pH, the distance between the interacting residues and the aromaticity of the Phe residue were critical to the stability of the helix. Furthermore statistics showed that 60% of cation/π interactions in proteins were at least partially solvent-exposed indicating that these interactions play an important role in stabilising the protein on the solvent-exposed surface.[96,97,101,106] The binding energy of the cation/π interaction in proteins can also be enhanced by a mixture of organic/aqueous solvents and Kostic and co-workers[94] studied association constants of protected single amino acids in chloroform/methanol/water mixtures, and found that the Lys-Phe and Lys-Tyr were -14.2 and -12.1 kJ.mol^{-1} respectively (-3.4 and -2.9 kcal.mol^{-1}), whereas these values become -10.0 and -8.78 kJ.mol^{-1} in water (-2.4 and -2.1 kcal.mol^{-1}). Clearly, cation/π interactions are ubiquitous in biological systems and contribute to the stabilisation of the geometry of proteins, both in α-helical structures[107] and in designed β-hairpins.[108]

1.4.1.2 – Binding of Acetylcholine

Acetylcholine esterase hydrolyses acetylcholine (ACh) to choline and acetate, and is viewed as a perfect target for demonstrating the importance of cation/π interactions within biological systems.[109] Prior to the determination of the structure of the esterase, it was assumed that the quaternary ammonium ion of ACh was stabilised by an anionic unit present in the binding site. However, the X-ray structure of the esterase showed that the active site, which was at the bottom of a deep cavity surrounded by 14 aromatic residues, possesses an aromatic Trp residue which could interact with the quaternary ammonium cation of ACh. This Trp was thus crucial in the active site.[93]

Further work established that the protonated buffer molecule **52**, and the Trp of the binding site of ACh-binding protein are stabilised by cation/π interactions and the protonated ammonium centre is surrounded by four aromatic residues which permit a short contact distance between the cation and the Trp residue (4.1 Å) as depicted in Figure 46.[110] Similar

cation/π interactions have been subsequently observed for a large number of nicotinic ACh receptor agonists.[111]
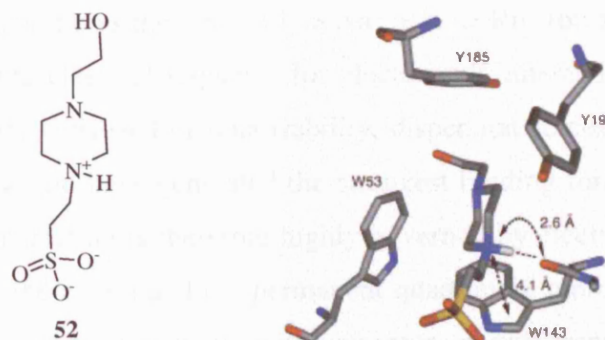
Figure 46 Cation/π interaction between *N*-2-hydroxyethylpiperazine-*N'*-2-ethane sulfonic acid 52 and Trp in the ACh binding site of an ACh-binding protein

1.4.2 – Energetic and geometric features of cation/π interactions

The early gas phase studies of Kebarle[112] revealed that the K^+-water interaction energy was surprisingly weaker than that of the K^+-benzene complex (75 and 79 kJ.mol^{-1} respectively). Subsequently, Meot-Ner[113] established that a more complicated cation could also bind strongly with an aromatic system, as exemplified by the case of the NH_4^+-benzene complex whose binding energy was similar to that of the K^+-benzene complex. Although alkylation of the ammonium cation can decrease the strength of the binding force, the energy of the NMe_4^+-benzene complex was calculated to be 38 kJ.mol^{-1}, and, as such, was comparable with that of the NMe_4^+-water interaction (Table 9)

Cation	Molecule	Experimental binding energy kJ.mol^{-1} (kcal.mol^{-1})	Computational binding energy kJ.mol^{-1} (kcal.mol^{-1})
Li^+	C_6H_6	160.1 (38.3)	183.1 (43.8)
Na^+	C_6H_6	117.0 (28.0)	113.3 (27.1)
K^+	C_6H_6	80.3 (19.2)	62.7 (15.0)
K^+	H_2O	74.8 (17.9)	-
NH_4^+	C_6H_6	80.7 (19.3)	74.8 (17.9)
NMe_4^+	C_6H_6	39.3 (9.4)	42.6 (10.2)

Table 9 Binding energies ΔH in kJ.mol^{-1} (kcal.mol^{-1}) of different complexes estimated by *ab initio* calculations and experimental values under gas-phase conditions

As the theoretical and gas phase results are in agreement, cation/π interactions are generally investigated by computational studies. Comparison of these interactions in alkali metal cation-benzene complexes shows the trend: $Li^+ > Na^+ > K^+ > Rb^+$ (66 kJ.mol^{-1} by *ab initio* calculations) which is the classical sequence for electrostatic interactions. If the cation/π interaction predominantly consisted of polarisability, dispersion forces or charge transfer, the largest cation, Rb^+ would have generated the strongest binding force. Since this is not the case, the cation/π interaction is therefore highly governed by electrostatic attraction of the interaction between the cation and the permanent quadrupole moment associated with the π-system. However, participation of donor-acceptor, charge-transfer and dispersion forces may become significant with a large organic ion as the polarisability could become more important than in the case of Na^+.[114] The optimised geometry of the K^+-benzene complex shows the cation positioned above the benzene along the 6-fold axis and the distance between the centre of the Na^+ cation and that of the benzene ring is estimated at 2.4 Å. *Ab initio* computational studies[115] of the Na^+-π system indicated that the electrostatic interactions between the charged species and the quadrupole moment of the aromatic ring contribute predominantly to the stabilisation of the complex. Moreover, replacing the alkali metal ion by NH_4^+ did not affect the contribution of the electrostatic potential to the total binding energy. Computational calculations of the H_3O^+-benzene complex led to the conclusion that the monodentate complex was the most stable, with a binding energy of -114.5 kJ.mol^{-1} (*vs.* -103.2 kJ.mol^{-1} for the tridentate complex).[116] IR and NMR experiments of the H_3O^+-benzene complex[117] showed that the hydronium cation can bind to aromatic systems in a similar fashion to that of K^+ cation leading the authors to suggest that the electron-rich arene can participate in the biological transport of a proton *via* the complexation of the hydronium ion with π-systems.

1.4.3 – Cation/π interactions in synthetic receptors

As several forces contribute to molecular binding, such as hydrophobic interactions in water, studies of the contribution of a specific interaction are far from trivial and the most convincing evidence for the cation/π interaction arises from systematic studies of a series of analogous molecules. Indeed, a large series of measurements on the complexation of

substrates with a designed receptor in solution can provide some insight into the importance of non-covalent interactions, such as the cation/π interaction.

1.4.3.1 – Host-guest complexation in aqueous solvents

In water, a cation is highly solvated and the binding cavities of the synthetic receptors must therefore compete with solvation to bind the cation tightly. Fortunately however, some synthetic receptors can attract the cation away from the water and into the hydrophobic cavity leading to a strong attractive interaction with the organic cation. The necessity of using water as solvent is to mimic physiological conditions in order to give some insight into biological recognition. To solubilise the receptor in water, a polar group is often inserted, for example a charged functionality, however the cation can also interact with the receptor though conventional electrostatic interaction between charged species and this can complicate the interpretation of the origins of the complexation.

Dougherty and co-workers have performed an extensive study of cation/π interactions with the series of cyclophanes **53** in which the anionic carboxylates enable the species to be soluble in water (Figure 47).

53a

53b R = cyclohexyl
53c R = 2,5-furan
53d R = 2,5-thiophene
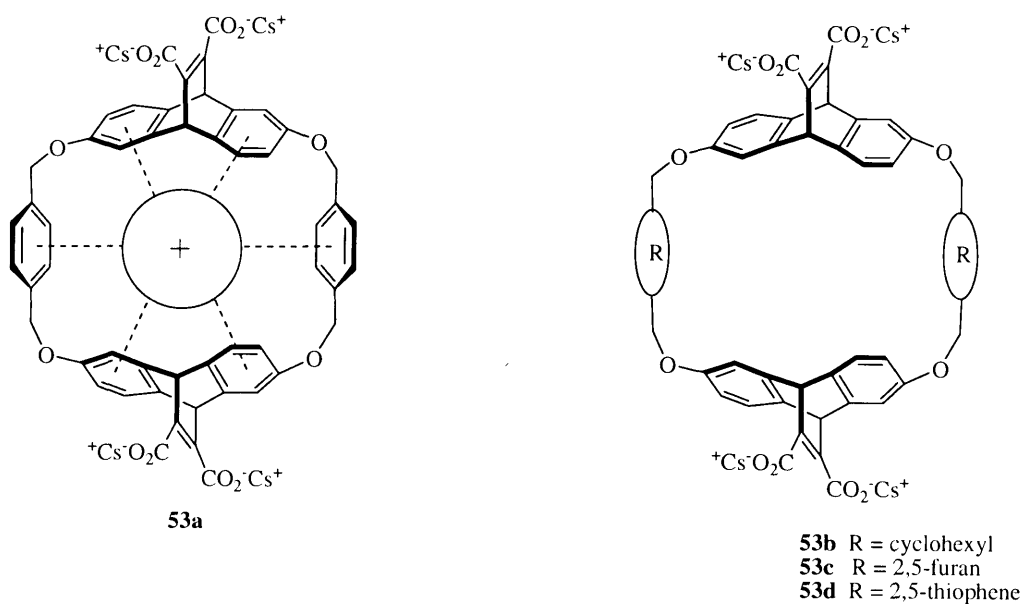
Figure 47 Synthetic receptors used to study the cation/π interactions

Surprisingly, the cyclophane **53a** was found to be a better receptor for quaternary ammonium and iminium ions than for the corresponding neutral molecules.[92,118] Therefore the complex of **53a** with the methylquinolinium cation **54b** was more stable than that with the neutral quinoline **54c** although the cationic substrate was more highly solvated (Table 10). Replacement of the two benzene rings of **53a** by cyclohexyl units, leading to **53b** affected the strength of the interaction and the cation was bound less tightly to **53b** than to **53a**, proving once again that the stabilisation of the cation in the hydrophobic cavity was by electrostatic interactions with the π-systems. Additionally, in the presence of two further electron rich systems, such as furan **53c**) or thiophene (**53d**) replacing the two original benzene rings reduced the binding strength to the quaternary ammonium substrates.[119]
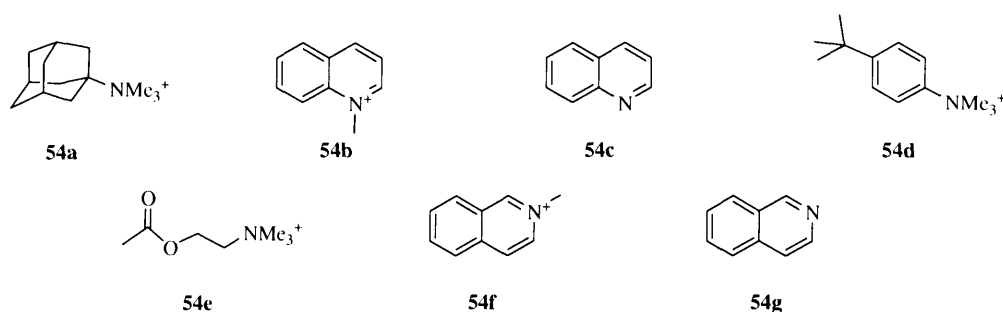
Figure 48   Examples of substrates used for complexation studies with the receptors **53**

In the complexation of the receptor **53a** with the substrate **54d**, the polar group NMe_3^+ is inserted into the hydrophobic cavity of the receptor, not the hydrophobic *t*-butyl group. Binding studies of these receptors with the neurotransmitter Acetylcholine (ACh) **54e** indicated that the magnitude of the association constant K_a ($K_a = 2 \times 10^4$ M^{-1}) was comparable to that of natural ACh receptors (Table 10).[120]

	54a	**54b**	**54c**	**54e**	**54f**	**54g**
-ΔG° kJ.mol^{-1} (kcal.mol^{-1})	28.0 (6.7)	31.8 (7.6)	22.6 (5.4)	24.2 (5.8)	30.1 (7.2)	26.3 (6.3)

Table 10   Free enthalpy of complexation ΔG° for the 1:1 complexes of **53a** in aqueous deuterated borate buffer (pD = 9)

Schneider and co-workers[1d,121] corroborated these observations through an investigation of the binding of the cyclophanes 55 in water The positively charged azacyclophane 55a bound arene and nucleoside molecules more strongly than its saturated analogues and this binding energy was reduced from 4.18 to 5.43 kJ.mol^{-1} (1 to 1.3 kcal.mol^{-1}) on removal of an aromatic unit. Receptors 55b and 55c were also synthesised, when the anionic charge by insertion of benzyl ring was removed from the hydrophobic cavity.
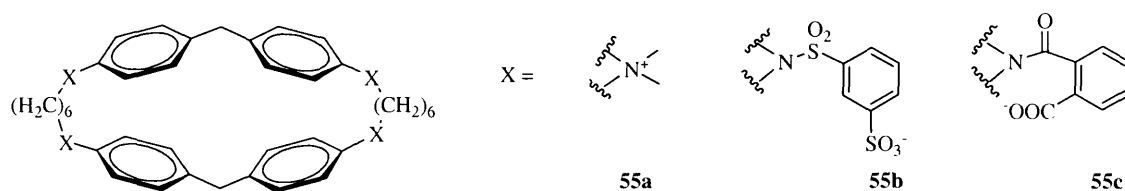
Figure 49 Schneider's synthetic receptors

Neutral aromatic substrates exhibited a stronger binding interaction in the positively charged cavity of the receptor 55a than in the cavities of 55b and 55c. However, similar affinities between aliphatic substrates and the three receptors 55 indicated that hydrophobic interactions could be the driving force for complex formation. Further experiments were performed with these receptors to quantify the cation/π interaction and Schneider's group proved that the binding energy was proportional to the number of aromatic rings surrounding the cationic centre, i.e. the free energy increased with the number of phenyl rings involved, and that each cation/π interaction contributed up to -2.1 kJ.mol^{-1} (-0.5 kcal.mol^{-1}) of binding energy per phenyl ring.

Schwabacher[122] also studied the complexation of charged cyclophanes 56a and 56b, which have a similar structure but oppositely charged cavity with the idea that comparison of the binding magnitude of the same substrate with these two receptors would provide some valuable insights into the cation/π interaction.

56a X = P(CH₃)₂⁺
56b X = PO₂⁻

57a R = H, X = SO₃⁻
57b R = CH₂CO₂H, X = SO₃⁻
57c R = CH₂CO₂H, X = H

58
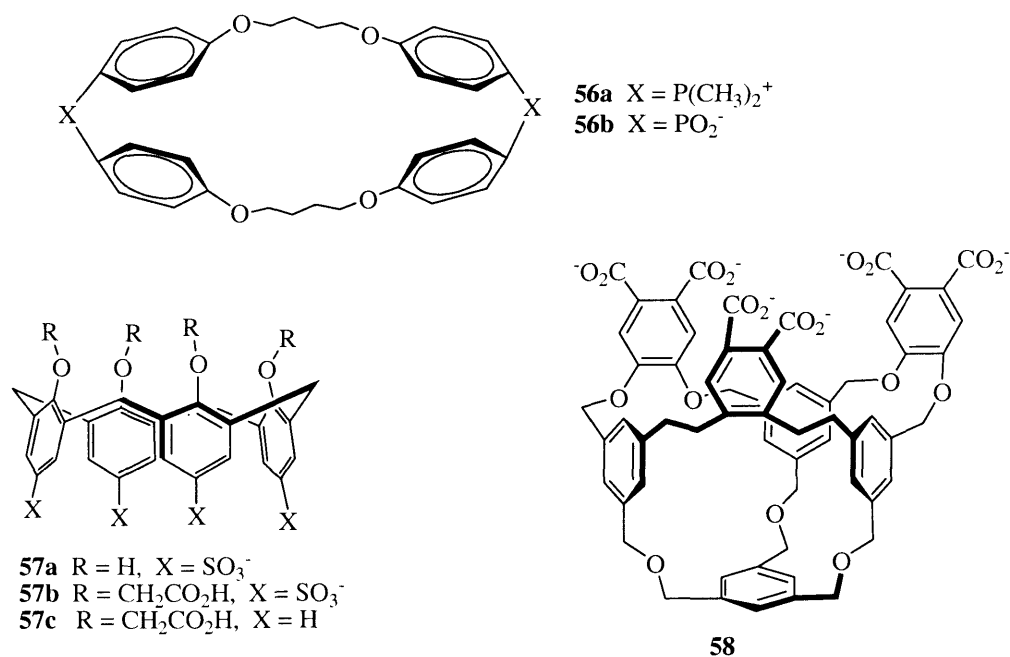
Figure 50 Representation of several synthetic receptors. The cavity of the receptor **56a** is positively charged, whereas the binding cavity of **56b** is negative.

Unlike the cyclophane receptor **55a** where the charged units were introduced to solubilise the receptor in water and were positioned far away from the binding cavity, the charge in the receptors **56** are adjacent to the binding cavity in order to study their participation in the complexation of aromatic substrates. From these studies, the authors found a stronger binding interaction between naphthalene and the cationic receptor **56a** than that for the receptor **56b**, demonstrating once again the participation of the cation/π interaction in stabilisation of the complex.

Additional studies of host-guest complexes in water led to the synthesis of new receptors, such as **57** and **58**, which have been shown to be the most efficient receptors for ammonium and iminium cations to date, and several reviews are dedicated to the investigations of their properties.[123] Under slightly acidic conditions, the phenyl groups of the calix[4]arene **57a**[124] are bound with a trimethylanilinium substrate and on increasing the pH, the phenolic groups are ionized with the receptor becoming much more electron-rich, inducing a stronger cation/π interaction, which can overcome the hydrophobic interaction that dominates complexation at low pH.

As several X-ray structures of proteins display a carboxylate group close to the face of the aromatic ring, Smithrud[125] mimicked this observation with his receptors **59** (Figure 51). From his studies, Arg and Lys derivatives are bound to the receptor **59a** in water ($\Delta G° = -5.02$ to -6.27 kJ.mol^{-1}) while no binding is observed on the aromatic surface of **59b**, highlighting the role of the aromatic ring in the stabilisation of a salt bridge.
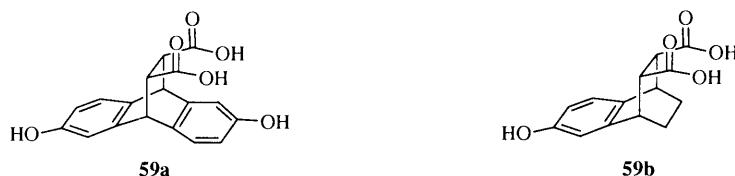
Figure 51 Smithrud's synthetic receptors to demonstrate the role of the aromatic system in molecular recognition

Diederich and co-workers[126] designed the tricyclic inhibitors **60** to bind in the ᴅ-pocket of thrombin as a Trp lies at the bottom of this hydrophobic pocket as depicted in Figure 52.

Figure 52 Schematic representation of the binding mode of the designed inhibitor ±-**60a** in the active site of thrombin and structure of the *tert*-butyl analogue **60b**

Protein crystallography indicated that there was a cation/π interaction between the ammonium tail of the inhibitor **60a** and the Trp215 aromatic residue. Replacing the
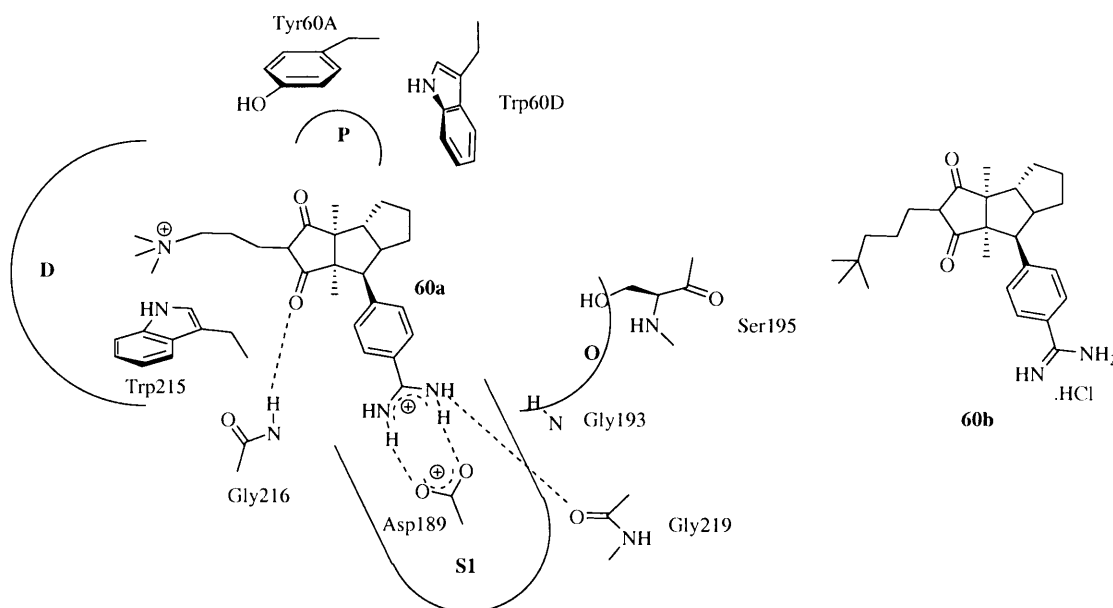
tert-butyl derivative **60b** with the ammonium derivative **60a**, the free enthalpy energy increased by 11.7 kJ.mol^{-1} ($2.8 \text{ kcal.mol}^{-1}$) because of cation/$\pi$ interaction.

Recently, studies of cation/π interactions in aqueous solution involving cationic amino acids in proteins have attracted attention.[127] For example, Schrader and co-workers designed amino-acid receptors to study the binding interactions of Lys, His and Arg,[128] adrenaline,[129] and small peptides[130] *via*. ion-pairing and cation/π interactions (Figure 53).
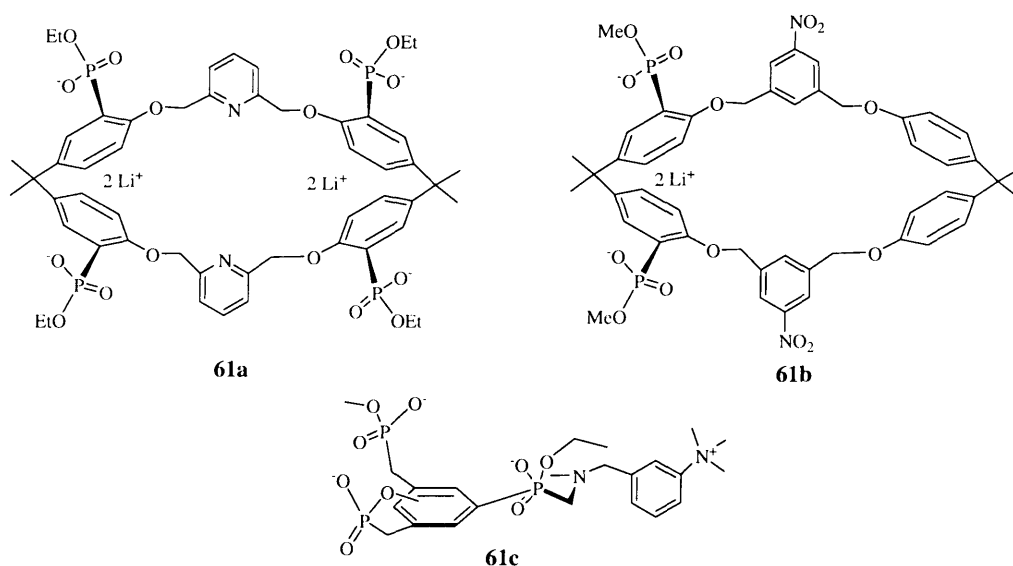
Figure 53   Amino-acid receptors **61a**, **61b** and **61c** for amino-acids, adrenaline and small peptides respectively

Additionally, many novel receptors have recently been designed for selective a cation binding.[131] Thus, all of the receptors investigated have brought to light the importance of the cation/π interaction in the stabilisation of the structure of proteins and demonstrated that this interaction is viable in aqueous solution.

1.4.3.2 – Host-guest complexation in organic solvents

An aqueous solution requires the presence of hydrophilic functional groups in the receptor to provide solubilisation of the receptor, and therefore, necessitates a contribution from Coulombic interactions which can interfere with cation/π interactions. Moreover, the association energy must be greater than the solvation penalty caused by the complexation of the substrate. Therefore, organic solvents are a good alternative to use in order to

eliminate the importance of the hydrophobic driving force that can dominate attraction in aqueous solution.

NMR studies of the neutral calix[4]arene **57c** (Figure 50) in organic solvents indicated that the positively charged part of trimethyloctylammonium was bound in the cavity.[124a]

63a R = CH$_2$CO$_2$H
63b R = CH$_3$

62
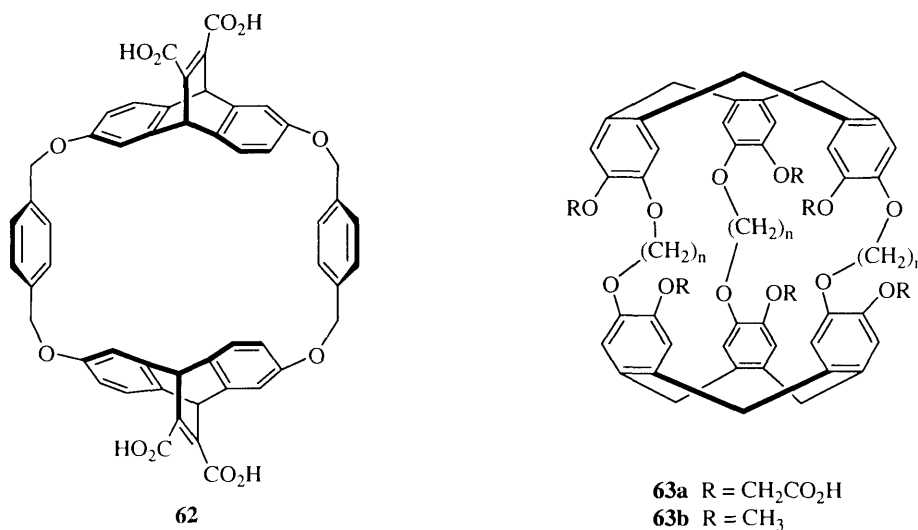
Figure 54 Receptors for studies in organic solvents

However, NMR experiments in chloroform on the receptor **62**,[118] (Figure 54) which is a neutral analogue of **53a**, revealed the ability of **62** to bind positively charged substrates, such as the adamantyltrimethylammonium cation **54a**, however no complexation was observed with neutral hosts such as quinoline and isoquinoline. The free energy enthalpies $\Delta G°$ of the complexes of ammonium cations and the receptor **62** lie in the range of 8.4-12.5 kJ.mol^{-1} (2-3 kcal.mol^{-1}) and these important results show the crucial role of the positive charge and the stabilisation of the complex by CH/π interactions. Using cryptophane **63b**, Collet[132] established the unprecedented complexation of the NMe$_4^+$ cation in (CDCl$_2$)$_2$ with an association constant K_a of 2.25 x 10^5 M^{-1}, which corresponds to a $\Delta G°$ value of -30.9 kJ.mol^{-1} (-7.4 kcal.mol^{-1}). In solution, this is larger than that of the NMe$_4^+$-benzene complex as calculated by gas-phase experiments ($\Delta G° = $ -14.6 kJ.mol^{-1}). Strong binding interactions have also been observed between the receptor **63a** (with n = 3) and choline, acetylcholine, and various quaternary ammonium ions, but these were weaker than those obtained with a larger cavity (with n = 5), thereby demonstrating that a loose association was preferred over a tight fitting.[132]

Closed and open cyclophane receptors, **64a** and **64b** respectively,[133] have been used to complex with NMe_4^+ (tetramethylammonium picrate TMAP) or ACh (acetylcholine picrate AChP), and both receptors gave similar association constants with both picrate salts (Table 11).

64a   **64b**

65a R = H
65b R = Me
65c R = Ts
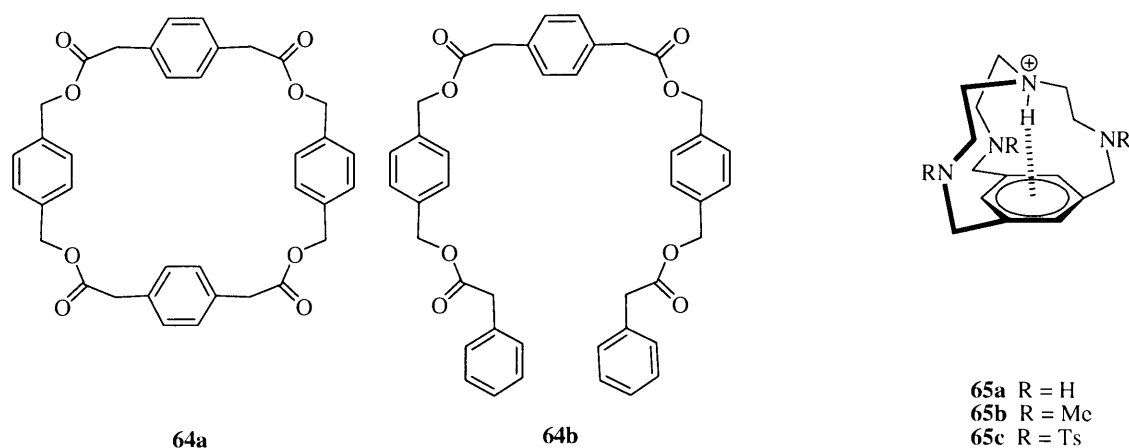
Figure 55   Structures of the close-chain and open-chain receptor **64a** and **64b** and the protonated azaphane **65** which exhibits a cation/π interaction

	TMAP		AChP	
	K_a (M^{-1})	$\Delta G°$ kJ.mol^{-1} (kcal.mol^{-1})	K_a (M^{-1})	$\Delta G°$ kJ.mol^{-1} (kcal.mol^{-1})
64a	29.7	-8.36 (-2.00)	13.1	-6.31 (-1.51)
64b	17.0	-6.98 (-1.67)	17.6	-7.06 (-1.69)

Table 11   Association constants K_a (M^{-1}) in CDCl$_3$ and free energies of binding $\Delta G°$ (kJ.mol^{-1} and kcal.mol^{-1}) for the 1:1 complexes of TMAP and AChP with cyclic and open-chain esters

Thus, Roelens and his group argued that the cation/π interaction was a sizable attractive force even without a preorganised structure of the receptor, which contradicts the rules established by Etter, emphasizing the importance of a preorganised structure for a better molecular recognition.[26] Furthermore, by comparison of the association constants of further analogous receptors in which the number of aromatic rings was variable, they established that the free energy increased per additional aromatic ring. The cavity of the azaphane **65**[134] is much too small to bind to alkali cations but is suitable for the inclusion of a proton. Its structure has been designed such that the lone pair of the nitrogen atom is directed towards the central cavity and the X-ray crystal structure of protonated **65a** revealed a distance of 2.13 Å between the proton and the benzene ring. This is in fact less than the sum of the van

der Waals radii of H and C. The N-π distance of protonated **65a** was measured to be 2.97 Å whereas the same distance in the neutral derivative was calculated to be 3.01 Å. Thus, protonation of the **65a** leads to a constriction of the cavity due to the formation of a NH^+/π interaction.

Host-guest complexation in organic solution is accordingly an active research area for probing the importance of cation/π interactions and cyclophanes,[135] crown ethers,[136] cyclic peptides[137] and other calix[4]arenes[138] have all been designed as cation receptors. Comparison of the experimental results obtained from these synthetic receptors with those from advanced computational studies highlight the complexity of this interaction.

1.5 – Conclusions and perspectives

Over the last thirty years, supramolecular chemistry, crystallographic databases, gas-phase studies and theoretical investigations have all combined to enhance our knowledge of non-covalent aromatic interactions and highlight their importance in biology. Research on such aromatic interactions has indicated that the aromatic ring can behave as a hydrogen bond acceptor, although weaker than the classical hydrogen bond, and furthermore, that electrostatic forces are the predominant interactions which govern aromatic interactions. Although the aromatic ring has a large contact surface, thereby increasing van der Waals interactions and the desolvation penalty, this large surface enables several interactions to occur with one aromatic ring, and this fact must be taken into account when estimating the total binding energy. A detailed understanding of these interactions and the development of the general rules for the behaviour of aromatic systems have yet to be established. However, with increasing interest in this area, an understanding of aromatic interactions may lead to the introduction of powerful computer models for accurate prediction of models in drug design and molecular recognition.

Although well documented, π-π interactions still attract interest, in order to optimise the geometry of the edge-to-face and parallel-displaced stackings, and also to provide more accurate energy models. By way of contrast, X-H/π interactions are less investigated. Cation/π interactions are also well documented due to their importance in biological systems but, additional aromatic interactions still present a challenge for chemists, biologists and physicists as they cannot be accurately measured. Furthermore, since

solvation plays a vital role in complex formation within biological and chemical systems but is not fully understood, much research remains to be done in this area.

Many synthetic systems have been designed to investigate the magnitude of aromatic interactions but straightforward comparison of different aromatic interactions remains problematic. For example, comparison of the O-H/π and N-H/π interactions has never been experimentally performed on the same synthetic system due to the difficulty of changing one parameter without modifying the complete system. Varying distances and angles in these systems would affect the aromatic interactions, and therefore a synthetic model molecule is required to rationalise the relative strengths of these different aromatic interactions in comparable systems.

CHAPTER 2

RESULTS AND DISCUSSION

2.1 – Objectives

As we have hopefully gathered from the foregoing introduction, although considerable research efforts have been devoted towards studying non-covalent interactions involving an aromatic system, there have been relatively few studies to quantify these phenomena in terms of functional group-arene interactions due to the difficulty in measuring such small energies. This objective was accordingly the focus of our own work. In a previous study within our group,[139] a system was designed in which such weak interactions can be quantified by a dynamic NMR study of conformational equilibria. Thus, the propanoanthracene skeleton **66** was selected to examine through space π-interactions with various functional groups (Scheme 2).
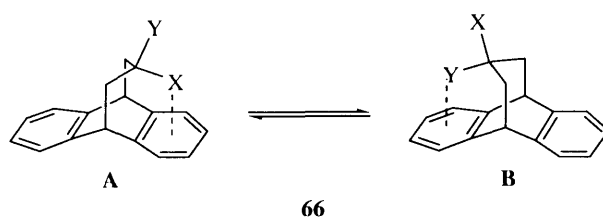
Scheme 2 Conformational equilibrium of the propanoanthracene **66**

This framework consists of a rigid structure containing two independent aromatic systems and a flexible three-membered ring bridge, whose central carbon atom can possess two different functional groups X and Y. The flexibility of the bridge can place either of these substituents in proximity to the centres of one of the aromatic rings, thus leading to through space interactions which are large enough to be measured. As different substituents will affect the conformational equilibrium between **A** and **B**, the relative abundance of each conformer in solution provides a measure of the relative interaction energies. Thus, the propanoanthracene skeleton can be envisaged as a conformational balance to compare the relative strengths of the interactions between aromatic rings and functional groups. However, when X = Y = CH_2 are formally joined to form a cyclopropane unit, this molecule is perfectly symmetrical and hence was used as our standard since any interactions between the aromatic ring and either of the substituents will be identical.

The conformational equilibria of this system can be quantified using NMR spectroscopy. Experiments at low temperature will reduce the conformational motion of the flexible bridge and thus allow a measurement of which conformer is preferred. The proportion of each conformer in solution can be calculated using the coupling constants between the protons on the bridge (Scheme 3).
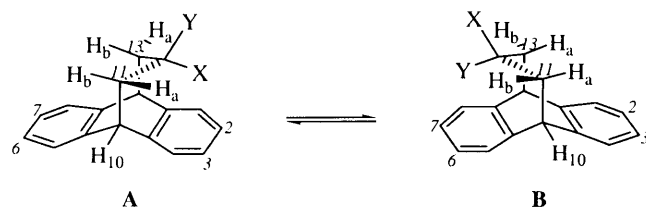
Scheme 3 Detailed structure of the propanoanthracene **66**

Thus, the coupling constants between H_{10} and H_{11a} and those between H_{10} and H_{11b} are characteristic of each conformer. The conformational equilibrium can be calculated from the observed coupling constants, which will lie between that of the theoretical 100% conformer **A** and that of the theoretical 100% conformer **B**, depending on the extent of the equilibrium. Additionally, and of great significance for our work, is that the conformational ratio of **A** and **B** is expected to be highly sensitive to the effects of solvent and temperature and these dependences could be investigated in the evaluation of the coupling constants.

With a suitable framework for the study of weak interactions between functional groups and aromatic systems in hand, we then turned our attention towards an appropriate starting material, which could be easily functionalised in order to develop a diverse array of geminally substituted compounds. We decided to utilise the known symmetrical aromatic ketone **67**, as the carbonyl moiety could be readily elaborated to give a range of derivatives with the essential three-membered propano bridge in place (Scheme 4).
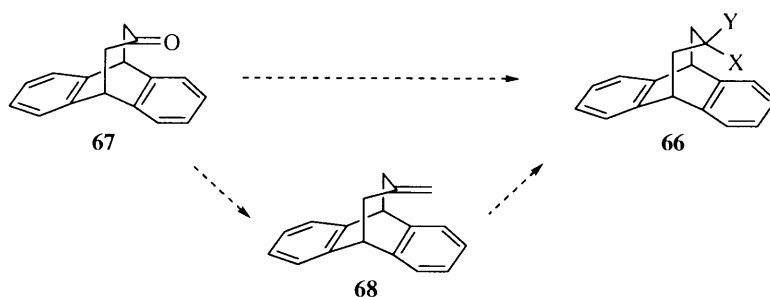
Scheme 4

In addition to the ketone **67**, access to the alkene **68** was also considered to be of value in expanding the range of available derivatives.

2.2 – Synthesis of propanoanthracenes

2.2.1. - Ketone 67

Ketone **67** was originally synthesised by Hoffmann and Karama[140] by the two-step route shown in Scheme 5. In the first step, tetrabromoacetone[141] was prepared by the reaction of bromine, hydrobromic acid and acetone in the absence of light for ten days. Subsequent reaction of tetrabromoacetone with anthracene in the presence of a zinc/copper couple in dioxane at 80 °C led to the cycloaddition product **67** in 22% yield. In this reaction, the intermediate oxoallyl carbocation **69** underwent a [4+3] cycloaddition with anthracene to afford **70**, which was reduced *in situ* to give the desired ketone **67**. However our initial attempts using this method[139] yielded the expected compound **67** in a low yield of 3% with a significant amount of polymeric material being formed, and final purification of the ketone was far from trivial.
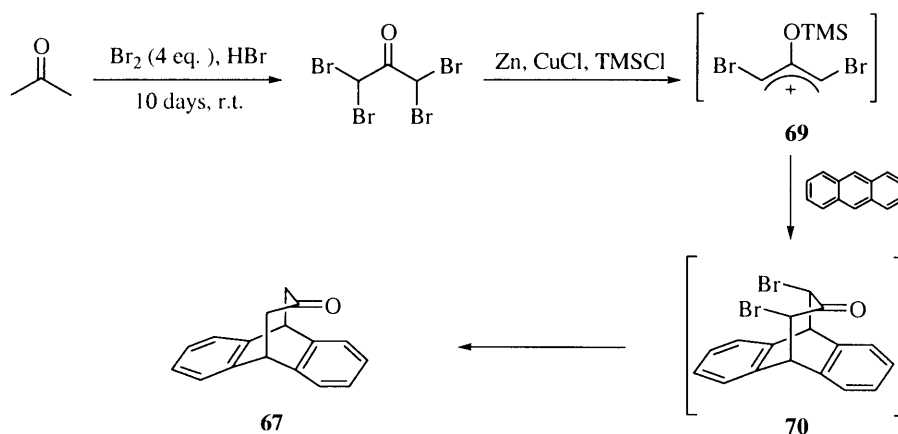
Scheme 5 First synthetic pathway for the ketone **67** developed by Hoffmann and Karama

Thus, Motherwell and Nic[139] developed a synthetic route to **67** incorporating a base-induced rearrangement of α-bromoaldehyde **72**, into α-hydroxyketone **73**, based on a similar reaction of 1-bromo-1-formyl-bicyclo[2,2,2]octane[142] by Corey. The use of potassium hydroxide as the base and THF as the solvent resulted in the highest yield and

purity of **73**. The α-bromoaldehyde **72**[143] was synthesised by the Diels-Alder reaction of 2-bromopropenal and anthracene, and was subsequently treated with potassium hydroxide in THF, presumably to generate *in situ* 9,10-dihydro-11-formyl-11-hydroxy-9,10-ethanoanthracene, which then underwent spontaneous rearrangement to α-hydroxyketone **73**. Deoxygenation of **73** with samarium diiodide then gave the desired compound **67** (Scheme 6).
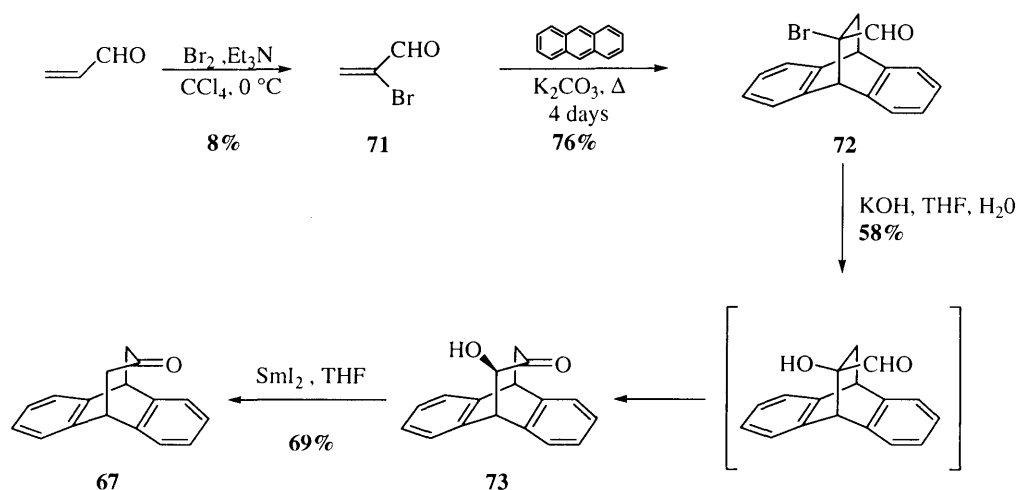
Scheme 6 Synthetic pathway for the ketone **67** developed by Motherwell and Nic

Whilst this route clearly provided access to the ketone **67**, the isolation and purification of dienophile **71** proved troublesome and it was only obtained in approximately 10% yield due to its inherent instability. The subsequent Diels-Alder reaction was therefore carried out immediately after distillation.

As bromination of acrolein was the most problematic step, a new route to the α-bromoaldehyde obviating the need for the preparation of 2-bromopropenal **71** was accordingly developed. In the event, though the simple expedient of carrying out the Diels-Alder reaction between acrolein and anthracene as the first step followed by bromination of the cycloadduct, the desired compound was routinely produced in good overall yield.

Aldehyde **74** was initially synthesised following the procedure of Weiss and Rush[144] using a sealed tube heated at 180 °C for 2.5 hours. Thus, the Diels-Alder adduct **74** was isolated in very good yield (Scheme 7).
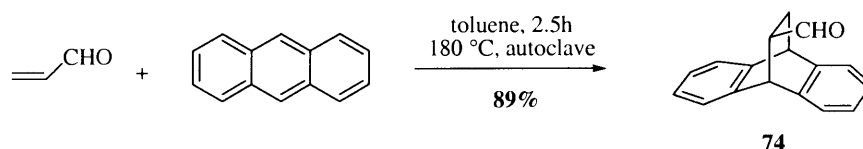
Scheme 7

Since microwave irradiation is an efficient alternative for conventional heating in cycloaddition reactions and, in particular, for Diels-Alder reactions,[145] we were, of course, attracted to this possibility. However, the use of polar solvents is crucial for effective microwave heating and the original thermal cycloaddition reaction was carried out in non-polar toluene. Due to the poor solubility of anthracene in polar solvents, the use of a solvent mixture capable of solubilising the starting material while still able to absorb microwave irradiation was investigated. The highest reaction temperature was reached when using a 1:4 mixture of acetonitrile in toluene. Although a short reaction time was expected using microwave heating, complete conversion required a temperature of 165 °C for 90 minutes in order to provide **74** in virtually quantitative yield (Scheme 8).

Subsequent bromination of the aldehyde **74** using bromine in either CH$_2$Cl$_2$ at room temperature[146] or in dioxane at -5 °C[147] gave the α-bromoaldehyde **72** in very good yield. This indicated that that dioxane had no obvious deleterious or positive effect on the bromination and as a result, CH$_2$Cl$_2$ was chosen as the more efficient solvent for this reaction (Scheme 8).
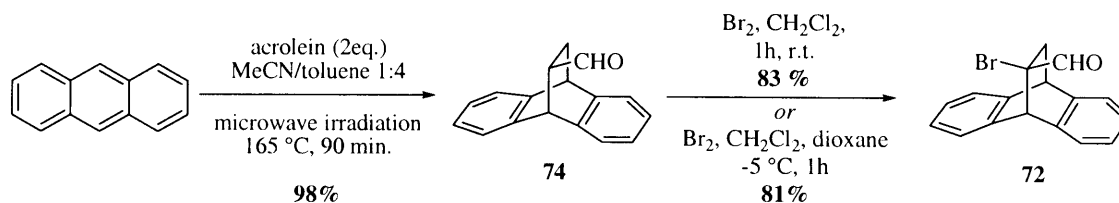
Scheme 8

α-Bromoaldehyde **72** was converted into α-hydroxyketone **73** following the procedure previously developed within the group (Scheme 6). Interestingly, in addition to **73**, the rearrangement step provided the byproduct **75**. Initially, we considered that **73** and **75** were in equilibrium, an equilibrium similar to that seen in the Amidori rearrangement, which occurs for α-hydroxyketones as shown in Scheme 9.
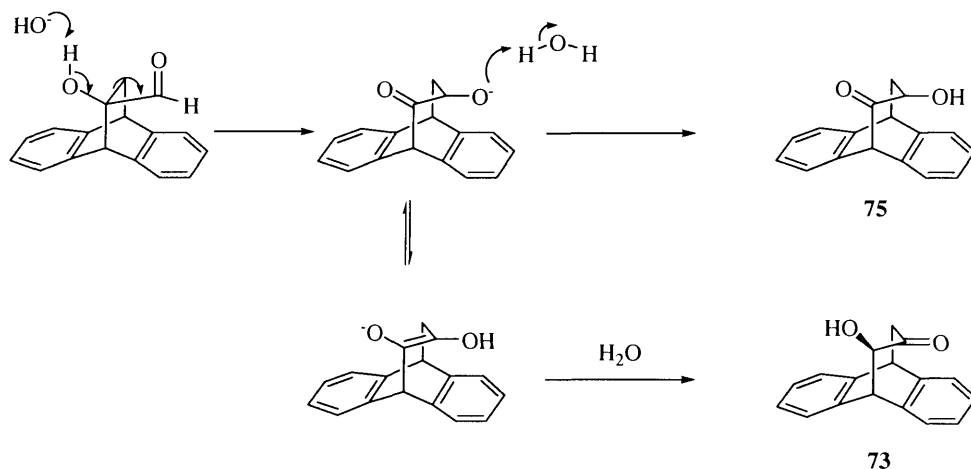
Scheme 9 First supposed mechanism for the formation of **73** and **75**

Although this mechanism would indicate that the equilibrium could be shifted in favour of the formation of **73**, all of our attempts to isomerise the byproduct **75**, using MgSO$_4$, Amberlyst 15 or KOH, failed. Alternatively, the following mechanism would account for the formation of both regioisomers, and also explain the failure of our attempted isomerisations (Scheme 10).
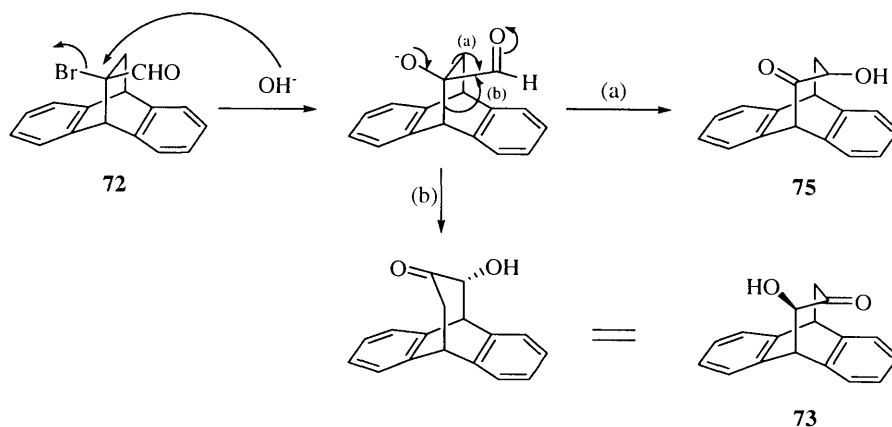
Scheme 10 Supposed mechanism for the formation of the two α-hydroxyketones **73** and **75**

As demonstrated in Scheme 10, initial displacement of Br⁻ by OH⁻ leads to the possibility of either of two groups migrating. Pathway (a) leads to the formation of **75** while **73** is obtained via pathway (b). Compound **73** was isolated as the major product possibly as a consequence of the operation of strain effects which should favour location of the sp^2 carbonyl carbon on the central atom of the bridge. The yield of this reaction is limited by the formation **75**.
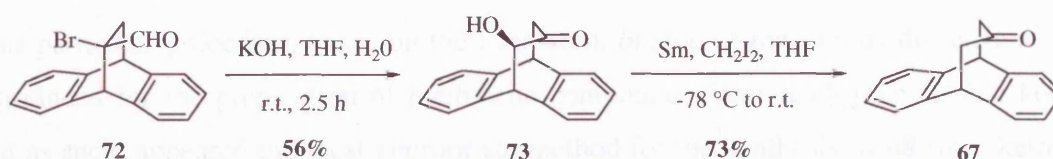
Scheme 11

Finally, the sequential electron transfer based reduction of **73** using freshly prepared samarium diiodide afforded the expected ketone **67** in good yield (Scheme 11). This modified and more efficient route allowed us to synthesise the key compound **67** with its structure confirmed by X-Ray studies, in 31% overall yield.
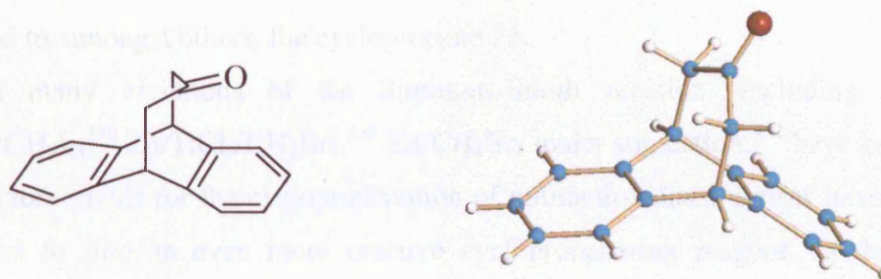
Figure 56   X-Ray structure of the ketone **67**

2.2.2 – Synthesis of alkene 68 and its cyclopropane analogue 76

In order to access alkene **68** from our ketone **67**, a number of possible methods for exomethylenation was explored. For example, the method of Oshima and co-workers for methylenation, converted the cyclic ketone **77** into the alkene **78** using a dihalogenomethane, zinc and titanium tetrachloride (Scheme 12).[148]
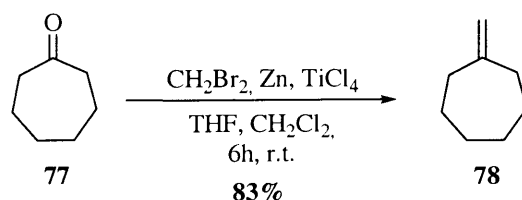
Scheme 12

This particular procedure, based on the formation, *in situ,* of the Lombardo reagent[149] was introduced for the preparation of methylene compounds from readily enolisable ketones, and as such, appeared the most appropriate method for the synthesis of **68** from ketone **67** (Scheme 13).
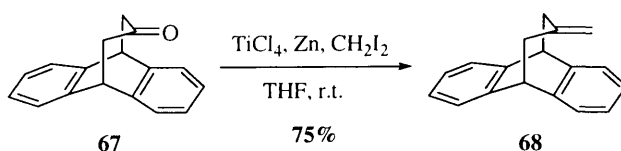
Scheme 13

The alkene **68** allowed us to expand the series of required derivatives and was the precursor compound to, amongst others, the cyclopropane **76**.

Although many variations of the Simmons-Smith reaction, including the use of $Zn/CuCl/CH_2I_2$,[150] $Zn/TiCl_4/CH_2Br_2$,[151] Zn/CH_2Br_2 under sonication,[152] have been reported, unsatisfactory yields for the cyclopropanation of unfunctionalised olefins have encouraged researchers to find an even more reactive cyclopropanating reagent. In the event, the Furukawa modification, namely treatment of Et_2Zn with CH_2I_2, proved to be the most convenient method for cyclopropanation of alkene **68**.[153] The progress of the reaction could not be followed by chromatography since the starting material and the cyclopropane have the same R_f. However, on quenching the reaction after 2 days at room temperature, complete conversion of alkene **68** to cyclopropane **76** was achieved (Scheme 14).

Scheme 14

= 80 =
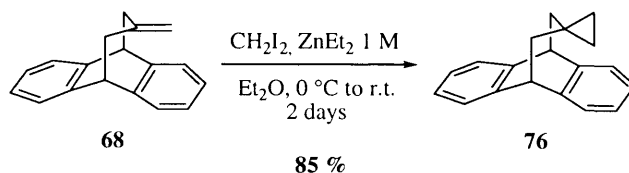
The signal of the protons of the cyclopropane unit appeared as a singlet at -0.15 ppm in the ^{1}H NMR spectrum, highlighting the symmetry of the entire molecule and the equivalence of conformers **A** and **B**. Thus, conformational equilibria results of the motion of the bridge will not be affected by functional groups interacting with the aromatic rings and this derivative can be a standard for our studies upon the conformational equilibria.

2.2.3 – Synthesis of propanoanthracenes

With a suitable route to the desired ketone **67** and the alkene **68** now established, the preparation of the functionalised derivatives required for our studies was then pursued.

Our designed conformational balance was expected to be highly sensitive to small differences in the interaction energy between the aromatic system and the various functional groups but would also be affected by the steric bulk of the substituents. In this respect, it is relevant to note that the distance d between the functional group Y and the aromatic quaternary carbon varies from 2.8 Å (for Y = F) to 3.2 Å (for Y = S) (Figure 57). This distance is sufficiently close to the sum of the van der Waals radii of the aromatic carbons and the appropriate atoms to make the results of value for other systems.
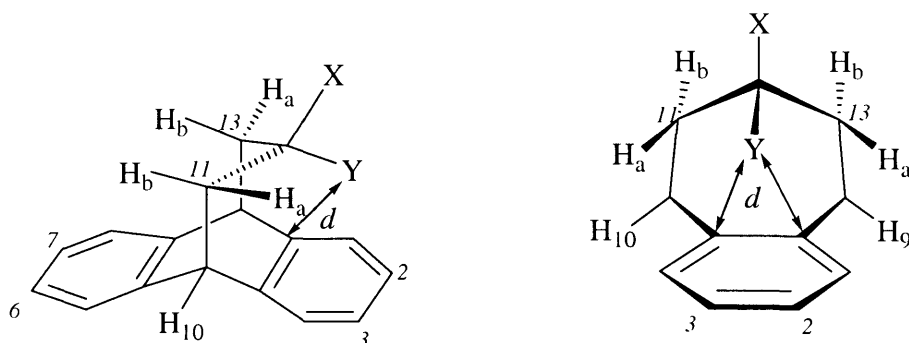
Figure 57   Distance d between the functional group Y and the aromatic quaternary carbon

As we have seen in the introductory review, formation of O-H/π hydrogen bonding between a hydroxy group and an aromatic system has been demonstrated and therefore the effects on the conformational equilibria of an oxygenated substituent as the functional group X, initially attracted our attention.

We therefore envisaged the synthesis of various alcohols where X represents the hydroxy group while Y is either a hydrogen atom, or one of the various simple but pertinent alkyl groups, differing in their orbital hybridisation. These alcohols in term would then provide direct access to the corresponding ethers, and comparison of the conformational equilibria of the ether derivatives and their hydroxy precursors would then allow us to gain some insight into the magnitude and nature of the hydrogen bonding. In the situation where X and Y form a cyclic unit containing an oxygen atom, the effects induced by the presence of the conformationally locked oxygen atom and the strained ring could then be studied. Finally, in similar fashion and in order to investigate the interactions of the amino group with an aromatic system, an analogous series of nitrogen derivatives were also synthesised.

2.2.3.1 – Synthesis of a series of propanoanthracenes bearing an oxygenated group on the central carbon of the flexible bridge

2.2.3.1.1 – Preparation of alcohol derivatives from the ketone 67

The first compound to be prepared was the secondary alcohol **77**, obtained by smooth reduction of ketone **67** by sodium borohydride in a mixture of THF and methanol (Scheme 15).
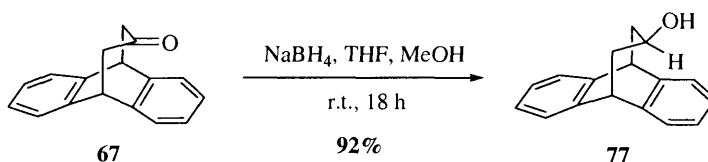
Scheme 15

As mentioned previously, we were interested in introducing various alkyl groups to the ketone functionality of **67**, offering a series of tertiary alcohols. Reaction of ketone **67** with methyl magnesium bromide provided a 1:1 mixture of desired tertiary alcohol **78** and recovered starting material. This was due to the Grignard reagent acting as a base, to form the magnesium enolate and leading to the recovery of starting material after aqueous work-up. However, alkyl cerium reagents have been reported to be very efficient in addition reactions to readily enolisable carbonyl compounds.[154] The use of a cerium based electrophile was therefore investigated for the synthesis of the tertiary alcohols. The

corresponding methyl cerium reagent was prepared according to a literature procedure[155] and its reaction with ketone **67** provided **78** as the sole product (Scheme 16).
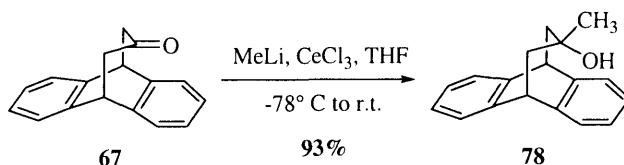
Scheme 16

As discussed earlier, the proximity of an aromatic ring with an unsaturated carbon-carbon bond generates an interaction of significant magnitude, as in case of the ethylene-benzene and acetylene-benzene complexes. Increasing the acidity of the proton of the substituent on the central carbon would modify the strength of the interactions between the bridge substituent and the aromatic ring, and to investigate this theory, an unsaturated alkyl group, containing either an sp^2 or sp hybridised carbon atom was introduced. To probe this particular interaction, vinylic alcohol **79** was our next target.

Sargent and co-workers[156] reported the reaction of cyclohexanone with 1.3 equivalents of vinyl magnesium bromide in THF leading to 1-vinylcyclohexyl alcohol. Under these conditions, only 12% conversion of ketone **67** into **79** was observed and increasing the number of equivalents did not improve the yield and byproducts were formed. However, the low yield of this reaction may arise from the poor solubility of vinyl magnesium bromide in THF at room temperature. However, by changing the reaction solvent to dichloromethane, an increased yield of 36%, of **79** was isolated and unreacted starting ketone was recovered (Scheme 17).
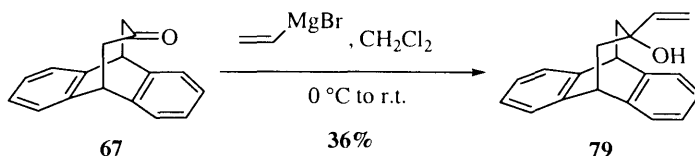
Scheme 17

In order to complete the series of alcohols, addition of an ethynyl moiety to the ketone **67** was carried out using the cerium reagent generated *in situ* from trimethylsilylacetylene,

cerium (III) chloride and *n*-butyllithium. All of the methods described in the literature[157,158,159] use the same methodology, the only variable being the number of equivalents of the organocerium reagent. On using two equivalents, the propargylic alcohol **80** was obtained in 38% yield with the remainder being recovered starting material. However, the use of 5 equivalents of the organocerium reagent led to complete conversion. Fluoride anion induced removal of the trimethylsilyl moiety[160] finally provided the desired propargylic alcohol **81** (Scheme 18).
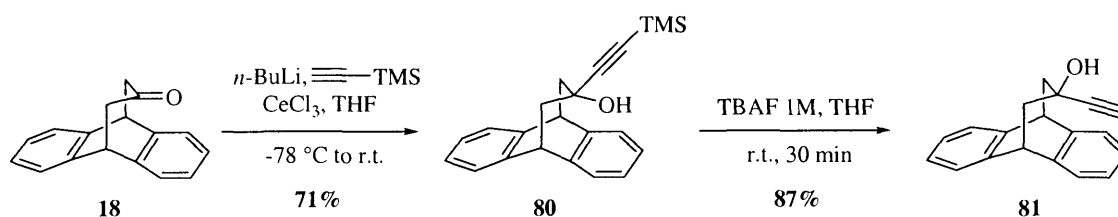
Scheme 18

Comparison of the terminal alkyne with cyano group also offered interesting possibilities and the cyanohydrin **83** was deemed to be a good substrate to provide this information. The use of TMSCN as the source of cyanide in the presence of a Lewis acid[161] offered a mild alternative for the synthesis of cyanohydrins and led to the formation of the intermediate silyl protected derivative **82** (Scheme 19).
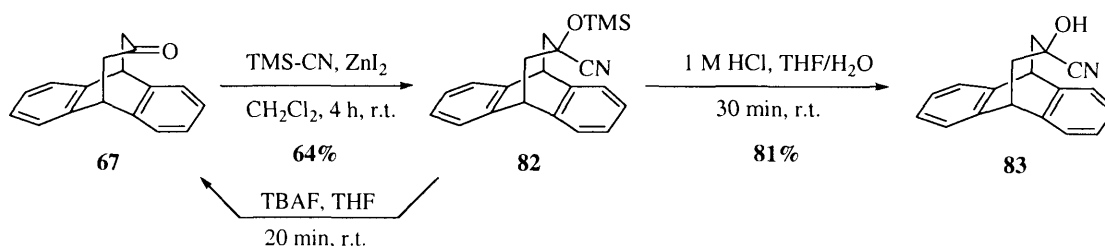
Scheme 19

Although **82** was easily synthesised, deprotection of the hydroxy group and purification of the free cyanohydrin **83** was more problematic. Under basic conditions, such as the use of tetrabutylammonium fluoride in THF, the only compound to be isolated was the ketone **67**, formed by loss of CN⁻ as depicted in Scheme 19. Removal of the trimethylsilyl group was then attempted in aqueous HCl but the resultant cyanohydrin appeared to be highly

insoluble in dichloromethane or diethyl ether since extraction of **83** into ethyl acetate and purification on silica gel led to regeneration of the starting ketone **67**, the only solution found in order to purify **83**, was to wash the white powder thoroughly with dichloromethane.

2.2.3.1.2 – *Synthesis of ether derivatives from the tertiary alcohols **78** and **81***

Since replacement of the proton of the hydroxy group by a methyl group would preclude any possibility of π-facial intramolecular hydrogen bonding, comparison of the alcohols with their corresponding ethers could also provide some valuable information on the relative strengths of the involved interactions. In the first instance, ether **84** was obtained by deprotonation of the tertiary alcohol **78** with potassium hydride and reaction of the resulting anion with dimethylsulfate (Scheme 20).
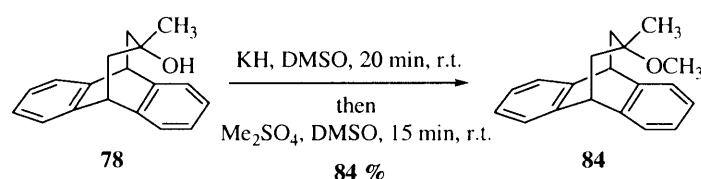
Scheme 20

Methylation of the propargylic alcohol **81** to give **85** was then attempted using the same procedure described for the formation of the ether **84**. However, under these conditions, ketone **67** was the only isolated product. Elimination of the protected ethynyl unit was also observed using the silylether **80** as the reactant (Scheme 21).
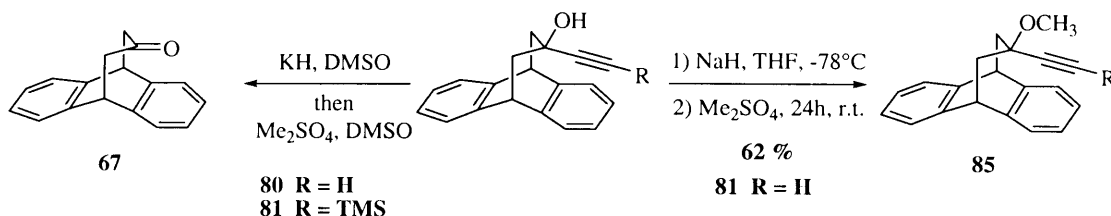
Scheme 21

At this stage, examination of the literature[162] revealed that acetone can in fact be used as a protecting group for terminal alkynes and deprotection can be induced under basic conditions with heating (Scheme 22).
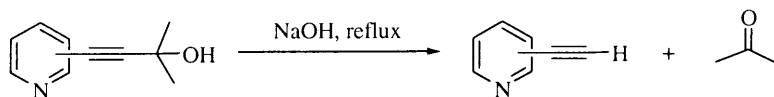
Scheme 22

In our case, the presence of the strong potassium base deprotonated the hydroxy group at room temperature leading to elimination of the ethynyl group and formation of the ketone **67**. As a result, the synthesis of ether **85** was investigated under different conditions. However, reaction of **81** with Me$_3$OBF$_4$ in dichloromethane[163] led to recovery of starting material. The ether **85** was finally obtained following procedure reported by Diederich and co-workers[164] for methylation of a tertiary alcohol group in the presence of NaH in THF (Scheme 21).

2.2.3.1.3 – Synthesis of the epoxide 86 and the oxetane 87

The epoxide and the oxetane were synthesised in order to provide a series of conformationally locked cyclic ethers for comparison with the acyclic variants described above. Thus, the alkene **68** reacted smoothly with *meta*-chloroperbenzoic acid in CH$_2$Cl$_2$ at room temperature to give the epoxide **86** in excellent yield (Scheme 23).
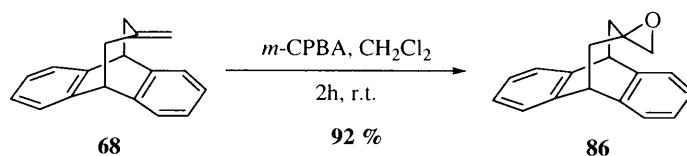
Scheme 23

Okuma and co-workers had previously described the ring expansion reaction of the epoxide moiety using dimethyloxosulfonium methylide *via in situ* formation of the ylide **88**[165] in the presence of strong base (Scheme 24).
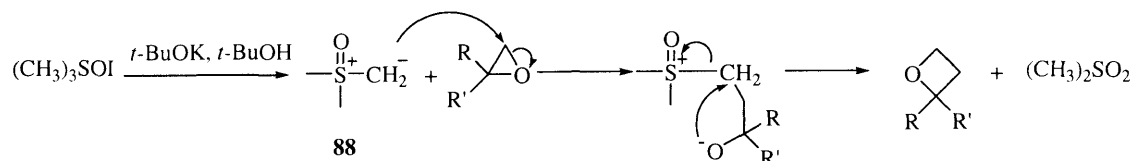
Scheme 24

Although this is a powerful nucleophilic methylene-transfer reagent, in our hands, only traces of the oxetane **87** were observed and the starting epoxide **86** was recovered. Curiously however, when the same reaction was performed using ketone **67** and a large excess of dimethyloxosulfonium methylide, a 1:1 mixture of epoxide **86** and oxetane **87** was produced (Scheme 25).
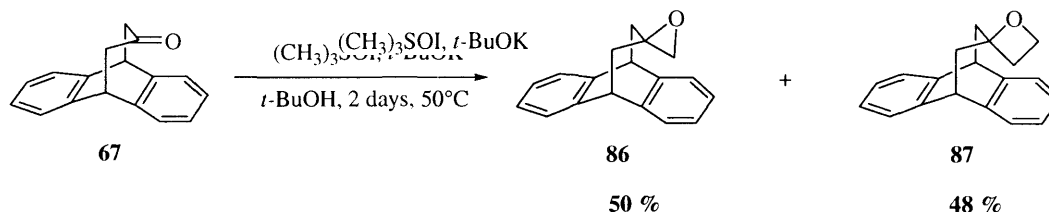
Scheme 25

Isolation of **86** and conversion to **87** was attempted by sequentially increasing the number of equivalents of reagent and the reaction time, but no further conversion was observed. As both the epoxide **86** and oxetane **87** were formed, the reaction pathway in Scheme 26 was proposed wherein, after reaction with one equivalent of ylide, a competition exists between ring closure to give the epoxide or nucleophilic attack of a second equivalent of ylide, followed by ring closure leading to oxetane **87**.
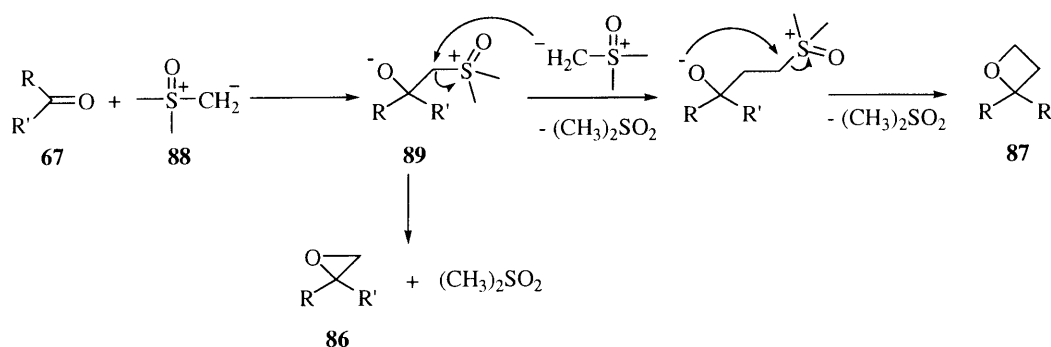
Scheme 26 Suggested mechanism for the formation of epoxide **86** and oxetane **87**

As equivalent yields of **86** and **87** were obtained, the rate of the ring closure reaction and that of the nucleophilic attack are similar, indicating that intermediate **89** may be stabilised by the presence of the two aromatic rings. The potassium cation can be envisaged as being coordinated to the negatively charged oxygen atom and to the aromatic ring, while, on the other side of the bridge, the positive charge on the sulphur atom may cause the sulfoxide moiety to become close to the aromatic system, facilitating the attack of a second equivalent of ylide, whilst slowing the rate of ring closure to form the desired epoxide **86** (Figure 58).

89
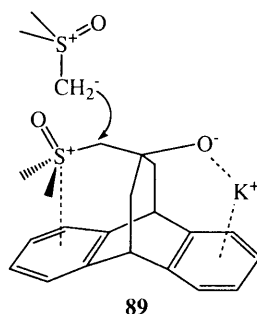
Figure 58

The failure of epoxide **86** to react with the ylide **88** indicated the poor electrophilicity of the carbon atom of the epoxide cyclic unit and that the opening of the ring appeared less trivial than expected. In order to study the reactivity of **86**, the opening of the epoxide unit to the diol **91** was attempted.

Initially, the reaction was investigated using various basic conditions, NaOH in DMSO at reflux,[166] KOH in THF[167] or LiOH in THF/H$_2$O at reflux,[168] but only the starting epoxide was observed. This transformation was then attempted in the presence of H$_2$SO$_4$ in THF/H$_2$O,[169] and after stirring overnight, the rearrangement product **92** was isolated as the sole product (Scheme 27). Under these acidic conditions, the carbocation intermediate was formed and instead of being trapped by a molecule of water, underwent a hydride shift (or loss of a proton to give an intermediate enol) to form aldehyde **92** (Scheme 27).
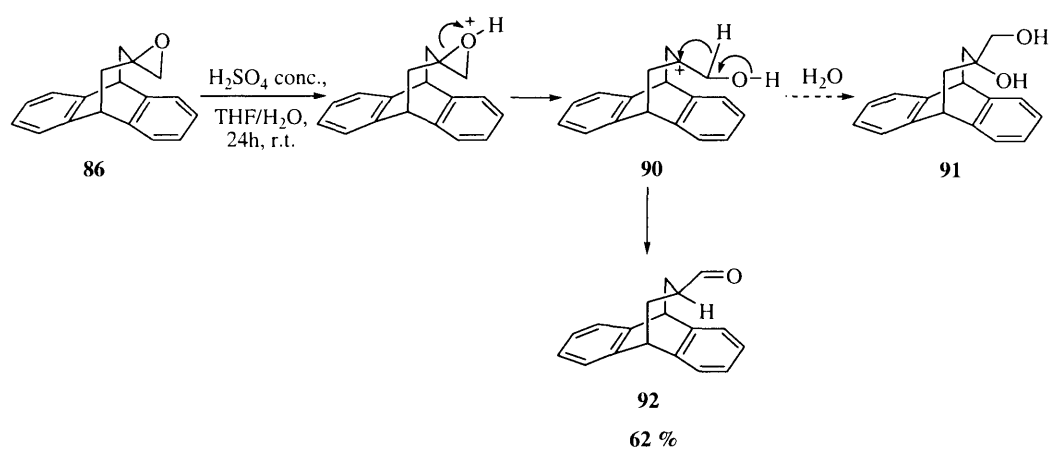
Scheme 27

As investigating a milder alternative to sulphuric acid for opening the epoxide, a catalytic amount of tosic acid in a mixture of THF and H$_2$O was used and led to the formation of product **92** as well as **93** as the major component (Scheme 28).
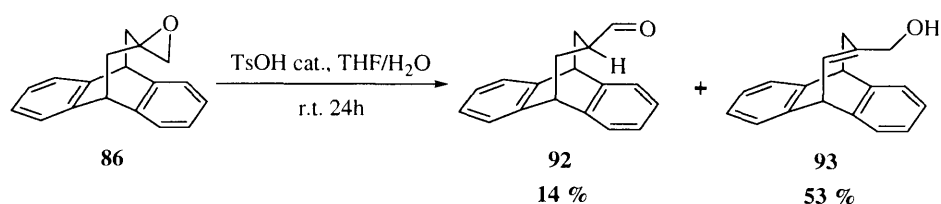
Scheme 28

Two different mechanisms can be envisaged for the formation of **93** from the intermediate carbocation **90**, either by elimination of a bridge proton *via* an E_1 mechanism as depicted in Scheme 29 or *via in situ* E_2 dehydration of the diol **91** involving protonation of the tertiary hydroxy group.
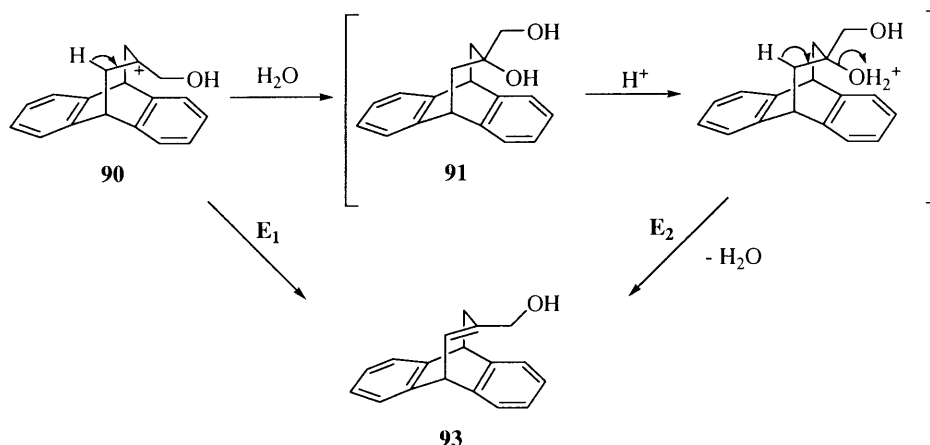
Scheme 29

2.2.3.1.4 – Replacement of the hydroxy group by a fluorine atom

The introduction of a fluorine into organic compounds can increase lipophilicity and consequently, absorption of fluorinated molecules into biological membranes.[170] In consequence, incorporation of a fluorine atom or fluorinated groups into biologically active compounds is an area of intense interest in medicinal chemistry, since the physical, chemical and biological properties of the parent molecule can be modified drastically. Substitution of a hydrogen atom by fluorine is an excellent strategy for reinforcing drug-receptor interactions (electronic modulation), facilitating the path through lipid bilayers (lipophilic modulation) and inducing conformational change metabolism (steric parameters). The van der Waals radius of the fluorine atom (1.47 Å) is between that of oxygen (1.52 Å) and a hydrogen atom (1.20 Å), also allowing it to be claimed as an isostere for the hydroxy group.

Therefore, studies on the replacement of the hydroxy group in **78** by a fluorine atom on the resultant conformational equilibria were of considerable interest. The synthesis of **94** from the tertiary alcohol was initially attempted in the presence of DAST. However, the high hydrolytic sensitivity of this common fluorinating agent led it to act as a proton source for dehydration of the tertiary alcohol to the alkene **95**. Even in the presence of an inorganic base to neutralise the acidity of the reaction mixture, only complete conversion into the alkene **95** was observed (Scheme 30).
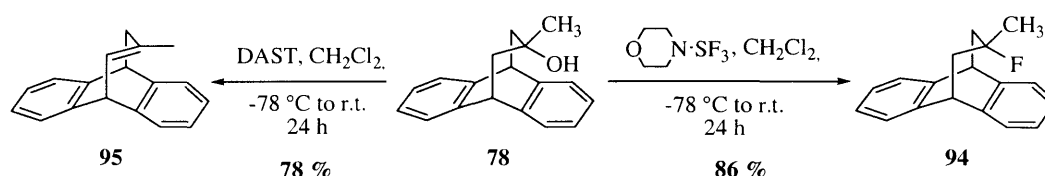
Scheme 30

Fortunately however, morpholinosulphur trifluoride, which has been shown to be a good alternative for nucleophilic fluorination due to its increased thermal stability, did lead to complete conversion of alcohol **78** into the derivative **94** (Scheme 30). Under these reaction conditions, compound **96** was also obtained by fluorination of the corresponding secondary alcohol **77** in 82% yield (Scheme 31).
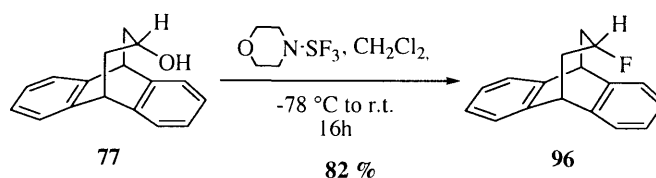
Scheme 31

2.2.3.2. – The synthesis of a series of propanoanthracenes bearing a nitrogen-containing functional group on the central carbon of the flexible bridge

With a series of propanoanthracenes bearing oxygen containing functional groups in hand, we then focused our attention on the synthesis of an analogous series of nitrogen containing functional groups.

Thus, the conformational equilibrium of oxazolidine **97** should provide a direct comparison of the degree of intramolecular interaction between the aromatic ring and each heteroatom (Scheme 32).
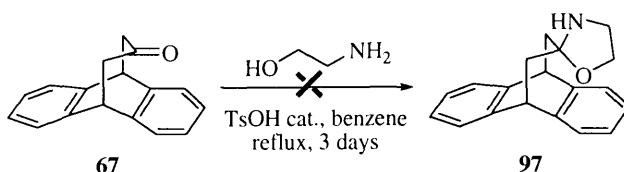
Scheme 32

The general method for oxazolidine formation as described by Hancock and Cope[171] was used, whereby ethanolamine was heated in the presence of **67** in benzene containing a catalytic amount of tosic acid, under Dean and Stark conditions. A large excess of ethanolamine and a six-hour reflux[172] provided a 1:1 mixture of the starting ketone **67** and the expected oxazolidine **97** by NMR spectroscopy (Scheme 32). Unfortunately, chromatography on silica gel or alumina led to decomposition of the oxazolidine **97**. Extending the reflux period to 5 days and using an excess of ethanolamine of 20 equivalents, did not displace the equilibrium in favour of complete conversion into **97**. Purification of **97** was further hindered due to its high moisture sensitivity.

2.2.3.2.1 – Synthesis of amine derivatives where the functional group is connected to the central atom of the flexible bridge

Replacing the hydroxy group of the tertiary alcohol **78** by an amino group would provide valuable information on the relative strengths of the interactions generated by the presence of a nitrogen _versus_ an oxygen atom with an aromatic ring. Coutts _et al._ reported the

synthesis of an amino substituted quaternary carbon **101** from the disubstituted alkene **98** in

three steps _via_ the β-iodo-isocyanate derivative (Scheme 33).[173]
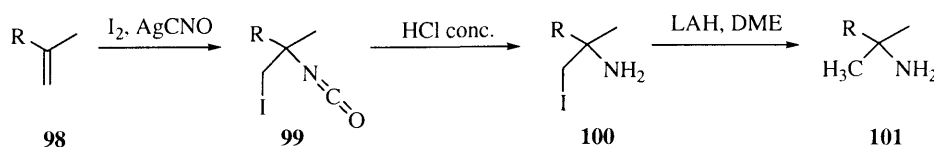
Scheme 33

According to this procedure, the alkene **68** should react with iodine and freshly prepared

silver isocyanate[174], but this reaction led to the recovery of the starting material

(Scheme 34).
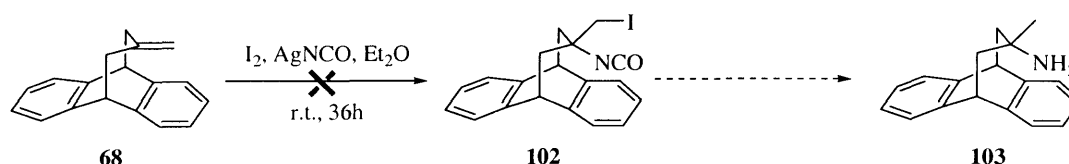
Scheme 34

In consequence, we investigated the nucleophilic addition of the methyl group to an

unsaturated nitrogen-containing functional group such as a substituted imine, seen as a

potential source of nitrogen to provide the amino functionality.

The stereoselective addition of organometallic reagents to N-(_tert_-butanesulfinyl)imines has

been previously described[175] and was accordingly selected (Scheme 35).
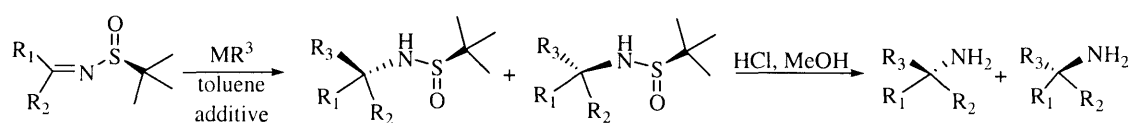
M =MgBr, Li,

Additive = Me_3Al, Et_2AlPh, $BF_3.Et_2O$, Et_2Zn, $CeCl_3$

Scheme 35

Thus, ketone **67** was transformed by the use of _tert_-butylsulfinamide into sulfinylimine

104, the precursor of tertiary sulfinamide **105** and quantitative conversion was achieved by

employing Ti(O-_i_Pr$_4$)[176] as the additive, with heating (Scheme 36).
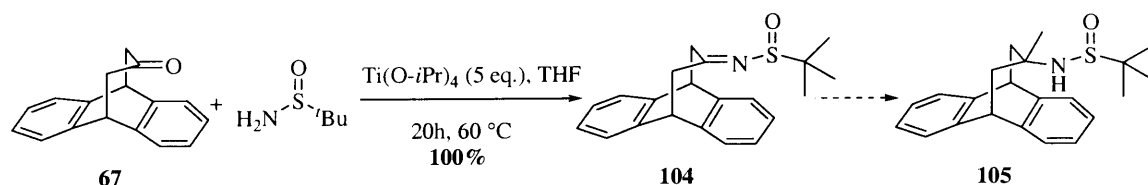
Scheme 36

A variety of methods were employed in attempted introduction of the methyl group to the sulfinylimine **104**, such as the use of methyllithium, methyl Grignard reagent, and alteration of the solvent or the additive. However, in all cases, the starting material **104** was recovered, either due to lack of reaction or because the organometallic reagent acted as a base instead of a nucleophile leading, after work-up, to the recovery of **104** without any trace of the expected sulfinylamine **105**.

A convenient protocol was eventually found though use of the Ritter reaction,[177] a common method to convert tertiary alcohols into amines. Jirgensons *et al.*[178] established a convenient method using chloroacetonitrile, to give the chloroacetamide **106** from the alcohol **78.** Subsequent cleavage of the acetyl group with thiourea quickly gave the intermediate isothiouronium salt which decomposed slowly to the desired amine **103** (Scheme 37).
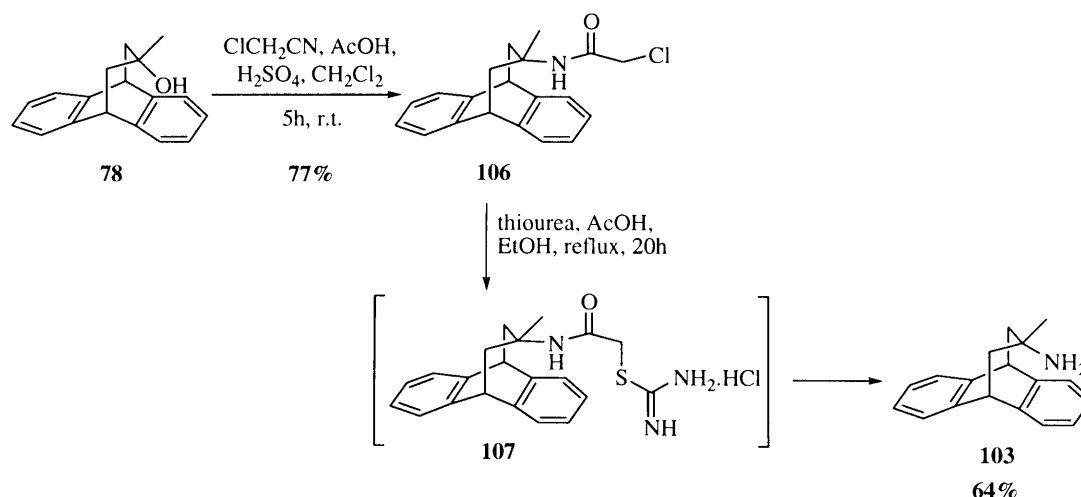
Scheme 37

Our next target molecule was the propargylic amine **108.** The reported syntheses of propargylic amines are based on the conversion of the hydroxy group of the propargylic alcohol analogues into a good leaving group which was subsequently displaced by sodium amide to provide the amino group.[179] However, reaction of the propargylic alcohol **81** with mesyl chloride under basic conditions[180] led to the elimination *in situ* of the newly formed leaving group as depicted in Scheme 38.
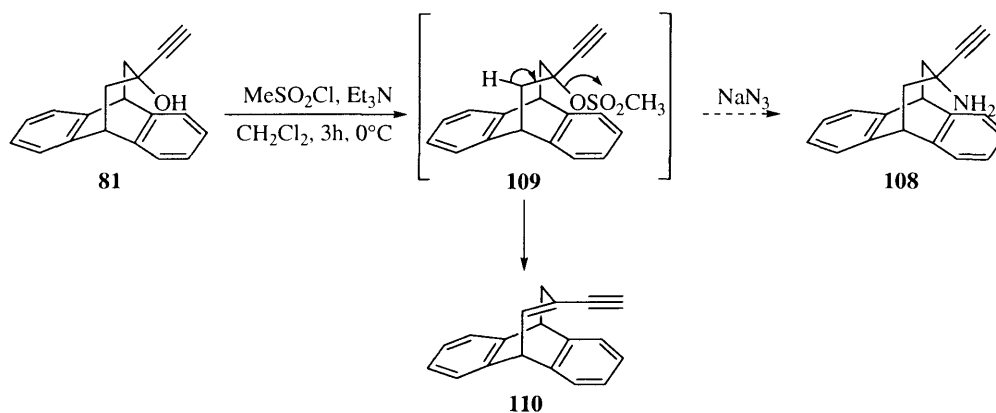
Scheme 38 Mechanism for the formation of **110**

The elimination reaction was shown to be much faster than the formation of **109** since **110** was the only isolated product and no trace of **109** was detected.

Previously, the Ritter reaction allowed the conversion of the tertiary alcohol **78** into **106** and the synthesis of propargylic amine **108** was attempted in an analogous manner. In this instance however, **111** was formed as the sole product (Scheme 39).
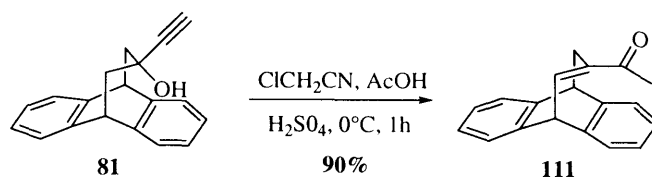
Scheme 39

Alternatively, acid-catalysed formation of **111** could occur by following the Rupe rearrangement of the tertiary α-acetylenic alcohols[181] and a speculative mechanism for the formation of **111** is shown in Scheme 40.

81

111
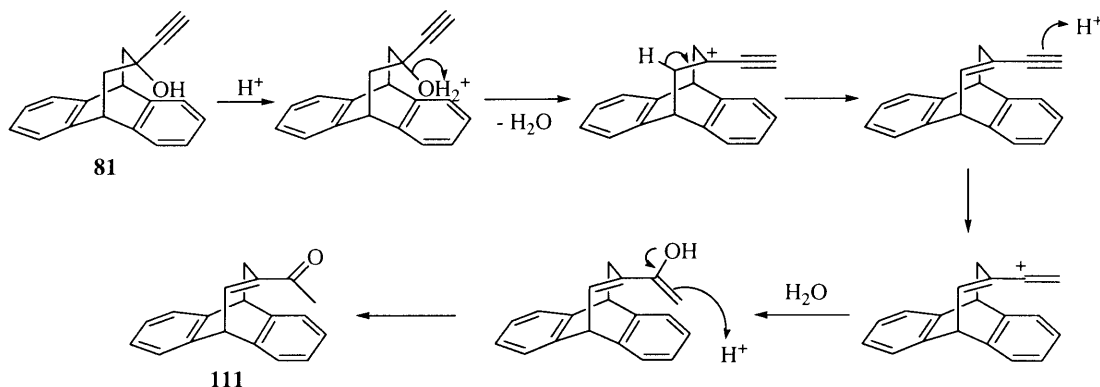
Scheme 40 Suggested mechanism for the formation **111** by elimination of the protonated hydroxy group followed by hydration of the triple bond

In a second approach which unfortunately paralleled our failure with the methyl Grignard reagent, reaction of ethynylmagnesium bromide or (trimethylsilyl)ethynylmagnesium bromide[182] with sulfinylimine **104** was likewise unsuccessful and the starting material was recovered.

Synthesis of the O-benzyloxime **113**[183] _via_ the oxime **112**[184] was then carried out in order to attempt subsequent addition of the ethynyl moiety. The nucleophilic addition to the C=N bond of an oxime functionality is a synthetically important and well-established method for preparing many types of nitrogen-containing compounds. Although, alkoxylamines have been synthesised by the reaction of oximes with organocerium reagents,[185] the present reaction using O-benzyloxime **113** resulted only in the recovery of starting material (Scheme 41).

67   **95 %**   **112**   **57 %**   **113**

TMS———$\equiv$, $CeCl_3$
_n_-BuLi, THF, -78°C to r.t.
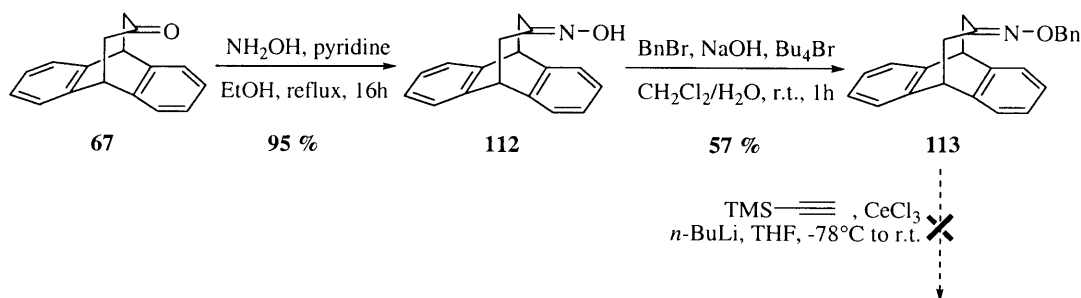
Scheme 41

In the event, the addition reaction of either an organolithium or organocerium reagent to oxime ether **113** was unachievable even if this method is a well established procedure.[186] Although recovery of the starting material could be due to a slow rate of reaction, it may also suggest that the organocerium reagent coordinated to the N atom and acted as a base, despite the fact that they are generally considered to be less basic and more nucleophilic than their lithium counterparts.

Another attempt to produce the propargylic amine **108** was initiated with the synthesis of the nitrone **114** from the ketone **67**. Merino and co-workers[187] have reported an improved method for the synthesis of nitrones by the activation of ketones with a stoichiometric amount of a Lewis acid, in particular $ZnCl_2$. Various procedures for the addition of organometallic reagents to the nitrone functionality are described in the literature,[188] but, in similar fashion to the sulfinylimine and the amine ether, none proved successful in forming the adduct **115** (Scheme 42).

Attempted conditions : (a) TMS-≡, Et_2Zn, toluene, r.t., 24h[189]

(b) TMS-≡, *n*-BuLi, THF, -78°C to r.t., 20h[190]

(c) TMS-≡, $CeCl_3$, *n*-BuLi, THF, -78°C to r.t.
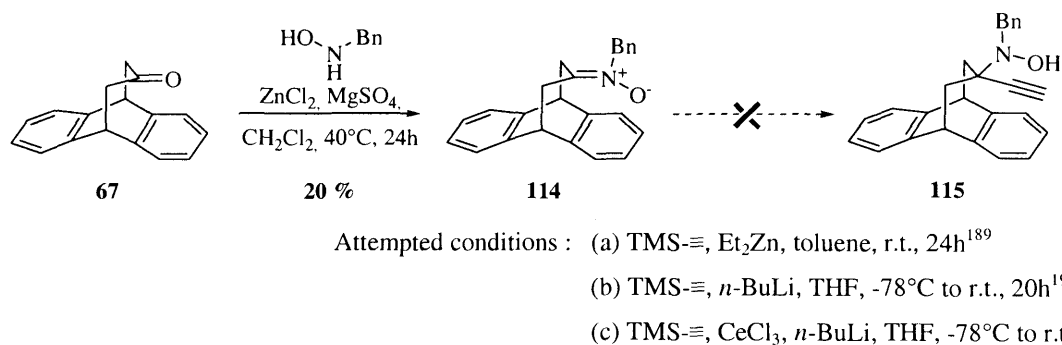
Scheme 42

In summary, the conversion of the hydroxy group into a leaving group leads to spontaneous elimination and the Rupe reaction occurs under acidic conditions instead of the expected Ritter reaction. Reactions of imine derivatives with organometallic reagents are either too slow or allow the reagent to act as a base. In all of these cases, reactions led to the recovery of starting material. Thus, the failure of all synthetic approaches and other priorities forced us to abandon the synthesis of propargylic amine **108**.

A further amino derivative capable of yielding valuable information was the derivative bearing an amino and a cyano group as substituents on the central carbon of the bridge. The conversion of a carbonyl group into an α-amino-nitrile in one pot, _via_ the formation of an iminium ion is, of course, the basis of the Strecker reaction. Thus, a combination of sodium cyanide and ammonium chloride under an atmosphere of ammonia [191] provided the amine **116** in 56% yield.
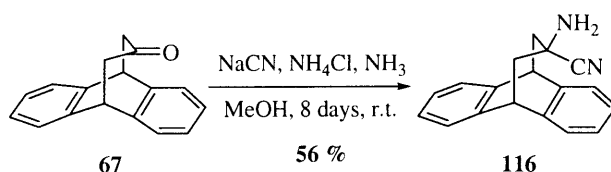
Scheme 43

Two types of intramolecular interactions with the aromatic unit may occur in the α-amino-nitrile derivative **116**. The first of these results from the presence of the electron deficient carbon atom of the cyano group whilst the other derives from the presence of the amino group which could, in similar fashion to the hydroxy group, have potential hydrogen bond donor capacity. This competition should affect the conformational equilibrium. In addition, comparison of this conformational balance with the results using the cyanohydrin **83**, would give a relative quantification of the strength of the intramolecular interactions involving the aromatic ring with either an amino or a hydroxy group.

2.2.3.2.2 – Synthesis of ammonium salts from the amines 103 and 116

As described in the introductory chapter, non-covalent interactions between charged species and aromatic rings have been widely explored since cation/π interactions in the active sites of enzymes are particularly useful for drug design in both synthetic and biological systems.[192] Host-guest complexation, based on cation/π interactions in organic solutions is currently an active research area and cyclophanes, cyclic peptides and molecular clefts are the most versatile hosts to explore these interactions.[119] Ma and Dougherty[93] established that there is an electrostatic attraction between a cation and the permanent quadrupole moment associated with a π-system. Based on the exchange from NH_4^+ to NMe_4^+ cation, they demonstrated that a large increase in the ionic radius, generated

a reduction in the cation-π interactions, as expected in an electrostatic model, especially as no hydrogen bonds of the type N-H•••π were involved.

Accordingly, the potential interactions between an ammonium cation and the aromatic system were crucial for our research programme. Further exploration of these cation/π interactions as a function of the solvent was perceived as being fundamentally important. We thus prepared the hydrochloride salts **117** and **118** (Scheme 44).

103 R = CH$_3$	**117** R = CH$_3$ 95%
116 R = CN	**118** R = CN 86%
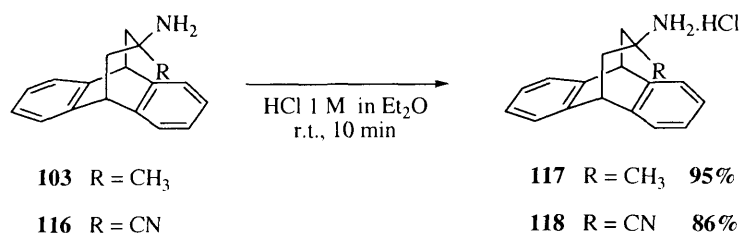
Scheme 44

The preparation of the mesylate salts **119** and **120** was also carried out from the corresponding free amines **103** and **116** respectively, in order to study the influence of these counter anions on the conformational equilibria.

103 R = CH$_3$	**119** R = CH$_3$ 78%
116 R = CN	**120** R = CN 81%
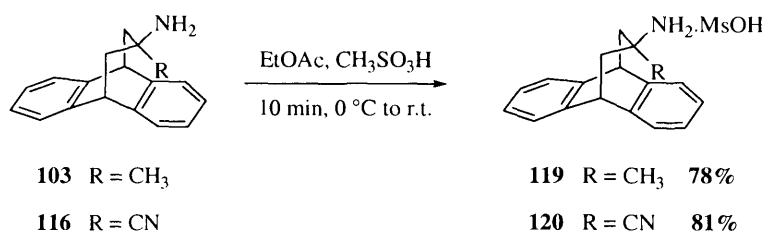
Scheme 45

2.2.3.2.3 – Synthesis of propanoanthracene derivatives where the functional groups X and Y form a N-spiro-heterocycle

Initially, it was desired to obtain the smallest possible nitrogen-containing ring on the central carbon of the flexible bridge. Thus, we focused our attention on the synthesis of the aziridine **121** in order to provide a direct comparison with its epoxide analogue. The first pathway attempted was based on the Staudinger reaction of intermediate azide **122** using

triphenylphosphine to afford the required aziridine **121**,[193,194] *via* the formation of an intermediate ylide, and driven by the loss of nitrogen (Scheme 46).

The formation of the desired azide **122** was achieved *via* SN2 opening of the epoxide **86** under harsh conditions.[195]
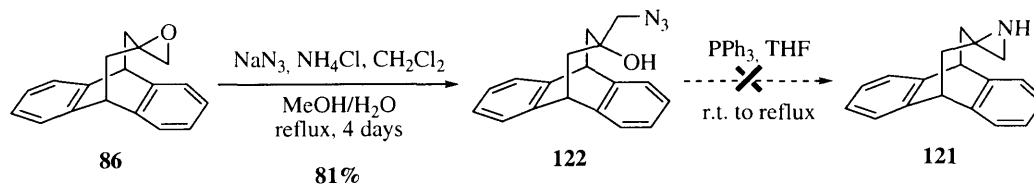
Scheme 46

However, reaction of **122** with triphenylphosphine in either toluene or THF did not give the desired aziridine **121** and **92** was the sole isolated product. Mechanism involving hydride migration is represented in Scheme 47.
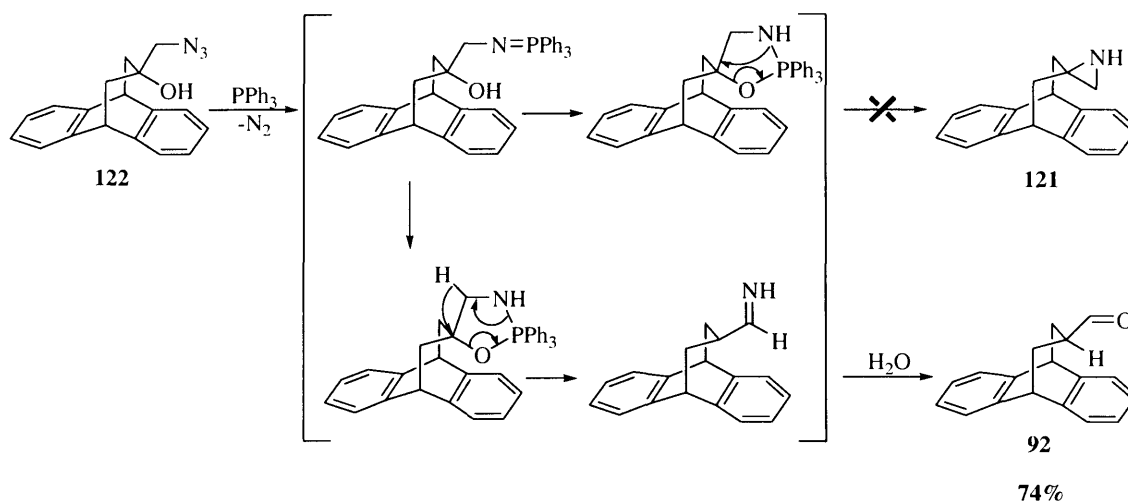
Scheme 47

Thus, another synthetic pathway was investigated. Atkinson and co-workers have previously described the synthesis of aziridines using *in situ* oxidation of 2,4-dinitrobenzenesulphenamide by lead tetraacetate and subsequent trapping of the nitrene by the corresponding precursor alkene.[196] Following this procedure, only the starting alkene **68** was recovered (Scheme 48). The lack of reactivity may be explained by the fact that the starting alkene **68** was not sufficiently electron-rich to enable the trapping of the sulphenylnitrene formed *in situ*.
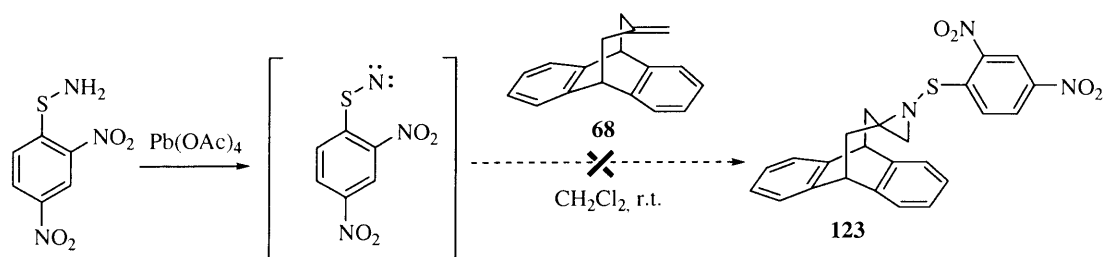
Scheme 48

The copper-catalysed olefin aziridination reaction in the presence of PhI=NTs is a well-established stereospecific route to aziridines.[197] In similar fashion however, reaction of alkene **68** with freshly prepared copper triflate (II) and PhI=NTs failed and the starting alkene was recovered (Scheme 49).
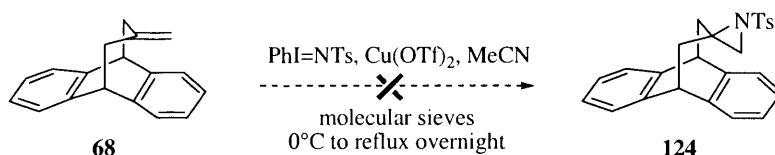
Scheme 49

Finally, the procedure described by Hassner[198] to form an aziridine led to success. This methodology involved the addition of IN_3 to a double bond followed by reduction of the azide group and elimination of iodide leading to an aziridine moiety. Modification of the first step by changing the solvent from acetonitrile[199] to dichloromethane[200] afforded the intermediate azide **125**, which was subsequently reduced to the aziridine **121** (Scheme 50).
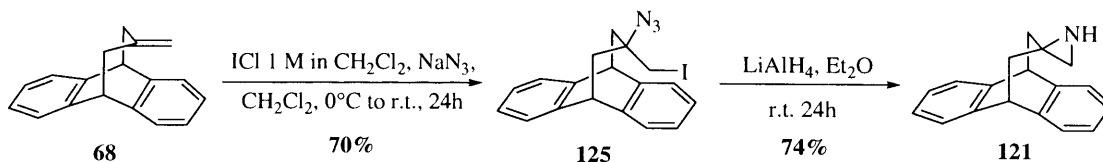
Scheme 50

In order to complete our series of propanoanthracene derivatives, we envisaged the synthesis of the azetidine **130** *via* the β-lactam **128**, following the pathway depicted in Scheme 51.
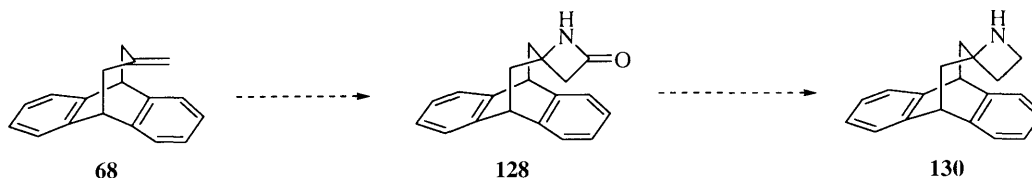
Scheme 51 Investigated retrosynthetic pathway for azetidine **129**

The most appropriate synthetic method for the required β-lactam was the [2+2] cycloaddition of chlorosulfonyl isocyanate with the alkene **68**.[201] Our first attempt[202,203] led to a mixture of the isomerised alkene **95** and the β-lactams **126** and **127** (Scheme 52).
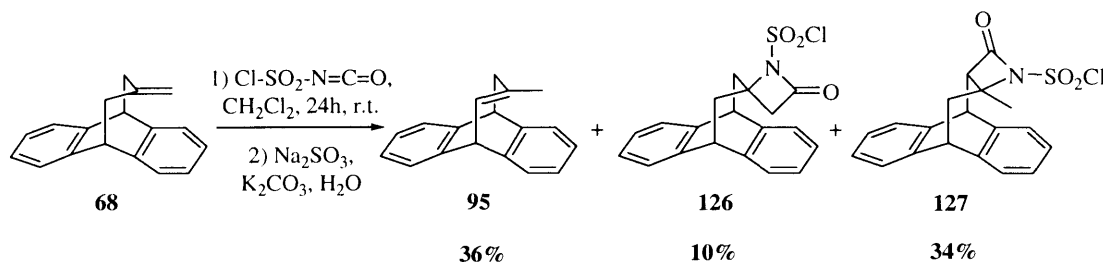
Scheme 52

Isomerisation of the alkene **68** most probably occurred as a result of acidic conditions[204] since the moisture sensitivity of chlorosulfonyl isocyanate provided some traces of HCl. As the two alkenes **68** and **95** were then in competition in the reaction mixture, **127** was formed as the cycloaddition adduct of chlorosulfonyl isocyanate with the isomerised alkene **95**. Moreover, although the reductive removal of the N-chlorosulfonyl group was expected during the second step, the recovered β-lactams still contained the chlorosulfonyl group. A large excess of DIBAH was therefore used in the reduction of **126** to the expected β-lactam **128** (Scheme 53) but this reducing agent was insufficiently powerful to convert the β-lactam into the azetidine.
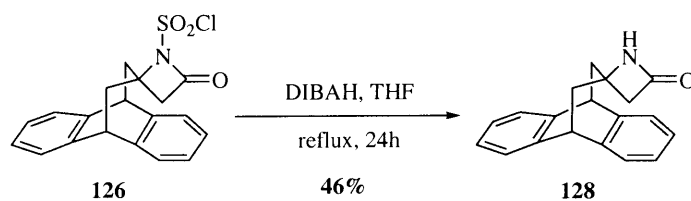
Scheme 53

Careful examination of the literature then revealed that Chmielewski and co-workers had faced the same difficulties in the reaction of alkenes with chlorosulfonyl isocyanate and found that by storing the reagent over potassium carbonate for 2 days and then performing the reaction in the presence of an inorganic base, isomerisation of the starting material was impeded.[205] Following this procedure, no trace of the isomerised alkene **95** nor the cycloadduct **127** were observed but these reaction conditions provided a mixture of the β-lactams **126** and **128** and the byproduct **129** (Scheme 54).
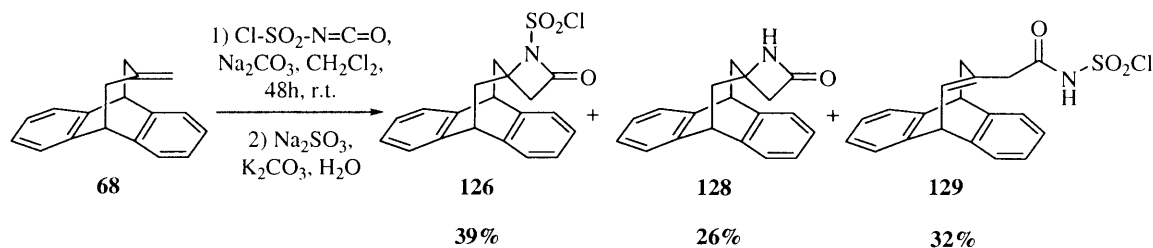
Scheme 54

In Scheme 55, the mechanism of the formation of β-lactam **126** can be represented by the pathway (a) whereas a competing elimination reaction[206] provides the byproduct alkene **129** following the pathway (b).
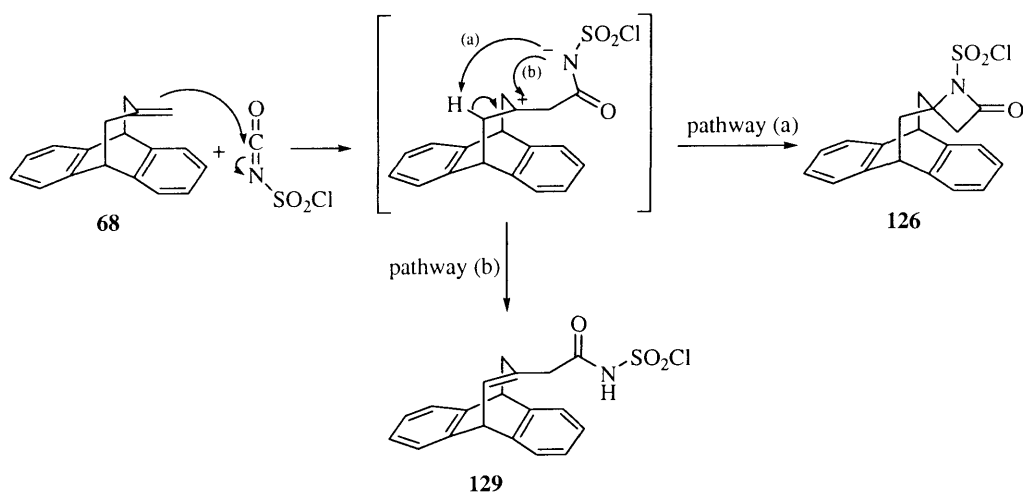
Scheme 55   Mechanisms suggested for the formation of **126** and **129**

Although the β-lactam **128** was not reduced by DIBAH, a large excess of lithium aluminium hydride provided the desired azetidine **130** in a good yield. Furthermore, **126** was directly converted into **130** using this reducing agent (Scheme 56).

126 R = SO$_2$Cl	64%
128 R = H	76%
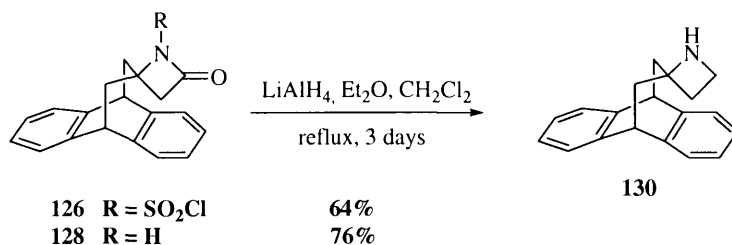
Scheme 56

Thus, the conformational equilibria of the azetidine **130** will be compared not only with that of the aziridine **120** in order to study the effects of the size of the functionalised ring on the strength of the intramolecular interactions, but also with that of the oxetane analogue **87**. Moreover, it will be possible to observe the influence of the more acidic proton in the amide functionality of the β-lactam **129** by comparison with the azetidine **130**.

2.2.3.3 – Substitution of the aromatic ring in propanoanthracenes

Even although the conformational equilibria are highly sensitive to the nature of the functional groups on the flexible bridge, they are also strongly dependent on the electron density of the aromatic scaffold. Modification of the electron density of the original aromatic ring *via* introduction of powerful electron withdrawing or donating groups on one of the aromatic rings would clearly alter the strength of the intramolecular interactions.

Initially, we investigated the mononitration of ketone **67** to make one of the aromatic rings electron deficient. Although the Barrett group[207] has reported the mononitration of naphthalene using nitric acid and a catalytic amount of ytterbium triflate, this procedure was not as selective as hoped and numerous inseparable nitrated products were formed with none being predominant. We were however attracted to a report by Ohwada *et al*[208] in which selective nitration of the analogue, dibenzobicyclo[2.2.2]octadienone **131**, on carbon C_2 was shown to provide a 1:1 mixture of ketones **132** and **133** (Scheme 57).
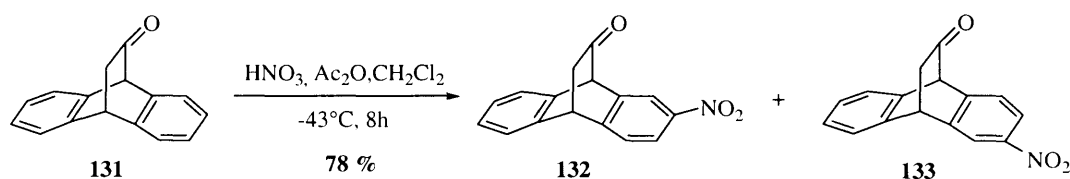
Scheme 57

Initially use of this method with ketone **67** led to the recovery of starting material, but after increasing the temperature to 0 °C, a mixture of two products, the mononitrated **134** and 2,6-dinitropropanoanthracenone **135**, were isolated in 8% and 6% yield respectively. Finally in the presence of nitromethane as co-solvent and at a lower reaction temperature,[209] **134** was formed as the sole product (Scheme 58).

Conditions:	**134**	**135**
HNO_3, Ac_2O, 0 °C, 24h	8 %	6 %
HNO_3, Ac_2O, $MeNO_2$ CH_2Cl_2, 0 °C, 24h	71%	0%
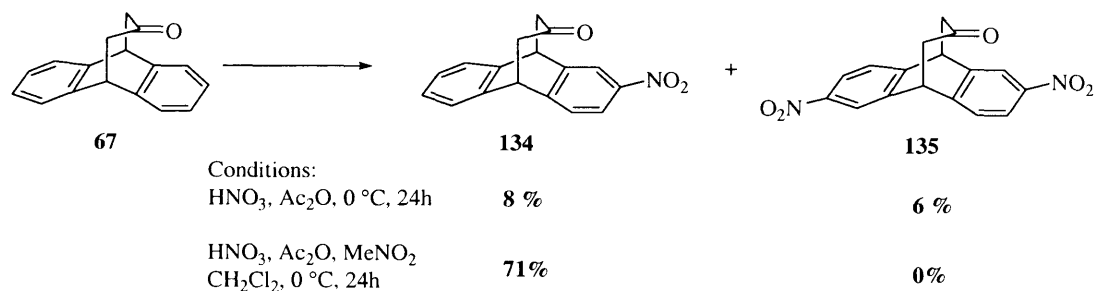
Scheme 58

The structure of **135** was established by ^{1}H NMR which clearly showed that nitration had occurred on both aromatic rings. Dinitration can occur on C_6 or C_7 leading to **135** and **136** respectively as shown in Figure 59 and in each case, the signal for the aromatic rings would be similar. However, the chemical shifts for H_9 and H_{10} were identical indicating that these protons were on the same chemical environment, corresponding to structure **135**.
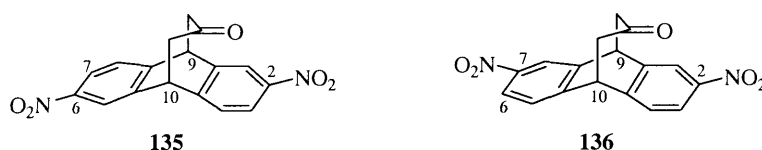
Figure 59   Structures of 2,6-dinitropropanoathracen-12-one **135** and 2,7-dinitropropanoanthracen-12-one **136**

From the results of the two procedures, reaction temperature and solvent were predominant factors for nitration. Although Masci studied the effects of organic solvents on electrophilic nitration of various aromatic systems,[210] and established that nitromethane gave the lowest reaction rate, there is no obvious correlation between the order of selectivity and physical or chemical properties of the solvents. In the present reaction, formation of the nitronium species needed to be carried out at 0 °C and then aged in an ice bath for a one day period, otherwise **135** was the only product. From these two crucial observations, decreasing the reaction rate of the aromatic nitration by changing the solvent and lowering the temperature ensures the highest selectivity and formation of **134**.
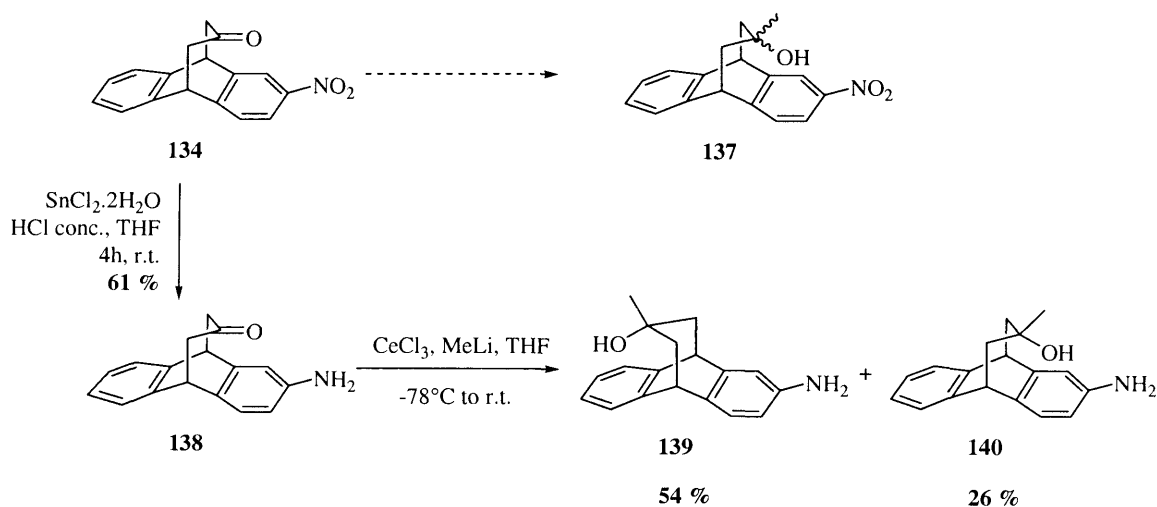
Scheme 59

The asymmetric ketone **134** contains one substituted, electron deficient aromatic ring, and a non-substituted, more electron rich aromatic system. This compound was prepared as a precursor for the tertiary alcohols **137** (Scheme 59). However, the nucleophilic addition of a methyl group to the ketone did not proceed using the procedure previously described for the parent alcohol **78** and modification of the number of organocerium equivalents used had no effect on the results.

Thus, amine **138** was suggested as a good alternative to the nitro product to provide the desired framework with two aromatic rings electronically different. This derivative, easily prepared by reduction of the nitro group[211] of **134** was then converted into two diastereoisomers **139** and **140** according to the procedure employed for the synthesis of the tertiary alcohol **78**. By increasing the number of equivalents of the organocerium reagent to 6, the corresponding alcohols were produced in good yield as a mixture of two separable diastereoisomers (Scheme 59).

Comparison of the conformational equilibria observed for tertiary alcohol **78** with that of the alcohols **139** and **140** was anticipated to provide valuable data on the effects of modification of the anisotropy of the ring current present in the aromatic ring and on the resultant strengths of the through space interactions generated by the presence of the hydroxy group. Investigation of various substituents on the aromatic ring, whilst varying the functional groups on the central carbon of the flexible bridge, will be highly informative and represents one of the longer term aims of this project.

2.2.4 – Synthetic summary

The series of propanoanthracenes with the central carbon atom of the flexible bridge substituted by oxygen, nitrogen and fluorine containing functional group as summarised in Figure 60, has been prepared.

R = H	77
R = CH$_3$	78
R = CH=CH$_2$	79
R = CCH	81
R = CN	83

R = CH$_3$	84
R = CCH	85

X = NH$_2$	103
X = NH$_2$.HCl	117
X = NH$_2$.MsOH	119

X = NH$_2$	116
X = NH$_2$.HCl	118
X = NH$_2$.MsOH	120

X = CH$_2$	76
X = O	86
X = NH	121

X = O	87
X = NH	130

128

R = H	96
R = CH$_3$	94

X = CH$_3$, Y= OH	139
X = OH, Y = CH$_3$	140
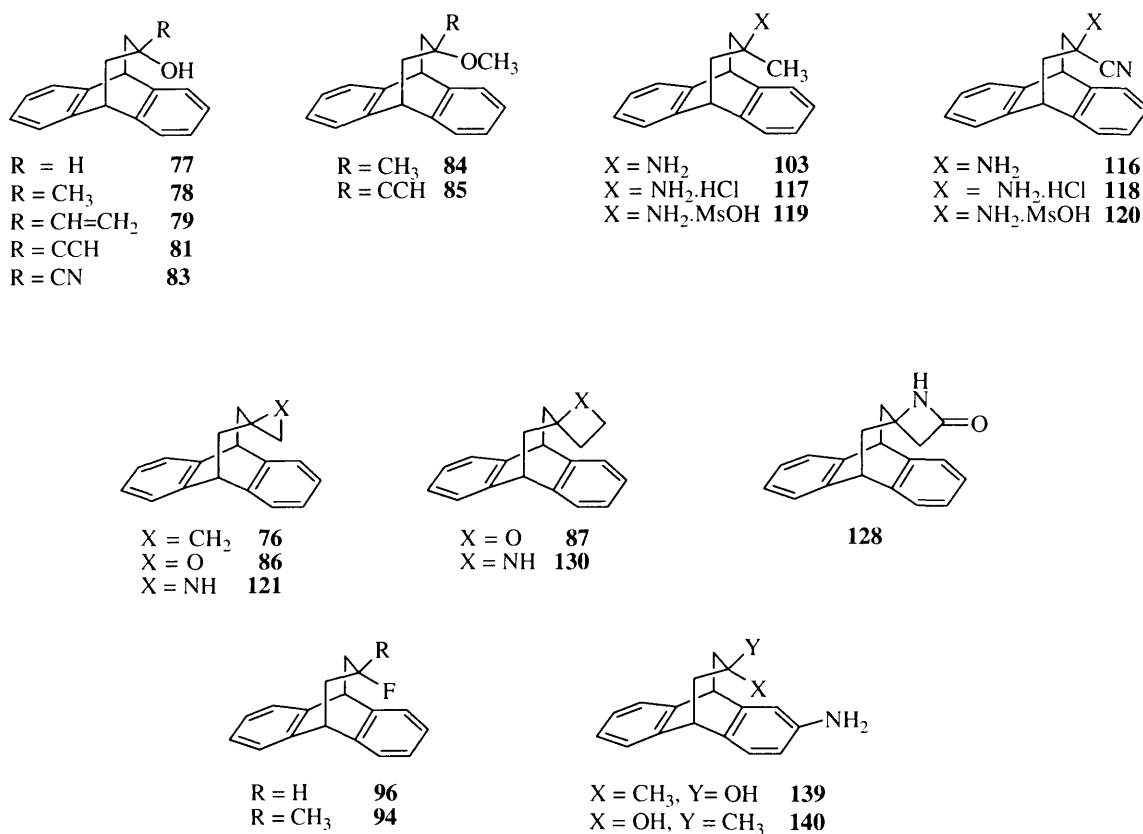
Figure 60

Each derivative of this series has been synthesised in order to measure the conformational preference and hence to compare the intramolecular non-covalent interactions which are preferred in the proximity of the precisely located aromatic ring.

2.3 – Experimental techniques used to estimate the conformational equilibria in solid and liquid states

2.3.1 – NMR spectroscopy

The structure of the molecules prepared has been especially designed to enable each derivative to be studied by NMR spectroscopy in order to bring to light the conformational preference of the substituents X and Y for each derivative and to measure this conformational equilibrium. However, their interconversion energy barriers are rather small and the usual approach of reaching the slow exchange limit on the NMR timescale by operating at low temperature failed. At 163 K, the symmetrical cyclopropane **76** presented a severely broadened ^{13}C resonance at 14 ppm in $CFCl_3$:CD_2Cl_2 (4:1) solution. A 50:50 ratio of resonance signals was expected at very low temperatures due to the symmetry of the molecule and, indeed, two separate signals of equal intensity and linewidth were detected in the solid-state ^{13}C CPMAS spectrum for the cyclopropane methylene carbons at 9.2 and 20.2 ppm at ambient temperature. Using these values as boundary values in the slow exchange region and assuming that the coalescence temperature in the solution state is less than 163 K, the interconversion energy barrier was estimated to be < 27 kJ.mol^{-1} from the following equation[212]:

$$\Delta G = RT_c \left[22.96 + \ln \frac{T_c}{\delta v} \right] \qquad \textbf{Equation (1)}$$

Where:

ΔG is the interconversion energy barrier (J.mol^{-1})

R is the universal gas constant (R = 8.315 J.K^{-1}.mol^{-1})

T_c is the coalescence temperature (in K)

δv is the difference of chemical shifts for the methylene carbons of the cyclopropane (in Hz)

As a consequence of this fast exchange rate between the two conformers **A** and **B** on the NMR time scale at room temperature, only averaged chemical shifts and coupling constants are observed. These can nevertheless be used to determine the ratio of **A** and **B** in solution.

2.3.1.1 - Dihedral angle

The torsional angle of our system is shown in the following Newman projection (Scheme 60).
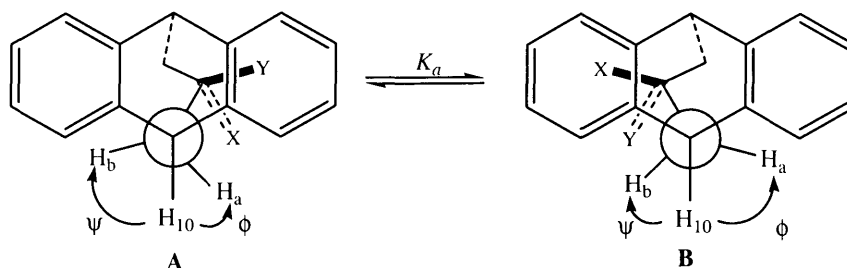
Scheme 60 Newman projection of the conformers **A** and **B**

If the conformer A predominates, the dihedral angle ψ would be larger than $60°$ giving $^3J_{10\text{-}11a} > {}^3J_{10\text{-}11b}$ from the Karplus equation. If the other conformer predominates, ϕ would be larger than $60°$ leading to $^3J_{10\text{-}11a} < {}^3J_{10\text{-}11b}$.

Theoretical calculations, performed by Dr. A. Aliev, have been used to predict the dihedral angles ϕ and ψ in this framework (Figure 61) and the results are given in more detail within the appendix for better coherence.
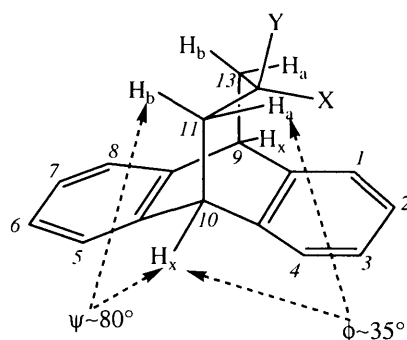
Figure 61 Dihedral angles of the series of derivatives **66**

Thus, the overall range of dihedral angles ϕ and ψ has been estimated to be $32\text{-}42°$ and $75\text{-}81°$ respectively (See Appendix 1) and are directly associated with the values of the coupling constants $^3J_{10\text{-}11a}$ and $^3J_{10\text{-}11b}$ for one conformer.

2.3.1.2 - Determination of the predominant conformer by NOE measurements

The nuclear Overhauser effect is a convenient method to determine the through space proximity of two nuclei. Its magnitude, called the NOE enhancement, is not dependent on the connectivity of the two nuclei but only on the internuclear distance r.[213] The NOE enhancement η is proportional to r^{-6}. As a result, the magnitude of NOE decreases suddenly on increasing the distance and therefore, it is a short-range effect. Furthermore, NOE enhancement exhibits the spatial arrangement of the molecule generated by the presence of intra- or intermolecular interactions. This NMR experiment can be important in determining the geometry of conformers in a rapidly exchanging mixture. The magnitude for the signal of each conformer reflects its spatial arrangement and is proportional to the population of the conformer in solution.

For example, selective excitation of the substituent $X = CH_3$ generated enhancements η_a and η_b on the protons H_{11a} and H_{11b}, respectively. The distances between the substituent X and H_{11a} and H_{11b}, r_a and r_b respectively, were estimated by gas phase optimised geometries for each derivative in both conformations and the results are reported in Appendix 2. However, the fast rotation of the methyl group of tertiary alcohol 78 along the $C_{12}-C_{Me}$ bond leads to an averaged position for the methyl protons corresponding of the averaged position H* and the approximative distances r_a and r_b for each conformer are reported in Figure 62.
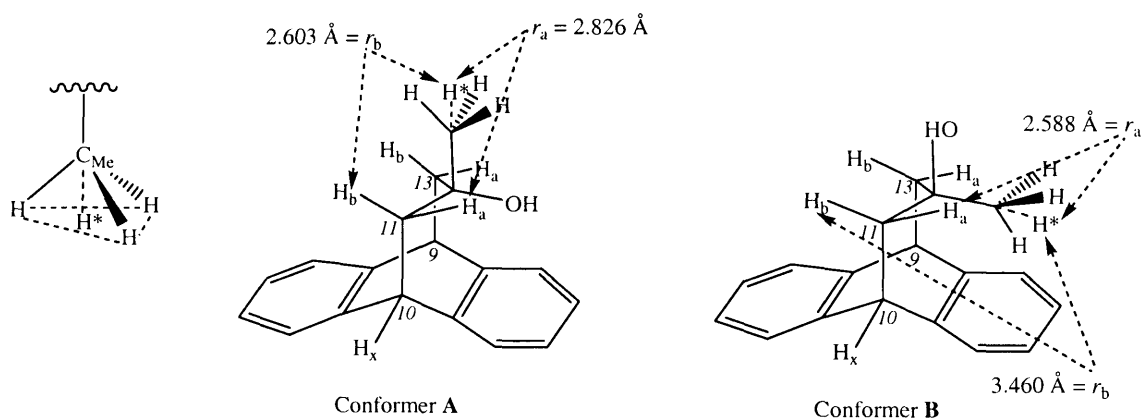
Figure 62   Determination of the averaged position H* and distances between the substituent on C_{12} and the bridgehead protons in the two conformations of 78

An example of NOE enhancement is shown in Figure 63 for the alcohol **78** after selective excitation at the frequencies of the signal corresponding to the methyl protons.
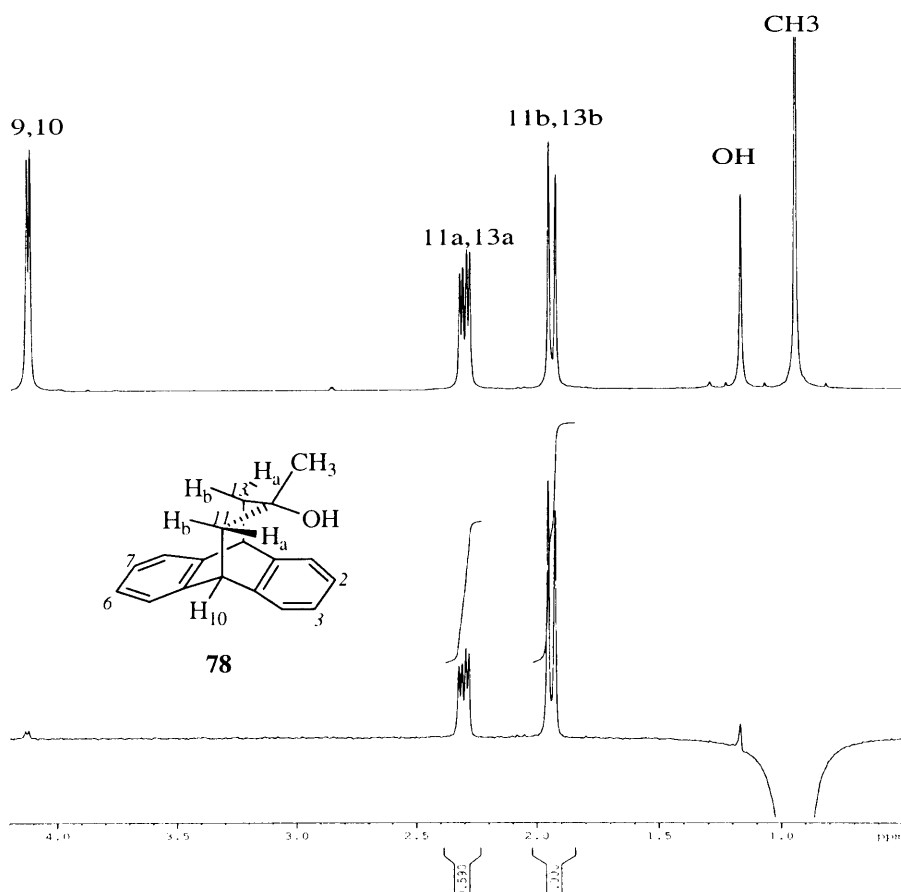
Figure 63   Top: ^{1}H NMR spectrum of **78** in CDCl$_3$ at 298 K. Bottom: selective NOE spectrum of **78** in CDCl$_3$ at 298 K.

Using the initial rate approximation,[213] the experimental enhancement ratio (η_a/η_b) leads to the determination of the predominant conformer by the equation:

$$\frac{\eta_a}{\eta_b} = \left(\frac{r_a}{r_b}\right)^{-6}$$

<div align="right">Equation (2)</div>

To illustrate the use of Eq (2), the enhancement ratio for protons H$_A$ and H$_B$ (η_A/η_B) was experimentally found to be 0.59 on the selective NOE spectrum (Figure 63). For the conformer **A** in which the hydroxy group lies above the aromatic ring, the distance ratio $(r_a/r_b)^{-6}$ was estimated to be 0.61 and agrees well with the experimental enhancement ratio,

<div align="center">= 112 =</div>

whereas the distance ratio for the conformer **B** was 5.71. Thus, the NOE experiment is an efficient method to determine the predominant conformer by comparison between the experimental and calculated enhancement ratios.

2.3.1.3 - Determination of the conformational populations using the coupling constants between the protons on the central bridge in $CDCl_3$ solutions

The coupling constants between the protons at the bridgehead, H_9 and H_{10}, and those on the bridge, H_{11} and H_{13} can give direct access to the population of each conformer **A** and **B** in solution, if the boundary coupling constants, $^3J_{10\text{-}11a}$ and $^3J_{10\text{-}11b}$, for both conformers are known. These boundary values are the coupling constants found for one conformer in solution. Thus, as the motion of the bridge is a fast process on the NMR time scale, conformational equilibrium induces the presence of both conformers in solution, and therefore, only average chemical shifts and coupling constants are observed in the NMR spectra. An exact measurement of these constants for each conformer was not possible due to conformational equilibria but estimation can be made due to the similarity in the framework of each compound. The largest coupling constants for **A** equals the smallest in **B** and the converse also applies as the result of the symmetry of the framework (Scheme 61).

| $^3J_{10\text{-}11a}$ | $=$ | $^3J_{10\text{-}11b}$ |
| $^3J_{10\text{-}11b}$ | $=$ | $^3J_{10\text{-}11a}$ |
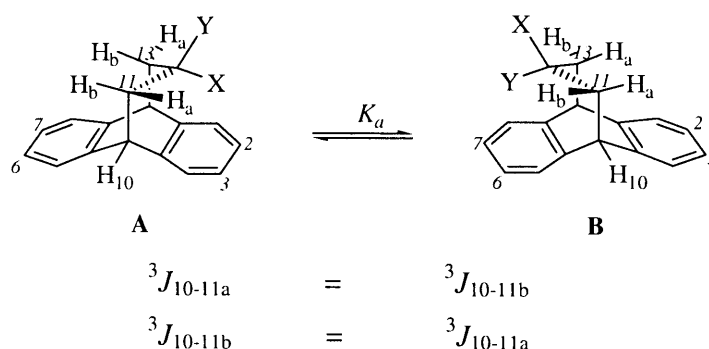
Scheme 61

The calculated boundary values, were found to be $^3J_{10\text{-}11a} = J_L = 7.3$ Hz when X is directed towards the aromatic ring, and $^3J_{10\text{-}11a} = J_S = 1.1$ Hz when X is away from the ring (See Appendix 1). Coupling constants, $^3J_{10\text{-}11a}$ and $^3J_{10\text{-}11b}$, for the disubstituted derivatives

are dependent on the dihedral angles ϕ and ψ and also on the electronegativity of the substituent. The electronegativity of the substituents in the series of derivatives synthesised is comparable, but this approximation cannot be validated for the presence of a fluorine or a hydrogen atom as the substituent. Therefore, the values of J_L and J_S for the derivatives with X =H are 7.9 Hz and 0.9 Hz respectively.

The population of the conformer **A**, for each derivative is called, P_A and that for the conformer **B** (P_B) is 1-P_A. For clarity, these conformation ratios will be given as percentages and, therefore $P_B = 100 - P_A$. Thus, the values for coupling constant between H_{10} and H_{11a} can be calculated from the following equation[139]:

$$^3J_{10,11a} = \frac{P_A}{100}.J_L + \left(1 - \frac{P_A}{100}\right).J_S \quad \text{and} \quad ^3J_{10,11b} = \frac{P_A}{100}.J_S + \left(1 - \frac{P_A}{100}\right).J_L \qquad \text{Equations (3) and (4)}$$

Where:

P_A the proportion of time spent in the conformer A

J_L the coupling constant between the protons H_{10} and H_{11a} in the conformer A

J_S the coupling constant between the protons H_{10} and H_{11a} in the conformer A

$^3J_{10-11a}$ the observed average coupling constant between the protons H_{10} and H_{11a}

$^3J_{10-11b}$ the observed average coupling constant between the protons H_{10} and H_{11b}

Consequently,

$$P_A = \frac{(J_L - {}^3J_{10,11b})}{(J_L - J_S)} \times 100 = \frac{({}^3J_{10,11a} - J_S)}{(J_L - J_S)} \times 100 \qquad \text{Equation (5)}$$

Furthermore, the equilibrium constant K_a can be directly calculated from the proportion of time spent in the conformer **A** by the equation (6):

$$K_a = \frac{P_A}{100 - P_A} \qquad \text{Equation (6)}$$

From equation (5), the sum of the coupling constants $^3J_{10-11a}$ and $^3J_{10-11b}$ are approximately equivalent to the sum of the boundary values J_L and J_S providing an internal check in the system studied. Therefore, the variation in the electronegativity of the substituent, as well as its orientation relative to the coupled proton pairs, does not have an effect on $(J_L + J_S)$ for a series of propanoanthracenes with the same framework. Assuming that the boundary values J_L and J_S are accurate within ±0.3 Hz, the error of the population measurements is estimated as ±5%. The agreement between the population values calculated using two

different $^{3}J_{10\text{-}11a}$ and $^{3}J_{10\text{-}11b}$ couplings for each compound is within 0-2%. In the case of the derivative **94**, $^{3}J_{HF}$ couplings are also used, and these vary over a significantly larger range of values than $^{3}J_{10\text{-}11a}$ or $^{3}J_{10\text{-}11b}$ providing a better accuracy for population estimated.

With a method to determine the conformational ratio now established, the free energy difference $\Delta G°$ at a given temperature can be calculated according to the following equation (5):

$$\Delta G° = -RT \ln K_a \qquad \text{Equation (5)}$$

$\Delta G°$ Free energy difference between conformers $(J.mol^{-1})$

R Universal gas constant $(R = 8.314 \ J.K^{-1}.mol^{-1})$

T Temperature (K)

K_a equilibrium constant determined from the conformational ratio

2.3.1.4 – Temperature dependence

Varying the temperature is another technique of generating perturbation in the conformational equilibria by slowing down the motion of the bridge and consequently increasing the lifetime of conformers on the NMR time scale. Initially, ^{1}H NMR studies at low temperature were attempted to determine the major conformer by reaching the slow exchange limit, but only the time averaged picture was observed until reaching the freezing point of the solvent. Nevertheless, conformational ratios and chemical shifts of the substituents are significantly affected by the change of temperature and enable the confirmation, and even the determination, of the more stable conformer of some derivatives. As with the coupling constants, the observed chemical shifts reflect the protons of the conformational balance and are an average between the theoretical chemical shifts of the protons of the conformer **A** and those of the conformer **B**, and consequently modifying the conformational ratio of one derivative affects the chemical shifts of the protons on the bridge and the substituents X and Y. The benzene ring current effect increases the electron density on the substituent directly above the π-system compared to that on the other conformer, thus the chemical shift of the substituent directed towards the aromatic ring would be upfield in comparison to its chemical shift in the other conformer. Since accurate determination of the theoretical chemical shifts of the protons of X and Y in each

conformer **A** and **B** is not possible, a less direct method based on temperature dependence would enable a significant modification of the conformational ratio by increasing the time spent in one of the conformers. The following case histories are illustrative.

2.3.1.4.1 – Effects of temperature on the conformational equilibrium of the ether 84

A relevant example to illustrate the effects of temperature gradient on the conformational ratio and chemical shifts is that of ether **84** at low temperatures. At ambient temperature, its conformational ratio is 70:30 in $CDCl_3$ and the Table 12 reports the ^1H NMR spectrum data of **84** at different temperatures in a 4:1 mixture of $CFCl_3:CD_2Cl_2$ while the ^1H NMR spectra are provided in Appendix 3.

84
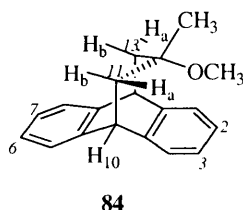
Figure 64

Temp. (K)	Δδ (ppm)				$^3J_{10-11a}$ (Hz)	$^3J_{10-11b}$ (Hz)	Ratio
	H_{11a}	H_{11b}	OCH_3	CH_3			
293	0.00	0.00	0.00	0.00	5.2	2.7	70:30
273	0.01	-0.02	-0.01	0.01	5.5	2.6	73:27
253	0.01	-0.04	-0.03	0.02	5.6	2.4	76:24
233	0.02	-0.06	-0.05	0.04	5.8	2.0	81:19
213	0.04	-0.08	-0.07	0.05	6.0	1.5	86:14
193	0.05	-0.10	-0.09	0.08	6.4	n/a	(85:15)[a]

[a] As the smallest coupling constant could not been measured in the ^1H NMR spectrum, the ratio is calculated from the biggest coupling constant and therefore is less accurate.

Table 12 Difference of chemical shifts from room temperature to the mentioned temperature and vicinal couplings of the ether **84** in $CFCl_3:CD_2Cl_2$ (4:1)

The conformational ratio is therefore dependent on the temperature as the major conformer becomes more populated on cooling, but the broadness of the signals of the protons H_{11a} and H_{11b} below 193 K impedes the accurate determination of the coupling constants $^3J_{10-11a}$ and $^3J_{10-11b}$. Another interesting effect of temperature is the shift of the NMR signals of the

protons of the substituents, as well as that of H_{11b}. The chemical shift of the signal of the protons of the methoxy group is slightly shifted upfield ($\Delta\delta_{OMe}$ = -0.09 ppm) at 193 K compared to the values at room temperature and this demonstrates the increase in time spent in this conformation with the methoxy group above the aromatic ring. In this conformer, the electron density of the protons of the methoxy group is enriched by the benzene ring current effect in comparison to their electron density in the other conformer. Since $\Delta\delta_{Me}$ is positive (+0.08 ppm), the population of the conformer bringing the methyl group spatially close to the aromatic ring becomes less populated on decreasing the temperature and corroborates the results obtained for the other substituent. Intriguingly, the variation in $\Delta\delta_{11a}$ is less significant than in $\Delta\delta_{11b}$ as the time spent in the more stable conformer increases. This observation can be explained by the geometry of the bridge in each conformer.
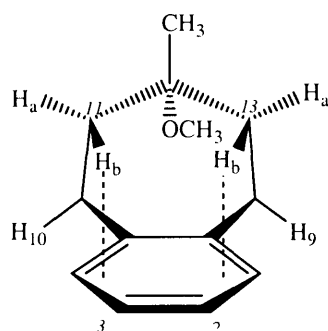
Figure 65   Structure of the major conformer of ether **84** with the methoxy group sitting above the aromatic ring. The protons H_b are affected by the close proximity to the π-system

As depicted in the Figure 65, the proton H_{11b} is relatively close to the aromatic ring in the major conformer and therefore a significant negative $\Delta\delta_{11b}$ is to be expected. Moreover, due to the orientation of the proton H_{11a}, the contribution of the aromatic system to the electron density of H_{11a} is fairly similar in both conformations. Therefore, the temperature dependence of the conformational equilibria and comparison of the chemical shifts of the protons of the substituents at various temperatures provides a further tool in the determination of the conformational equilibria.

2.3.1.4.2 – Studies of the propargylic alcohol **81** at low temperatures

On cooling, the population of one conformer increases from 52% at room temperature to 87% at 203 K along with a noteworthy upfield shift for the signal of the alkyne proton (Table 13 and appendix 4).

81
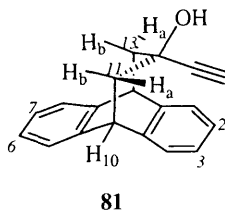
Figure 66

Temp. (K)	$\Delta\delta_{C\equiv CH}$ (ppm)	$^3J_{10\text{-}11a}$ (Hz)	$^3J_{10\text{-}11b}$ (Hz)	Ratio
253	-0.09	4.3	3.8	54:46
233	-0.28	4.9	3.4	62:38
223	-0.50	5.4	2.7	72:28
213	-0.76	6.1	2.1	82:18
203	-0.99	6.4	1.8	87:13
193	-1.18	6.2	n/a	n/a
183	-1.35	6.0	n/a	n/a

Table 13 Difference of chemical shifts of the signal of the alkyne proton and conformation ratio of **81** at various temperatures in $CFCl_3$:CD_2Cl_2 (4:1)

Although the negative $\Delta\delta_{C\equiv CH}$ at 183 K would indicate that the predominant conformer at this temperature would bring the alkyne proton spatially close to the aromatic system, comparison of $\Delta\delta_{C\equiv CH}$ with $\Delta\delta_{OMe}$ obtained for the ether **84** highlights the limits of accuracy of this method. Indeed, for a decrease of 100 K, $\Delta\delta_{C\equiv CH}$ is considerably larger than $\Delta\delta_{OMe}$ (-1.18 and -0.09 ppm respectively) and this large upfield shift may be induced by another phenomenon, such as the formation of an intermolecular C-H/π hydrogen bond which may enable the alkyne proton to lie closer to an external aromatic system. Therefore, low temperature studies alone cannot determine the structure of the predominant conformer of **81** and further analytical methods are required.

2.3.1.4.3 – Behaviour of aziridine 121 at low temperatures

The ^{1}H NMR spectrum of aziridine **121** exhibits an interesting feature on cooling due to the presence of the lone pair of electrons on the nitrogen atom. At 173 K, the signals of each proton adjacent to the nitrogen split into two as, at this temperature, the two protons of the CH_2 groups become inequivalent (Figure 68). This inequivalence arises as the fast inversion of the lone pair of electrons is and therefore this temperature corresponds normally to the coalescence temperature of the nitrogen inversion.

121
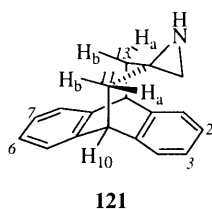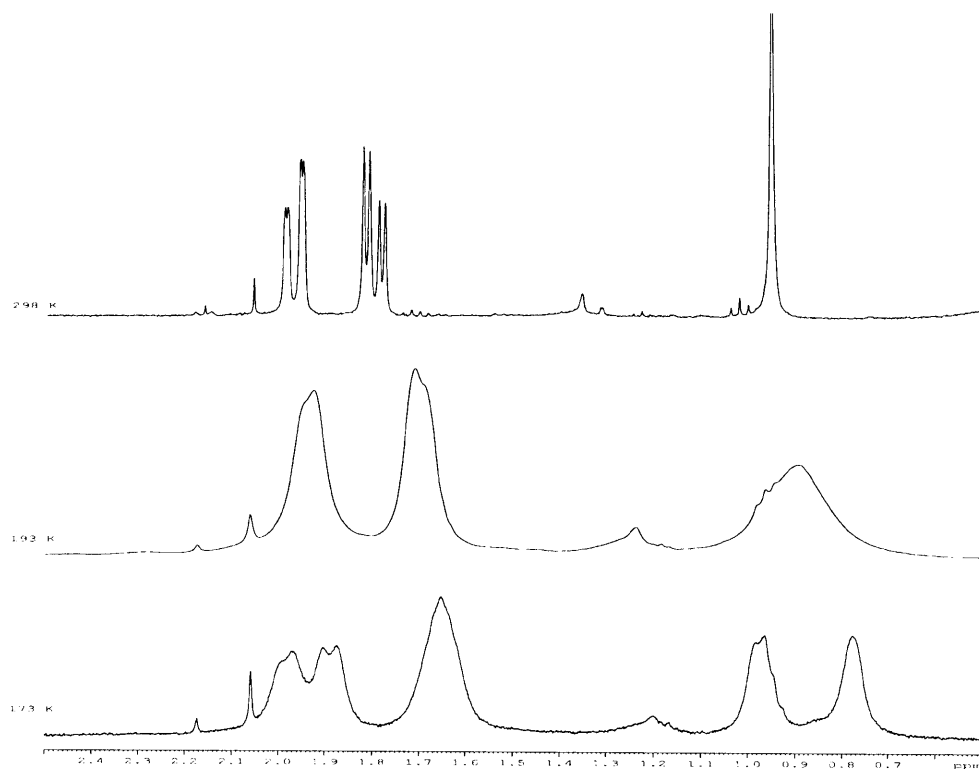
Figure 67

Figure 68 ^{1}H NMR spectra of aziridine **121** at low temperatures

= 119 =

Within the series of nitrogen-containing derivatives studied, the inversion barrier was reached only for **121**, presumably due to the strain within the spiro ring. From the literature, the interconversion energy of an aziridine has been reported to be much higher than that of azetidine or ammonia.[214] These energies have been estimated to be 79.9, 21 and 24.1 kJ.mol^{-1} respectively by *ab initio* MO calculations and dynamic ^{1}H NMR at 154 K. By way of comparison, the ^{1}H NMR spectrum of azetidine **130** did not demonstrate this phenomenon and this inversion at 173 K can be explained by the significant energy difference for inversion between the aziridine and azetidine.

2.3.2 – X-Ray studies

2.3.2.1 – Intermolecular interactions in the crystal structure of alcohol 78

Throughout our work, it was always of interest, when possible, to compare behaviour in the solid state with that in solution, particularly in view of the prevalence of crystallographic data based mining for the detection of non-covalent interactions. Once again, some relevant cases are outlined below. In the solid state, alcohol **78** exists in one only conformer, *i.e.* with the methyl group above the aromatic ring and the structure also exhibits two types of intermolecular interactions. The O-H proton of one molecule participates in a hydrogen bond with the oxygen atom of the hydroxy group of a second molecule, whereas the O-H proton of this second molecule takes part in an O-H/π interaction with the aromatic ring of a third molecule (Figures 69 and 70). Surprisingly, alcohol **78** exists in this conformer in the crystalline state, whereas NOE enhancement experiments in solution proved the predominance of the other conformer, in which an intramolecular O-H/π interaction occurs. This noteworthy result will be discussed in-depth in the following section. With conventional hydrogen bonding, the distance and the angle between the two hydroxy groups, found to be 1.85 Å and 161.2°, are comparable to the hydrogen bonding in water (1.88 Å and 162°).
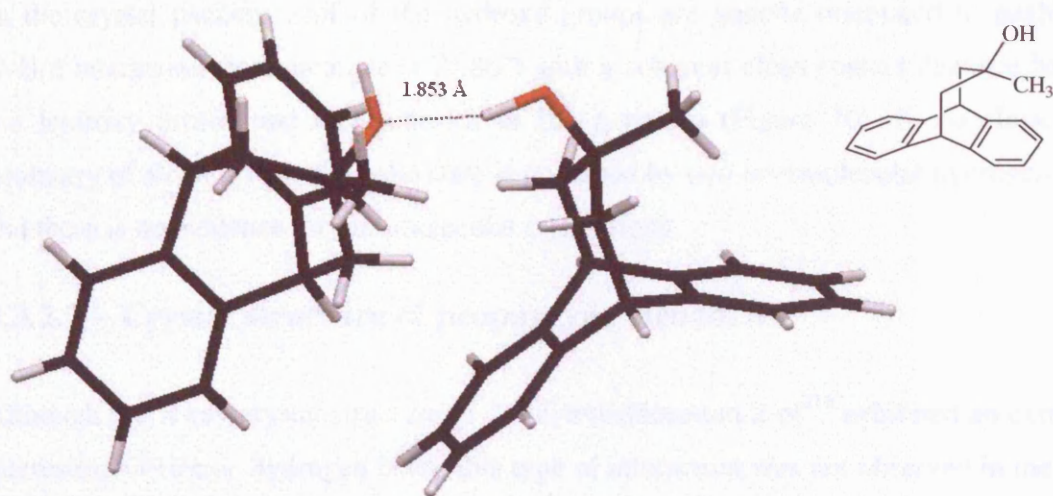
Figure 69   Crystal structure of alcohol **78** which presents a conventional hydrogen bonding between two hydroxy groups
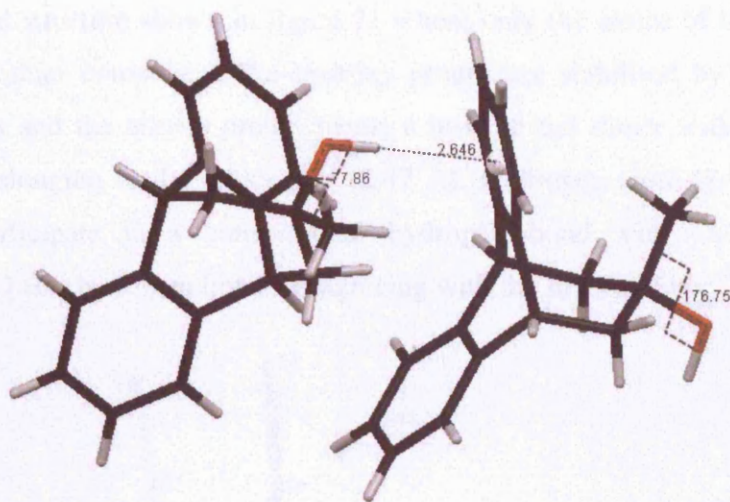
Figure 70   Intermolecular O-H/π hydrogen bonding

Furthermore, the O-H•••π-centre distance in the latter intermolecular interaction is less than 2.69 Å. In their *ab initio* studies of the water-benzene dimer, Tsuzuki and co-workers[79] determined the O-H•••π-centre distance in the monodentate complex, in which its geometry is comparable to the orientation of the hydroxy group towards the aromatic ring in our crystal structure of **78**, to be 3.4 Å. The significant difference in distance between the theoretical and experimental values may be explained by the fact that the hydroxy group is involved in two hydrogen bonds and the oxygen atom therefore becomes electron deficient.

In the crystal packing, half of the hydroxy groups are *gauche* orientated to enable this O-H/π interaction (torsion angle = 77.86°) with a coherent close contact distance between the hydroxy proton and the centroids of the π-system (Figure 70). In conclusion, the geometry of alcohol **78** in the solid state is governed by two intermolecular hydrogen bonds and there is no evidence for intramolecular interactions.

2.3.2.2 – Crystal structure of propargylic alcohol 81

Although the X-ray crystal structure of 2-ethynyladamantan-2-ol[215] exhibited an extremely interesting O-H/$\pi_{C\equiv C}$ hydrogen bond, this type of interaction was not observed in the X-ray structure of the propargylic alcohol **81**. Thus, the structure determination of the propargylic alcohol **81** revealed a disordered arrangement in which the substituents of the flexible bridge adopt two different geometries. The major component, present in a 70:30 ratio was the fully bonded structure shown in figure 71 where only the atoms of the minor part are shown. In the minor component, the hydroxy groups are stabilised by the formation of hydrogen bonds and the alkyne proton forms a head to tail dimer with lone pair of the oxygen atom belonging to the major unit (2.47 Å). Hydrogen atom H_1' is preferentially oriented to participate in a conventional hydrogen bond with O_1' rather than in intramolecular O-H/π hydrogen bonding, agreeing with the rules of Etter.[86]
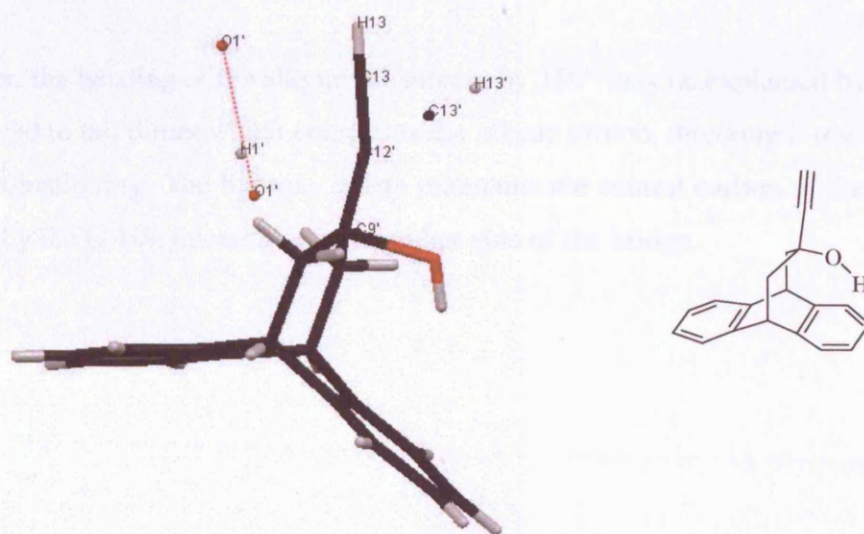
Figure 71   Disordered crystal structure of **81**. Only the atoms of the minor component are shown

Although two disordered components are observed in the crystalline state, they correspond to only one geometry of the two possible conformers. Both exhibit the hydroxy group directed towards the aromatic ring whilst the alkyne group tends to be oriented in favour of an intermolecular interaction.

The major component is present as a dimer in the unit cell and is stabilised by the contributions of both intra- and intermolecular interactions, O-H/π and C-H/π hydrogen bonds respectively (Figure 72).
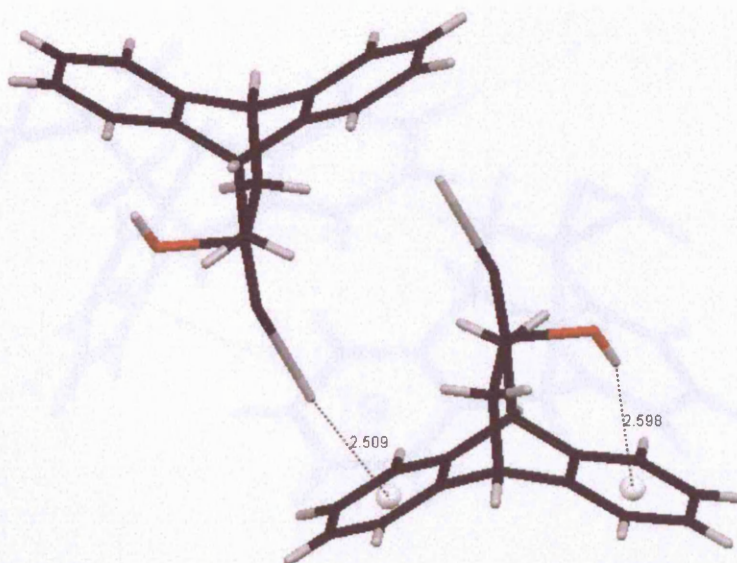
Figure 72 Crystal structure of the propargylic alcohol **81**

Moreover, the bending of the alkyne substituent by 159° may be explained by the formation of this head to tail dimer which constrains the alkyne proton, directing it towards the centre of the aromatic ring. The hydroxy group maintains the central carbon of the bridge in this position by the O-H/π interaction on the other side of the bridge.

2.3.2.4 – Crystal structure of epoxide 86

The conformer of the epoxide **86** with the oxygen atom directed away from the aromatic ring is the only conformation in the solid state. However, this structure does not exhibit any obvious close contacts between two molecules of **86** and therefore neither any inter- nor intramolecular interactions can justify the stabilisation of this conformer.
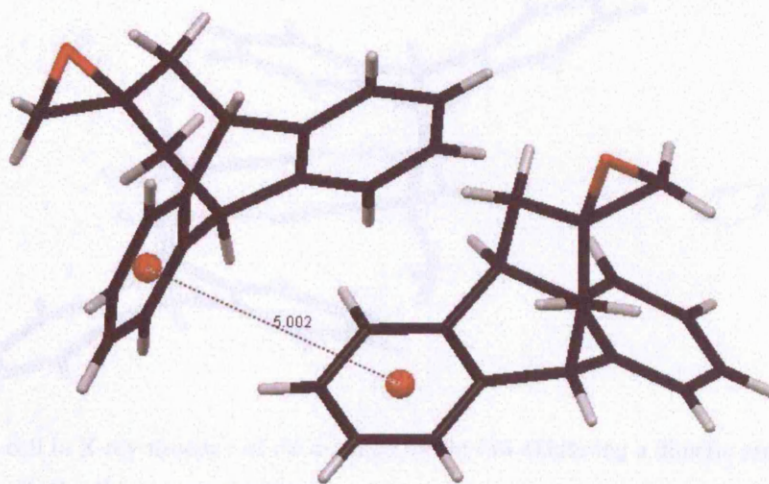
Figure 73   Crystal structure of the epoxide **86**

Although the stacking of molecules in the crystalline state enables intermolecular π-π interactions to occur in a displaced T-shaped geometry with a distance of 5.00 Å between the two aromatic centroids, which compares with that calculated for the benzene dimer in this particular stacking (5.10 Å).[6] Nevertheless, this close contact does not explain the crystallisation of the epoxide **86** as only one conformer since this interaction does not involve the flexible bridge.

2.3.2.2 – Intra- and intermolecular interactions in the crystal structure of α-amino nitrile 116

In similar fashion to the crystal structure of the alcohol **78**, only one conformer of the α-amino nitrile **116**, where the cyano group is directed towards the aromatic ring as illustrated in Figure 74, is observed by single crystal X-Ray diffraction.
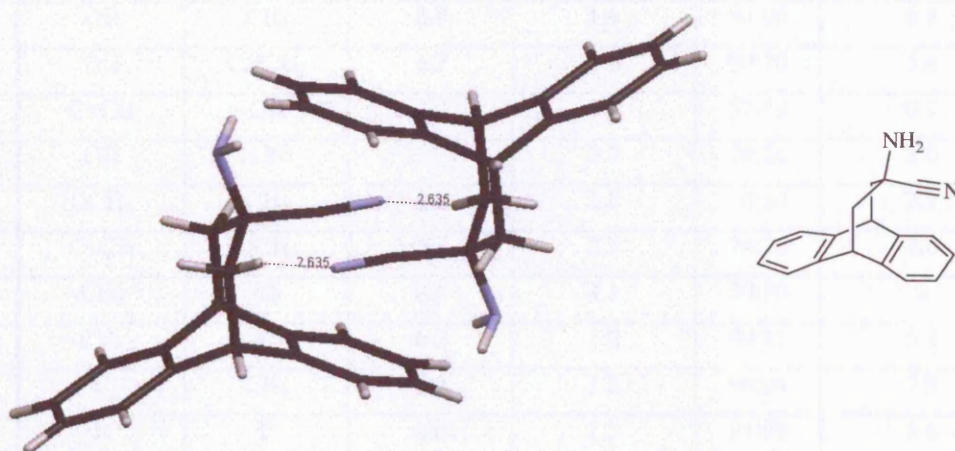
Figure 74   Unit cell in X-ray structure of the α-amino nitrile **116** exhibiting a dimeric arrangement stabilised by intermolecular C≡N•••H hydrogen bonding

The crystal structure of **116** in the unit cell exhibits a dimeric arrangement in which there is the formation of a hydrogen bond between the bridge proton, H_{11a}, and the nitrogen atom belonging to the cyano group. Desiraju reported the H•••O distance to be 2.59 Å in the C-H•••O hydrogen bond,[216] a value comparable to the distance obtained for the C≡N•••H intermolecular interaction. Furthermore, formation of this hydrogen bond in the solid state is supported by the C-H•••N angle of 168.4°, which corresponds well to the expected 180° angle for hydrogen bonds. Another interesting feature is the slight bending of the C-C≡N bond, which is also predicted by the geometric optimisation for a single molecule, indicating that this bending is not caused by crystal packing but rather by intramolecular interactions. This can be a result of the repulsive effects between the aromatic ring and the lone pair of the nitrogen. Therefore, the conformation of α-amino nitrile **116** in the solid state is governed by the contribution of multiple interactions, both attractive and repulsive.

Using these methods, the structures of the predominant conformers and conformational ratios have been determined for a series of propanoanthracene derivatives and the results are reported in Table 14.

	X-down	Y-up	$^3J_{10\text{-}11a}$ (Hz)	$^3J_{10\text{-}11b}$ (Hz)	P_A	ΔG° (kJ.mol^{-1})
77	H	OH	7.3	1.1	93:07	6.4
78	OH	CH_3	6.8	1.4	94:06	6.8
79	OH	$CHCH_2$	6.7	1.6	90:10	5.4
81	C≡CH	OH	4.2	3.9	52:48	0.2
83	OH	CN	5.7	2.7	74:26	2.6
84	OCH_3	CH_3	5.2	2.8	70:30	2.1
85	C≡CH	OCH_3	5.7	2.7	74:26	2.6
86	$-CH_2-$	-O-	4.1	4.1	50:50	0
87	$-CH_2-$	-O-	6.7	1.8	89:11	5.2
94	F	CH_3	6.2	1.8	96:04	7.9
96	H	F	6.0	1.5	91:09	5.6
103	NH_2	CH_3	6.0	2.3	79:21	3.3
116	CN	NH_2	7.0	1.2	96:04	7.9
117	NH_3Cl	CH_3	6.0	2.0	~82:18	~3.7
121	$-CH_2-$	-NH-	5.3	3.0	68:32	1.9
128	$-CH_2-$	-NH-	5.1	3.0	71:29	2.2
130	$-CH_2-$	-NH-	4.8	3.4	61:39	1.1
139	OH	CH_3	6.6	1.4	92:08	6.1
140	OH	CH_3	6.9	1.3	95:05	7.3

Table 14 Equilibrium Ratios, experimental coupling constants and Energy Differences between conformers of the propanoanthracenes in $CDCl_3$ at 298 K. Concentration C = 1-2 mg.mL^{-1}

Interestingly, concentration effects have been studied for the propargylic alcohol **84** in $CDCl_3$ and $C_6D_5\text{-}CD_3$ from 2 to 10 mg.mL^{-1} and no trace of formation of the dimer has been observed in any solvent.

The conformational ratios and the predominant conformers cannot be determined by using only one method and combination of these methods are required to elucidate the exact structures of the conformational balances. Moreover, several possible interpretations of the results obtained may arise due to the complexity of the systems studied. This will be

discussed in the following section, where Table 14 will also be analysed, and comparison of these results will be done to give the relative magnitudes of the different π-hydrogen bonds.

2.4 – Relative strengths of functional group-arene interactions in a series of propanoanthracene derivatives in $CDCl_3$ solution

2.4.1 – Introduction

The primary goal of this work is to gain insight into the relative magnitude of various intramolecular non-covalent π-interactions occurring in a series of propanoanthracene derivatives by determining the conformational equilibria. However, the stabilisation of one conformer over the other is a complex phenomenon in which numerous interactions also play crucial roles. As discussed in the introductory chapter, direct experimental investigations into such π-interactions cannot be carried out, and therefore, many research groups have circumvented this limitation by studying the behaviour of a molecular system through systematic variation of changing one parameter. Although our conformational balance has been designed to limit interference from other interactions on the equilibrium, dominant intermolecular interactions such as solvation effects, cannot be neglected and are, in fact of vital significance (vide infra). Indeed, the conformational equilibrium is inevitably affected by interactions between the substituents on the bridge and the solvent, since any attractive intermolecular forces between the solvent and a functional group could compete with a π-interaction. Although we have selected substituents on the bridge that would have comparable steric hindrance, the difference in van des Waals radii between these constituents can also cause interactions affecting the conformational equilibrium. Measurement of the conformational ratio has been obtained under comparable conditions of solvent and temperature for a series of derivatives, but these results cannot be attributed exclusively to the effects of the intramolecular π-interactions since many other forces are involved. Thus, there is a great challenge in calculating accurate binding energies. However, in this section, attempts have been made to provide quantitative data and to compare the conformational ratios of the series of derivatives reported in Table 14. From

examination of Table 14, the first interesting feature is the free energy difference between the two possible conformers which was estimated to be greater than 8 kJ.mol^{-1} at 298 K.

2.4.2 – Alcohol and ether derivatives – The importance of the O-H/π interaction

As we have seen, the assistance of the π-facial hydrogen bond between a hydroxy group and an aromatic ring is now a well established non-covalent interaction. For this reason, it was of particular interest to prepare a series of alcohol and ether derivatives within the propano-bridged anthracene system.

The population of the predominant conformer of the secondary alcohol **77** is 93% in solution. Previously, another member of our group[139] established that the structure of this major conformer is such as the hydrogen atom is positioned above the aromatic ring and this conformation agrees well with the results calculated in gas phase. Stabilisation of this conformation arises from the significant steric difference between the hydrogen atom and the hydroxy group as substituents on C_{12} as the formation of a hydrogen bond in the other conformation would not be strong enough to compensate for the difference in the van der Waals radius.

Conformational ratio
93:7

77
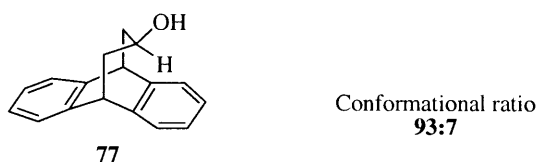
Figure 75   Representation of the predominant conformation of **77** in CDCl$_3$ solution

Although, stabilisation of the other conformer by π-hydrogen bonding in **77** or by electron repulsion between the fluorine atom and the electron rich aromatic centre in **94** can be expected, steric effects govern the stabilisation of one conformer over the other for these two derivatives.

One predominant conformer (> 90%) was also observed for tertiary alcohols **78, 79, 139** and **140** and NOE enhancements proved that the hydroxy group was directed towards the aromatic ring in this series of alcohols.

78

Conformational ratio
94:6

79

Conformational ratio
90:10

139

Conformational ratio
92:8

140

Conformational ratio
95:5
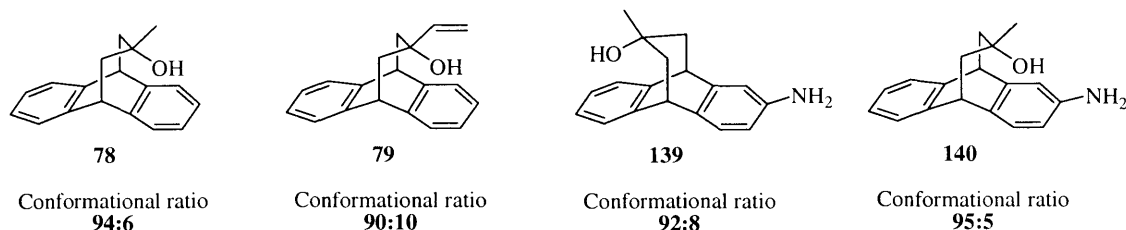
Figure 76   Representation of the predominant conformation of tertiary alcohols **78, 79, 139** and **140** in CDCl$_3$ solution

Stabilisation of the preferential orientation cannot be attributed exclusively to steric effects of an oxygen atom having a smaller van der Waals radius compared to that of the alkyl group, as an additional O-H/π interaction can significantly contribute to the stabilisation of this conformer.

The conformational ratios of derivatives **78** and **79** are 94 and 90% respectively with the hydroxy group orientated towards the aromatic ring (Figure 76) whereas both conformers of propargylic alcohol **81** are almost equally populated (52%). Initially, these alcohols were synthesised to investigate the effects of the hybridized orbitals of the carbon atom of the substituent on the conformational equilibria and resulted in showing that the ratio decreases on increasing the degree of insaturation of the carbon. Interaction energy of the ethylene-benzene complex has been calculated to be greater than 8.6 kJ.mol^{-1} in its optimised geometry.[41] Although free rotation of the vinyl group along the C$_{12}$-C$_{vinyl}$ bond can bring the terminal vinylic proton above the aromatic ring (Figure 77).

79
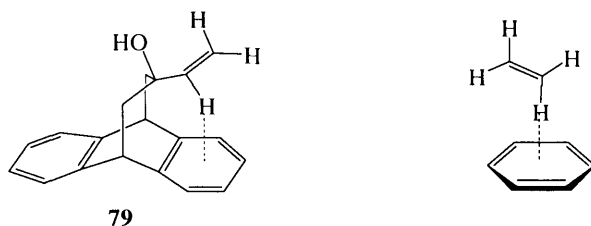
Figure 77   Less stabilised conformer of the tertiary alcohol **79** exhibiting a C-H/π interaction and comparison of its geometry with that of the ethylene-benzene complex

This conformer is far from being favoured as shown by the conformational ratio indicating a large preference for the other geometry. Thus, this C-H/π hydrogen bonding is not as strong as the O-H/π interaction occurring in the other conformation. However, the conformation ratio of **79** is slightly smaller than that of the methyl analogue **78** although a vinyl group is significantly larger than a methyl group and, therefore, the C-H/π interaction may be sufficiently strong to compensate for the difference of steric bulk between a vinyl and a methyl group and to slightly reduce the conformational ratio compared to that of **78**. The energy of interaction in the methane-benzene complex has been estimated to be smaller than that of the ethylene-benzene dimer (7.6 kJ.mol^{-1}) supporting our experimental observations.

The conformational ratio of the propargylic alcohol **81** is an exciting result since both conformers are equally populated in solution, demonstrating that the strength of the O-H/π interaction can be effectively counterbalanced by the terminal alkyne.

Conformational ratio
52:48

81
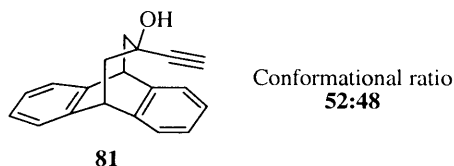
Figure 78   Representation of the predominant conformation of tertiary alcohols **78**, **79**, **139** and **140** in CDCl$_3$ solution

The ^{1}H NMR spectra of propargylic alcohol **81** was studied at low temperatures and the upfield shift of the signal of the alkyne proton on cooling was initially attributed to the spatially close presence of the aromatic ring. However, the X-ray crystal structure showed the formation of a dimer stabilised by intermolecular C-H/π hydrogen bonding between the alkyne proton and the aromatic system of the second molecule. Thus, based on the anisotropy of the ring current effect, formation of this intermolecular interaction may cause the significant upfield shift of the signal of the alkyne proton on cooling rather than the increase of time spent in the other conformer. Therefore, the predominant conformer at low temperature may well be dimeric species observed in the solid state, _i.e._ with the hydroxy group interacting with the aromatic ring and the alkyne group oriented towards the aromatic

ring of another molecule. Comparison of the results obtained in the solid state and solution leads to the conclusion that the behaviour of **81** in the solid state cannot be extrapolated to the solution case, and conversely.

The 93:7 conformational ratio of secondary alcohol **77** in favour of the hydrogen atom being above the aromatic ring demonstrates that the O-H/π hydrogen bond is not as strong as the influence due to the difference in van der Waals radii of the substituents and therefore highlights the relative weakness of this interaction. However, further evidence for the existence of this interaction can be demonstrated by comparison of the equilibrium ratios of the tertiary alcohol **78** with the methyl ether derivative **84**. Replacing the hydrogen of the hydroxy group of **78** by a methyl group, as in **84**, decreased the population from 94 to 70%, indicating that the favoured conformation of **78** is partially stabilised by the formation of intramolecular O-H/π interactions.

Conformational ratio
94:6

78

Conformational ratio
70:30

84

Conformational ratio
52:48

81

Conformational ratio
74:26

85
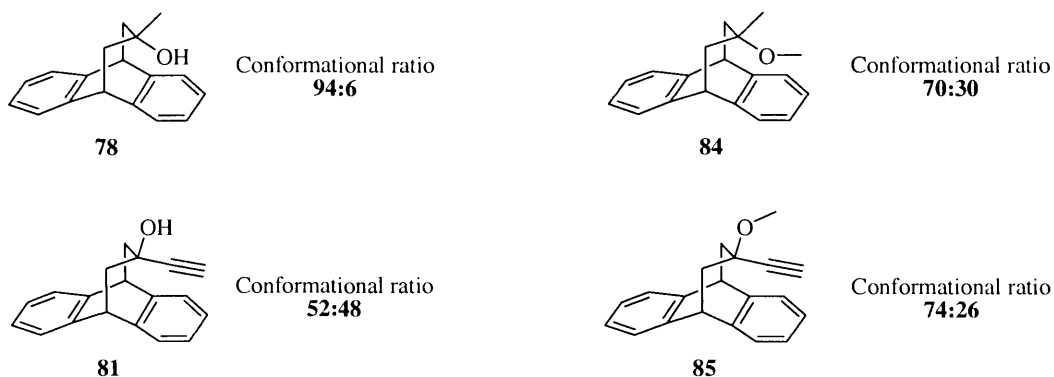
Figure 79   Representation of the predominant conformation of ethers **84** and **85** in CDCl$_3$ solution and comparison with the corresponding alcohols **78** and **81** respectively

However the conformer of **84** with the methyl group above the aromatic ring might be expected to be the major conformer on simple steric arguments. Free rotation around the C$_{12}$-O and O-CH$_3$ bonds, with C$_{12}$ as the centre carbon atom of the flexible bridge, can of course occur and can enable the terminal protons of the methoxy group to become closer to the centre of the ring than those of the methyl group as illustrated in Figure 80a. This degree of rotational freedom may also allow the methoxy group to be in the _gauche_-rotameric state in order to limit the steric hindrance of the methoxy group (Figure 80b).
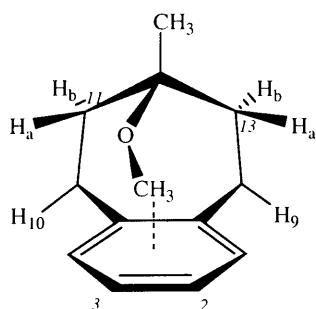
Figure 80a   Conformation of the ether **84** showing a π-interaction with the terminal protons of the methoxy group.
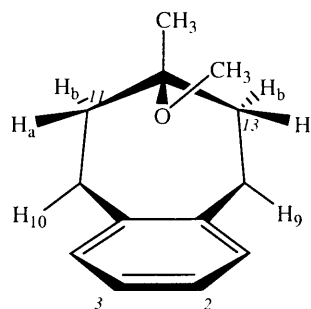
Figure 80b   Conformation of the ether **84** in the *gauche*-rotameric state.

The structure of the favoured conformer of the ether **85** showed a distinct preference for the terminal alkyne group to be above the aromatic ring and its relative proportion was larger than that of the propargyl alcohol **81** in $CDCl_3$ solution, due to the absence of the stabilising O-H/π interaction on the other side of the balance. Indeed, the conformational equilibrium of the propargylic alcohol **81** revealed that there was no preference for one conformer over the other due to the effective competition between the O-H/π interaction and the alkyne group. Removal of the former interaction, the C-H/π hydrogen bonding governed the conformation observed for the ether **85**.

2.4.3 – Aromatic interactions with a fluorine atom

At this stage, given that the replacement of an hydroxy group by a fluorine atom is a proven stratagem within the pharmaceutical industry, it was of particular interest to contrast the behaviour of the secondary and tertiary fluorides within the corresponding alcohols. The predominant conformation of the fluoride derivatives **94** and **96** in $CDCl_3$ solutions are illustrated in Figure 81.
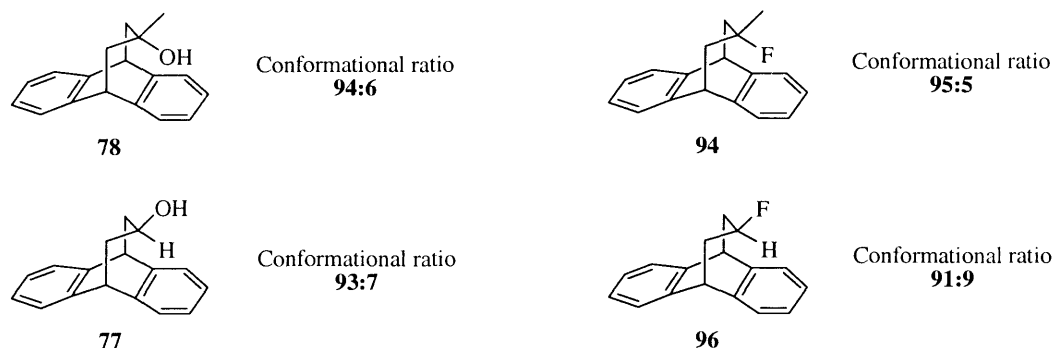
Figure 81   Representation of the predominant conformation of fluoride derivatives **94** and **96** in CDCl₃ solution and comparison with the corresponding alcohols **77** and **78**

The difference in the van der Waals radius of a methyl group and a fluorine atom justifies the preferential conformation of **94** exhibiting the fluorine atom directed towards the aromatic system. The predominant conformation of the fluoride **96** was determined based on the coupling constants between the proton on the centre carbon of the bridge and the bridgehead protons H_a and H_b. The Karplus equation provides two theoretical coupling constants $^3J_{12\text{-}Ha}$ and $^3J_{12\text{-}Hb}$ in the illustrated conformation, of 6.2 and 10.0 Hz respectively, whereas smaller coupling constants are expected for the other conformation ($^3J_{12\text{-}Ha}$ = 3.1 Hz and $^3J_{12\text{-}Hb}$ = 2.7 Hz). Experimentally, the resonance given by H_{12} in the ^1H NMR spectrum of **96** exhibits two large coupling constants agreeing well with those calculated for the illustrated conformation. Therefore, the combination of electron density of the fluorine atom and difference in van der Waals radius between hydrogen and fluorine atom explains the stabilisation of the preferential conformer having the hydrogen atom above the centre of the ring.

2.4.4 – Cyanohydrin and α-amino nitrile derivatives – The influence of the cyano group

One sole conformer was found in the crystal structure of the α-amino nitrile **116** in which the nitrile group was positioned above the aromatic ring. Moreover, solid state ^{13}C chemical shifts did not reveal any significant change when compared with the ^{13}C NMR shifts obtained in chloroform solution, indicating that the structure of the major conformer was similar in both the solid state and in solution. Interestingly, the NMR signal of the carbon

atom of the nitrile group appeared at 4 ppm towards higher field in the solid state, which is characteristic of a solid specific hydrogen bonding (Appendix 5). Stabilisation of this conformer may arise from an interaction between the electron rich aromatic ring and the electron deficient carbon atom of the nitrile group.

Conformational ratio
74:26

83

Conformational ratio
96:4

116

Figure 82 Conformational ratio of cyanohydrin **83** and representation of the predominant conformation of α-amino nitrile **116** in CDCl₃ solution

In solution, one conformer of the cyanohydrin **83** was significantly favoured and its conformational ratio was 74:26. However, neither of the two substituents contains a non-labile proton for NOE enhancements to be performed to determine the structure of the predominant conformer and this derivative could not be crystallised due to its instability in protic solvents. Thus, the structure of the more stable conformer could not be demonstrated experimentally. Although the C≡N/π interaction in the α-amino nitrile **116** is stronger than the N-H/π hydrogen bond allowing one conformer to be formed in 96%, the relative strength of the C≡N/π interaction versus the O-H/π hydrogen bond is unknown, and consequently the more stable conformation could not be estimated.

Conformational ratio
94:6

78

Conformational ratio
79:21

103

Conformational ratio
74:26

83

Conformational ratio
96:4

116
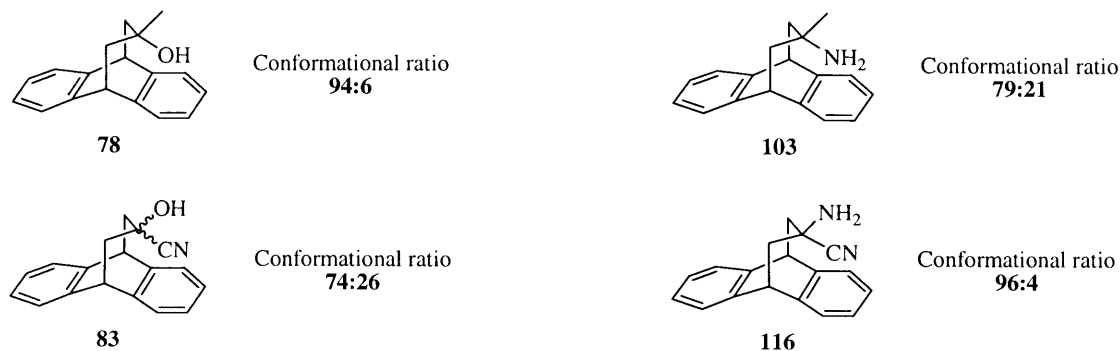
Figure 83 Conformational ratios of **78, 83, 103** and **116** in CDCl₃ solution in order to determine the structure of the predominant conformer of the cyanohydrin **83**

Interestingly, the difference of population of conformers of the amines **103** and **116** with their respective hydroxy analogues **78** and **83** is approximately equivalent. Since this change is induced by the replacement of an amino group by a hydroxy group, it seems reasonable to conclude that the more populated conformers of the nitriles **83** and **116** may have the same geometry, _i.e._ with the cyano group directed towards the aromatic ring.

The relative magnitudes of the N-H/π and the O-H/π interactions are shown by the comparison of the conformational population of the alcohol **78** with that of the amine **103**, which are 94:6 and 79:21 respectively.

Conformational ratio
94:6

78

Conformational ratio
79:21

103

Figure 84   Representation of the predominant conformation of alcohol **78** and amine **103** in CDCl₃ solution

Although the predominant conformer of **103** shows the amino group above the π-system, the stabilisation energy is less than that of **78**, indicating that the N-H/π hydrogen bonding is weaker than the corresponding O-H/π interaction which is in agreement with _ab initio_ calculations on water-benzene and ammonia-benzene complexes, where the stronger binding was found for the O-H/π interaction. Such results would be anticipated by most organic chemists who would consider an alcohol as a weak proton donor (acid) and an amine as a proton acceptor (base).

Conformational ratio
74:26

83

Conformational ratio
96:4

116

Figure 85   Representation of the predominant conformation of cyanohydrin **83** and α-amino nitrile **116** in CDCl₃ solution at 298 K

Based on the structure assumed for the major conformer of the cyanohydrin **83** showing the hydroxy group directed away from the aromatic ring, similar contribution from the O-H/π interactions to the stabilisation of cyanohydrin in its minor conformer, thus partially

compensating for the magnitude of the interaction between the cyano group and the aromatic ring on the other side of the conformational balance, leading to a 74:26 conformational ratio.

2.4.6 – An initial probe of the ammonium cation/π interaction

The poor solubility in $CDCl_3$ of the four ammonium salts prepared **117**, **118**, **119** and **120** resulted in broad resonances in the ^1H NMR spectra and measurements of the coupling constants were not sufficiently accurate to provide the conformational ratio. Fortunately, the slightly higher solubility of ammonium salt **117** permitted an approximate estimation of its conformational ratio to be 82:18, underlining the existence of a cation-π interaction.
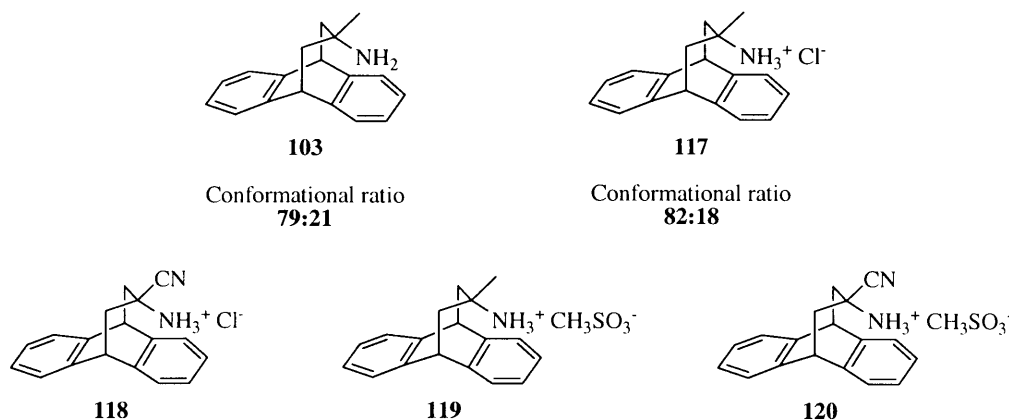
Figure 86 Representation of the predominant conformation of amine **103** and ammonium salt **117** in $CDCl_3$ solution. Structure of ammonium salts **118, 119** and **120** in $CDCl_3$ solution

The populational ratio of the conformers of its corresponding amine **103** was very similar and initially implied that the cation/π and N-H/π interactions may be of similar strengths, nevertheless, the difference in steric hindrance between an ammonium salt and a free amine substituent must be taken into account. On this basis, cation/π interaction may be slightly stronger than N-H/π hydrogen bonding in order to counteract steric interactions. Nevertheless, solvation effects must not be neglected as the poor affinity of the ammonium salt for chloroform may constrain this substituent above the aromatic ring and then may contribute to the stabilisation of the ammonium salt **117** in its predominant conformation.

2.4.7 – Influence of a spiro cyclic unit to the flexible bridge

Spiro heterocyclic derivatives have been prepared in order to study the effects of the locked conformation of the heterocyclic unit on the strength of the π-interactions.

The conformational ratio of the hemithioketal **141**[139] was 76:24 and the difference in energy between the two conformers was relatively large, *i.e.* 2.9 kJ.mol^{-1} (Figure 87). On the basis of steric grounds, it was assumed that the oxygen was positioned above the aromatic ring but this could not be confirmed experimentally. On further study of the ^{1}H NMR data, the opposite conformation appears to be more probable and in this orientation, the distance between the sulphur atom and the centre of the aromatic ring is ca. 3.2-4.2 Å. This is a remarkable observation since a sulphur atom is larger than an oxygen atom in terms of van der Waals radius. Stabilising effects of S-π interactions have been reported where the internuclear distance is between 3.5 and 4.9 Å[217] and the formation of this interaction can be attributed to the availability of the empty *3d*-orbitals on the sulphur atom combined with its enhanced polarisability.[16c]

Conformational ratio:
76:24

141
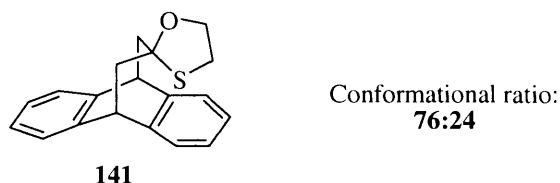
Figure 87   Structure of hemithioketal **141** in its favoured conformation in CDCl$_3$ solution

Further interesting features have been observed with the spiro-heterocycle derivatives **86**, **87**, **121** and **130**. Although epoxide **86** exists as one only conformer in the crystalline state, both structures are significantly populated in chloroform solution to give a 1:1 mixture of the conformers. The strained geometry of the three-membered ring locks the oxygen lone pairs but also effectively precludes interaction of either the oxygen atom or the methylene group with the aromatic ring and demonstrates the sensitivity of these non covalent interactions to the distance from the aromatic ring.

Increasing the size of the spiro cyclic unit brings either the oxygen atom or the methylene protons spatially closer to the centre of the aromatic ring and the most stable conformation

of the oxetane **87** has been shown earlier to have the oxygen atom away from the aromatic ring.

Conformational ratio
89:11

87
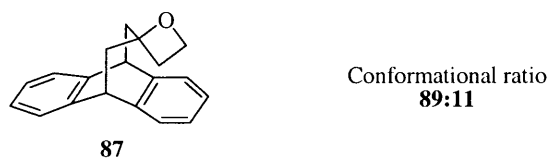
Figure 88   Representation of the predominant conformation of oxetane **87** in CDCl₃ solution

The strained cyclic unit impedes the free rotation along the C_{12}-O bond of the substituent and may force the two lone pairs of the oxygen atom to be positioned above the electron rich aromatic centre causing electronic repulsion. Thus, this conformation may become less stable than that with the oxygen atom directed away from the aromatic ring. Interestingly, the predominant conformer of the acyclic ether **84** shows the methoxy group above the aromatic ring whereas the opposite conformation is favoured for the oxetane **87**. Therefore, due to the structural similarity of the substituents, **84** being the acyclic analogue of **87**, the difference of preferential orientation for these two derivatives cannot be fully explained. Free rotation of the methoxy group along the C_{12}-O axis may bring the terminal protons of the methoxy group sufficiently close to the π-system to interact whereas the strained spiro cycle unit impedes this rotation and the stabilisation of its predominant conformer may basically be the result of electronic repulsion.

Both conformers of aziridine **121** are significantly populated with a slight preference for the nitrogen atom oriented away from the aromatic ring (68:32).

121

Conformational ratio
68:32

128

Conformational ratio
71:29

130

Conformational ratio
61:39
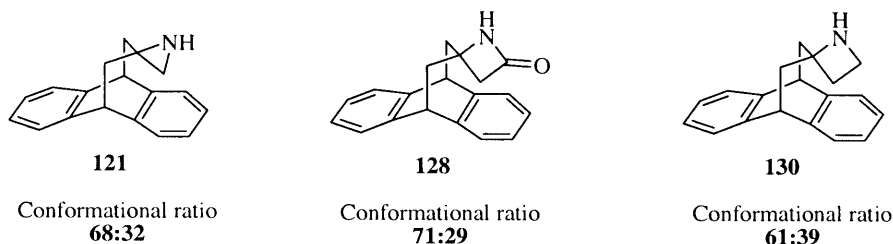
Figure 89   Representation of the predominant conformation of N-spiro-heterocycles **121**, **128** and **130** in CDCl₃ solution

As the epoxide **86** does not show any preference in its conformation due to the strained spiro unit maintaining the substituents too far from the aromatic ring for interaction, the

same observation may be applicable to the aziridine **121**. Furthermore, the geometry of the nitrogen atom may bring its electron lone pair too close to the π-system, thus generating electronic repulsion in the less stable conformation and this repulsive force could justify the slight preference for the nitrogen atom away from the aromatic ring. The significant population of the less stable conformer of **121** indicated the sensitivity of these intramolecular interactions when compared to the conformational ratio of the epoxide **86**.

The structures of the preferred conformer of azetidine **130** and β-lactam **128** are similar to that of the oxetane **87** with a population of 61 and 71% respectively. Stabilisation of the minor conformer may arise from a weak N-H/π interaction, which nevertheless may not sufficiently compensate for the repulsion between the electron lone pair of the nitrogen atom and the aromatic ring. Interestingly, the minor conformer of the β-lactam **128** is less stabilised than the azetidine **130** in its minor conformation although the N-H proton of a β-lactam unit is more acidic than that of the azetidine. This contraction may be explained by the difference of geometry between the two heterocyclic units. Indeed, the β-lactam moiety is planar with the N-H proton pointing towards the centre of the aromatic ring, whereas this proton is oriented towards the edge of the aromatic ring for the azetidine derivative (Figure 90)
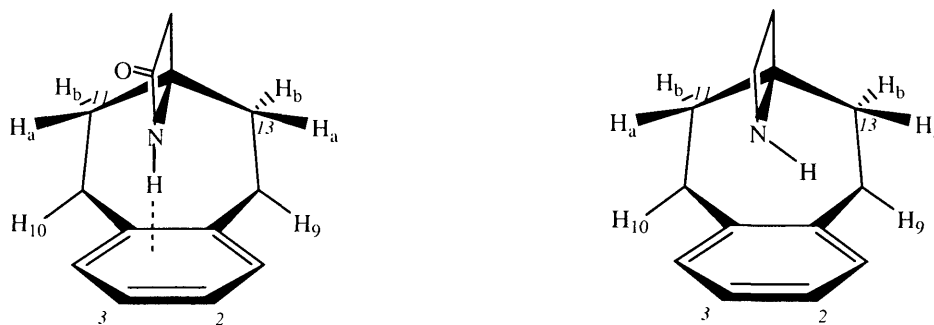
Figure 90 Representation of the structure of β-lactam **128** and azetidine **130** in their minor conformation in CDCl₃ solution

Therefore, the major conformation of the spiro cyclic derivatives shows there is a balance between repulsion of the electron lone pair and the weak attractive force of X-H/π hydrogen bonding. Moreover, the strength of the aromatic interactions is greatly affected by the internuclear distance of the participating partners.

2.4.8 – Influence of the electron density of the aromatic ring on the magnitude of the O-H/π interaction
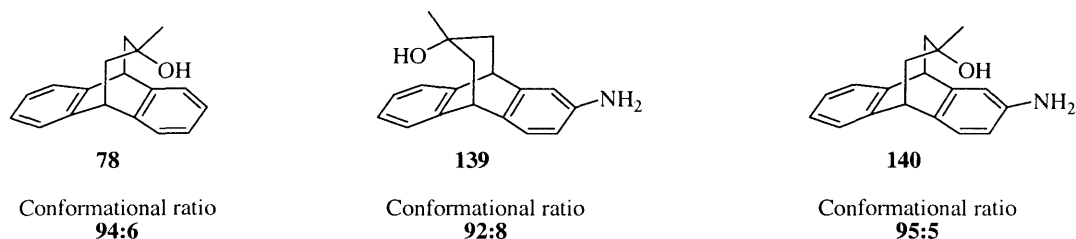
Figure 91 Representation of the predominant conformation of tertiary alcohols **78**, **139** and **140** in CDCl₃ solution

Due to the presence of the amino group on the aromatic ring, the π-system of the derivatives **139** and **140** is electron rich in comparison to the alcohol **78**. Nevertheless, the ratio of the two conformers in **140** (95:05) is very similar to that of **78**. Therefore, this modification of the electron density on the aromatic ring does not apparently strongly perturb the strength of the π-facial intramolecular hydrogen bond in these systems. In addition, the hydroxy group of alcohol **139** lies above the non-substituted aromatic ring in the predominant conformer which is populated to 92%. Despite the conformational ratio of **140** being slightly larger, this difference cannot be attributed to the influence of the amino group on the aromatic ring because of experimental error.

2.4.9 – Some preliminary conclusions from the studies in CDCl₃ solution

Propanoanthracenes act as torsion balances allowing the comparison of various aromatic interactions. The differences in interaction energies in $CDCl_3$ solutions, directly obtained from the conformational ratio, were substantial and proved the usefulness of this approach. Indeed, this study demonstrated the predominance of these interactions limiting steric hindrance and electronic repulsion and also dependence of interactions on the distance to an aromatic system. Moreover, the strength of π-interactions has been shown to be highly dependent on the acidity of the proton of the functional group, for example the interaction observed with a terminal alkyne group is effectively as strong as a O-H/π hydrogen bond, and that the behaviour of the π-hydrogen bond is similar to that of a classical hydrogen bond (similar in angle and distance) and its significance has been clearly highlighted. Additionally, the interaction involving an aromatic ring and a nitrile group is noteworthy. Variation of the anisotropy of the ring current of the aromatic ring in the aniline derivative studied did not however appear to play a crucial role in the strength of the aromatic interactions with a hydroxy group in these systems in $CDCl_3$ solution.

2.5 – Solvent dependence studies

The influence of the effects of solvation on non-covalent interactions is a topic of paramount importance in molecular recognition.[218] In the case of π-facial hydrogen bonded systems, the magnitude of stabilising energy provided by the weak non-covalent interaction can be similar to that due to solvation in certain relatively polar solvents. For this reason, we elected to investigate the solvent dependence of the conformational equilibrium of the propanoanthracene derivatives in nine different solvents at room temperature. Within the range of solvents used, C_6D_{12} and CCl_4 are relatively inert because of their apolar and aprotic properties, and the behaviour of the conformational balance in these solvents should be approximately similar to that in the gas phase. The aromatic rings in benzene and toluene, when used as solvents, may also act as a hydrogen bond acceptor even if their dielectric constants are rather low (2.3 and 2.4 respectively). Although the dielectric constant of $CDCl_3$ is only slightly larger than toluene (4.8), the acidity of the deuterium atom of this molecule may generate further specific interactions between the substituents on the flexible bridge or the π-systems of the propanoanthracenes. In the other solvents used, their high polarity and hydrogen-bonding capacity may engender significant modifications of the conformational equilibria. The measurements of the conformational ratios of propanoanthracenes for the series of solvents are reported in Appendix 6 as a Table and show dramatic changes on modifying solvent.

In order to have a representative overview of the solvent effects on the conformational equilibria for a series of derivatives, solvent studies were firstly summarised as various graphs depending on the dielectric constants of the solvent on the horizontal axis in this chapter, but this representation did not provide some explicit results. However, it appeared that perturbations of the conformational equilibria were more dependent on the hydrogen bond acceptor capacity of solvents than on the dielectric constant and that the reason why this horizontal axis unit was elected (Figure 92b). An example of this observation is illustrated in Figure 92 for the alcohol **78**.
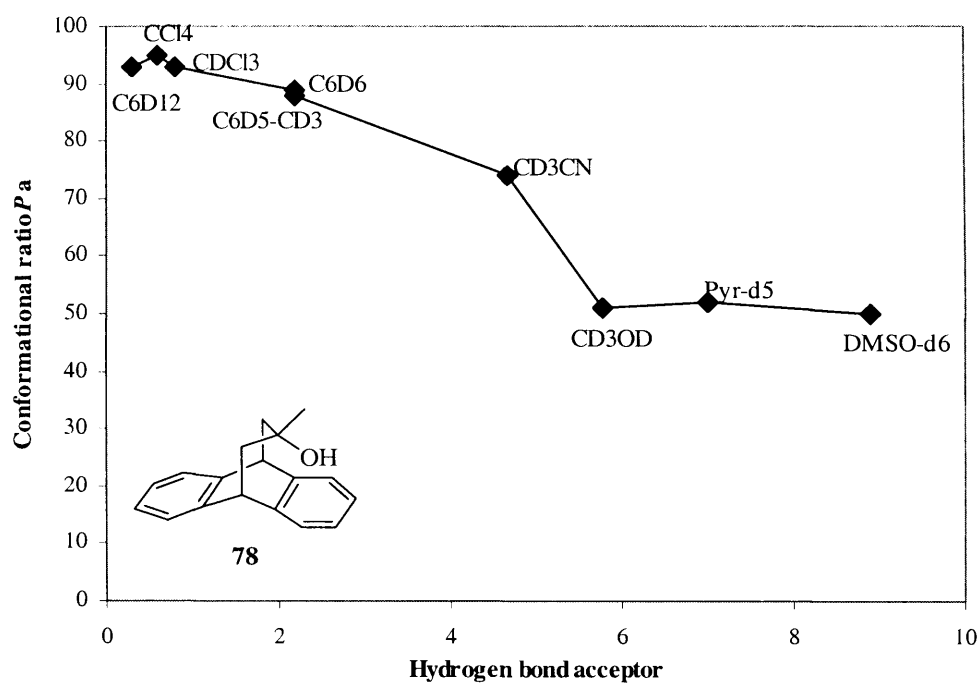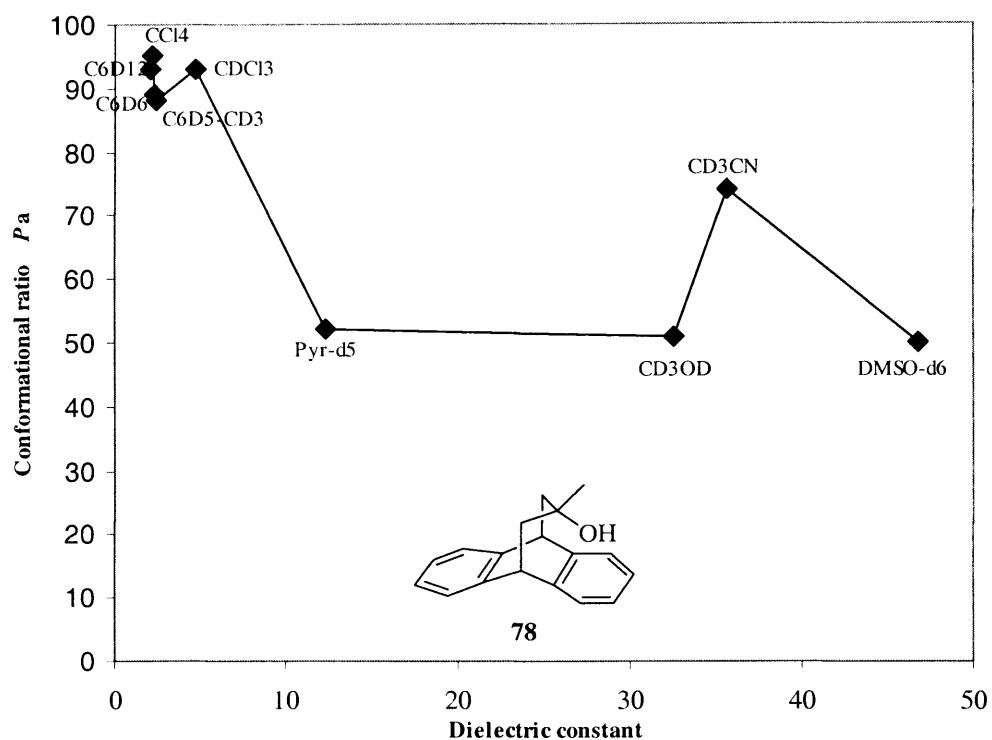
Top: **Figure 92a** Conformational ratio of **78** in different solvents depending on the dielectric constant of the solvent. Bottom: **Figure 92b**   Conformational ratio of **78** in different solvents depending on the hydrogen bond acceptor capacity of the solvents.

2.5.1 – Effects of the solvent nature on the conformational equilibrium of ether derivatives

As we have seen, the conformational equilibrium of epoxide **86** in CDCl₃, previously discussed in chapter 2.4.7, brought to light the possible distance dependence of the π-facial interactions, especially in terms of comparison with the simple methyl ether **84**. The perturbations of the conformational equilibrium of **86** illustrated in Figure 93, are significant and certainly result from the magnitude of the solvent-solute interactions. Unfortunately however, the geometry of the predominant conformer of **86** cannot be determined by NOE enhancements since the resonance of the methylene groups in the ^{1}H NMR spectrum overlaps with those of the bridgehead protons in each solvent.
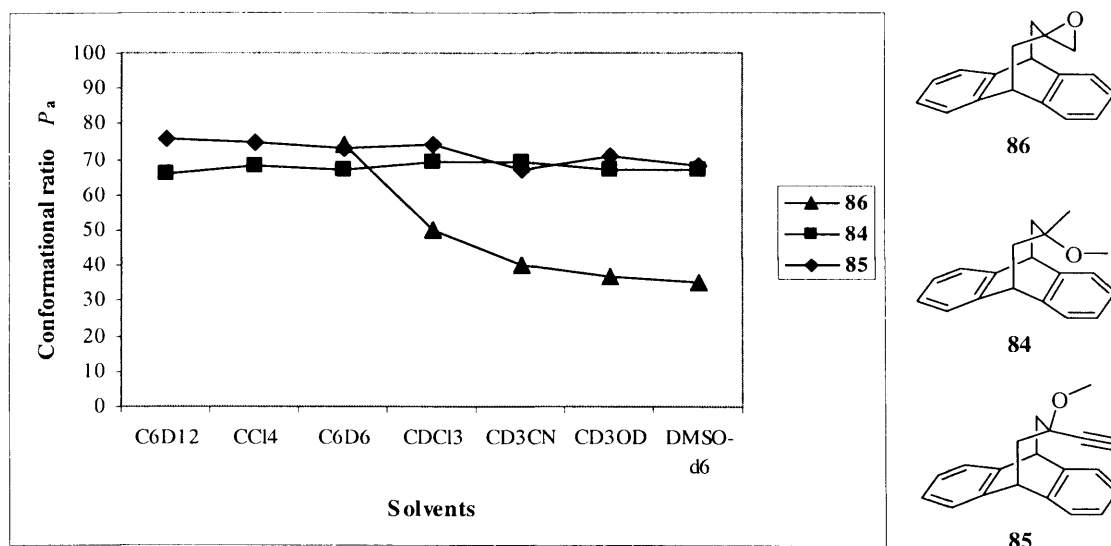
Figure 93 Conformational ratio of epoxide **86** and ethers **84** and **85** in a range of solvents at 298 K.

In the ^{1}H NMR spectrum of **86** in C₆D₆, the resonances of H_{11b} and H_{13b} are further upfield than those of H_{11a} and H_{13a} but the opposite chemical shifts were observed in polar solvents, such as CD₃CN, as illustrated in Figure 94. Therefore, an inversion of the predominant conformation occurred on changing the solvent from C₆D₆ to more polar one.
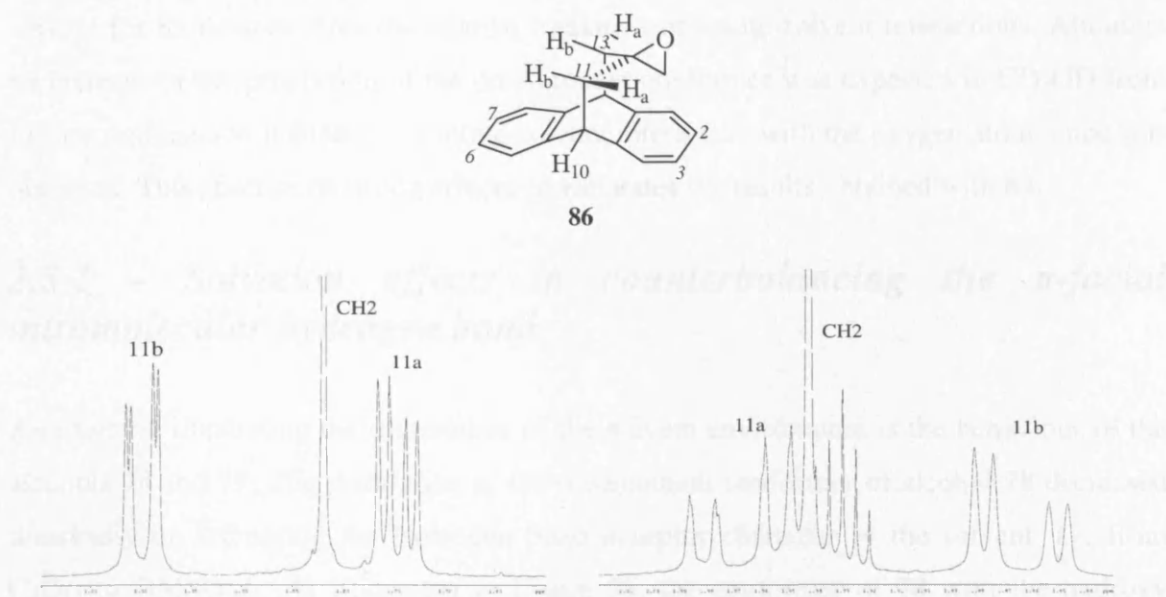
Figure 94 Left: enlargement of ^{1}H NMR spectrum of **86** in C_6D_6. Right: enlargement of ^{1}H NMR spectrum of **86** in CD_3CN

As the major conformation of **86** could not be established experimentally, an explanation of these interactions causing the variation of the conformational ratio in the series of solvents cannot be made.

However, in ethers **84** and **85** the population of the predominant conformer is not greatly affected by the nature of solvent as shown in Figure 93 thus highlighting that solvation effects with ether functionality are weak. In the previous chapter, it was argued that a possible π-interaction involving the proton of the methoxy group of **84** could also justify the preferential stabilisation of the conformer with the methoxy group above the aromatic ring. However, possible solute-solvent interaction with the oxygen atom in a protic environment is clearly not sufficiently strong to compete with the observed preference and illustrates the weakness of the hydrogen bond donor character of ether functionality.

Somewhat surprisingly, despite the presence of the more acidic alkyne proton of the terminal alkyne which could interact with a polar solvent or form a C-H/π interaction with C_6D_6 thereby stabilising the minor conformer, no dramatic changes were observed for the ether **85** in polar solvents. In his paper, Hunter[218] has established that solvent-solvent interactions are energetically favoured when a benzene ring and an alkyne proton are solvated in methanol or DMSO. The similarity of the conformational ratios on changing the

solvent for **85** demonstrates the relative weakness of solute-solvent interactions. Although an increase of the proportion of the predominant conformer was expected in CD_3OD from further stabilisation induced by a solute-solvent interaction with the oxygen atom, none was observed. This absence of strong effects corroborates the results obtained with **84**.

2.5.2 – Solvation effects in counterbalancing the π-facial intramolecular hydrogen bond

An example illustrating the importance of the solvent environment is the behaviour of the alcohols **78** and **79**. The population of the predominant conformer of alcohol **78** decreased drastically on increasing the hydrogen bond acceptor character of the solvent, *i.e.* from C_6D_{12} to DMSO-d_6. As illustrated in Figure 95, the conformer of **78** with the hydroxy group directed towards the aromatic ring was preferred to the extent of 85% in apolar solvents due to the influence of the O-H/π interaction, whilst solvents capable of forming hydrogen bond with the hydroxy group tended to stabilise the minor conformer. Furthermore, similar behaviour was observed for the alcohol **79** in the series of solvents studied (Appendix 7).
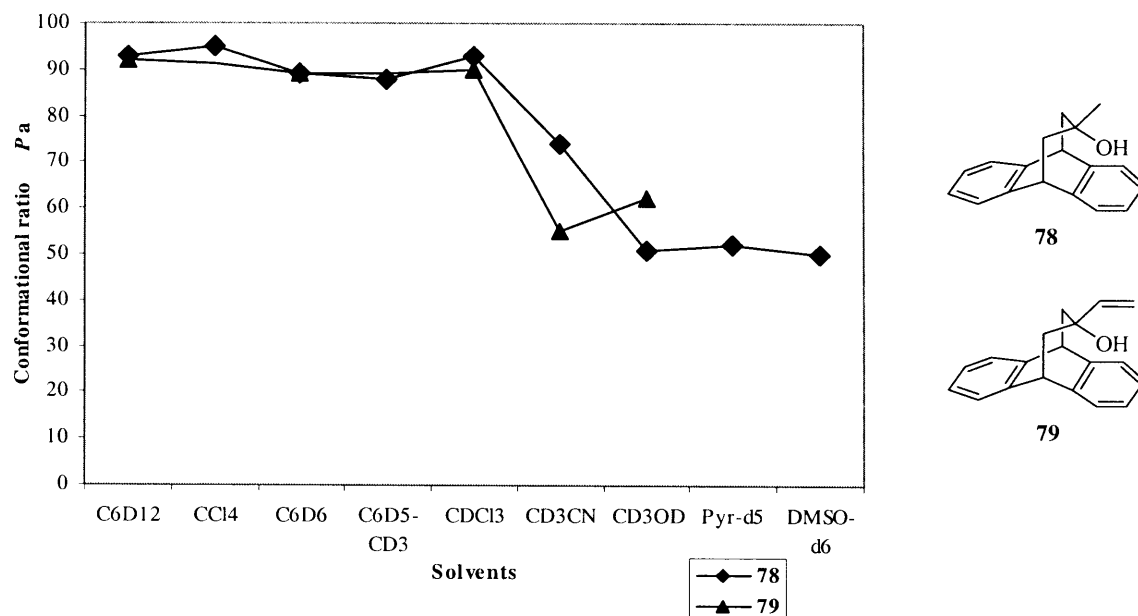
Figure 95 Conformational ratio of alcohols **78** and **79** in a range of solvents at 298 K.

Thus, for example, CD₃OD or DMSO-d_6 which can participate in hydrogen bonding clearly dominated the conformational equilibria and counterbalanced the intramolecular π-facial hydrogen bond (Figure 96).

Conformer **A**   Conformer **B**
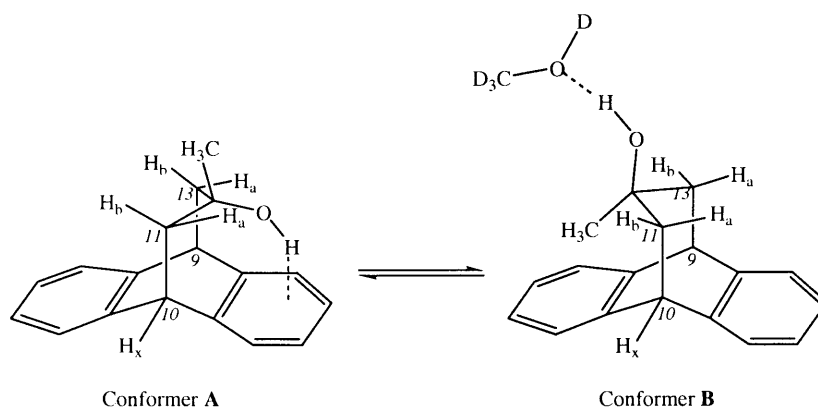
Figure 96   Conformational equilibrium of **78** between conformer **A** stabilised by the intramolecular O-H/π interaction and conformer **B** stabilised by solute-solvent interactions in CD₃OD

Interestingly, the conformational ratios of **78** in CD₃OD and in DMSO-d_6 are 51 and 50% respectively, revealing that the hydrogen bond donor properties of methanol do not significantly participate in the solvation of the hydroxy group but the solute-solvent interaction is governed primarily by the hydrogen bond acceptor properties of the solvent. This observation corroborates the absence of solvation dependence previously observed for the ethers **84** and **85** in which the ether functionality does not appear to participate in strong solute-solvent interactions even in protic solvents.

Furthermore, despite the stabilisation of the "minor conformer" in DMSO-d_6, both conformers **A** and **B** are equally populated for the alcohols **78** and **79**, showing that the solute-solvent interaction may not be sufficiently strong to compensate for the O-H/π interaction occurring in the other conformation. Since the lone pairs of the oxygen atom of the hydroxy group do not participate in a solute-solvent interaction, the strength of the O-H/π interaction and the hydrogen bond between the hydroxy proton and the solvent is comparable in this system.

2.5.3 – Some observations on the cyano and terminal alkyne groups

The conformational ratio of α-amino nitrile **116** is not greatly affected by the nature of the solvents studied and the possible aromatic interaction with the cyano group stabilises this conformation to the extent of 95% in apolar aprotic solvents. In polar solvents, the structure showing the amino group directed away from the π-system is the only conformer present, suggesting that solvation effects may also further stabilise the interaction between the amino group and the polar solvent. Although the observed changes are of the order of the error involved in the measurement, the gradual increase in the ratio of the conformer having the amino group directed away from the aromatic ring as a function of solvent polarity supports the idea that solvation of the nitrile group is not of great importance.
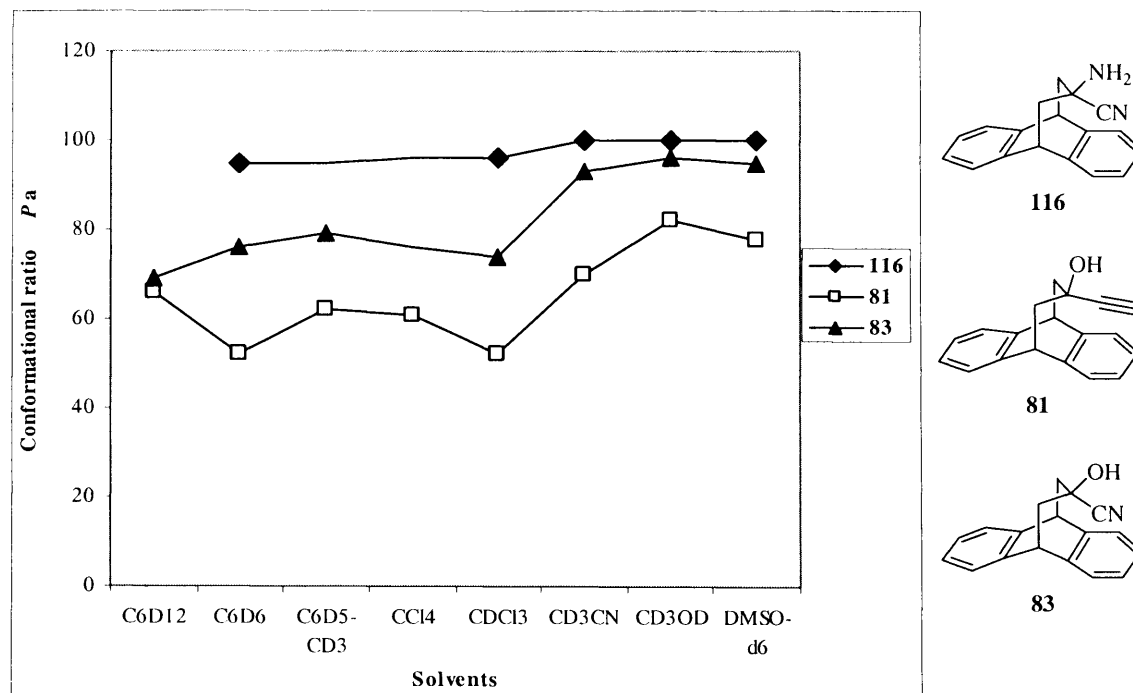
Figure 97   Conformational ratio of alcohols **81**, **83** and α-amino nitrile **116** in a range of solvents at 298 K.

As we have already stated, the predominant conformer of the cyanohydrin **83** in $CDCl_3$ is populated to the extent of 74%, but its structure could not be determined experimentally. However, it is interesting to note that solvent effects on its population are similar to those on the conformational ratio of the propargylic alcohol **81** as illustrated in Figure 97. In both

of these derivatives, formation of an O-H/π interaction is in competition with a small linear diatomic group possessing an sp hybridised carbon atom.

In CDCl₃, the two conformers of the propargylic alcohol **81** are equally populated. However, in polar solvents, the conformer with the hydroxy group directed away from the aromatic ring is favoured, demonstrating the participation of a solute-solvent interaction to the total stabilisation (Figure 98). Furthermore, NOE enhancements performed in every solvent studied confirmed this effect.
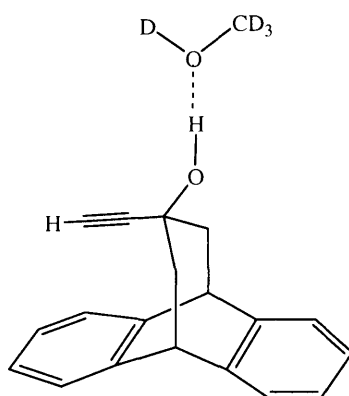
Figure 98 Structure of the predominant conformer of **81** (82%) in CD₃OD with solvation of the hydroxy group

As illustrated in Figure 97, solvent effects on the conformational ratio of **83** and **81** are comparable, and it is tempting to speculate that, by analogy, the predominant conformer of **83** also prefers the hydroxy group to be directed away from the aromatic system. Indeed, this conformation could be stabilised by a contribution from an intramolecular π-interaction with the cyano group and an intermolecular hydrogen bond between the polar solvent and the hydroxy group, vindicating the 95% ratio of the predominant conformer.

2.5.4 – Solute-solvent interactions with nitrogen-containing functional groups

In figure 99, the conformational ratios of amine **103** can be compared with those of the corresponding alcohol **78** in the range of solvents studied and indicate that the solvent dependence of the predominant conformer of **103** is much less important when compared to the sensitivity of the conformational equilibrium of **78**.
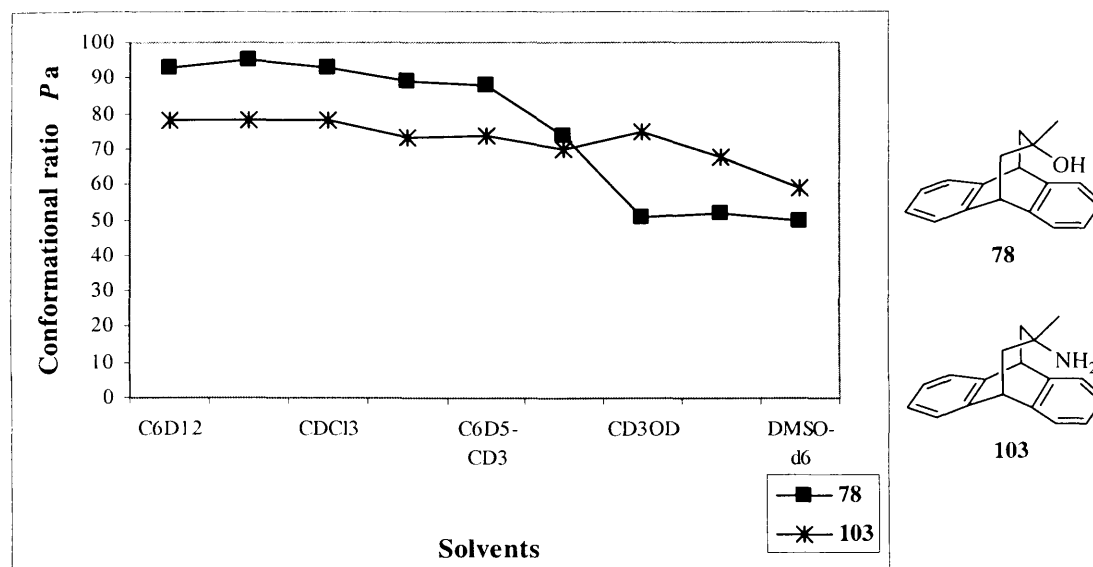
Figure 99 Conformational ratio of amine **103** and analogous alcohol **78** in a range of solvents at 298 K.

Nevertheless, polar solvents can partially stabilise the less populated conformer of **103** in which the amino group is directed away from the aromatic ring, although this phenomenon is only observed in pyridine-d_5 and DMSO-d_6, highlighting the poor hydrogen bond donor capacity of an amino group when compared to that of a hydroxy group.

The solvent dependence of the conformational equilibrium of aziridine **121** is comparable to that of ethers **84** and **85** and indicates therefore that the stabilisation of the predominant conformer of **121** does not depend on solvation of the N-H proton but may depend on the electronic repulsive interactions between the lone pair of the nitrogen atom and the aromatic ring.
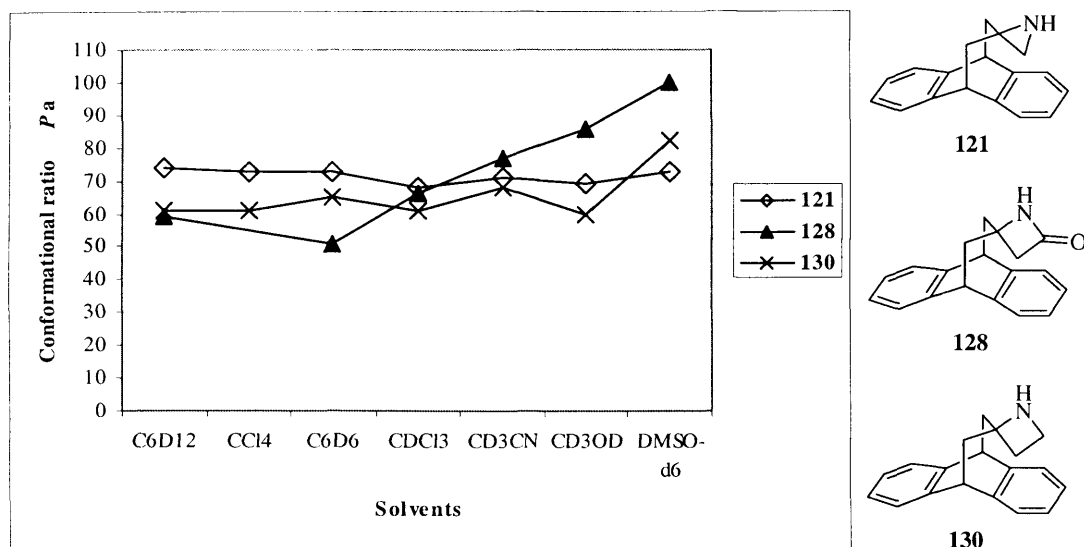
Figure 100 Conformational ratio of N-spiro-heterocycles **121**, **128** and **130** in a range of solvents at 298 K.

The importance of the acidity of the proton of the amino or amido group is clearly demonstrated on comparing the solvent effects on the conformational equilibria of **128** and **130**. Indeed, the structure of the major conformer of both derivatives shows the N-H group directed away from the aromatic ring with solute-solvent interactions further stabilising this conformation. Although solvation in CD_3CN and DMSO-d_6 only increases the population of the major conformer of azetidine **130**, the stable conformer of β-lactam **128** becomes more populated on increasing the hydrogen-bond acceptor property of the solvent as illustrated in Figure 100. This difference of behaviour between azetidine and β-lactam derivatives is due to the N-H proton of the β-lactam being more acidic than that of the azetidine and therefore interacting more strongly with polar solvents by hydrogen bonding.

2.5.5 – Solvation effects on cation/π interactions

A restricted series of solvents was used for the ammonium salts **117**, **118**, **119** and **120** due to their insolubility in apolar solvents. Nevertheless, variation of the conformational ratio of **117** (Figure 101) shows some interesting features in terms of the solvation of the ammonium group.
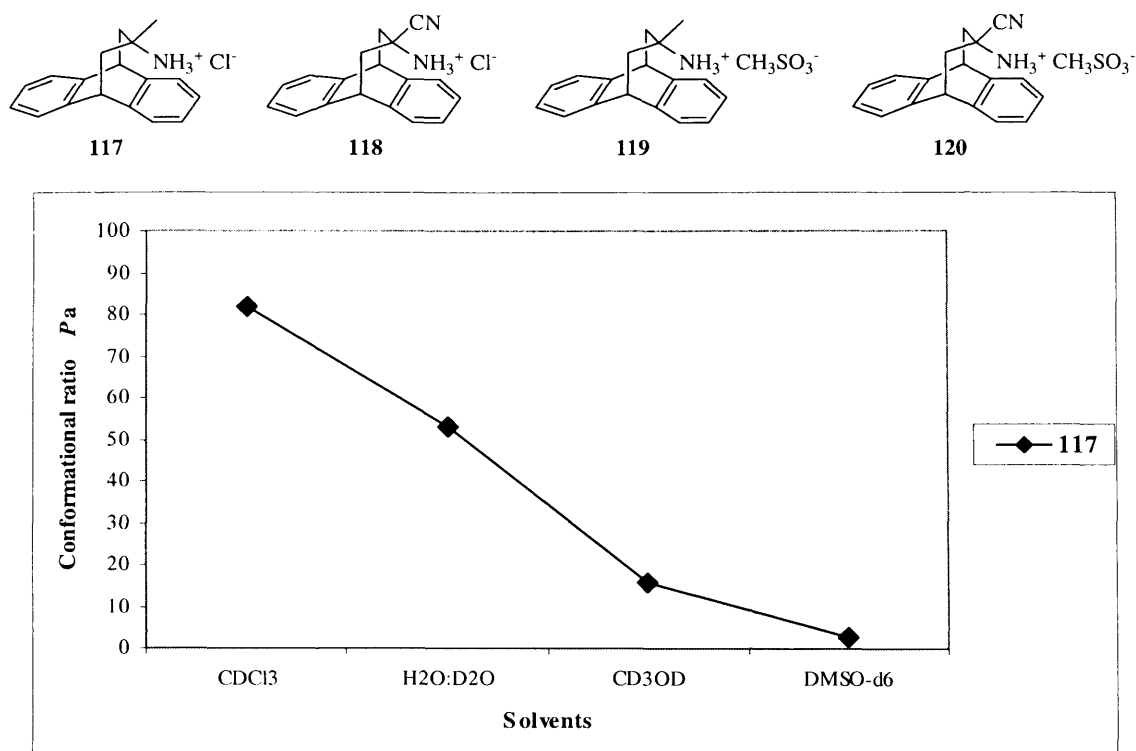
Figure 101 Conformational ratio of ammonium salt **117** in a range of solvents at 298 K

In $CDCl_3$, the predominant conformer of **117** is stabilised by a cation/π interaction whereas solvation of this derivative by DMSO-d_6 enables the formation of a hydrogen bond between the solvent and the protonated ammonium group, leading to a preference for the other conformer. This complete inversion of conformation brings to light the weakness of the cation/π interaction compared to the strength of the solvation of cation in DMSO-d_6. Within the range of weak non-covalent interactions, it was nevertheless fascinating to note the 50:50 equilibrium of salt **117** in water. It is interesting to note that both conformers of the tertiary alcohol **78** are equally populated in this solvent because of the persistence of the

O-H/π interaction, indicating that the cation/π interaction may be weaker than an O-H/π hydrogen bond.

It is nevertheless remarkable that in a 1:9 mixture of $D_2O:H_2O$, both conformers **A** and **B** are equally populated, contradicting the expected preferential stabilisation of the conformer with the ammonium group directed away from the aromatic ring because of the high polarity of the solvent (Conformer **A** in Figure 102). However, the possibility cannot be excluded that the small size of a water molecule may enable it to insert into the cavity between the protonated amino functionality and the aromatic ring. Thus, a molecule of water may lie above the aromatic ring stabilised by an O-H/π interaction allowing the solvation of the protonated amino group directed towards the aromatic ring, as illustrated in Figure 102.

Conformer **A**   Conformer **B**
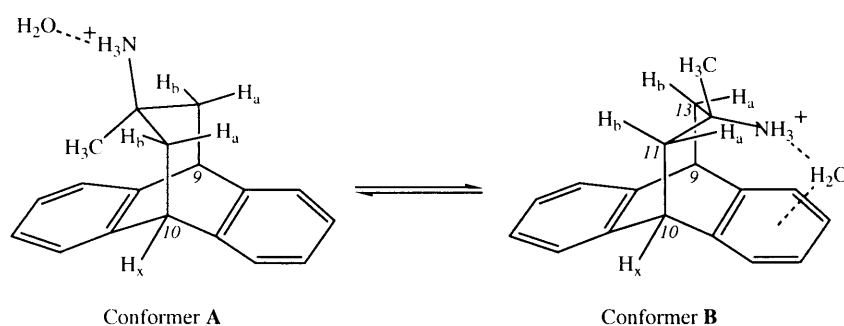
Figure 102   Conformational equilibrium of the ammonium salt **117**. Conformer **B** is stabilised by the inclusion of a molecule of water in the solute cavity between the aromatic ring and the protonated amino group.

The influence effects of the nature of the counteranion on the conformational ratio have also been investigated in a series of polar solvents in order to modify the acidity of the proton of the ammonium group and vary the strength of the cation/π interaction. However, replacement of a chloride by a methanesulfonate anion did not greatly affect the conformational equilibrium and the strength of the solute-solvent interaction in **119** was similar to that in **117** in polar solvents. In the range of solvents studied, the predominant conformer exhibited the ammonium group directed away from the aromatic ring.

As discussed, the neutral α-amino nitrile **116** shows only the one conformer with the amino group directed away from the aromatic ring in polar solvents. Consequently, protonation of the amino group did not affect the population of the observed conformer since solvation of the ammonium group in polar solvents can presumably contribute to the total stabilisation

energy of this conformer. Indeed, only one conformer of the ammonium salts **118** and **120** is stabilised by a combination of solute-solvent interaction and aromatic interaction with the cyano group. Because of the insolubility of these two ammonium salts in $CDCl_3$, it was not possible to study the competition between the two aromatic interactions induced by the nature of the substituents of the bridge. Given that the preferred conformation of cyanohydrin **83** places the nitrile group over the aromatic ring, it is tempting to speculate that replacement of the hydroxy group by an ammonium cation should increase the population of the conformer.

From these studies, the relative weakness of the cation/π interactions when compared with the hydroxy group was highlighted, and this bonding can exist only in apolar solvents due to the preferential solvation of the cation in methanol-d_4 or DMSO-d_6. Furthermore, the possible inclusion of a small molecule between the cation unit and the aromatic ring can compete with the solute-solvent interaction and could play a crucial role in the conformational equilibrium.

2.5.6 – *Conformational ratio of fluorinated derivatives in various solvents*

The nature of the solvent does not strongly influence the conformational equilibria in **94** and **96**, as illustrated in Figure 103 and therefore the governing forces in the stabilisation of one conformer over the other are either based on the difference of van der Waals radii or electronic repulsion with the π-system. Indeed, for the fluoride **96**, any form of π-hydrogen bond involving the proton on the central carbon of the flexible bridge would not be possible due to the large distance between this proton and the aromatic system. Furthermore, if such an interaction had occurred, solute-solvent interaction would have appeared in polar solvents, thus generating a decrease in the conformational ratio of **96**, but this was not observed.
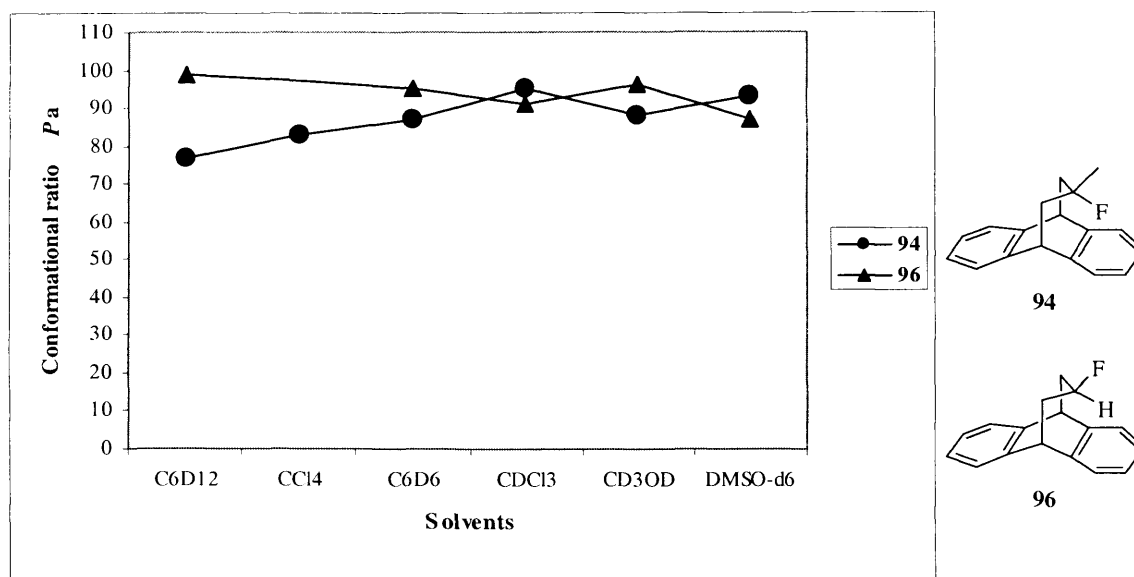
Figure 103   Conformational ratio of fluorides **94** and **96** in a range of solvents at 298 K

Of significance for drug and catalyst design however is the observation that the predominant conformers of alcohol **78** and fluoride **94** exhibit the same orientation in $CDCl_3$ with the methyl group directed away from aromatic ring, and are similarly populated. The strength of intramolecular $O-H/\pi$ hydrogen bonding is however highly dependent on the solvent whereas the conformational equilibrium of **94** is not significantly affected. Thus, replacing a hydroxy group by a fluorine atom may maintain an aromatic interaction even in polar solvents.

As we have stressed throughout, the influence of solvation is a critical parameter in any study of weak interactions. In this respect, propanoanthracenes have been proved to be very useful for the investigation of solvation phenomena, revealing that solute-solvent interactions can either compete or contribute to the total stabilisation energy of a given conformational balance. However, the dielectric constant of the solvent did not play an important role in the formation of solute-solvent interactions which were governed by the hydrogen bond acceptor capacity of the solvent. Additionally, the preference to place the nitrile group over the aromatic group was shown to be greater than that of $O-H/\pi$ interaction. The solvent dependence of the π-hydrogen bonds has also been highlighted as

the conformational equilibria of the ethers and fluorides were not significantly affected, proving that these preferences can persist in any solvent. Another interesting feature was the possible stability of the inclusion of a molecule of water between the aromatic system and a cationic functional group with interactions as strong as cation/π interactions.

CHAPTER 3

CONCLUSIONS AND PERSPECTIVES

3.1 – Preparation and analysis of conformational balances

The primary objective of the present work was to use the flexible bridge of 9,10-propanoanthracenes as conformational balances in order to provide further understanding of through space non-covalent aromatic interactions with different functional groups and to investigate the solvent dependence of these interactions.

3.1.1 – Synthesis of propanoanthracenes

In the first instance, it was necessary to improve the synthetic route to the ketone **67** from anthracene and this was achieved giving the precursor of a series of propanoanthracenes in 31% yield over the four steps and in higher purity on a larger scale than the synthetic route described in the literature (22% yield).
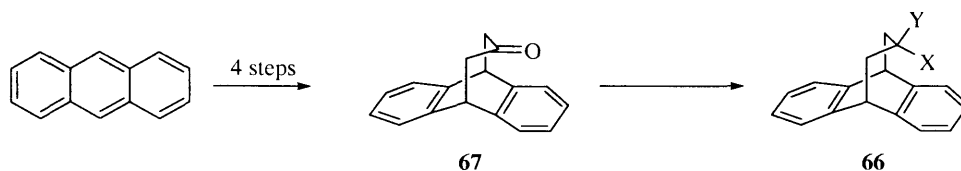
Scheme 62

Building on the earlier study in the group, the ketone served as the basis for the construction of a wide range of new derivatives **66** with various functional groups X and Y on the flexible bridge. A limitation on the number of reactions that could be performed on the central carbon atom of the bridge was the propensity for elimination to lead to an unsaturated bond on the bridge. Hence, alkylation of the carbonyl group required the use of organocerium reagents and the presence of strong bases in reaction mixtures was avoided.

3.1.2 – Conformational equilibria of propanoanthracenes

Differences in aromatic interaction energies between functional groups were significant and demonstrated the efficacy of the developed methods. Firstly, the conformational equilibria appeared to be highly sensitive to the environment and behaved differently in the solid state to being in solutions. Moreover, the effects of the solvent on the conformational equilibria were sufficiently large to be observed and, with appropriate functional groups, were significant when the solvents exhibited an important hydrogen bond acceptor capacity. The distance dependence of aromatic interactions was also established to some extent and the distance between the nuclei of the two partners of this interaction were comparable to that of a hydrogen bond. In addition to the crucial role of π-hydrogen bonding, the prevalence of the aromatic interaction generated by the presence of a nitrile group was of particular interest, and was stronger than the O-H/π interaction. Another interesting feature was the preference of a terminal alkyne group for the aromatic ring and the fact that this counterbalances the O-H/π hydrogen bond in chloroform.

3.2 – Future scope for extending the types of aromatic interactions investigated

3.2.1 – Modification of the electron density of the aromatic system

As discussed in chapter 2.4.8, the presence of an amino group on one of the aromatic rings did not affect the conformational equilibrium significantly, as can be seen from the similarly of the conformational ratios of **78**, **139** and **140**. The synthesis of a series of propanoanthracenones in which the aromatic ring is substituted with a chloride atom has been attempted using the synthetic pathway described for the preparation of ketone **67** (Scheme 63).
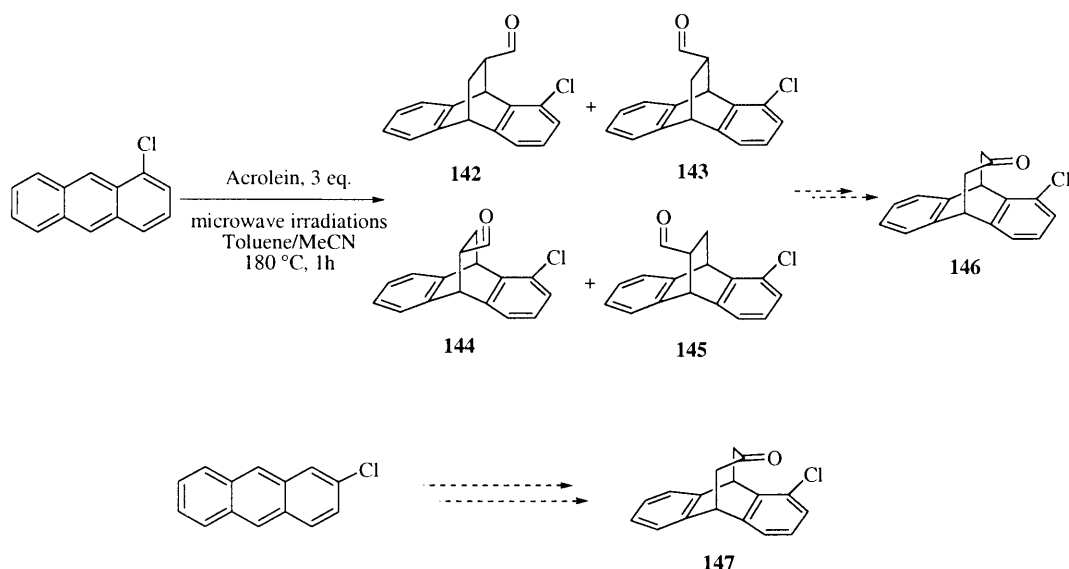
Scheme 63   Synthetic route to prepare propanoanthrancenones **146** and **147** from the corresponding chloroanthracenes.

However, the Diels-Alder reaction between acrolein and chloroanthracene provided four inseparable diastereoisomers and optimising the reaction conditions led to the use of an excess of acrolein, which polymerised under microwave irradiation and purification of the diastereoisomers became far from trivial. Therefore, future syntheses of ketones **146** and **147** should be attempted following another pathway.

As hexafluorination of an aromatic system inverts the quadrupole moment of the aromatic ring, ketones **148** and **149** could be envisaged as common intermediates for the series of derivatives **150** and **151** with either one or both of the aromatic rings tetrafluorinated (Scheme 64).
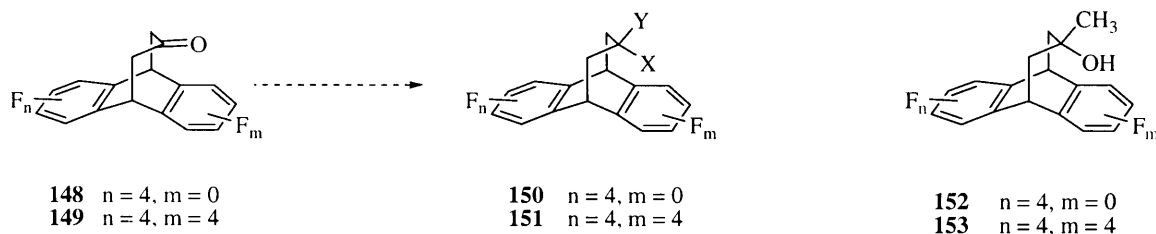
Scheme 64

The preparations of 1,2,3,4-tetrafluoroanthracene and 1,2,3,4,5,6,7,8-octafluoroanthracene have been described in the literature[219] and these anthracenes could be seen as dienes for the Diels-Alder condensation,[220] taking place as the first step of the synthesis of ketones **148** and **149** respectively. Recently, studies of aromatic interactions with fluorinated systems have become of increasing interest,[221] especially with respect to pharmaceutical applications. Therefore, investigation of the conformational equilibria of alcohols **152** and **153** would give some insight into the importance of the electron density of the aromatic ring on the magnitude of the O-H/π interactions and on cation/π interaction with a fluorinated aromatic ring.

For a better understanding of the influence of the electron density of the aromatic ring on the magnitude of the aromatic interactions, the comparison of the conformational equilibria of the two series of balances **154** and **155**, where the aromatic substituents are carefully chosen, *i.e.* with considerable electron donating or electron withdrawing power, would also be very useful.
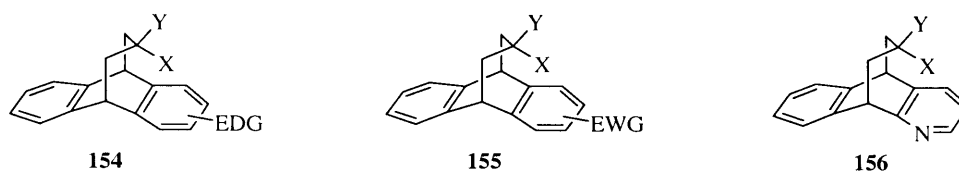
Figure 104

Moreover, the position of the substituent on the aromatic ring may also play a role in terms of the orientation of dipoles and comparison of the conformational equilibria of compounds with the same substituents on the bridge but having a substituent in different positions on the aromatic ring could give further insight into the interactions. In addition, studies of the conformational equilibrium of balances **156** in which one aromatic ring is replaced by a heterocyclic system such as pyridine, pyrrole or furan, should be investigated.

3.2.2 – Investigation of other functional groups on the centre carbon of the flexible bridge

In order to complete our comparative study of the substituent effects on aromatic interaction, another synthetic pathway to the propargylic amine **108** should be attempted

since all of our efforts thus far have failed. Conversion of this amine into the ammonium salt would then enable a comparison with the acetylenic alcohol. Additionally, the behaviour of the electron deficient carbon atom of a nitrile group warrants further investigation (Figure 105).
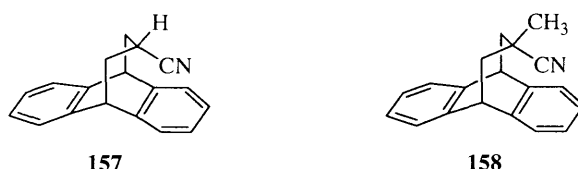
Figure 105

We note parenthetically that the synthesis of alcohol **159** was attempted as the presence of the three fluorine atoms would decrease the electron density of the trifluoromethyl carbon. However, the reactions of ketone **67** with TMS-CF$_3$ using various catalysts[222] or the reaction with CF$_3$COONa[223] failed with only the starting material being isolated (Scheme 65).

Conditions: TMS-CF$_3$, TBAF[222a]

TMS-CF$_3$, CsF, TMS-imidazole[222b]

TMS-CF$_3$, (Ph$_3$SnF$_2$)(Bu$_4$N)[222c]

CF$_3$COONa, CuI[223]
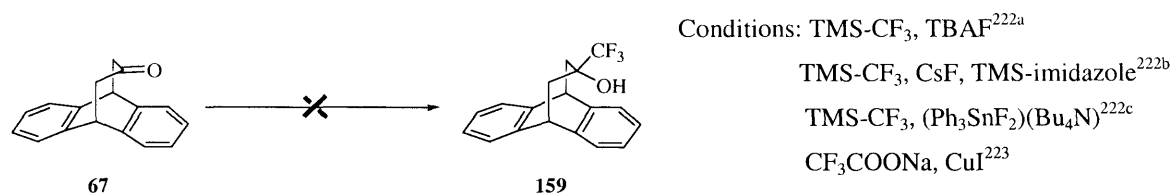
Scheme 65   Attempted reactions for the synthesis of alcohol **159**

Hemithioketal **141** showed the sulphur atom directed towards the aromatic ring and the oxygen atom directed away, thus indicating the importance of the polarisability of the sulphur atom compared to that of an oxygen atom. Moreover, a series of balances with oxygen-containing substituents has been prepared for this study and comparison with sulphur-containing analogues would be of interest. Therefore, it would be useful to synthesise the series of compounds depicted in Figure 106.
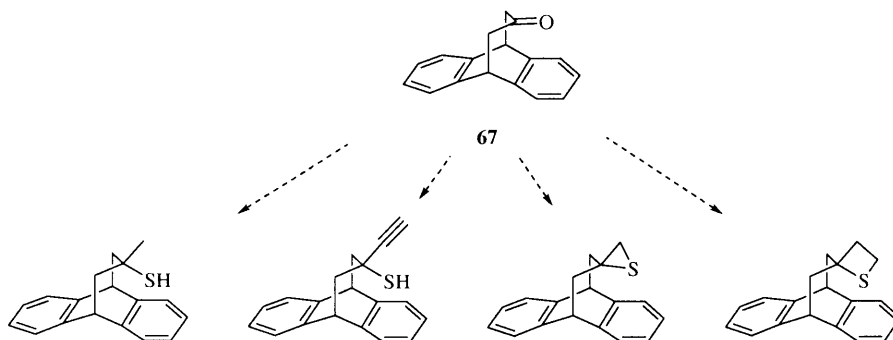
Figure 106 Range of derivatives with a sulphur-containing substituent on the central carbon of the bridge

The presence of further halogen atoms as substituents on the bridge could be obtained by the addition of a hydrogen halide to the alkene **95** and would lead to a series of derivatives **160**.

X = Cl, Br
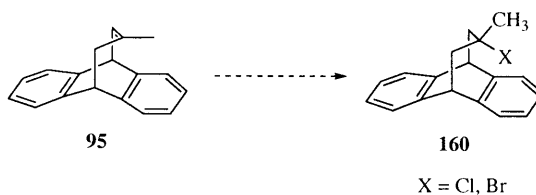
Scheme 66

Comparison of the conformational equilibria of compounds of this series with that of the fluorinated derivative **96** would lead to an estimation of the steric and electronic effects of the halogen atoms on the equilibria.

3.2.3 – Analysis of the conformational equilibria

A crucial observation emerging from our studies has been the differing behaviour of the observed conformational equilibria in the solid state and in solution. In crystal structures, intermolecular interactions play an important role in the orientation of the molecules and a study of the conformational equilibria of the derivatives at different concentrations would indicate the concentration limits when intermolecular interactions become prevalent over the intramolecular aromatic interactions occurring in the system. At this limiting concentration, the behaviour of the conformational balance should be comparable to that in

the solid state and these studies on concentration effects could also be performed in a range of solvents. Clearly, a considerable amount of work remains to be done in this area.

CHAPTER 4

EXPERIMENTAL

4.1 – General information

Melting points were determined using a Reichert hot-stage apparatus and are uncorrected. Recrystallisation solvents are recorded when this operation was performed. Infrared (IR) were recorded on a Perkin-Elmer 1605 Fourier transform spectrometer, and were recorded as thin films (KBr) of either pure sample or of solution of sample in the stated solvent. Absorption maxima are reported in wave-numbers (cm^{-1}).

^1H NMR spectra were recorded at 300 MHz on a Bruker AMX300 spectrometer, at 400 MHz on a Bruker AMX400 spectrometer or at 500 MHz on a Bruker Avance 500 spectrometer in the stated solvent, using residual protic solvent $CHCl_3$ ($\delta=7.24$ ppm, s) as an internal standard. Spin multiplicities are indicated by the following symbols: s (singlet), d (doublet), t (triplet), m (multiplet), br (broad) or a combination of these. NMR data are reported as follows: number of protons, multiplicity, coupling constants (J values). Varient temperature NMR experiments were carried out either on a Bruker AMX400 spectrometer or on a Bruker Avance 500 spectrometer. 1D-NOE and 2D-noesy NMR experiments were carried out on a Bruker Avance 500 spectrometer.

The ^{13}C NMR spectra were recorded at 75 MHz on a Bruker AMX300 spectrometer, at 100 MHz on a Bruker AMX400 spectrometer or at 125 MHz on a Bruker Avance 500 spectrometer in the stated solvent, using the central reference of residual $CHCl_3$ ($\delta=77.0$ ppm, t) as the internal standard. Chemical shifts are reported to the nearest 0.1 ppm. If more than one peak is observed within 0.1 ppm accuracy, the numbers of peaks will be indicated. Variable temperature NMR measurements were carried out using either AMX400 or AVANCE500 spectrometers. Selective NOE and 2D NOESY experiments were measured using AVANCE500, equipped with z-gradient facilities.

Solid-state ^{13}C spectra were recorded at 75.5 MHz using a standard 7 mm double-resonance magic-angle spinning (MAS) probe on MSL300 (Bruker). Samples in zirconia rotors of 7 mm external diameter were spun at 5 kHz with stability better than ±3 Hz. Spectra were

recorded using cross-polarization (CP), MAS and high-power ^{1}H decoupling. Typical acquisition conditions for ^{13}C CPMAS experiments were: ^{1}H 90° pulse duration = 4 μs; contact time = 5 ms; recycle delay = 3 s. Dipolar-dephased ^{13}C CPMAS spectra were also acquired in order to emphasise peaks due to nuclei, which are either remote from protons or have substantial motional averaging of dipolar interactions with protons.[224] Typical dephasing delay used was 40 μs. Variable delay dipolar-dephased ^{13}C CPMAS spectra were also measured. Fifty different values of the dipolar-dephasing delay (t_{dd}) between 1 μs and 50 μs were used. The observed curve of intensity changes in the dipolar-dephased CPMAS spectra is best described as a Gaussian decay and was fitted to the following function:[225]

$$I=I_0 \exp(-t_{dd}^2/T_{dd}^2)$$

The time constant T_{dd} in the above is used in this work for the comparison of the dephasing rates of various ^{13}C sites and is equal to $T_2 \sqrt{2}$ of reference.[225]

Mass spectra and accurate mass measurements were recorded on a Micromass 70-SE Magnetic Sector spectrometer at the University College London Chemistry Department. Elemental analyses were performed by University College London Chemistry Department microanalytical laboratory.

X-Ray crystal structures were determined using a Bruker Smart Apex diffractometer by Dr. D. Tocher at the University College London Chemistry Department. Microwave irradiation reactions were performed in Novartis, London with an Emrys Optimizer supplied by Personal Chemistry.

Thin layer chromatography (TLC) was performed on aluminium sheets pre-coated with Merck silica gel 60 F254, and visualized with ultraviolet light (254 nm), plus either basic potassium permanganate or cerium-ammonium-molybdate solution. Flash column chromatography was performed using BDH silica gel (40-60 μm).

All reactions using anhydrous solvents were carried out in oven-dried glassware under a nitrogen atmosphere. Diethyl ether and tetrahydrofuran were distilled from sodium-benzophenone ketyl. Toluene was distilled from sodium. Methanol was distilled from magnesium turnings and iodine. Dichloromethane was distilled from calcium hydride. DMSO was distilled from calcium hydride at reduced pressure and stored over 4 Å

molecular sieves. Immediately prior to use, tetrachloromethane was distilled under nitrogen from phosphorous pentoxide. Triethylamine was distilled from potassium hydroxide and stored over potassium hydroxide. _tert_-Butyl alcohol was dried with K_2CO_3, filtered, distilled under nitrogen and stored over 4 Å molecular sieves. Acetic anhydride was purified by fractional distillation and stored over 4 Å molecular sieves. Nitromethane was dried over $CaCl_2$, distilled to remove the water/nitromethane azeotrope, and kept over 4 Å molecular sieves under nitrogen. Anthracene was crystallised from ethyl acetate. Diiodoethane was purified by dissolving in ether and washing with 1 M sodium thiosulphate. Potassium _tert_-butoxide was purified by sublimation. Unless otherwise indicated, all reagents were obtained from commercial suppliers and were used without purification.

4.2 – Calculations

Force field and DFT calculations were carried out using PCMODEL (version 8.5, Serena Software)[226] and Gaussian 03,[227] respectively. Geometry optimisations were done using either B3LYP/6-31G(d) or B3LYP/6-31+G(d) levels of theory. Solution state calculations used IEFPCM model, as implemented in Gaussian 03. ^{1}H and ^{13}C NMR chemical shifts relative to TMS were computed at B3LYP/6-311+G(2d,p) level, whereas vibrational frequencies were calculated at B3LYP/6-31G(d) and B3LYP/6-31+G(d) levels, using scaling factors of 0.9613[228] and 0.9763,[229] respectively. The overall rms error for the frequency calculations by B3LYP/6-31G(d) has been reported to be 34 cm^{-1}.[228]

4.3 – Calculated and experimental errors

Assuming that the boundary values J_L and J_S are accurate within ±0.3 Hz, the error of the population measurements is estimated as ±5%. The agreement between the population values calculated using two different $^3J_{10\text{-}11a}$ and $^3J_{10\text{-}11b}$ couplings for each compound is within 0-2%.

4.4 – Experimental procedure

2-Bromopropenal 71[142]

71

C_3H_3BrO 134.96 g.mol^{-1}
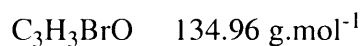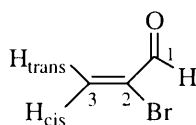
A solution of bromine (5.6 mL, 148 mmol) in CCl_4 (12 mL) was added dropwise to a solution of freshly distilled acrolein (dried with anhydrous copper sulphate and distilled) (10 mL, 148 mmol) in CCl_4 (100 mL) at 0 °C under nitrogen atmosphere and the resulting mixture was stirred vigorously. Triethylamine (20.6 mL, 148 mmol) was added dropwise and the stirring continued for 2 h at 0 °C. The mixture was then filtered through celite to remove the salts formed and the residue was concentrated under reduced pressure. The resulting oil was dried over molecular sieves (3 Å) at 4 °C overnight. Distillation of the crude product at reduce pressure provided the *title compound* **71** (1.69 g, 8%) as a colourless oil.

B.p. 43 °C / 23 torr (lit.[230] 46-48 °C / 28 torr); **IR** (nujol) v_{max} 1700 (s), 1599 (s), 900 (s) cm^{-1}; **^{1}H NMR** (300 MHz, $CDCl_3$) 9.12 (1H, d, $^3J_{3cis,CHO}$ = 0.5 Hz, CHO), 6.83 (1H, d, $^2J_{3cis,3trans}$= 2.2 Hz, H_3), 6.80 (1H, d, $^2J_{3cis,3trans}$= 2.2 Hz, H_3); **^{13}C NMR** (75 MHz, $CDCl_3$) 186.2 (CHO), 137.7 (C_3), 132.7 (C_2).

11-Bromo-9,10-dihydro-11-formyl-9,10-ethanoanthracene 72[143]

72

$C_{17}H_{13}BrO$ 313.19 g.mol^{-1}
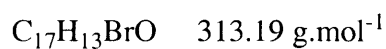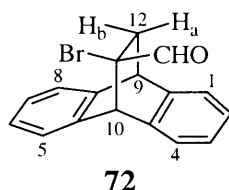
Freshly distilled 2-bromopropenal **71** (1.69 g, 12 mmol), anthracene (1.05 g, 5.9 mmol), potassium carbonate (200 mg) and hydroquinone (20 mg) were stirred in toluene (11 mL) for 4 days in an oil bath maintained at 100 °C. After cooling to room temperature, the solution was filtered and concentrated under reduced pressure to give a brown oil. The crude product was purified by flash column chromatography (silica gel, 1:9 EtOAc/P.E. 40-60 °C) to provide the *title compound* **72** (1.40 g, 76%) as white square crystals.

M.p. 133-134 °C (EtOAc-P.E.); **IR** (CDCl$_3$) ν_{max} 3074 (w), 3027 (m, H$_{ar}$), 2957 (w), 2830 (w), 1728 (s, CHO), 1460 (m) cm^{-1}; **^{1}H NMR** (300 MHz, CDCl$_3$) 9.30 (1H, s, CHO), 7.44-7.07 (8H, m, H$_{ar}$), 4.70 (1H, s, H$_{10}$), 4.36 (1H, dd, $^3J_{9,12a}$ = 2.7 Hz, $^3J_{9,12b}$ = 2.8 Hz, H$_9$), 3.00 (1H, dd, $^3J_{9,12b}$ = 2.8 Hz, $^2J_{12a,12b}$ = 14.2 Hz, H$_{12b}$), 2.17 (1H, dd, $^3J_{9,12a}$ = 2.7 Hz, $^2J_{12a,12b}$ = 14.2 Hz, H$_{12a}$); **^{13}C NMR** (75 MHz, CDCl$_3$) 189.0 (CHO), 143.0 (C$_q$), 142.8 (C$_q$), 138.6 (C$_q$), 137.8 (C$_q$), 127.7 (CH), 127.1 (CH), 126.5 (CH), 126.3 (CH), 123.9 (CH), 123.5 (CH), 68.9 (C$_{11}$), 52.5 (C$_{10}$), 43.9 (C$_9$), 38.2 (C$_{12}$).

Dihydro-11-formyl-9,10-ethanoanthracene 74[144]

74

$C_{17}H_{14}O$ 234.29 g.mol^{-1}
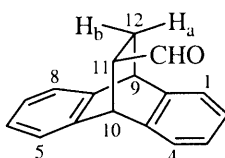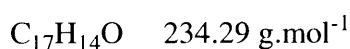
An Emrys Optimizer microwave tube (20ml capacity) equipped with a magnetic stirrer bar, was charged with anthracene (3.34 g, 19 mmol) in toluene (10 mL) and acetonitrile (2.5 mL). Acrolein (2.7 mL, 2.1 g, 38 mmol) was added in a single portion. The vessel was sealed with a crimped septum and exposed to microwave heating for 1.5 h at 165 °C. Upon completion of the heating, the tube was cooled rapidly by the Emrys Optimizer using compressed air and the mixture was filtered and concentrated under reduced pressure. Flash column chromatography (silica gel, 1:10 EtOAc/P.E. 40-60 °C) yielded the *title compound* **74** (4.40 g, 98%) as a white solid.

M.p. 97-100 °C (EtOAc-P.E.) (lit[144] 95-96 °C); **HRMS** found: M$^+$, 234.10504. $C_{17}H_{14}O$ requires 234.10446; **IR** (CH_2Cl_2) v_{max} 3022 (m, H_{ar}), 2947 (w), 2872 (s), 2820 (s), 2713 (s, CHO), 1720 (s, CHO), 1456 (m), 1391 (w), 1169 (s), 1024 (s), 937 (s), 735 (m), 579 (s), 550 (s) cm^{-1}; ^{1}**H NMR** (300 MHz, CDCl$_3$) 9.44 (1H, d, $^3J_{11,CHO}$ = 1.8 Hz, CHO), 7.34-7.28 (4H, m, H_{ar}), 7.15-7.07 (4H, m, H_{ar}), 4.72 (1H, d, $^3J_{10,11}$ = 2.5 Hz, H$_{10}$), 4.43 (1H, dd, $^3J_{9,12a}$ = 2.7 Hz, $^3J_{9,12b}$ = 2.8 Hz, H$_{12}$), 2.77 (1H, dddd, $^3J_{11,CHO}$ = 1.8 Hz, $^3J_{10,11}$ = 2.5 Hz, $^3J_{11,12b}$ = 4.7 Hz, $^3J_{11,12a}$ = 10.4 Hz, H$_{11}$), 2.11 (1H, ddd, $^3J_{9,12b}$ = 2.8 Hz, $^3J_{11,12b}$ = 4.7 Hz, $^2J_{12a,12b}$ = 12.8 Hz, H$_{12b}$), 1.99 (1H, ddd, $^3J_{9,12a}$ = 2.7 Hz, $^3J_{11,12b}$ = 10.4 Hz, $^2J_{12a,12b}$ = 12.8 Hz, H$_{12a}$); ^{13}**C NMR** (75 MHz, CDCl$_3$) 202.6 (CHO), 144.1 (C$_q$), 143.8 (C$_q$), 142.2 (C$_q$), 139.4 (C$_q$), 126.5 (CH), 126.3 (CH), 126.1 (CH), 126.0 (CH), 124.5 (CH), 123.6 (CH), 123.5 (CH), 123.4 (CH), 51.2 (C$_{11}$), 45.3 (C$_9$), 43.7 (C$_{10}$), 28.8 (C$_{12}$); **EI-MS**, *m/z* (relative intensity) 234 ([M]$^+$, 35), 202 (10), 178 ([C$_{12}$H$_{10}$]$^+$, 100).

11-Bromo-9,10-dihydro-11-formyl-9,10-ethanoanthracene 72

72

$C_{17}H_{13}BrO$ 313.19 g.mol^{-1}
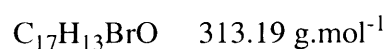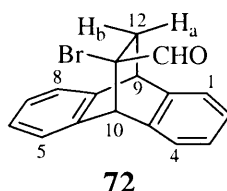
Method A

A solution of bromine (0.91 mL, 0.28 g, 18 mmol) in anhydrous CH_2Cl_2 (50 mL) was added dropwise to a solution of **74** (4.25 g, 18 mmol) in anhydrous CH_2Cl_2 (25 mL). After stirring for 2 h at 25 °C, the reaction mixture was concentrated under reduced pressure and the residue was purified by flash column chromatography (silica gel, 1:20 EtOAc/P.E. 40-60 °C) to give the *title compound* **72** (4.69 g, 83%) as white square crystals.

Method B

A mixture of bromine (0.26 mL, 5.0 mmol) and dioxane (0.75 mL) in anhydrous CH_2Cl_2 (3.5 mL) was added dropwise to a solution of **74** (1.17 g, 5.0 mmol) in CH_2Cl_2 (2.5 mL) below -5 °C and under nitrogen atmosphere. After stirring for 1 h, the solution was warmed to room temperature and treated with a solution of Na_2CO_3 (0.39 g) in H_2O (1.6 mL). The organic layer was separated and the aqueous layer was extracted with CH_2Cl_2 (3 x 3 mL). The combined organic layers were washed with brine (5 mL), dried over $MgSO_4$ and concentrated under educed pressure. Purification of the crude product by flash column chromatography (silica gel, 1:20 EtOAc/P.E. 40-60 °C) afforded the *title compound* **72** (1.27 g, 81%) as white square crystals.

The spectroscopic data obtained were identical to those previously described

9,10-Dihydro-11-hydroxy-9,10-propanoanthracen-12-one 73 and 9,10-dihydro-12-hydroxy-9,10-propanoanthracen-11-one 75[139]

$C_{17}H_{14}O_2$ 250.29 g.mol⁻¹ $C_{17}H_{14}O_2$ 250.29 g.mol⁻¹
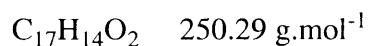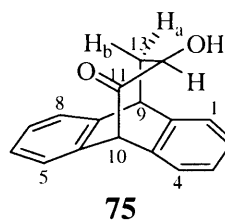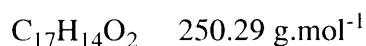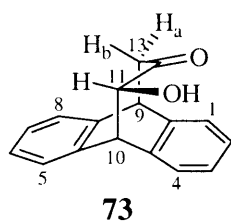
Aqueous KOH solution (3 M, 70 mL) was added to a stirred solution of the α-bromoaldehyde **74** (4.38 g, 14 mmol) in THF (175 mL) at air atmosphere. The solution was stirred vigorously for 2.5 h and neutralised by slow addition of aqueous HCl solution (2 M). The phases were separated and the aqueous layer was extracted with CH_2Cl_2 (3 x 150 mL). The combined organic layers were washed with brine (75 mL), dried over $MgSO_4$, filtered and concentrated under reduced pressure. Crystallisation from EtOAc and P.E. 40-60 °C gave the *title compound* **73** (1.96 g, 56%) as a white solid. Flash column chromatography (silica gel, 1:10 EtOAc/P.E. 40-60 °C) of the mother liquor and subsequent crystallisation from EtOAc yielded the *title compound* **75** (0.98 g, 28%) as a light yellow solid.

9,10-Dihydro-11-hydroxy-9,10-propanoanthracen-12-one 73

M.p. 183-184 °C (EtOAc) (lit[139] 186-187 °C (EtOAc)); **HRMS** found: M^+, 250.09997. $C_{17}H_{14}O_2$ requires 250.09937; **IR** (CH_2Cl_2) v_{max} 3492 (br, OH), 3037 (m, H_{ar}), 2945 (w), 2895 (w), 1689 (s, C=O), 1475 (s), 1452 (s), 1410 (s, OH), 1088 (s), 1064 (s, OH), 1031 (s), 829 (s), 767 (s), 738 (s), 706 (s), 642 (s) cm⁻¹; **¹H NMR** (400 MHz, CDCl₃) 7.51-7.49 (1H, m, H_{ar}), 7.40-7.38 (2H, m, H_{ar}), 7.31-7.27 (3H, m, H_{ar}), 7.21-7.10 (2H, m, H_{ar}), 4.38 (1H, d, $^3J_{10,11}$ = 4.4 Hz, H_{10}), 4.31 (2H, t, $^3J_{10,11}$ = 4.4 Hz, $^3J_{9,13a}$ = 6.7 Hz, H_9, H_{11}), 3.99 (1H, t, $^3J_{10,OH}$ = 1.3 Hz, OH), 3.16 (1H, dd, $^3J_{9,13a}$ = 6.7 Hz, $^2J_{13a,13b}$ = 15.2 Hz, H_{13a}), 2.81 (1H, d, $^2J_{13a,13b}$ = 15.2 Hz, H_{13b}); **¹³C NMR** (100 MHz, CDCl₃) 208.3 (C_{12}), 143.4 (C_q), 139.9 (C_q), 139.4 (C_q), 138.2 (C_q), 128.1 (CH), 127.6 (CH), 127.4 (CH), 127.3 (CH), 127.0

(CH), 126.9 (CH), 126.0 (CH), 125.6 (CH), 81.4 (C_{11}), 52.2 (C_{10}), 50.0 (C_{13}), 43.6 (C_9); **EI-MS**, *m/z* (relative intensity) 250 ([M]$^+$, 6), 234 ([$C_{17}H_{14}O$]$^+$, 96), 215 (44), 191 ([$C_{15}H_{11}$]$^+$, 100), 189 (100), 178 ([$C_{12}H_{10}$]$^+$, 100), 165 (61), 152 (74), 138 (100); **Anal.** Found: C, 81.73; H, 5.74. Calcd for $C_{17}H_{14}O_2$: C, 81.58; H, 5.64.

9,10-dihydro-12-hydroxy-9,10-propanoanthracen-11-one 75

M.p. 191 °C (EtOAc) (lit^{139} 186-190 °C (EtOAc)); **HRMS** found: M$^+$, 250.10003. $C_{17}H_{14}O_2$ requires 250.09937; **IR** (KBr) v_{max} 3479 (s, OH), 3450 (br, OH), 3034 (m, H_{ar}), 2943 (w), 2852 (w), 1707 (s, C=O), 1476 (s), 1456 (s), 1077 (s), 1043 (m), 784 (m), 763 (s), 755 (m), 699 (s), 652 (s) cm^{-1}; **^{1}H NMR** (400 MHz, CDCl$_3$) 7.45-7.43 (2H, m, H_{ar}), 7.23-7.36 (6H, m, H_{ar}), 4.86 (1H, s, H_{10}), 4.28 (1H, d, $^3J_{9,13b}$ = 1.2 Hz, $^3J_{9,13a}$ = 6.9 Hz, H_9), 4.12 (1H, dt, $^3J_{12,OH}$ = 3.3 Hz, $^3J_{12,13a}$ = 9.0 Hz, $^3J_{12,13b}$ = 9.8 Hz, H_{12}), 3.33 (1H, d, $^3J_{12,OH}$ = 3.3 Hz, OH), 3.00 (1H, ddd, $^3J_{9,13a}$ = 6.9 Hz, $^3J_{12,13a}$ = 9.0 Hz, $^2J_{13a,13b}$ = 12.8 Hz, H_{13a}), 1.83 (1H, ddd, $^3J_{9,13b}$ = 1.2 Hz, $^3J_{12,13b}$ = 9.8 Hz, $^2J_{13a,13b}$ = 12.8 Hz, H_{13b}); **^{13}C NMR** (100 MHz, CDCl$_3$) 204.6 (C_{11}), 143.0 (C_q), 139.3 (C_q), 136.6 (C_q), 134.4 (C_q), 128.3 (CH), 128.2 (CH), 127.6 (CH), 126.9 (x 2, CH), 126.5 (x 2, CH), 125.9 (CH), 72.7 (C_{12}), 60.4 (C_{10}), 43.9 (C_9), 42.8 (C_{13}); **EI-MS**, *m/z* (relative intensity) 250 ([M]$^+$, 0.6), 234 ([$C_{17}H_{14}O$]$^+$, 0.3), 191 ([$C_{15}H_{11}$]$^+$, 20), 189 (22), 179 (99), 178 ([$C_{12}H_{10}$]$^+$, 100), 176 (73), 165 (12), 152 (42), 139 (10), 89 (34), 76 (31).

9,10-Dihydro-9,10-propanoanthracen-12-one 67
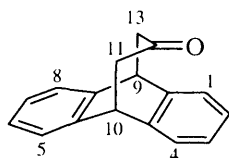
67

$C_{17}H_{14}O$ 234.29 g.mol^{-1}

In a glove box, samarium powder (1.80 g, 12 mmol) was placed into a three-necked flask fitted with a dropping funnel and a nitrogen inlet adaptor. A solution of diiodoethane (1.69 g, 6 mmol) in freshly distilled cold THF (60 mL) was placed into the dropping funnel

and the solution was bubbled with nitrogen for 30 min. The solution was added dropwise to the samarium powder over 1 h and the dark blue solution was left to stir for a further hour. The flask was cooled to -78 °C under a nitrogen atmosphere and 80% of a solution of α-hydroxyketone **73** (1.50 g, 6 mmol) in anhydrous THF (25 mL) was added dropwise. The mixture was allowed to warm to room temperature before adding the final 20%, then the mixture was poured into a saturated aqueous K_2CO_3 solution (100 mL) and the layers separated. The aqueous layer was extracted with CH_2Cl_2 (3 x 50 mL) and the combined organic layers washed with brine (50 mL), dried over $MgSO_4$, filtered and concentrated under reduced pressure. The product was purified by flash column chromatography (silica gel, gradient elution from 1:10 to 1:5 EtOAc/P.E. 40-60 °C) to yield the *title compound* **67** (1.02 g, 73%) as white needles.

M.p. 236-237 °C (EtOAc) (lit[140] 220 °C); **HRMS** found: M^+, 234.10460. $C_{17}H_{14}O$ requires 234.10446; **IR** (CH_2Cl_2) v_{max} 3037 (m, H_{ar}), 2927 (m), 2897 (m), 1684 (s, C=O), 1454 (s), 1398 (s), 1115 (s), 985 (s), 766 (s), 708 (s), 683 (s), 592 (s) cm^{-1}; ^{1}**H NMR** (400 MHz, $CDCl_3$) 7.38-7.36 (4H, m, H_{ar}), 7.28-7.26 (4H, m, H_{ar}), 4.29 (2H, t, $^3J_{10,11}$ = $^3J_{9,13}$ = 3.9 Hz, H_9, H_{10}), 2.87 (4H, d, $^3J_{10,11}$ = $^3J_{9,13}$ = 3.9 Hz, H_{11}, H_{13}); ^{13}**C NMR** (100 MHz, $CDCl_3$) 209.3 (C_{12}), 141.7 (C_q), 124.0 (CH), 126.0 (CH), 51.1 (C_{11}, C_{13}), 43.4 (C_9, C_{10}); **EI-MS**, m/z (relative intensity), 234 ($[M]^+$, 100), 215 (56), 191 ($[C_{15}H_{11}]^+$, 100), 189 (72), 178 ($[C_{12}H_{10}]^+$, 100), 165 (45), 152 (22), 63 (34); **Anal.** Found: C, 86.92; H, 5.95. Calcd for $C_{17}H_{14}O$: C, 87.15; H, 6.02.

9,10-dihydro-12-methylene-9,10-propanoanthracene 68[139]

68

$C_{18}H_{16}$ 232.32 g.mol^{-1}
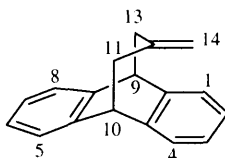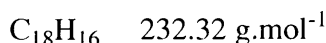
Diiodomethane (0.84 mL, 2.68 g, 10 mmol) was added to a suspension of zinc dust (1.2 g, 18 mmol) in anhydrous THF (20 mL). After stirring for 30 min, the solution was cooled to 0 °C and a 1 M solution of TiCl$_4$ in CH$_2$Cl$_2$ (2 mmol, 2.0 mL) was added over 10 min. After the dark brown mixture was stirred for 30 min at room temperature, a solution of the ketone **67** (468 mg, 2.0 mmol) in anhydrous THF (10 mL) was added dropwise and stirred for a further 3h. The solution was poured into a saturated aqueous solution of NaHCO$_3$ (50 mL), filtered and extracted with CH$_2$Cl$_2$ (3 x 30 mL). The combined organic layers were washed with brine, dried over MgSO$_4$ and concentrated under reduced pressure. Purification of the crude mixture by flash column chromatography (silica gel, 1:10 EtOAc/P.E. 40-60 °C) gave the *title compound* **68** (348 mg, 75%) as white square crystals.

M.p. 158 °C (lit^{139} 159-160 °C); **HRMS**: found: M$^+$, 232.12235. $C_{18}H_{16}$ requires 232.12519; **IR** (CH$_2$Cl$_2$) v_{max} 3070 (m), 3039 (m), 3019 (m, H$_{ar}$), 2976 (m), 2937 (s), 2898 (s), 1637 (s), 1476 (s), 1454 (s), 1424 (s), 1115 (s), 992 (s), 895 (s), 767 (s), 697 (s), 598 (s), 500(s) cm^{-1}; ^{1}**H NMR** (400 MHz, CDCl$_3$) 7.29-7.25 (4H, m, H$_1$, H$_4$, H$_5$, H$_8$), 7.19-7.16 (4H, m, H$_2$, H$_3$, H$_6$, H$_7$), 4.46 (2H, s, H$_{14}$), 4.09 (2H, t, $^3J_{10,11}$ = $^3J_{9,13}$ = 4.1 Hz, H$_9$, H$_{10}$), 2.61 (4H, d, $^3J_{10,11}$ = $^3J_{9,13}$ = 4.1 Hz, H$_{11}$, H$_{13}$); ^{13}**C NMR** (100 MHz, CDCl$_3$) 144.8 (C$_{12}$), 142.9 (C$_q$), 126.2 (CH), 125.5 (CH), 115.5 (C$_{14}$), 45.9 (C$_9$, C$_{10}$), 41.6 (C$_{11}$, C$_{13}$); **EI-MS**, *m/z* (relative intensity), 232 ([M]$^+$, 100), 217 (72), 202 (7), 191 ([C$_{15}$H$_{11}$]$^+$, 20), 189 (72), 178 ([C$_{12}$H$_{10}$]$^+$, 86), 165 (5), 152 (8); **Anal.** Found: C, 92.90; H, 7.01. Calcd for C$_{18}$H$_{16}$: C, 93.06; H, 6.94.

12,12-Cyclopropyl- 9,10-dihydro-9,10-propanoanthracene 76
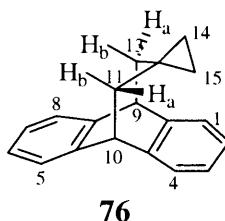
76

$C_{19}H_{18}$ 246.35 g.mol^{-1}

Diethylzinc (1 M solution in Et_2O, 1.7 mL, 1.7 mmol) was carefully added over 5 min to a solution of the alkene **68** (80 mg, 0.34 mmol) in anhydrous Et_2O (5 mL) at 0 °C, followed by addition of CH_2I_2 (274 μL, 3.4 mmol) over 2 min. The mixture was stirred at 0 °C for 4 h, warmed to room temperature and stirred for 20 h. The solution was quenched with water (5 mL) and brine (5 mL), extracted with CH_2Cl_2 (3 x 5 mL) and the combined organic layers were dried over Na_2SO_4 and concentrated under reduced pressure. Flash column chromatography (silica gel, gradient of elution 1:20 to 1:4 EtOAc/P.E. 40-60 °C) provided the *title compound* **76** (71 mg, 85%) as a white solid.

M.p. 117-119 °C; **HRMS**: found: $[M+H]^+$, 247.14848. $[C_{19}H_{18}+H]$ requires 247.14867; **IR** (CH_2Cl_2) ν_{max} 3060 (s, cyclopropyl), 2997 (s), 2912 (m), 2841 (s), 1473 (s), 1456 (s), 1175 (s), 1113 (s), 1031 (w), 1018 (s), 989 (w), 879 (w), 741 (m), 710 (s), 592 (s), 471 (d, cyclopropyl) cm^{-1}; **^{1}H NMR** (400 MHz, $CDCl_3$) 7.26-7.23 (4H, m, H_1, H_4, H_5, H_8), 7.16-7.14 (4H, m, H_2, H_3, H_6, H_7), 4.03 (2H, t, $^3J_{10,11} = {}^3J_{9,13} = 4.1$ Hz, H_9, H_{10}), 1.65 (4H, d, $^3J_{10,11} = {}^3J_{9,13} = 4.1$ Hz, H_{11}, H_{13}), -0.22 (4H, s, H_{14}, H_{15}); **^{13}C NMR** (75 MHz, $CDCl_3$) 143.5 (C_q), 125.9 (CH), 125.6 (CH), 46.6 (C_9, C_{10}), 41.7 (C_{11}, C_{13}), 15.5 (C_{12}), 13.6 (C_{14},C_{15}); **CI (methane)-MS**, *m/z* (relative intensity), 247 ($[M+H]^+$, 88), 217 (12), 206 (28), 192 ($[C_{15}H_{12}]^+$, 20), 191 ($[C_{15}H_{11}]^+$, 79), 189 (72), 178 ($[C_{12}H_{10}]^+$, 100); **Anal.** Found: C, 92.28; H, 7.72. Calcd for $C_{19}H_{18}$: C, 92.64; H, 7.36.

9,10-Dihydro-12-hydroxy-9,10-propanoanthracene 77[139]

77

$C_{17}H_{16}O$ 236.31 g.mol^{-1}
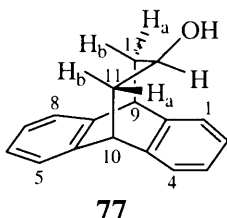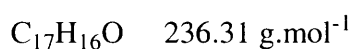
Sodium borohydride (360 mg, 10 mmol) was added as a single portion to a solution of ketone **67** (234 mg, 1.0 mmol) in anhydrous THF (9 mL) and anhydrous MeOH (5 mL). After 18 h of stirring, the reaction mixture was poured into water (20 mL) and extracted with CH_2Cl_2 (3 x 10 mL). The organic layer was washed with brine (10 mL), dried over $MgSO_4$ and concentrated under reduced pressure. The product was purified by flash column chromatography (silica gel, 1:4 EtOAc/P.E. 40-60 °C) to yield the *title compound* **77** (217 mg, 92%) as a white solid.

M.p. 122-123 °C (EtOAc-P.E.) (lit^{231} 114-116 °C); **HRMS** found: M$^+$, 236.12036. $C_{17}H_{16}O$ requires 236.12011; **IR** (CH_2Cl_2) v_{max} 3344 (br, OH), 3020 (m, H_{ar}), 2927 (s), 2854 (w), 1473 (s), 1456 (s), 1286 (s, OH), 1105 (s, OH), 1032 (s), 765 (s), 737 (br), 702 (w), 665 (s), 596 (s) cm^{-1}; ^{1}**H NMR** (500 MHz, $CDCl_3$) 7.29-7.27 (4H, m, H_1, H_4, H_5, H_8), 7.22-7.19 (4H, m, H_2, H_3, H_6, H_7), 4.11 (2H, dd, $^3J_{10,11b} = {}^3J_{9,13b} = 1.1$ Hz, $^3J_{10,11a} = {}^3J_{9,13a} = 7.1$ Hz, H_9, H_{10}), 3.22 (1H, m, H_{12}), 2.37 (2H, ddd, $^3J_{10,11a} = {}^3J_{9,13a} = 7.1$ Hz, $^3J_{12,11a} = {}^3J_{12,13a} = 10.3$ Hz, $^2J_{11a,11b} = {}^2J_{13a,13b} = 13.1$ Hz, H_{11a}, H_{13b}), 1.75 (1H, br, OH), 1.48 (2H, ddd, $^3J_{10,11b} = {}^3J_{9,13b} = 1.1$ Hz, $^3J_{11b,12} = {}^3J_{13b,12} = 6.1$ Hz, $^2J_{11a,11b} = {}^2J_{13a,13b} = 13.1$ Hz, H_{11b}, H_{13b}); ^{13}**C NMR** (125 MHz, $CDCl_3$) 144.4 (C_q), 140.6 (C_q), 127.5 (CH), 126.5 (CH), 126.4 (CH), 126.0 (CH), 125.9 (CH), 125.6 (CH), 125.4 (CH), 125.2 (CH), 68.2 (C_{12}), 44.0 (C_9, C_{10}), 39.1 (C_{11}, C_{13}); **EI-MS**, *m/z* (relative intensity), 236 ([M]$^+$, 73), 218 ([M-H$_2$O]$^+$, 100), 203 (33), 192 ([$C_{15}H_{12}$]$^+$, 91), 191 ([$C_{15}H_{11}$]$^+$, 96) 189 (38), 178 ([$C_{12}H_{10}$]$^+$, 100), 165 (22), 152 (15); **Anal**. Found: C, 86.74; H, 6.91. Calcd for $C_{17}H_{16}O$: C, 86.40; H, 6.82.

9,10-Dihydro-12-hydroxy-12-methyl-9,10-propanoanthracene 78[139]

78

$C_{18}H_{18}O$ 250.33 g.mol^{-1}
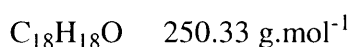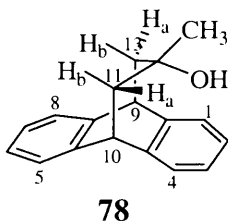
Cerium (III) chloride heptahydrate (1.12 g, 3 mmol) was ground in a mortar and placed in a three-necked flask fitted with a dropping funnel and a nitrogen inlet adaptor. The flask was evacuated (0.1 mmHg) and immersed in an oil bath at 140 °C without stirring for 1 h and then stirred for a further 1 h. The flask was cooled in an ice bath under nitrogen and anhydrous THF (7.5 mL) was added all at once with vigorous stirring. The ice bath was removed and the suspension was stirred overnight at room temperature. The flask was cooled to -78 °C under nitrogen and MeLi (1.6 M in Et$_2$O, 1.87 mL, 3 mmol) was added dropwise and the light yellow suspension was stirred for 1 h. A solution of the ketone **67** (351 mg, 1.5 mmol) in anhydrous THF (7.5 mL) was added dropwise and the reaction mixture was stirred for 2 h, then warmed up to 0 °C. The mixture was poured into an aqueous HCl solution (2 M, 30 mL) and extracted with CH$_2$Cl$_2$ (3 x 15 mL). The combined organic layers were washed with brine (15 mL), dried over MgSO$_4$ and concentrated under reduced pressure. Flash column chromatography (silica gel, gradient elution from 1:10 to 1:5 EtOAc/P.E. 40-60 °C) gave the *title compound* **78** (349 mg, 93%) as a white solid.

M.p. 130-132 °C (EtOAc-P.E) (lit[139] 128-129 °C (EtOAc-P.E.)); **HRMS:** found: M$^+$, 250.13523. C$_{18}$H$_{18}$O requires 250.13576; **IR** (CH$_2$Cl$_2$) v$_{max}$ 3587 (s, OH), 3441 (br, OH), 2974 (w, CH$_3$), 2928 (s), 2851 (w), 1475 (s), 1454 (s), 1373 (s, CH$_3$), 1288 (w, OH), 1225 (w), 1176 (w), 1109 (s, OH), 1086 (s, C-OH), 1057 (w), 1032 (w), 881 (w), 771 (s), 746 (s), 667 (s, C-OH), 596 (s) cm^{-1}; **^{1}H NMR** (500 MHz, CDCl$_3$) 7.38-7.36 (2H, m, H$_1$, H$_4$), 7.27-7.25 (2H, m, H$_5$, H$_8$), 7.23-7.21 (2H, m, H$_2$, H$_3$), 7.17-7.14 (2H, m, H$_6$, H$_7$), 4.12 (2H, dd, $^3J_{10,11b}$ = $^3J_{9,13b}$ = 1.4 Hz, $^3J_{10,11a}$ = $^3J_{9,13a}$ = 6.8 Hz, H$_9$, H$_{10}$), 2.30 (2H, ddd, $^4J_{11a,13a}$ = 1.9

Hz, $^3J_{10,11a}$ = $^3J_{9,13a}$ = 6.8 Hz, $^2J_{11a,11b}$ = $^2J_{13a,13b}$ = 14.5 Hz, H$_{11a}$, H$_{13a}$), 1.93 (2H, dd, $^3J_{10,11b}$ = $^3J_{9,13b}$ = 1.4 Hz, $^2J_{11a,11b}$ = $^2J_{13a,13b}$ = 14.5 Hz, H$_{11b}$, H$_{13b}$), 1.14 (1H, br, OH), 0.93 (3H, s, CH$_3$); ^{13}C NMR (100 MHz, CDCl$_3$) 144.2 (C$_q$), 141.6 (C$_q$), 126.9 (CH), 126.4 (CH), 125.9 (CH), 125.2 (CH), 72.7 (C$_{12}$), 44.9 (C$_9$, C$_{10}$), 44.6 (C$_{11}$, C$_{13}$), 32.8 (CH$_3$); EI-MS, *m/z* (relative intensity), 250 ([M]$^+$, 35), 232 ([M-H$_2$O]$^+$, 82), 217 (81), 192 ([C$_{15}$H$_{12}$]$^+$, 96), 178 ([C$_{12}$H$_{10}$]$^+$, 100); Anal. Found: C, 86.23; H, 7.34. Calcd for C$_{18}$H$_{18}$O: C, 86.36; H, 7.25.

9,10-Dihydro-12-hydroxy-12-vinyl-9,10-propanoanthracene 79
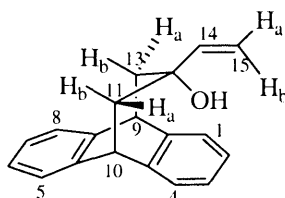
79

C$_{19}$H$_{18}$O   262.35 g.mol^{-1}

A solution of the ketone **67** (117 mg, 0.5 mmol) in CH$_2$Cl$_2$ (2.5 mL) was added dropwise at 0 °C to vinylmagnesium bromide (1 M solution in THF, 650 µL, 0.65 mmol). After complete addition, the mixture was stirred for 1 h keeping the reaction temperature below 10 °C then warmed up to room temperature and the stirring continued for a further 1.5 h. Then a saturated ammonium chloride solution (5 mL) was carefully added dropwise and the resulting mixture was filtered and washed thoroughly with CH$_2$Cl$_2$ (3 x 5 mL). The filtrate was dried over MgSO$_4$, filtered and concentrated under reduced pressure. Flash column chromatography (silica gel, gradient of elution 1:20 to 1:4 EtOAc/P.E. 40-60 °C) provided the *title compound* **79** (47 mg, 36%) as a white solid.

M.p. 138-140 °C (EtOAc); **HRMS**: found: M$^+$, 263.14275. C$_{19}$H$_{18}$O requires 263.14358; **IR** (CH$_2$Cl$_2$) v$_{max}$ 3583 (s, OH), 3070 (w, C=CH$_2$), 3020 (m, H$_{ar}$), 2918 (s), 1634 (w, CH=CH$_2$), 1475 (s), 1454 (s), 1410 (br, OH), 1219 (s), 1122 (s, OH), 1003 (s, C=CH$_2$), 930 (s, C=CH$_2$), 823 (w), 766 (s), 737 (s), 706 (s), 673 (s), 596 (s) cm^{-1}; ^{1}H NMR (500 MHz, CDCl$_3$) 7.40-7.37 (2H, m, H$_1$, H$_4$), 7.30-7.27 (2H, m, H$_5$, H$_8$), 7.25-7.22 (2H, m, H$_2$, H$_3$),

7.20-7.16 (2H, m, H_6, H_7), 5.49 (1H, dd, $^3J_{14,15a}$ = 10.6 Hz, $^3J_{14,15b}$ = 17.0 Hz, H_{14}), 5.08 (1H, dd, $^2J_{15a,15b}$ = 1.6 Hz, $^3J_{14,15b}$ = 17.0 Hz, H_{15b}), 4.85 (1H, dd, $^2J_{15a,15b}$ = 1.6 Hz, $^3J_{14,15a}$ = 10.6 Hz, H_{15a}), 4.15 (2H, dd, $^3J_{10,11b}$ = $^3J_{9,13b}$ = 1.6 Hz, $^3J_{10,11a}$ = $^3J_{9,13a}$ = 6.7 Hz, H_9, H_{10}), 2.22 (2H, ddd, $^4J_{11a,13a}$ = 1.9 Hz, $^3J_{10,11a}$ = $^3J_{9,13a}$ = 6.7 Hz, $^2J_{11a,11b}$ = $^2J_{13a,13b}$ = 14.7 Hz, H_{11a}, H_{13a}), 2.04 (2H, dd, $^3J_{10,11b}$ = $^3J_{9,13b}$ = 1.6 Hz, $^2J_{11a,11b}$ = $^2J_{13a,13b}$ = 14.7 Hz, H_{11b}, H_{13b}), 1.26 (1H, br, OH); ^{13}**C NMR** (125 MHz, $CDCl_3$) 145.8 (C_{14}), 144.1 (C_q), 141.7 (C_q), 127.0 (CH), 126.3 (CH), 126.1 (CH), 126.0 (CH), 111.2 (C_{15}), 74.6 (C_{12}), 66.0 (C_{15}), 44.8 (C_9, C_{10}), 43.3 (C_{11}, C_{13}); **CI(methane)-MS**, *m/z* (relative intensity) 263 ([M]$^+$, 19), 245 (90), 235 (100), 234 (79), 217 (21), 192 ([$C_{15}H_{12}$]$^+$, 74), 191 ([$C_{15}H_{11}$]$^+$, 85), 178 ([$C_{12}H_{10}$]$^+$, 49) 165 (8); **Anal.** Found: C, 86.43; H, 6.83. Calcd for $C_{19}H_{18}O$: C, 86.99; H, 6.92.

9,10-Dihydro-12-hydroxy-12-(trimethylsilyl)ethynyl-9,10-propanoanthracene 80

80

$C_{22}H_{24}OSi$ 332.16 g.mol^{-1}
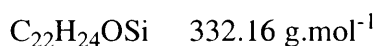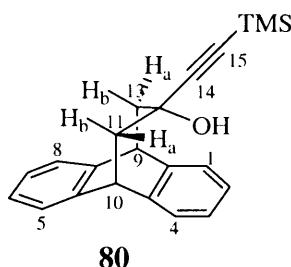
Cerium (III) chloride heptahydrate (0.96 g, 2.5 mmol) was ground in a mortar and placed in a three-necked flask fitted with a dropping funnel and a nitrogen inlet adaptor. The flask was evacuated (0.1 mmHg) and immersed in an oil bath at 140 °C without stirring for 1 h and then stirred for a further 1 h. The flask was cooled in an ice bath under nitrogen and anhydrous THF (12.5 mL) was added all at once with vigorous stirring. The ice bath was removed and the suspension was stirred overnight at room temperature. A 1.37 M solution of *n*-BuLi in hexanes (1.82 mL, 2.5 mmol) was added dropwise to a solution of trimethylsilylacetylene (352 µL, 2.5 mmol) in anhydrous THF (3.5 mL) at 0 °C. The yellow mixture was stirred for 30 min and cooled to -78 °C. Meanwhile, the suspension of cerium (III) chloride in THF was cooled to -78 °C before the dropwise addition of the organolithium solution *via* a canula. The mixture was stirred for 2 h at -78 °C and a

solution of ketone **67** (117 mg, 0.5 mmol) in anhydrous THF (12.5 mL) was added dropwise. After 4 h of stirring at 0 °C, the resulting mixture was warmed to room temperature, poured into a saturated aqueous NH_4Cl solution (50 mL), filtered through celite and extracted with EtOAc (3 x 25 mL). The combined organic layers were washed with brine (25 mL), dried over $MgSO_4$ and concentrated under reduced pressure. Flash column chromatography (silica gel, 1:10 EtOAc/P.E. 40-60 °C) gave the *title compound* **80** (118 mg, 71%) as a white solid.

M.p. 111-114 °C; **HRMS**: found: $[M+H]^+$, 333.16755. $[C_{22}H_{24}OSi+H]^+$ requires 333.16746; **IR** (CH_2Cl_2) v_{max} 3566 (s, OH), 3414 (br, OH), 3022 (m, H_{ar}), 2957 (s), 2926 (s), 2852 (w), 2170 (s, C≡C), 1475 (s), 1456 (s), 1323 (w, OH), 1290 (w, OH), 1248 (s, $Si(CH_3)_3$), 1082 (s, OH), 1018 (m), 993 (s), 920 (s), 843 (d, $Si(CH_3)_3$), 766 (s), 734 (s), 696 (s), 633 (w), 598 (s), 569 (s) cm^{-1}; **^{1}H NMR** (500 MHz, $CDCl_3$) 7.28-7.26 (2H, m, H_1, H_4), 7.25-7.23 (2H, m, H_5, H_8), 7.15-7.12 (4H, m, H_2, H_3, H_6, H_7), 4.10 (2H, dd, $^3J_{10,11b} = {}^3J_{9,13b}$ = 3.9 Hz, $^3J_{10,11a} = {}^3J_{9,13a}$ = 4.6 Hz, H_9, H_{10}), 2.47 (2H, ddd, $^4J_{11a,13a}$ = 1.1 Hz, $^3J_{10,11a} = {}^3J_{9,13a}$ = 4.6 Hz, , $^2J_{11a,11b} = {}^2J_{13a,13b}$ = 14.1 Hz, H_{11a}, H_{13a}), 2.18 (2H, dd, $^3J_{10,11b} = {}^3J_{9,13b}$ = 3.9 Hz, $^2J_{11a,11b} = {}^2J_{13a,13b}$ = 14.1 Hz, H_{11b}, H_{13b}), 1.62 (1H, br, OH), -0.02 (9H, s, $Si(CH_3)_3$); **^{13}C NMR** (125 MHz, $CDCl_3$) 143.0 (C_q), 142.1 (C_q), 126.6 (CH), 126.4 (CH), 126.0 (CH), 125.7 (CH), 109.8 (C_{14}), 86.4 (C_{15}), 69.4 (C_{12}), 44.33 (C_{11}, C_{13}), 44.29 (C_9, C_{10}), -0.15 ($Si(CH_3)_3$); **CI(methane)-MS**, *m/z* (relative intensity), 332 ($[M]^+$, 29), 315 (100), 299 (55), 243 (35), 241 (44), 215 (7), 192 ($[C_{15}H_{12}]^+$, 49), 191 ($[C_{15}H_{11}]^+$, 38), 178 ($[C_{12}H_{10}]^+$, 50), 165 (3).

9,10-Dihydro-12-ethynyl-12-hydroxy-9,10-propanoanthracene 81

81
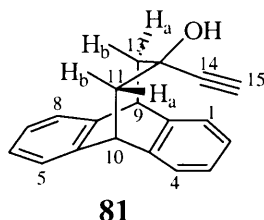
$C_{19}H_{16}O$ 260.33 g.mol^{-1}
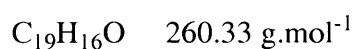
A solution of TBAF in THF (1 M, 0.36 mL, 0.36 mmol) was added dropwise to a solution of the tertiary alcohol **80** (118 mg, 0.36 mmol) in THF (1.5 mL) and the resulting solution was stirred for 30 min. The reaction mixture was quenched with Et$_2$O (1.5 mL) and saturated aqueous NH$_4$Cl solution (3 mL), extracted with Et$_2$O (3 x 1.5 mL), dried over MgSO$_4$ and concentrated under reduced pressure. Flash column chromatography (silica gel, 1:10 EtOAc/P.E. 40-60 °C) provided the _title compound_ **81** (82 mg, 87%) as a white solid.

M.p. 138-141 °C (EtOAc); **HRMS:** found: M$^+$, 260.12229. C$_{19}$H$_{16}$O requires 260.12011; **IR** (CH$_2$Cl$_2$) v_{max} 3562 (s, OH), 3430 (br, OH), 3298 (s, C≡CH), 3022 (m, H$_{ar}$), 2924 (s), 2852 (w), 2108 (w, C≡CH), 1580 (s), 1475 (s), 1456 (s), 1290 (s, OH), 1221 (w), 1175 (d), 1107 (s), 1074 (s), 1059 (s), 1030 (s, C-OH), 993 (s), 895 (w), 768 (s), 737 (m), 704 (s), 660 (s, C-OH), 638 (s, C≡CH), 598 (d), 557 (s), 463 (s) cm^{-1}; ^{1}**H NMR** (500 MHz, CDCl$_3$) 7.32-7.30 (2H, m, H$_1$, H$_4$), 7.28-7.26 (2H, m, H$_5$, H$_8$), 7.19-7.16 (4H, m, H$_2$, H$_3$, H$_6$, H$_7$), 4.14 (2H, dd, $^3J_{10,11b}$ = $^3J_{9,13b}$ = $^3J_{10,11a}$ = $^3J_{9,13a}$ = 4.1 Hz, H$_9$, H$_{10}$), 2.48 (2H, dd, $^3J_{10,11b}$ = $^3J_{9,13b}$ = 4.0 Hz, $^2J_{11a,11b}$ = $^2J_{13a,13b}$ = 14.2 Hz, H$_{11b}$, H$_{13b}$), 2.26 (2H, ddd, $^4J_{11a,13a}$ = 1.1 Hz, $^3J_{10,11a}$ = $^3J_{9,13a}$ = 4.2 Hz, , $^2J_{11a,11b}$ = $^2J_{13a,13b}$ = 14.2 Hz, H$_{11a}$, H$_{13a}$), 2.10 (1H, s, H$_{15}$), 1.68 (1H, br, OH); ^{13}**C NMR** (125 MHz, CDCl$_3$) 142.6 (C$_q$), 142.1 (C$_q$), 126.7 (CH), 126.4 (CH), 126.0 (CH), 125.8 (CH), 88.0 (C$_{14}$), 70.3 (C$_{12}$), 69.1 (C$_{15}$), 44.3 (C$_{11}$, C$_{13}$), 44.2 (C$_9$, C$_{10}$); **EI-MS**, _m/z_ (relative intensity), 260 ([M]$^+$, 47), 242 ([M-H$_2$O]$^+$, 90), 192 ([C$_{15}$H$_{12}$]$^+$, 76), 191 ([C$_{15}$H$_{11}$]$^+$, 100), 178 ([C$_{12}$H$_{10}$]$^+$, 92), 165 (15), 152 (9); **Anal.** Found: C, 87.59; H, 6.23. Calcd for C$_{18}$H$_{16}$O: C, 87.66; H, 6.19.

12-Cyano-9,10-dihydro-12-hydroxytrimethylsilyl-9,10-propanoanthracene 82

82

$C_{21}H_{23}NOSi$ 333.50 g.mol^{-1}
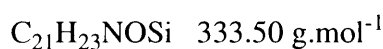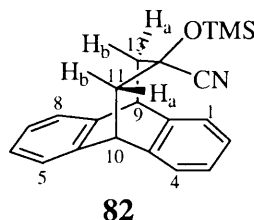
Trimethylsilylcyanide (0.3 mL, 2.2 mmol) was added dropwise to a solution of ketone **67** (234 mg, 1.0 mmol) in anhydrous CH_2Cl_2 (5 mL) in the presence of ZnI_2 (13 mg, 0.04 mmol). The resulting mixture was stirred for 4 h and concentrated under reduced pressure. The crude product was purified by flash column chromatography (silica gel, gradient elution from 1:20 to 1:6.7 EtOAc/P.E. 40-60 °C) to yield the *title compound* **82** (213 mg, 64%) as a white solid.

M.p. 126-129 °C; **HRMS**: found: M$^+$, 333.15436. $C_{21}H_{23}NOSi$ requires 333.15488; **IR** (CH_2Cl_2) v_{max} 3049 (s), 3024 (m, H$_{ar}$), 2956 (s), 2929 (s), 2856 (w), 2204 (w, CN), 1475 (s), 1458 (s), 1292 (w), 1254 (m, Si(CH$_3$)$_3$), 1097 (s, OSi), 1067 (s), 1032 (w), 895 (s, OSi), 872 (s), 847 (s, Si(CH$_3$)$_3$), 739 (m), 704 (s), 599 (w), 573 (s, CN) cm^{-1}; ^{1}**H NMR** (500 MHz, CDCl$_3$) 7.39-7.35 (2H, m, H$_1$, H$_4$), 7.32-7.28 (4H, m, H$_5$, H$_8$, H$_2$, H$_3$), 7.20-7.17 (2H, m, H$_6$, H$_7$), 4.19 (2H, dd, $^3J_{10,11b}$ = $^3J_{9,13b}$ = 1.7 Hz, $^3J_{10,11a}$ = $^3J_{9,13a}$ = 6.7 Hz, H$_9$, H$_{10}$), 2.76 (2H, ddd, $^4J_{11a,13a}$ = 1.2 Hz, $^3J_{10,11a}$ = $^3J_{9,13a}$ = 6.7 Hz, , $^2J_{11a,11b}$ = $^2J_{13a,13b}$ = 14.1 Hz, H$_{11a}$, H$_{13a}$), 2.01 (2H, dd, $^3J_{10,11b}$ = $^3J_{9,13b}$ = 1.7 Hz, $^2J_{11a,11b}$ = $^2J_{13a,13b}$ = 14.1 Hz, H$_{11b}$, H$_{13b}$), 0.13 (9H, s, Si(CH$_3$)$_3$); ^{13}**C NMR** (125 MHz, CDCl$_3$) 143.5 (C$_q$), 139.7 (C$_q$), 127.3 (CH), 126.7 (CH), 126.6 (CH), 125.3 (CH), 121.3 (CN), 70.1 (C$_{12}$), 43.6 (C$_{11}$, C$_{13}$), 43.4 (C$_9$, C$_{10}$), 1.4 Si(CH$_3$)$_3$); **EI-MS**, *m/z* (relative intensity), 333 (M$^+$, 34), 318 (18), 243 (100), 192 ([C$_{15}$H$_{12}$]$^+$, 27), 191 ([C$_{15}$H$_{11}$]$^+$, 47), 178 ([C$_{12}$H$_{10}$]$^+$, 58).

12-Cyano-9,10-dihydro-12-hydroxy-9,10-propanoanthracene 83

83

$C_{18}H_{15}NO$ 261.32 g.mol^{-1}
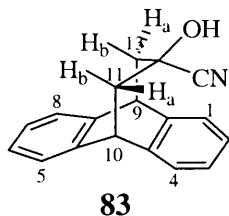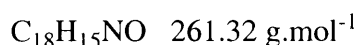
To a stirred solution of the protected alcohol **82** (213 mg, 0.64 mmol) in THF (40 mL) an aqueous HCl solution (1M, 20 mL) was added dropwise. The mixture was stirred for 30 min, diluted with Et$_2$O (100 mL), extracted with Et$_2$O (3 x 50 mL), washed with brine (50 mL) and dried over Na$_2$SO$_4$. After removal of the solvents under reduced pressure, the remaining white powder was washed thoroughly with CH$_2$Cl$_2$ (2 x 100 mL) to afford the *title compound* **83** (160 mg, 96%) as a relatively unstable white powder which was used without further purification.

M.p. 194-195 °C; **HRMS**: found: M$^+$, 261.11429. C$_{18}$H$_{15}$NO requires 261.11536; **IR** (KBr) v_{max} 3323 (br, OH), 3035 (w), 2930 (s), 2243 (s, CN), 1477 (s), 1456 (s), 1419 (s), 1352 (s), 1288 (w), 1169 (w), 1107 (w), 1053 (s, OH), 1030 (s), 997 (w), 773 (s), 754 (s), 704 (s), 648 (s), 596 (s), 571 (s, CN) cm^{-1}; ^{1}**H NMR** (400 MHz, CDCl$_3$) 7.36-7.33 (2H, m, H$_1$, H$_4$), 7.32-7.30 (2H, m, H$_5$, H$_8$), 7.28-7.26 (2H, m, H$_2$, H$_3$), 7.21-7.19 (2H, m, H$_6$, H$_7$), 4.20 (2H, dd, $^3J_{10,11b}$ = $^3J_{9,13b}$ = 2.8 Hz, $^3J_{10,11a}$ = $^3J_{9,13a}$ = 5.7 Hz, H$_9$, H$_{10}$), 2.68 (2H, ddd, $^4J_{11a,13a}$ = 1.2 Hz, $^3J_{10,11a}$ = $^3J_{9,13a}$ = 5.7 Hz, , $^2J_{11a,11b}$ = $^2J_{13a,13b}$ = 14.1 Hz, H$_{11a}$, H$_{13a}$), 2.15 (2H, dd, $^3J_{10,11b}$ = $^3J_{9,13b}$ = 2.8 Hz, $^2J_{11a,11b}$ = $^2J_{13a,13b}$ = 14.1 Hz, H$_{11b}$, H$_{13b}$), 2.09 (1H, br, OH); ^{13}**C NMR** (100 MHz, CDCl$_3$) 142.4 (C$_q$), 140.1 (C$_q$), 127.4 (CH), 126.9 (CH), 126.5 (CH), 125.7 (CH), 121.3 (CN), 69.4 (C$_{12}$), 43.1 (C$_9$, C$_{10}$), 42.1 (C$_{11}$, C$_{13}$); **EI-MS**, *m/z* (relative intensity), 261 ([M]$^+$, 21), 243 ([M-H$_2$O]$^+$, 30), 234 ([M-HCN]$^+$, 32), 215 (13), 192 ([C$_{15}$H$_{12}$]$^+$, 38), 191 ([C$_{15}$H$_{11}$]$^+$, 100), 178 ([C$_{12}$H$_{10}$]$^+$, 65), 165 (18), 152 (11); **Anal.** Found: C, 82.17; H, 5.90; N, 5.21. Calcd for C$_{18}$H$_{15}$NO: C, 82.73; H, 5.79; N, 5.36.

9,10-Dihydro-12-methoxy-12-methyl-9,10-propanoanthracene 84[139]

84

$C_{19}H_{20}O$ 264.36 g.mol^{-1}
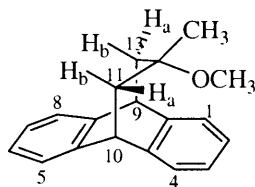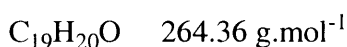
Tertiary alcohol **78** (125 mg, 0.5 mmol) was added as a single portion to a stirred suspension of oil free potassium hydride (30 mg, 0.75 mmol) in anhydrous DMSO (5 mL) and the dark red mixture stirred for 20 min. Dimethyl sulphate (126 mg, 95 μL, 1 mmol) was added dropwise and the light yellow solution was stirred for further 15 min. The reaction mixture was poured into water (10 mL), extracted with CH_2Cl_2 (3 x 5 mL), dried over $MgSO_4$ and concentrated under reduced pressure. Flash column chromatography (silica gel, 1:20, EtOAc/P.E. 40-60 °C) gave the _title compound_ **84** (111 mg, 84%) as a white solid.

M.p. 116 °C (EtOAc) (lit[139] 115-116 °C (EtOAc); **HRMS**: found: M$^+$, 265.15983. $C_{19}H_{20}O$ requires 265.15923; **IR** (CH_2Cl_2) v_{max} 3022 (m, H_{ar}), 2920 (br), 2852 (s), 2822 (s, O-CH_3), 1476 (s), 1456 (s), 1373 (s, CH_3), 1354 (s), 1292 (s), 1238 (w), 1176 (s), 1119 (s, C-O-C), 1086 (s), 1070 (s, C-O-C), 1030 (s), 943 (s), 908 (s), 854 (s), 812 (s), 763 (br), 706 (s), 656 (s), 596 (s) cm^{-1}; ^{1}**H NMR** (400 MHz, CDCl$_3$) 7.26-7.24 (4H, m, H$_1$, H$_4$, H$_5$, H$_8$), 7.15-7.10 (4H, m, H$_2$, H$_3$, H$_6$, H$_7$), 4.04 (2H, dd, $^3J_{10,11b}$ = $^3J_{9,13b}$ = 2.7 Hz, $^3J_{10,11a}$ = $^3J_{9,13a}$ = 5.2 Hz, H$_9$, H$_{10}$), 2.73 (3H, s, OCH$_3$), 2.28 (2H, ddd, $^4J_{11a,13a}$ = 1.4 Hz, $^3J_{10,11a}$ = $^3J_{9,13a}$ = 5.2 Hz, $^2J_{11a,11b}$ = $^2J_{13a,13b}$ = 14.4 Hz, H$_{11a}$, H$_{13a}$), 1.80 (2H, dd, $^3J_{10,11b}$ = $^3J_{9,13b}$ = 2.7 Hz, $^2J_{11a,11b}$ = $^2J_{13a,13b}$ = 14.4 Hz, H$_{11b}$, H$_{13b}$), 0.74 (3H, s, CH$_3$); ^{13}**C NMR** (100 MHz, CDCl$_3$) 144.2 (C$_q$), 142.9 (C$_q$), 126.1 (CH), 125.8 (CH), 125.3 (CH), 124.9 (CH), 76.4 (C$_{12}$), 47.9 (OCH$_3$), 44.7 (C$_9$, C$_{10}$), 40.0 (C$_{11}$, C$_{13}$), 28.0 (CH$_3$); **CI(methane)-MS**, _m/z_ (relative intensity) 323 (46), 266 ([M+H]$^+$, 56), 233 ([M-MeOH+H]$^+$, 100), 193 ([C$_{15}$H$_{12}$+H]$^+$, 61), 179 ([C$_{12}$H$_{10}$+H]$^+$,

55), 155 (51), 119 (51); **Anal.** Found: C, 86.42; H, 7.58. Calcd for $C_{19}H_{20}O$: C, 86.32; H, 7.63.

9,10-Dihydro-12-ethynyl-12-methoxy-9,10-propanoanthracene 85

85

$C_{20}H_{18}O$ 274.36 g.mol^{-1}
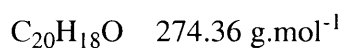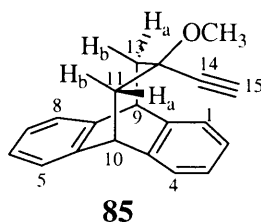
A solution of the tertiary alcohol **81** (105 mg, 0.51 mmol) in anhydrous THF (7.5 mL) was added dropwise to a suspension of 60% sodium hydride dispersion in mineral oil (22 mg, 0.56 mmol) in anhydrous THF (4.5 mL) at -78 °C. The reaction mixture was slowly warmed to 0 °C and stirred for 20 further minutes. Dimethylsulphate (0.2 mL, 2.0 mmol) was added dropwise and the solution was stirred for 2 days at room temperature. After dilution in hexanes (10 mL) and addition of a aqueous KOH solution (1 M, 15 mL), the mixture was stirred for 2 h, poured into a saturated aqueous NH_4Cl solution (15 mL) and extracted with CH_2Cl_2 (3 x 15 mL). The combined organic layers were washed with brine (15 mL), dried over $MgSO_4$ and concentrated under reduced pressure. The crude product was purified by flash column chromatography (silica gel, gradient elution from 1:6.7 to 1:3.3 EtOAc/P.E. 40-60 °C) to afford the *title compound* **85** (87 mg, 62%) as a white solid.

M.p. 158-159 °C (EtOAc); **HRMS**: found: M$^+$, 274.13495. $C_{20}H_{18}O$ requires 274.13576; **IR** (CH_2Cl_2) v_{max} 3265 (s, C≡CH), 2928 (s), 2818 (w, OCH_3), 2109 (w, C≡CH), 1476 (w), 1456 (s), 1290 (w), 1259 (w), 1173 (w), 1111 (w), 1080 (s, OCH_3), 1061 (w), 1030 (s), 987 (w), 862 (w), 810 (w), 773 (w), 760 (s, CH_3), 677 (w), 654 (w, C≡CH), 592 (s) cm^{-1}; ^1H **NMR** (400 MHz, $CDCl_3$) 7.27-7.24 (4H, m, H_1, H_4, H_5, H_8), 7.17-7.12 (4H, m, H_2, H_3, H_6, H_7), 4.13 (2H, dd, $^3J_{10,11b} = {}^3J_{9,13b} = 2.7$ Hz, $^3J_{10,11a} = {}^3J_{9,13a} = 5.7$ Hz, H_9, H_{10}), 3.10 (3H, s, OCH_3), 2.53 (2H, ddd, $^4J_{11a,13a} = 1.2$ Hz, $^3J_{10,11a} = {}^3J_{9,13a} = 5.7$ Hz, , $^2J_{11a,11b} = {}^2J_{13a,13b} = 13.9$ Hz, H_{11a}, H_{13a}), 2.07 (2H, dd, $^3J_{10,11b} = {}^3J_{9,13b} = 2.7$ Hz, $^2J_{11a,11b} = {}^2J_{13a,13b} = 13.9$ Hz, H_{11b}, H_{13b}), 2.01 (1H, s, H_{15}); ^{13}C **NMR** (100 MHz, $CDCl_3$) 143.6 (C_q), 141.7 (C_q), 126.2 (CH),

126.1 (CH), 126.1 (CH), 125.0 (CH), 84.7 (C_{14}), 73.9 (C_{15}), 72.0 (C_{12}), 49.8 (C_9, C_{10}), 44.0 (OCH_3), 41.1 (C_{11}, C_{13}); **EI-MS**, _m/z_ (relative intensity), 274 ($[M]^+$, 79), 259 (13), 242 ($[M-MeOH]^+$, 100), 192 ($[C_{15}H_{12}]^+$, 84), 191 ($[C_{15}H_{11}]^+$, 69), 178 ($[C_{12}H_{10}]^+$, 68), 165 (7); **Anal.** Found: C, 87.41; H, 6.65. Calcd for $C_{20}H_{18}O$: C, 87.56; H, 6.61.

9,10-Dihydro-12,12-oxiranyl-9,10-propanoanthracene 86

86
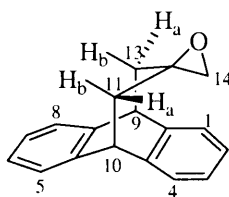
$C_{18}H_{16}O$ 248.32 g.mol^{-1}

3-chloroperoxybenzoic acid (77 %, 0.25g, 1.1 mmol) was added as a single portion to a stirred solution of the alkene **68** (0.1 g, 0.43 mmol) in CH_2Cl_2 (5 mL). After 2 h of stirring, the reaction mixture was poured into an aqueous solution of sodium thiosulphate (10 mL) and extracted with CH_2Cl_2 (3 x 5 mL). The combined organic layers were washed with brine (5 mL), dried over $MgSO_4$ and concentrated under reduced pressure. The crude product was purified by flash column chromatography (silica gel, 1:10 EtOAc/P.E. 40-60 °C) to yield the _title compound_ **86** (98 mg, 92%) as white needles.

M.p. 169-170 °C (EtOAc); **HRMS:** found: M^+, 248.12013. $C_{18}H_{16}O$ requires 248.12011; **IR** (CH_2Cl_2) v_{max} 3032 (m, epoxide and H_{ar}), 2945 (s), 2910 (m), 2854 (w), 1491 (s), 1477 (s), 1456 (s), 1434 (w), 1385 (w), 1175 (w), 1113 (s), 1014 (s), 895 (s, epoxide), 796 (s, epoxide), 764 (s), 714 (s), 631 (w), 594 (s) cm^{-1}; ^{1}**H NMR** (400 MHz, $CDCl_3$) 7.35-7.26 (4H, m, H_1, H_4, H_5, H_8), 7.22-7.17 (4H, m, H_2, H_3, H_6, H_7), 4.18 (2H, t, $^3J_{10,11} = {}^3J_{9,13} = 4.1$ Hz, H_9, H_{10}), 2.06 (2H, s, H_{14}), 2.02 (4H, d, $^3J_{10,11} = {}^3J_{9,13} = 4.1$ Hz, H_{11}, H_{13}); ^{13}**C NMR** (100 MHz, $CDCl_3$) 143.0 (C_q), 142.3 (C_q), 126.6 (CH), 126.5 (CH), 125.8 (CH), 125.7 (CH), 56.8 (C_{12}), 54.7 (C_{14}), 44.7 (C_9, C_{10}), 41.0 (C_{11}, C_{13}); **EI-MS**, _m/z_ (relative intensity), 248 ($[M]^+$, 25), 217 (19), 193 (50), 191 ($[C_{15}H_{11}]^+$, 30), 189 (72), 179 (22), 178 ($[C_{12}H_{10}]^+$, 86), 152 (6); **Anal.** Found: C, 87.25; H, 6.43. Calcd for $C_{18}H_{16}O$: C, 87.06; H, 6.49.

9,10-Dihydro-12,12-oxiranyl-9,10-propanoanthracene 86 and 9,10-dihydro-12,12-oxetanyl-9,10-propanoanthracene 87

86
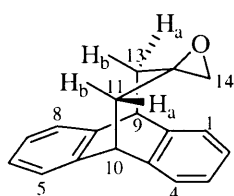
$C_{18}H_{16}O$ 248.32 g.mol^{-1}
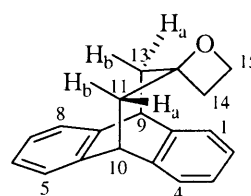
87

$C_{19}H_{18}O$ 262.35 g.mol^{-1}

A solution of t-BuOK (224 mg, 2.0 mmol) in anhydrous t-BuOH (25 mL) was added to a stirred mixture of trimethyloxosulfonium iodide (440 mg, 2.0 mmol) in anhydrous t-BuOH (4 mL) at 50 °C, followed by slow addition of a solution of ketone **67** (117 mg, 0.5 mmol) in anhydrous t-BuOH (2 mL). The resulting mixture was stirred at 50 °C for 3 days. The reaction was quenched by water (10 mL) then extracted with CH_2Cl_2 (3 x 5 mL). The combined organic layers were washed with brine (5 mL), dried over $MgSO_4$ and concentrated under reduced pressure. Flash column chromatography (silica gel, gradient of elution 1:12.5 to 1:4 EtOAc/P.E. 40-60 °C) afforded the title compounds **86** (62 mg, 50%) and **87** (63.3 mg, 48%) as white solids.

9,10-Dihydro-12,12-oxiranyl-9,10-propanoanthracene 86

The spectroscopic data obtained were identical to those previously described

9,10-dihydro-12,12-oxetanyl-9,10-propanoanthracene 87

M.p. 136-138 °C; **HRMS**: found: M$^+$, 262.13607. $C_{19}H_{18}O$ requires 262.13576; **IR** (CH_2Cl_2) v_{max} 2872 (s), 1475 (s), 1454 (s), 1223 (s, C-O-C), 1175 (s, C-O-C), 1099 (s, C-O-C), 1016 (s), 968 (s), 767 (s), 746 (s), 706 (s), 590 (s), 469 (C-O-C) cm^{-1}; ^{1}**H NMR** (400 MHz, $CDCl_3$) 7.31-7.26 (4H, m, H_1, H_4, H_5, H_8), 7.17-7.13 (4H, m, H_2, H_3, H_6, H_7), 4.34 (2H, t, $^3J_{14,15}$ = 7.8 Hz, H_{15}), 4.16 (2H, dd, $^3J_{10,11b}$ = $^3J_{9,13b}$ = 1.8 Hz, $^3J_{10,11a}$ = $^3J_{9,13a}$ = 6.6 Hz, H_9, H_{10}), 2.70 (2H, ddd, $^4J_{11a,13a}$ = 1.3 Hz, $^3J_{10,11a}$ = $^3J_{9,13a}$ = 6.6 Hz, $^2J_{11a,11b}$ = $^2J_{13a,13b}$ =

13.6 Hz, H_{11a}, H_{13a}), 1.98 (2H, dd, $^3J_{10,11b} = {}^3J_{9,13b} = 1.8$ Hz, $^2J_{11a,11b} = {}^2J_{13a,13b} = 13.6$ Hz, H_{11b}, H_{13b}), 1.59 (2H, t, $^3J_{14,15} = 7.8$ Hz, H_{14}); ^{13}**C NMR** (100 MHz, CDCl$_3$) 143.8 (C$_q$), 140.9 (C$_q$), 126.2 (CH), 126.0 (CH), 125.2 (CH), 87.2 (C$_{12}$), 66.0 (C$_{15}$), 44.1 (C$_{11}$, C$_{13}$), 43.8 (C$_9$, C$_{10}$), 36.2 (C$_{14}$); **EI-MS**, m/z (relative intensity) 262 ([M]$^+$, 100), 234 (25), 217 (85), 215 (40), 192 ([C$_{15}$H$_{12}$]$^+$, 53), 191 ([C$_{15}$H$_{11}$]$^+$, 78), 178 ([C$_{12}$H$_{10}$]$^+$, 100), 165 (14), 152 (11).

12-Formyl-9,10-dihydro-9,10-propanoanthracene 92

92
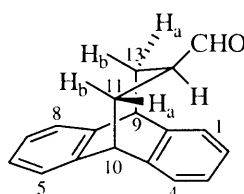
C$_{18}$H$_{16}$O   248.32 g.mol^{-1}

To a solution of epoxide **86** (102 mg, 0.41 mmol) in THF (5 mL) and H$_2$O (1 mL), two drops of concentrated sulphuric acid were added. After stirring overnight, the reaction mixture was neutralized by addition of saturated aqueous NaHCO$_3$ solution, extracted with Et$_2$O (3 x 5 mL) and the combined organic layers were washed with brine and dried over MgSO$_4$. After concentration under reduced pressure, the crude mixture was purified by flash column chromatography (silica gel, 1:10 EtOAc/P.E. 40-60 °C) to afford the _title compound_ **92** (63 mg, 62%) as a white solid.

M.p. 166-168 °C (EtOAc); **HRMS**: found: M$^+$, 248.12034. C$_{18}$H$_{16}$O requires 248.12011; **IR** (CH$_2$Cl$_2$) v_{max} 3024 (m, H$_{ar}$), 2926 (s), 2856 (s), 2816 (w, CHO), 2717 (s, CHO), 1716 (s, CHO), 1473 (s), 1456 (s), 1362 (w, CHO), 1109 (w), 1055 (w), 1032 (s), 897 (w), 769 (s), 739 (m), 704 (s), 575 (s) cm^{-1}; ^{1}**H NMR** (400 MHz, CDCl$_3$) 9.29 (1H, s, CHO), 7.30-7.25 (4H, m, H$_1$, H$_4$, H$_5$, H$_8$), 7.22-7.19 (2H, m, H$_2$, H$_3$), 7.16-7.13 (2H, m, H$_6$, H$_7$), 4.12 (2H, dd, $^3J_{10,11b} = {}^3J_{9,13b} = 2.3$ Hz, $^3J_{10,11a} = {}^3J_{9,13a} = 5.8$ Hz, H$_9$, H$_{10}$), 2.25 (2H, ddd, $^4J_{11a,13a} = 1.0$ Hz, $^3J_{10,11a} = {}^3J_{9,13a} = 5.8$ Hz, $^2J_{11a,11b} = {}^2J_{13a,13b} = 13.5$ Hz, H$_{11a}$, H$_{13a}$), 2.08 (1H, m, H$_{12}$), 1.93 (2H, ddd, $^3J_{10,11b} = {}^3J_{9,13b} = 2.3$ Hz, $^3J_{11a,12} = {}^3J_{11b,12} = 9.8$ Hz, $^2J_{11a,11b} = {}^2J_{13a,13b} = $

13.5 Hz, H_{11b}, H_{13b}); ^{13}C NMR (75 MHz, CDCl$_3$) 203.3 (CHO), 143.8 (C$_q$), 142.1 (C$_q$), 126.9 (CH), 126.8 (CH), 126.2 (CH), 125.4 (CH), 68.2 (C$_{12}$), 62.4 (C$_{14}$), 44.7 (C$_9$, C$_{10}$), 40.4 (C$_{11}$, C$_{13}$); EI-MS, m/z (relative intensity) 248 ([M]$^+$, 68), 217 (7), 191 ([C$_{15}$H$_{11}$]$^+$, 46), 178 ([C$_{12}$H$_{10}$]$^+$, 100); Anal. Found: C, 87.29; H, 6.42. Calcd for C$_{18}$H$_{16}$O: C, 87.06; H, 6.49.

12-Formyl-9,10-dihydro-9,10-propanoanthracene 92 and
9,10-dihydro-12-hydroxymethyl-9,10-prop-11-enoanthracene 93
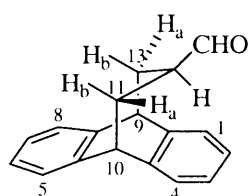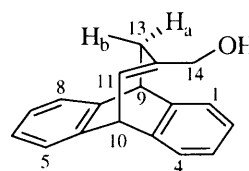
92	**93**
C$_{18}$H$_{16}$O 248.32 g.mol^{-1}	C$_{18}$H$_{16}$O 248.32 g.mol^{-1}

To a solution of epoxide **86** (26 mg, 0.1 mmol) in a mixture of THF (2.5 mL) and H$_2$O (0.5 mL) a pinch of tosic acid was added. After stirring overnight, the reaction mixture was neutralized with a saturated aqueous NaHCO$_3$ solution, extracted with CH$_2$Cl$_2$ (3 x 3 mL) and the combined organic layers were washed with brine and dried over MgSO$_4$. After concentration under reduced pressure, the crude product was purified by flash column chromatography (silica gel, gradient of elution 1:10 to 1:4 EtOAc/P.E. 40-60 °C) to afford the *title compounds* **92** (3.5 mg, 14%) and **93** (13 mg, 53%) as white solids.

12-Formyl-9,10-dihydro-9,10-propanoanthracene 92

The spectroscopic data obtained were identical to those previously described

9,10-Dihydro-12-hydroxymethyl-9,10-prop-11-enoanthracene 93

M.p. 176-177 °C (EtOAc); HRMS: found: M$^+$, 248.11990. C$_{18}$H$_{16}$O requires 248.12011; IR (CH$_2$Cl$_2$) ν_{max} 3689 (s, OH), 3441 (br, OH), 3010 (s, C=CH), 2922 (s), 2852 (w), 1473 (s), 1454 (s), 1412 (s, OH), 1383 (s), 1115 (s, OH), 1085 (s), 1032 (w), 999 (s), 887 (s), 831 (s, C=CH), 764 (s), 748 (s) cm^{-1}; ^{1}H NMR (400 MHz, CDCl$_3$) 7.37-7.35 (2H, m, H$_1$, H$_4$),

7.23-7.21 (2H, m, H_5, H_8), 7.18-7.11 (4H, m, H_2, H_3, H_6, H_7), 6.32 (1H, dt, $^4J_{11,13b} = 1.5$ Hz, $^3J_{10,11} = 8.5$ Hz, H_{11}), 4.25 (1H, d, $^3J_{10,11} = 8.5$ Hz, H_{10}), 4.17 (1H, t, $^3J_{9,13a} = {}^3J_{9,13b} = 3.6$ Hz, H_9), 3.71 (2H, d, $^2J_{CHH,CHH} = 1.1$ Hz, H_{14}), 2.51 (2H, dd, $^4J_{11,13b} = 1.5$ Hz, $^3J_{9,13a} = {}^3J_{9,13b} = 3.6$ Hz, H_{13}), 1.27 (1H, br, OH); ^{13}C NMR (75 MHz, CDCl$_3$) 145.5 (C$_q$), 141.1 (C$_q$), 135.7 (C$_{12}$), 127.4 (CH), 126.2 (CH), 126.0 (CH), 125.9 (CH), 124.1 (C$_{13}$), 45.6 (C$_9$, C$_{10}$), 34.0 (C$_{11}$), 29.7 (C$_{14}$); CI(methane)-MS, *m/z* (relative intensity) 248 ([M]$^+$, 20), 231 (100), 217 (8), 191 ([C$_{15}$H$_{11}$]$^+$, 7), 145 (20).

9,10-Dihydro-12-methyl-9,10-prop-11-enoanthracene 95

95
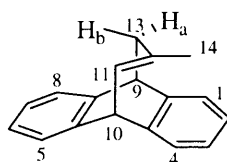
C$_{18}$H$_{16}$ 232.32 g.mol^{-1}

Diethylaminosulfur trifluoride (140 μL, 1.1 mmol) was added as a single portion to a solution of alcohol **78** (125 mg, 0.5 mmol) in anhydrous THF (5 mL) at -78 °C. The reaction mixture was stirred for 1.5 h, warmed to room temperature, poured into water (5 mL) and extracted with CH$_2$Cl$_2$ (3 x 2.5 mL). The combined organic layers were washed with brine (5 mL), dried over MgSO$_4$ and concentrated under reduced pressure. Purification of the crude product by flash column chromatography (silica gel, 1:10 EtOAc/P.E. 40-60 °C) afforded the *title compound* **95** (90 mg, 78%) as a white solid.

M.p. 162-166 °C; **HRMS**: found: M$^+$, 232.12541. C$_{18}$H$_{16}$ requires 232.12519; **IR** (CH$_2$Cl$_2$) v_{max} 3020 (m, H$_{ar}$), 2922 (m), 2873 (w), 2818 (w), 1473 (s), 1454 (s), 1445 (s), 1421 (s), 1292 (s), 1173 (s), 1136 (s), 1115 (w), 1029 (s), 949 (s), 877 (s), 822 (m), 765 (s), 742 (s), 702 (s), 687 (s), 596 (s), 472 (s), 436 (s) cm^{-1}; ^{1}H NMR (300 MHz, CDCl$_3$) 7.39-7.34 (2H, m, H$_1$, H$_4$) 7.26-7.23 (2H, m, H$_5$, H$_8$), 7.20-7.13 (4H, m, H$_2$, H$_3$, H$_6$, H$_7$), 6.07 (1H, dt, $^4J_{11,13b} = 1.7$ Hz, $^3J_{10,11} = 8.6$ Hz, H$_{11}$), 4.19 (1H, d, $^3J_{10,11} = 8.6$ Hz, H$_{10}$), 4.12 (1H, t, $^3J_{9,13} = 3.6$ Hz, H$_9$), 2.42 (2H, m, H$_{13}$), 1.44 (3H, s, H$_{14}$); ^{13}C NMR (75 MHz, CDCl$_3$) 146.1 (C$_q$),

141.4 (C_q), 132.3 (C_{12}), 125.9 (CH), 123.9 (C_{13}), 46.0 (C_9, C_{10}), 38.1 (C_{11}), 25.3 (C_{14}); **EI-MS**, *m/z* (relative intensity), 232 (M^+, 43), 217 (21), 191 ($[C_{15}H_{11}]^+$, 41), 178 ($[C_{12}H_{10}]^+$, 100).

9,10-Dihydro-12-fluoro-12-methyl-9,10-propanoanthracene 94[139]
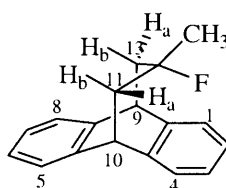
94

$C_{18}H_{17}F$ 252.33 g.mol^{-1}

Morpholinosulphur trifluoride (1g, 5.7 mmol) was added dropwise at -78 °C under a nitrogen atmosphere to a solution of tertiary alcohol **78** (285 mg, 1.14 mmol) in anhydrous CH_2Cl_2 (30 mL) and the mixture was then stirred for 24 h at room temperature. The reaction mixture was concentrated under reduced pressure, and water (50 mL) was carefully added to the residue. The resulting solution was extracted with CH_2Cl_2 (3 x 25 mL), the combined organic layers were washed with water (25 mL) and saturated aqueous $NaHCO_3$ solution (25 mL), and then dried over Na_2SO_4. The solvent was removed under reduced pressure and the crude product was purified by flash column chromatography (silica gel, 1:20 EtOAc/P.E. 40-60 °C) to yield the *title compound* **94** (248 mg, 86%) as a white solid.

M.p. 105-107 °C (lit[139] 108-112 °C); **IR** (KBr) v_{max} 3024 (w, H_{ar}), 2966 (m), 2929 (m), 1478 (m), 1455 (m), 1379 (m, CF), 1127 (m), 1082 (s), 854 (s), 828 (s), 769 (s), 745 (s), 596 (s), 495 (s) cm^{-1}; **^{1}H NMR** (300 MHz, CDCl$_3$) 7.33-7.27 (4H, m, H_1, H_4, H_5, H_8), 7.21-7.15 (4H, m, H_2, H_3, H_6, H_7,), 4.10 (2H, dd, $^3J_{10,11b} = {}^3J_{9,13b} = 1.8$ Hz, $^3J_{10,11a} = {}^3J_{9,13a} = 6.2$ Hz, H_9, H_{10}), 2.46 (2H, dddd, $^4J_{11a,13a} = 1.9$ Hz, $^3J_{10,11a} = {}^3J_{9,13a} = 6.2$ Hz, $^2J_{11a,11b} = {}^2J_{13a,13b} = 15.0$ Hz, $^3J_{11a,F} = {}^3J_{13a,F} = 20.9$ Hz, H_{11a}, H_{13a}), 1.97 (2H, ddd, $^3J_{10,11b} = {}^3J_{9,13b} = 1.8$ Hz, $^2J_{11a,11b} = {}^2J_{13a,13b} = 15.0$ Hz, $^3J_{11b,F} = {}^3J_{13b,F} = 34.3$ Hz, H_{11b}, H_{13b}), 1.08 (3H, d, $^3J_{CH3,F} = 21.2$ Hz, CH$_3$); **^{13}C NMR** (75 MHz, CDCl$_3$) 144.1 (C_q), 141.9 (C_q), 126.3 (CH), 126.2

(CH), 125.6 (CH), 125.3 (CH), 96.4 (d, J = 167.4 Hz, C_{12}), 44.4 (d, C_9, C_{10}); 42.3 (d, J = 21.3 Hz, C_{11}, C_{13}), 30.6 (d, J = 24.4 Hz, CH_3); ^{19}**F NMR** (376 MHz, $CDCl_3$) -123.0 (m); **EI-MS**, *m/z* (relative intensity) 252 ($[M]^+$, 73), 232 (27), 217 (84), 192 (46), 191 ($[C_{15}H_{11}]^+$, 100), 178 ($[C_{12}H_{10}]^+$, 79), 165 (14), 152 (12), 84 (28); **Anal.** Found: C, 85.81; H, 6.92. Calcd for $C_{18}H_{17}F$: C, 85.68; H, 6.79.

9,10-Dihydro-12-fluoro-9,10-propanoanthracene 96

96

$C_{17}H_{15}F$ 238.30 g.mol^{-1}
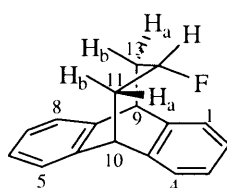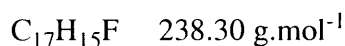
Morpholinosulphur trifluoride (305 μL, 2.5 mmol) was added dropwise at -78 °C under a nitrogen atmosphere to a solution of secondary alcohol **77** (119 mg, 0.5 mmol) in anhydrous CH_2Cl_2 (12 mL) and the mixture was then stirred for 16 h at room temperature. The reaction mixture was concentrated under reduced pressure, and water (20 mL) was carefully added to the residue. The resulting solution was extracted with CH_2Cl_2 (3 x 10 mL), the combined organic layers were washed with water (10 mL) and saturated aqueous $NaHCO_3$ solution (10 mL), then dried over Na_2SO_4. The solvent was removed under reduced pressure and the crude product was purified by flash column chromatography (silica gel, 1:20 EtOAc/ P.E. 40-60 °C) to yield the *title compound* **96** (98 mg, 82%) as a white solid.

M.p. 134-137 °C; **HRMS** found: $[M+H]^+$, 239.12397; $[C_{17}H_{15}F+H]^+$ requires 239.12360; **IR** (KBr) v_{max} 3030 (w, H_{ar}), 2929 (m), 2862 (w), 1471 (m), 1456 (m), 1383 (w), 1368 (m, CF), 1288 (s), 1261 (s), 1111 (s), 1051 (s), 1030 (s), 995 (br), 864 (s), 798 (s), 769 (m), 752 (s), 660 (s), 596 (s) cm^{-1}; ^{1}**H NMR** (500 MHz, C_6D_6) 7.02-6.99 (6H, m, H_{ar}), 6.96-6.94 (2H, m, H_{ar}), 4.07 (1H, ddd, $^3J_{12,11a}$ = $^3J_{12,13a}$ = 6.0 Hz, $^3J_{12,11b}$ = $^3J_{12,13b}$ = 9.9 Hz, $^2J_{12,F}$ = 46.3 Hz, H_{12}), 3.72 (2H, ddd, $^3J_{10,11b}$ = $^3J_{9,13b}$ = 1.5 Hz, $^4J_{9,F}$ = $^4J_{10,F}$ = 2.4 Hz, $^3J_{10,11a}$ =

$^3J_{9,13a}$ = 7.1 Hz, H_9, H_{10}), 2.31 (2H, dddd, $^4J_{11a,13a}$ = 1.0 Hz, $^3J_{12,11a}$ = $^3J_{12,13a}$ = 6.0 Hz,

$^3J_{10,11a}$ = $^3J_{9,13a}$ = 7.1 Hz, $^2J_{11a,11b}$ = $^2J_{13a,13b}$ = 13.4 Hz, H_{11a}, H_{13a}), 1.67 (2H, ddd, $^3J_{10,11b}$ =

$^3J_{9,13b}$ = 1.5 Hz, $^3J_{12,11b}$ = $^3J_{12,13b}$ = 9.9 Hz, $_{,11b}$ = $^2J_{13a,13b}$ = 13.4 Hz, H_{11b}, H_{13b}); ^{13}C NMR

(125 MHz, $CDCl_3$) 146.2 (C_q), 141.2 (C_q), 126.7 (CH), 126.5 (CH), 125.7 (CH), 125.5

(CH), 90.6 (d, J = 167.6 Hz, C_{12}), 46.0 (d, J = 11.0 Hz, C_9, C_{10}); 36.48 (d, J = 19.4 Hz, C_{11},

C_{13}); ^{19}F NMR (376 MHz, $CDCl_3$) -174.0 (m); CI (methane)-MS, m/z (relative intensity)

238 ([M]$^+$, 100), 218 (70), 203 (28), 192 ([$C_{15}H_{12}$]$^+$, 93), 191 ([$C_{15}H_{11}$]$^+$, 100), 178

([$C_{12}H_{10}$]$^+$, 73), 165 (10), 152 (12), 105 (12).

12-(_tert_-Butylsulfinimino)-9,10-dihydro-9,10-propanoanthracene 104
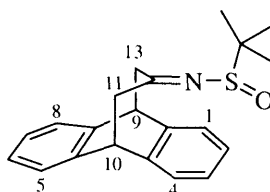
104

$C_{21}H_{23}NOS$ 337.49 g.mol^{-1}

Ti(O-iPr)$_4$ (690 µL, 2.5 mmol) was added dropwise under nitrogen atmosphere to a mixture of ketone **67** (117 mg, 0.5 mmol) and _tert_-butylsulfinamide (121 mg, 1.0 mmol) in anhydrous THF (5 mL) and the resulting solution was heated at 60 °C for 20 h. After cooling to room temperature, brine (5 mL) was added and the solution filtered through celite and extracted with CH_2Cl_2 (3 x 5 mL). The combined organic layers were dried over Na_2SO_4, filtered and concentrated under reduced pressure. Flash column chromatography (silica gel, 1:4 EtOAc/P.E. 40-60 °C) yielded to the _title compound_ **104** (168 mg, quantitative) as a white solid.

M.p. 141-146 °C; **HRMS**: found: [M+H], 338.15823. [$C_{21}H_{23}NOS+H$] requires 338.15785; **IR** (CH_2Cl_2) v_{max} 3022 (m, H_{ar}), 2897 (w), 2860 (w), 1607 (d, C=N-SO), 1475 (s), 1454 (s), 1414 (s), 1391 (d, C(CH$_3$)$_3$), 1358 (s, SO$_2$), 1287 (w), 1169 (s, S=O), 1113 (w), 1074 (s, S=O), 1034 (w), 997 (s), 947 (d), 769 (s), 756 (s), 739 (s), 717 (s), 602 (s, S=O), 586 (s) cm^{-1}; **^{1}H NMR** (400 MHz, $CDCl_3$) 7.33-7.30 (4H, m, H_1, H_4, H_5, H_8), 7.21-

7.17 (4H, m, H_2, H_3, H_6, H_7), 4.21 (2H, dd, $^3J_{10,11} = {}^3J_{9,13} = 3.3$ Hz, $^3J_{10,11} = {}^3J_{9,13} = 4.2$ Hz, H_9, H_{10}), 3.50 (1H, dd, $^3J_{10,11} = {}^3J_{9,13} = 3.3$ Hz, $^2J_{11a,11b} = {}^2J_{13a,13b} = 16.4$ Hz, H_{11a} or H_{13a}), 3.27 (1H, dd, $^3J_{10,11} = {}^3J_{9,13} = 4.2$ Hz, $^2J_{11a,11b} = {}^2J_{13a,13b} = 16.4$ Hz, H_{11a} or H_{13a}), 2.92 (2H, ddd, $^3J_{10,11} = {}^3J_{9,13} = 3.3$ Hz, $^3J_{10,11} = {}^3J_{9,13} = 4.2$ Hz, $^2J_{11a,11b} = {}^2J_{13a,13b} = 16.4$ Hz, H_{11b}, H_{13b}), 0.97 (9H, s, $(CH_3)_3$); ^{13}C NMR (100 MHz, $CDCl_3$) 184.0 (C_{12}), 142.1 (C_q), 141.9 (C_q), 141.8 (C_q), 126.9 (CH), 126.8 (CH), 126.0 (CH), 125.9 (CH), 125.8 (CH), 56.4 ($C(CH_3)_3$), 47.4 (C_{11} or C_{13}), 44.4 (C_9 or C_{10}), 44.0 (C_9 or C_{10}), 42.8 (C_{11} or C_{13}), 21.9 (CH_3); CI(methane)-MS, m/z (relative intensity), 338 ($[M+H]^+$, 42), 282 (100), 281 (60), 264 (77), 235 (95), 233 (90), 217 (35), 191 ($[C_{15}H_{11}]^+$, 37), 178 ($[C_{12}H_{10}]^+$, 65), 122 (46); Anal. Found: C, 74.71; H, 6.86; N, 4.00; S, 9.82. Calcd for $C_{21}H_{23}NOS$: C, 74.74; H, 6.87; N, 4.15; S, 9.50.

12-(2-Chloroacetamido)-9,10-dihydro-12-methyl-9,10-propanoanthracene 106
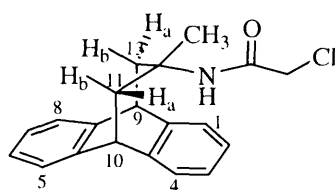
106

$C_{20}H_{20}ClNO$ 325.83 g.mol^{-1}

Glacial acetic acid (240 μL) was slowly added to a solution of the tertiary alcohol **78** (250 mg, 1.0 mmol) and chloroacetonitrile (390 μL, 6.0 mmol) in CH_2Cl_2 (2.5 mL) at 0 °C, followed by a dropwise addition of concentrated H_2SO_4 (500 μL, 9.0 mmol), within keeping the temperature below 10 °C. The mixture was slowly warmed to room temperature and stirred for 5 h. Then the resulting solution was poured into ice-water (5 mL), filtered, washed with a saturated aqueous $NaHCO_3$ solution (5 mL) and extracted with CH_2Cl_2 (3 x 5 mL). The combined organic layers were washed three times with brine (5 mL), dried over $NaSO_4$ and concentrated under reduced pressure. The crude product was purified by flash column chromatography (silica gel, 1:5 EtOAc/P.E. 40-60 °C) to afford the *title compound* **106** (296 mg, 91%) as a white solid.

M.p. 137-141 °C (EtOAc-P.E); **HRMS**: found: M$^+$, 326.13179. $C_{20}H_{20}ClNO$ requires 326.13116; **IR** (CH_2Cl_2) v_{max} 3048 (s, NHCO), 3350 (w), 3022 (m, H_{ar}), 2930 (s), 2858 (w), 1666 (s, C=O), 1529 (s, NH), 1475 (s), 1456 (s), 1408 (s), 1377 (s, CH_3), 1296 (CH_2Cl), 1176 (w), 1121 (s), 1097 (s), 1032 (s), 978 (w), 768 (s), 737 (s), 702 (s), 596 (s), 530 (s) cm^{-1}; ^{1}**H NMR** (500 MHz, $CDCl_3$) 7.29-7.28 (2H, m, H_1, H_4), 7.25-7.23 (2H, m, H_5, H_8), 7.18-7.16 (2H, m, H_2, H_3), 7.14-7.12 (2H, m, H_6, H_7), 5.30 (2H, br, NH_2), 4.08 (2H, dd, $^3J_{10,11b} = {}^3J_{9,13b} = 1.0$ Hz, $^3J_{10,11a} = {}^3J_{9,13a} = 7.1$ Hz, H_9, H_{10}), 3.41 (3H, s, CH_2Cl), 2.79 (2H, ddd, $^4J_{11a,13a} = 1.7$ Hz, $^3J_{10,11a} = {}^3J_{9,13a} = 7.1$ Hz, , $^2J_{11a,11b} = {}^2J_{13a,13b} = 15.1$ Hz, H_{11a}, H_{13a}), 1.74 (2H, dd, $^3J_{10,11b} = {}^3J_{9,13b} = 1.0$ Hz, $^2J_{11a,11b} = {}^2J_{13a,13b} = 15.1$ Hz, H_{11b}, H_{13b}), 1.21 (3H, s, CH_3); ^{13}**C NMR** (125 MHz, $CDCl_3$) 163.8 (C=O), 144.5 (C_q), 141.4 (C_q), 127.1 (CH), 126.3 (CH), 125.9 (CH), 125.2 (CH), 56.7 (C_{12}), 44.8 (C_9, C_{10}), 42.7 (CH_2Cl), 40.4 (C_{11}, C_{13}), 29.8 (CH_3); **CI (Methane)-MS**, m/z (relative intensity), 326 (M$^+$, 75), 290 ([M+HCl]$^+$, 74), 261 (74), 233 (100), 217 (73), 192 ([$C_{15}H_{12}$]$^+$, 64), 191 ([$C_{15}H_{11}$]$^+$, 76), 178 ($C_{12}H_{10}$]$^+$, 71), 165 (32), 122 (66).

12-Amino-9,10-dihydro-12-methyl-9,10-propanoanthracene 103
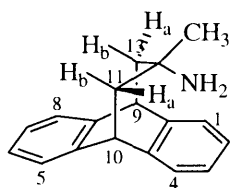
103

$C_{18}H_{19}N$ 249.35 g.mol^{-1}

A mixture of the chloroacetamide **106** (296 mg, 0.91 mmol), thiourea (84 mg, 1.1 mmol) in glacial acetic acid (0.4 mL) and EtOH (14 mL) was heated at reflux for 20 h. The mixture was poured into water (30 mL) and neutralized with an aqueous KOH solution (3 M) until a slightly basic pH was reached. The product was extracted with CH_2Cl_2 (15 mL), washed with brine (3 x 15 mL) and concentrated under reduced pressure. The crude product was purified by flash column chromatography (1:4:45 triethylamine/MeOH/EtOAc) to yield the *title compound* **103** (222 mg, 68 %) as a light yellow solid.

M.p. 154-156 °C (EtOAc-P.E); **HRMS:** found: M^+, 249.15198. $C_{18}H_{19}N$ requires 249.15174; **IR** (CH_2Cl_2) v_{max} 3379 (s, NH_2), 3026 (m, H_{ar}), 2960 (s, CH_3), 2906 (s), 2839 (w), 1580 (m, NH_2), 1475 (s), 1456 (s), 1427 (w), 1375 (s, CH_3), 1175 (w), 1113 (s), 1030 (s), 903 (w), 850 (s), 766 (m), 739 (s), 706 (s), 663 (s), 609 (w), 596 (s), 506 (s) cm^{-1}; ^1H **NMR** (400 MHz, $CDCl_3$) 7.35-7.30 (2H, m, H_1, H_4), 7.28-7.23 (2H, m, H_5, H_8), 7.21-7.17 (2H, m, H_2, H_3), 7.16-7.14 (2H, m, H_6, H_7), 4.11 (2H, dd, $^3J_{10,11b} = {}^3J_{9,13b} = 2.4$ Hz, $^3J_{10,11a} = {}^3J_{9,13a} = 5.8$ Hz, H_9, H_{10}), 2.05 (2H, ddd, $^4J_{11a,13a} = 1.0$ Hz, $^3J_{10,11a} = {}^3J_{9,13a} = 5.8$ Hz, , $^2J_{11a,11b} = {}^2J_{13a,13b} = 14.2$ Hz, H_{11a}, H_{13a}), 1.94 (2H, dd, $^3J_{10,11b} = {}^3J_{9,13b} = 2.4$ Hz, $^2J_{11a,11b} = {}^2J_{13a,13b} = 14.2$ Hz, H_{11b}, H_{13b}), 0.80 (2H, br, NH_2), 0.75 (3H, s, CH_3); ^{13}C **NMR** (100 MHz, $CDCl_3$) 144.1 (C_q), 142.3 (C_q), 126.5 (CH), 126.2 (CH), 126.1 (CH), 125.3 (CH), 51.6 (C_{12}), 45.5 (C_{11}, C_{13}), 45.3 (C_9, C_{10}), 34.8 (CH_3); **EI-MS**, m/z (relative intensity),249 ($[M]^+$, 51), 234 (57), 217 (39), 192 ($[C_{15}H_{12}]^+$, 100), 191 ($[C_{15}H_{11}]^+$, 71), 178 ($[C_{12}H_{10}]^+$, 57), 165 (16), 144 (25); **Anal.** Found: C, 86.48; H, 7.65; N, 5.58. Calcd for $C_{18}H_{19}N$: C, 86.70; H, 7.68; N, 5.62.

12-Ethynyl-9,10-dihydro-9,10-prop-11-enoanthracene 110
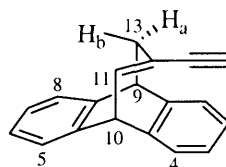
110

$C_{19}H_{14}$ 242.31 g.mol^{-1}

Propargyl alcohol **81** (130 mg, 0.5 mmol) was dissolved in anhydrous CH_2Cl_2 (1 mL) and distilled triethylamine (105 µL, 0.75 mmol) was added dropwise. After cooling to 0 °C, methanesulfonyl chloride (51 µL, 0.65 mmol) was added dropwise. The resulting mixture was stirred at 0 °C for 6 h, then dissolved in CH_2Cl_2 (5 mL). The solution was first washed with a mixture of brine (2.5 mL) and aqueous HCl solution (3M, 2.5 mL) and then with a saturated $NaHCO_3$ aqueous solution (5 mL). The product was dried over $MgSO_4$, concentrated under reduced pressure and purified by flash column chromatography (silica

gel, 1:5 EtOAc/P.E. 40-60 °C) to afford the _title compound_ **110** (70 mg, 58%) as a white solid.

M.p. 188-191 °C; **HRMS**: found: M^+, 243.11674. $C_{19}H_{14}$ requires 243.11737; **IR** (CH_2Cl_2) v_{max} 3284 (s, $C\equiv CH$), 3022 (m, H_{ar}), 2883 (w), 2110 (w, $C\equiv CH$), 1475 (s), 1456 (s), 1175 (s), 1031 (m), 889 (s), 835 (w, C=C), 769 (s), 739 (m), 704 (s), 652 (s), 631 (s), 615 (s), 590 (s) cm^{-1}; **^{1}H NMR** (300 MHz, $CDCl_3$) 7.40 (2H, m, H_1, H_4), 7.28-7.16 (6H, m, H_2, H_3, H_5, H_6, H_7, H_8), 6.78 (1H, dt, $^5J_{11,CCH}$ = 0.6 Hz, $^4J_{11,13b}$ = 2.1 Hz, $^3J_{10,11}$ = 8.6 Hz, H_{11}), 4.30 (1H, d, $^3J_{10,11}$ = 8.6 Hz, H_{10}), 4.16 (1H, t, $^3J_{9,13a}$ = $^3J_{9,13b}$= 3.7 Hz, H_9), 2.64 (2H, dd, $^3J_{11,13b}$ = 2.1 Hz, $^3J_{9,13a}$ = $^3J_{9,13b}$ = 3.7 Hz, H_{13}), 2.55 (1H, d, $^5J_{11,CCH}$ = 0.6 Hz, $C\equiv CH$); **^{13}C NMR** (75 MHz, $CDCl_3$) 144.5 (C_q), 142.2 (C_q), 140.6 (C_q), 139.3 (C_{11}), 126.6 (CH), 126.3 (CH), 126.2 (CH), 125.9 (CH), 125.7 (CH), 124.5 (CH), 118.2 (C_{12}), 85.9 ($C\equiv CH$), 72.6 ($C\equiv CH$), 46.1 (C_{10}), 45.5 (C_9), 37.2 (C_{13}); **CI(methane)-MS**, _m/z_ (relative intensity) 243 ($[M]^+$, 100), 228 (9), 191 ($[C_{15}H_{11}]^+$, 23), 178 ($[C_{12}H_{10}]^+$, 6) 165 (18), 119 (11), 91 (22).

12-Acetyl-9,10-dihydro-9,10-prop-11-enoanthracene 111
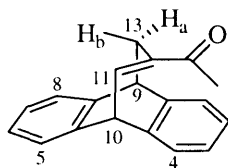
111

$C_{19}H_{16}O$ 260.33 g.mol^{-1}

Propargyl alcohol **81** (69 mg, 0.26 mmol) was dissolved in Et_2O (1.5 mL) and sodium cyanide (13 mg, 0.26 mmol) in glacial acetic acid (330 µL) was added at once. Concentrated sulphuric acid (65 mg) in glacial acetic acid (330 µL) was added dropwise over 10 min and the resulting mixture stirred overnight. The reaction solution was quenched by NaOH (150 mg) in H_2O (500 µL), stirred for 2 h, then diluted with Et_2O (1.5 mL) and the ethereal layer collected. The aqueous layer was extracted with Et_2O (3 x 1.5 mL) and the combined organic layers were washed with brine, dried over $MgSO_4$ and concentrated under reduced pressure. The crude residue was purified by flash column

chromatography (silica gel, gradient of elution 1:5 to 1:2 EtOAc/P.E. 40-60 °C) to afford the _title compound_ **111** (60.7 mg, 90%) as a white solid.

M.p. 224-228 °C (EtOAc-P.E. 40-60 °C); **HRMS**: found: M^+, 26012031. $C_{19}H_{16}O$ requires 260.12011; **IR** (CH_2Cl_2) ν_{max} 3022 (m, H_{ar}), 2892 (d), 1651 (m, C=O), 1627 (m, C=O), 1475 (s), 1456 (s), 1418 (s), 1387 (s), 1355 (s), 1331 (s), 1232 (s), 1173 (s), 1157 (s), 1116 (s), 1033 (s), 986 (s), 946 (d), 863 (s), 835 (s), 738 (m), 705 (s), 683 (s), 625 (s), 683 (s), 595 (s) cm^{-1}; **^{1}H NMR** (300 MHz, $CDCl_3$) 7.45 (1H, dt, $^4J_{11,13} = 1.9$ Hz, $^3J_{10,11} = 8.6$ Hz, H_{11}), 7.39 (2H, m, H_{ar}), 7.29-7.16 (6H, m, H_{ar}), 4.46 (1H, d, $^3J_{10,11} = 8.6$ Hz, H_{10}), 4.25 (1H, t, $^3J_{9,13} = 3.8$ Hz, H_9), 2.70 (2H, dd, $^4J_{11,13}= 1.9$ Hz, $^3J_{9,13} = 3.8$ Hz, H_{13}), 2.15 (3H, s, CH_3); **^{13}C NMR** (75 MHz, $CDCl_3$) 199.7 (C=O), 143.2 (C_q), 143.0 (C_{11}), 140.9 (C_q), 137.2 (C_q), 127.0 (CH), 126.3 (CH), 126.2 (CH), 124.5 (CH), 45.8 (C_9 or C_{10}), 45.0 (C_9 or C_{10}), 31.7 (C_{13}), 25.0 (CH_3); **EI-MS**, _m/z_ (relative intensity) 260 ([M]$^+$, 100), 245 (10), 217 (87), 216 (22), 215 (73), 202 (37), 191 ([$C_{15}H_{11}$]$^+$, 16), 178 ([$C_{12}H_{10}$]$^+$, 38); **Anal.** Found: C, 87.14; H, 6.18. Calcd for $C_{19}H_{16}O$: C, 87.56; H, 6.19.

9,10-Dihydro-12-hydroxyimino-9,10-propanoanthracene 112

112

$C_{17}H_{15}NO$ 249.31 g.mol^{-1}
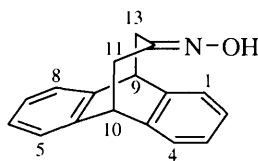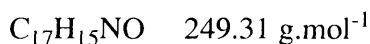
A mixture of ketone **67** (468 mg, 2.0 mmol), hydroxylamine hydrochloride (688 mg, 10.0 mmol), pyridine (1.3 mL) and ethanol (4 mL) was refluxed for 16 h and then concentrated _in vaccuo_. Aqueous HCl solution (1 M) was added to neutralise the reaction mixture and the resulting solution was diluted in water (5 mL) and EtOAc (5 mL). The organic layer was extracted with EtOAc (5 mL), washed with water (3 x 5 mL), dried over MgSO$_4$, filtered and concentrated under reduced pressure. Flash column chromatography

(silica gel, 1:4 EtOAc/P.E. 40-60 °C) yielded the *title compound* **112** (474 mg, 95%) as a white solid.

M.p. 158-160 °C; **HRMS** found: M^+, 249.11497. $C_{17}H_{15}NO$ requires 249.11536; **IR** (CH_2Cl_2) v_{max} 3200 (br, OH), 3045 (m, H_{ar}), 2898 (m), 1636 (s, C=N), 1475 (s), 1456 (s), 1423 (s), 1340 (w), 1178 (s), 1119 (w), 1011 (d), 984 (s), 960 (s), 928 (w), 770 (s), 733 (s), 708 (s), 594 (s), 580 (s) cm^{-1}; **^{1}H NMR** (300 MHz, $CDCl_3$) 8.47 (1H, br, NOH), 7.33-7.27 (4H, m, H_{ar}), 7.22-7.16 (4H, m, H_{ar}), 4.18 (2H, t, $^3J_{10,11} = {}^3J_{9,13} = 4.0$ Hz, H_9, H_{10}), 3.00 (2H, dd, $^4J_{11a,13a} = 0.7$ Hz, $^3J_{10,11} = {}^3J_{9,13} = 4.0$ Hz, H_{11} or H_{13}), 2.74 (2H, dd, $^4J_{11a,13a} = 0.7$ Hz, $^3J_{10,11} = {}^3J_{9,13} = 4.0$ Hz, H_{11} or H_{13}); **^{13}C NMR** (75 MHz, $CDCl_3$) 157.4 (C_{12}), 142.2 (C_q), 142.1 (C_q), 126.8 (CH), 126.7 (CH), 125.9 (CH), 44.4 (C_9 or C_{10}), 43.8 (C_9 or C_{10}), 38.9 (C_{11} or C_{13}), 33.3 (C_{11} or C_{13}); **EI-MS**, *m/z* (relative intensity), 249 ($[M]^+$, 46), 232 (95), 215 (15), 191 ($[C_{15}H_{11}]^+$, 44), 189 (21), 178 ($[C_{12}H_{10}]^+$, 100), 165 (9), 152 (16); **Anal.** Found: C, 81.66; H, 6.09; N, 5.57. Calcd for $C_{17}H_{15}NO$: C, 81.90; H, 6.06; N, 5.62.

12-(Benzyloxy)imino-9,10-dihydro-9,10-propanoanthracene 113

113

$C_{24}H_{21}NO$ 339.43 g.mol^{-1}
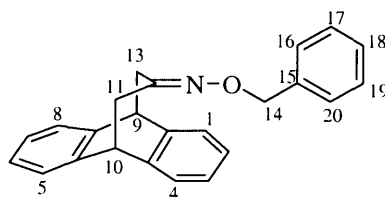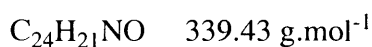
A solution of the oxime **112** (85 mg, 0.34 mmol) and benzyl bromide (200 μL, 1.7 mmol) in anhydrous CH_2Cl_2 (10 mL) was added to an aqueous NaOH solution (50%, 20 mL) and a catalytic amount of tetrabutylammonium bromine. The resulting two-phase system was stirred vigorously at room temperature for 1 h. Then CH_2Cl_2 (10 mL) was added, the organic layer washed with aqueous HCl solution (1M, 10 mL), followed by brine (10 mL), and dried over Na_2SO_4. The crude product was concentrated under reduced pressure and

purified by flash column chromatography (silica gel, 1:10 EtOAc/P.E. 40-60 °C) to afford the _title compound_ **113** (485 mg, 57%) as a white solid.

M.p. 142-144 °C (EtOAc); **HRMS** found: M^+, 339.16191. $C_{24}H_{21}NO$ requires 339.16231; **IR** (CH_2Cl_2) v_{max} 3030 (m, H_{ar}), 2910 (m), 1650 (m, C=N), 1475 (s), 1452 (s), 1423 (s), 1365 (s), 1175 (s), 1111 (s), 1082 (w), 1051 (s), 1012 (s), 905 (s), 885 (s), 858 (s), 820 (w), 765 (m), 725 (s), 696 (s), 596 (s), 548 (s) cm^{-1}; **^{1}H NMR** (400 MHz, $CDCl_3$) 7.37-7.33 (4H, m, H_{ar}), 7.29-7.26 (3H, m, H_{17}, H_{18}, H_{19}), 7.25-7.22 (4H, m, H_{ar}), 7.09 (2H, m, H_{16}, H_{20}), 4.96 (2H, s, H_{14}), 4.21 (2H, dt, $^3J_{10,11} = {}^3J_{9,13} = 4.0$ Hz, H_9, H_{10}), 3.10 (2H, d, $^3J_{10,11} = {}^3J_{9,13}$ = 4.0 Hz, H_{11} or H_{13}), 2.82 (2H, d, $^3J_{10,11} = {}^3J_{9,13} = 4.0$ Hz, H_{11} or H_{13}); **^{13}C NMR** (100 MHz, $CDCl_3$) 157.1 (C_{12}), 142.4 (C_q), 142.2 (C_q), 138.3 (C_{15}), 129.0 (CH), 128.2 (CH), 127.3 (CH), 127.2 (CH), 126.8 (CH), 126.7 (CH), 125.9 (CH), 125.8 (CH), 75.1 (C_{14}), 44.7 (C_9 or C_{10}), 44.1 (C_9 or C_{10}), 39.1 (C_{11} or C_{13}), 34.2 (C_{11} or C_{13}); **EI-MS**, _m/z_ (relative intensity), 339 ($[M]^+$, 100), 322 (9), 232 (12), 215 (15), 192 ($[C_{15}H_{12}]^+$, 3), 191 ($[C_{15}H_{11}]^+$, 5), 178 ($[C_{12}H_{10}]^+$, 8).

_N_-Benzyl-9,10-dihydro-9,10-propanoanthracen-12-ylideneamine _N_-oxide 114
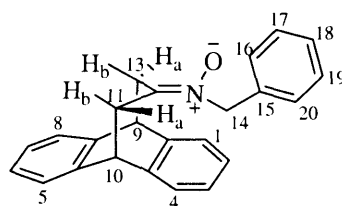
114

$C_{24}H_{21}NO$ 339.43 g.mol^{-1}

_N_-Benzylhydroxylamine was prepared from _N_-benzylhydroxylamine hydrochloride (1 g, 6.2 mmol) stirred for 30 minutes with a saturated K_2CO_3 aqueous solution (10 mL). The resulting suspension was extracted with CH_2Cl_2 (3 x 10 mL) and the combined organic layers were dried over $MgSO_4$, filtered and concentration under reduced pressure gave _N_-benzylhydroxylamine as a white powder.

To a well-stirred solution of ketone **67** (561 mg, 2.4 mmol) in anhydrous CH_2Cl_2 (17 mL), $ZnCl_2$ (1 M solution in Et_2O, 2.4 mL), *N*-benzylhydroxylamine (596 mg, 4.8 mmol) and anhydrous magnesium sulphate (288 mg, 2.4 mmol) were added sequentially. After stirring at 40 °C for 24 h, the crude mixture was cooled to room temperature and filtered. The filtrate was concentrated under reduced pressure and the residue was chromatographed on silica gel through a short column using EtOAc as an eluent to give the *title compound* **114** (160 mg, 20 %) as a colourless oil.

HRMS found: M^+, 339.16195. $C_{24}H_{21}NO$ requires 339.16231; **IR** (CH_2Cl_2) v_{max} 3030 (m, H_{ar}), 2928 (m), 1686 (br), 1601 (w), 1475 (s), 1456 (s), 1400 (s), 1157 (m), 1117 (s), 1032 (w), 986 (w), 966 (br, N-O), 870 (s), 737 (br), 694 (s), 644 (s), 594 (s), 511 (s) cm^{-1}; **^1H NMR** (400 MHz, $CDCl_3$) 7.34 (2H, m, H_{ar}), 7.22 (9H, m, H_{ar}), 7.1 (2H, m, H_{ar}), 4.99 (2H, s, H_{14}), 4.29 (1H, t, $^3J_{10,11}$ or $^3J_{9,13}$ = 3.9 Hz, H_9 or H_{10}), 4.19 (1H, t, $^3J_{10,11}$ or $^3J_{9,13}$ = 4.0 Hz, H_9 or H_{10}), 3.24 (2H, dd, $^4J_{11a,13b}$ = 1.9 Hz, $^3J_{10,11}$ or $^3J_{9,13}$ = 4.0 Hz, H_{11} or H_{13}), 3.01 ($^4J_{11a,13b}$ = 1.9 Hz, $^3J_{10,11}$ or $^3J_{9,13}$ = 3.9 Hz, H_{11} or H_{13}); **^{13}C NMR** (75 MHz, $CDCl_3$) 146.5 (C_{12}), 142.1 (C_q), 140.6 (C_q), 132.9 (C_{15}), 129.1 (CH), 128.8 (CH), 128.5 (CH), 128.0 (CH), 127.3 (CH), 127.2 (CH), 126.9 (CH), 126.0 (CH), 125.7 (CH), 63.6 (C_{14}), 43.6 (C_9 or C_{10}), 43.5 (C_9 or C_{10}), 37.8 (C_{11} or C_{13}), 37.3 (C_{11} or C_{13}); **EI-MS**, *m/z* (relative intensity), 339 ($[M]^+$, 12), 203 (17), 191 ($[C_{15}H_{11}]^+$, 34), 178 ($[C_{12}H_{10}]^+$, 61), 91 (100).

12-Amino-12-cyano-9,10-dihydro-propanoanthracene 116

116

$C_{18}H_{16}N_2$ 260.33 $g.mol^{-1}$
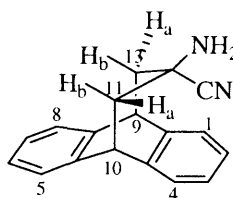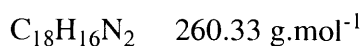
Ketone **67** (117 mg, 0.5 mmol) was placed into a flask and anhydrous methanol saturated with ammonia (5 mL) was added *via* a canula before addition of NaCN (78 mg, 1.6 mmol)

and NH_4Cl (77 mg, 1.5 mmol), each as a single portion. Bubbling of ammonia was continued for a further 1 h to ensure the saturation of ammonia in the solution. The mixture was stirred for 8 days with a daily bubbling of ammonia to ensure saturation then concentrated under reduced pressure. Water (5 mL) was added to the residue and the product was extracted with CH_2Cl_2 (3 x 5 mL). The combined organic layers were washed with a saturated aqueous $NaHCO_3$ solution (5 mL), followed by water (5 mL) and dried over Na_2SO_4. Crystallisation from EtOAc and P.E. 40-60 °C gave the *title compound* **116** (73 mg, 56%) as white square crystals.

M.p. 154-156 °C (EtOAc); **HRMS**: found: M^+, 260.13192. $C_{18}H_{16}N_2$ requires 260.13135; **IR** (CH_2Cl_2) v_{max} 3358 (s, NH_2), 3290 (s, NH_2), 3022 (m, H_{ar}), 2926 (s), 2854 (w), 2218 (s, CN), 1581(br, NH_2), 1475 (s), 1456 (s), 1267 (s, C-C-N), 1176 (w), 1103 (s), 1058 (s), 1030 (s), 850 (br, NH_2), 769 (s), 735 (s), 702 (s), 654 (s), 598 (s), 567 (s, $C{\equiv}N$) cm^{-1}; ^1H **NMR** (300 MHz, $CDCl_3$) 7.37-7.24 (6H, H_{ar}), 7.19-7.14 (2H, H_2, H_3), 4.19 (2H, dd, $^3J_{10,11b}$ = $^3J_{9,13b}$ = 1.3 Hz, $^3J_{10,11a}$ = $^3J_{9,13a}$ = 7.0 Hz, H_9, H_{10}), 2.63 (2H, ddd, $^4J_{11a,13a}$ = 1.3 Hz, $^3J_{10,11a}$ = $^3J_{9,13a}$ = 7.0 Hz, $^2J_{11a,11b}$ = $^2J_{13a,13b}$ = 13.2 Hz, H_{11a}, H_{13a}), 1.86 (2H, dd, $^3J_{10,11b}$ = $^3J_{9,13b}$ = 1.3 Hz, $^2J_{11a,11b}$ = $^2J_{13a,13b}$ = 13.2 Hz, H_{11b}, H_{13b}), 1.67 (2H, broad, NH_2); ^{13}C **NMR** (75 MHz, $CDCl_3$) 143.5 (C_q), 139.6 (C_q), 127.5 (CH), 127.0 (CH), 126.8 (CH), 125.5 (CH), 123.9 (CN), 50.6 (C_{12}), 43.7 (C_9, C_{10}), 41.7 (C_{11}, C_{13}); **EI-MS**, *m/z* (relative intensity), 260 $([M]^+, 15)$, 243 $([M-NH_3]^+, 10)$, 233 $([M-HCN]^+, 90)$, 215 (46), 192 $([C_{15}H_{12}]^+, 84)$, 191 $([C_{15}H_{11}]^+, 77)$, 178 $([C_{12}H_{10}]^+, 62)$, 165 (15), 152 (9); **Anal.** Found: C, 82.73; H, 6.25; N, 10.58. Calcd for $C_{18}H_{16}N_2$: C, 83.04; H, 6.19; N, 10.76.

12-Amino-9,10-dihydro-12-methyl-9,10-propanoanthracene hydrochloride 117

117

$C_{18}H_{20}ClN$ 285.81 g.mol^{-1}
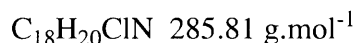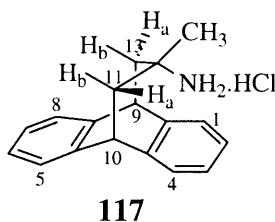
HCl (2 M solution in Et$_2$O, 1 mL, 2 mmol) was added dropwise to a solution of amine **103** (25 mg, 0.1 mmol) in CH$_2$Cl$_2$ (0.3 mL) with stirring. A white precipitate appeared instantly. After stirring for a further 10 min, the solution was filtered and the white powder washed with CH$_2$Cl$_2$ (2 x 1 mL) to afford the _title compound_ **117** (24 mg, 95%) as a white powder.

M.p. 146-149 °C (EtOAc-P.E); **HRMS**: found: M$^+$, 249.15132. C$_{18}$H$_{20}$ClN requires 249.15174; **IR** (KBr) v$_{max}$ 2918 (br), 2794 (br, NH$_3^+$), 2684 (br, NH$_3^+$), 2359 (br, NH$_3^+$), 1508 (s, NH$_3^+$), 1493 (s), 1477 (s), 1456 (s), 1439 (s), 1389 (s, CH$_3$), 1367 (w), 1323 (w), 1288 (w), 1263 (w), 1188 (s), 1157 (w), 1105 (s), 1032 (s), 943 (w), 916 (w), 762 (s), 744 (s), 706 (w), 661 (s), 594 (s), 557 (br) cm^{-1}; ^{1}**H NMR** (500 MHz, CDCl$_3$) 7.39-7.38 (2H, m, H$_1$, H$_4$), 7.26-7.22 (4H, m, H$_2$, H$_3$, H$_5$, H$_8$), 7.16-7.15 (2H, m, H$_6$, H$_7$), 6.82 (3H, br, NH$_3$), 4.12 (2H, dd, $^3J_{10,11b}$ = $^3J_{9,13b}$ = 1.3 Hz, $^3J_{10,11a}$ = $^3J_{9,13a}$ = 6.4 Hz, H$_9$, H$_{10}$), 2.58 (2H, ddd, $^4J_{11a,13a}$ = 0.7 Hz, $^3J_{10,11a}$ = $^3J_{9,13a}$ = 6.4 Hz, $^2J_{11a,11b}$ = $^2J_{13a,13b}$ = 15.8 Hz, H$_{11a}$, H$_{13a}$), 1.83 (2H, dd, $^3J_{10,11b}$ = $^3J_{9,13b}$ = 1.3 Hz, $^2J_{11a,11b}$ = $^2J_{13a,13b}$ = 15.8 Hz, H$_{11b}$, H$_{13b}$), 1.23 (3H, s, CH$_3$); ^{13}**C NMR** (125 MHz, CDCl$_3$) 142.8 (C$_q$), 139.8 (C$_q$), 128.4 (CH), 127.0 (CH), 126.9 (CH), 125.5 (CH), 58.2 (C$_{12}$), 43.9 (C$_{11}$, C$_{13}$), 40.1 (C$_9$, C$_{10}$), 30.0 (CH$_3$); **EI-MS**, _m/z_ (relative intensity),249 ([M]$^+$, 84), 234 (85), 217 (21), 192 ([C$_{15}$H$_{12}$]$^+$, 100), 191 ([C$_{15}$H$_{11}$]$^+$, 67), 178 ([C$_{12}$H$_{10}$]$^+$, 65), 165 (8), 144 (9), 117 (8).

12-Amino-12-cyano-9,10-dihydro-9,10-propanoanthracene hydrochloride 118

118

$C_{18}H_{17}ClN_2$ 296.79 g.mol^{-1}
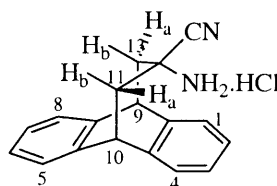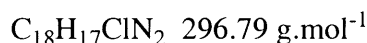
HCl (2 M in Et2O, 2 mL, 4 mmol) was added dropwise to a solution of amine **116** (26 mg, 0.1 mmol) in CH_2Cl_2 (0.2 mL) and the solution stirred for 10 min. The white precipitate was filtered and washed with CH_2Cl_2 (2 x 0.5 mL) to provide the *title compound* **118** (25.5 mg, 86%) as a white powder.

M.p. 163-165 °C; **HRMS**: found: M$^+$, 296.10876 $C_{18}H_{17}ClN_2$ requires 296.10803; **IR** (KBr) ν_{max} 3427 (br), 2750 (br, NH$_3^+$), 2644 (br, NH$_3^+$), 2555 (br, NH$_3^+$), 2361 (s, NH$_3^+$), 1593 (br), 1508 (s, NH$_3^+$), 1491 (s), 1475 (s), 1458 (s), 1323 (s), 1155 (s, C-C-N), 1117 (w), 1049 (s), 1032 (s), 1020 (w), 768 (s), 752 (s), 702 (w), 598 (s), 567 (s), 457 (s) cm^{-1}; **^{1}H NMR** (400 MHz, DMSO-d_6) 9.25 (3H, br, NH$_3$), 7.45-7.41 (2H, m, H$_{ar}$), 7.38-7.35 (2H, m, H$_{ar}$), 7.32-7.29 (2H, m, H$_{ar}$), 7.22-7.19 (2H, m, H$_{ar}$), 4.38 (2H, dd, $^3J_{10,11b} = {}^3J_{9,13b} = 1.0$ Hz, $^3J_{10,11a} = {}^3J_{9,13a} = 7.4$ Hz, H$_9$, H$_{10}$), 2.88 (2H, ddd, $^4J_{11a,13a} = 1.8$ Hz, $^3J_{10,11a} = {}^3J_{9,13a} = 7.4$ Hz, $^2J_{11a,11b} = {}^2J_{13a,13b} = 14.2$ Hz, H$_{11a}$, H$_{13a}$), 1.99 (2H, dd, $^3J_{10,11b} = {}^3J_{9,13b} = 1.0$ Hz, $^2J_{11a,11b} = {}^2J_{13a,13b} = 14.2$ Hz, H$_{11b}$, H$_{13b}$); **^{13}C NMR** (75 MHz, DMSO-d_6) 143.1 (C$_q$), 139.7 (C$_q$), 128.2 (CH), 127.0 (CH), 126.8 (CH), 125.5 (CH), 122.9 (CN), 51.2 (C$_{12}$), 43.8 (C$_9$, C$_{10}$), 41.2 (C$_{11}$, C$_{13}$); **EI-MS**, *m/z* (relative intensity),296 ([M]$^+$, 3), 260 ([M-HCl]$^+$, 20), 233 (100), 215 (44), 192 ([C$_{15}$H$_{12}$]$^+$,84), 191 ([C$_{15}$H$_{11}$]$^+$, 78), 178 ([C$_{12}$H$_{10}$]$^+$, 53), 165 (12).

12-Amino-9,10-dihydro-12-methyl-9,10-propanoanthracene mesylate 119
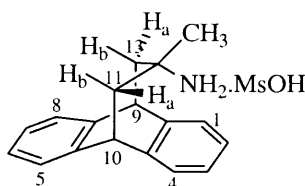

119

$C_{19}H_{23}NO_3S$ 345.46 g.mol^{-1}

Methanesulfonic acid (6.5 μL, 0.1 mmol) in EtOAc (40 μL) was added dropwise to a mixture of amine **103** (26 mg, 0.1 mmol) in CH_2Cl_2 (200 μL) and EtOAc (120 μL) at 0 °C. The resulting orange solution was warmed to room temperature and stirred for a further 1 h. After concentration under reduced pressure, crystallisation of the crude product from Et_2O and EtOAc afforded the _title compound_ **119** (27 mg, 78%) as white square crystals.

M.p. 141-145 °C (Et_2O-EtOAc); **HRMS**: found: M$^+$, 345.13978 $C_{19}H_{23}NO_3S$ requires 345.13986; **IR** (KBr) v_{max} 3022 (m, H_{ar}), 2935 (br, NH_3^+), 1524 (s, NH_3^+), 1477 (s), 1454 (s), 1392 (w, CH_3), 1315 (w), 1202 (br, SO_3), 1155 (s), 1109 (s), 1049 (s), 768 (s), 741 (w), 665 (w), 596 (s), 555 (s) cm^{-1}; ^{1}**H NMR** (500 MHz, CD_3OD) 7.35-7.32 (4H, m, H_{ar}), 7.23-7.18 (4H, m, H_{ar}), 4.23 (2H, dd, $^3J_{10,11b} = ^3J_{9,13b} = 2.0$ Hz, $^3J_{10,11a} = ^3J_{9,13a} = 6.3$ Hz, H_9, H_{10}), 2.66 (3H, s, CH_3SO_3H), 2.27 (2H, ddd, $^4J_{11a,13a} = 1.1$ Hz, $^3J_{10,11a} = ^3J_{9,13a} = 6.3$ Hz, $^2J_{11a,11b} = ^2J_{13a,13b} = 14.3$ Hz, H_{11a}, H_{13a}), 1.96 (2H, dd, $^4J_{13a,Me} = 0.7$ Hz, $^3J_{10,11b} = ^3J_{9,13b} = 2.0$ Hz, $^2J_{11a,11b} = ^2J_{13a,13b} = 14.3$ Hz, H_{11b}, H_{13b}), 0.57 (3H, t, $^4J_{13a,Me} = 0.7$ Hz, CH_3); ^{13}**C NMR** (100 MHz, $CDCl_3$) 143.2 (C_q), 140.4 (C_q), 126.7 (CH), 126.6 (CH), 125.8 (CH), 125.1 (CH), 55.2 (C_{12}), 43.4 (CH_3SO_3H), 39.9 (C_{11}, C_{13}), 37.9 (C_9, C_{10}), 28.4 (CH_3); **EI-MS**, _m/z_ (relative intensity), 345 ([M]$^+$, 2), 249 ([M-MsOH]$^+$, 67), 234 (65), 192 ([$C_{15}H_{12}$]$^+$, 100), 178 ([$C_{12}H_{10}$]$^+$, 47), 144 (15).

12-Amino-12-cyano-9,10-dihydro-9,10-propanoanthracene mesylate 120

120

$C_{19}H_{20}N_2O_3S$ 356.44 g.mol^{-1}
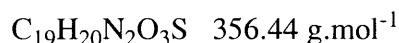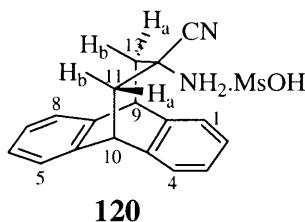
Methanesulfonic acid (6.5 µL, 0.1 mmol) in EtOAc (40 µL) was added dropwise to a mixture of amine **116** (26 mg, 0.1 mmol) in CH_2Cl_2 (200 µL) and EtOAc (120 µL) at 0 ° C and a white precipitate instantly appeared. The solution was warmed to room temperature and stirred for 10 min before filtration. The white precipitate was washed with CH_2Cl_2 (2 x 0.5 mL) to yield the *title compound* **120** (29 mg, 81%) as a white powder.

M.p. 162-167 °C (EtOAc-P.E); **HRMS**: found: M$^+$, 356.12013. $C_{19}H_{20}N_2O_3S$ requires 356.11946; **IR** (KBr) v_{max} 2829 (br, NH_3^+), 1553 (s), 1514 (s), 1475 (s), 1458 (s), 1325 (w, SO_2), 1182 (m, SO_2), 1151 (s), 1049 (s, SO_3H), 1034 (s, SO_3H), 767 (s), 702 (w), 557 (s, CN), 459 (s) cm^{-1}; **^{1}H NMR** (500 MHz, CDCl$_3$) 7.41-7.40 (2H, m, H_{ar}), 7.36-7.34 (2H, m, H_{ar}), 7.30-7.28 (2H, m, H_{ar}), 7.20-7.18 (2H, m, H_{ar}), 4.37 (2H, dd, $^3J_{10,11b} = {}^3J_{9,13b} = 1.0$ Hz, $^3J_{10,11a} = {}^3J_{9,13a} = 7.4$ Hz, H$_9$, H$_{10}$), 2.85 (2H, ddd, $^4J_{11a,13a} = 1.9$ Hz, $^3J_{10,11a} = {}^3J_{9,13a} = 7.4$ Hz, $^2J_{11a,11b} = {}^2J_{13a,13b} = 14.2$ Hz, H$_{11a}$, H$_{13a}$), 2.65 (3H, s, **CH$_3$SO$_3$H**), 1.98 (2H, dd, $^3J_{10,11b} = {}^3J_{9,13b} = 1.0$ Hz, $^2J_{11a,11b} = {}^2J_{13a,13b} = 14.2$ Hz, H$_{11b}$, H$_{13b}$); **^{13}C NMR** (100 MHz, CD$_3$OD) 142.9 (C$_q$), 138.3 (C$_q$), 127.6 (CH), 126.9 (CH), 126.8 (CH), 125.1 (CH), 116.9 (CN), 51.0 (C$_{12}$), 42.2 (C$_{11}$, C$_{13}$), 37.8 (C$_9$, C$_{10}$); **EI-MS**, m/z (relative intensity),356 ([M]$^+$, 3), 260 (26), 233 (100), 215 (52), 192 ([C$_{15}$H$_{12}$]$^+$, 87), 191 ([C$_{15}$H$_{11}$]$^+$, 69), 178 ([C$_{12}$H$_{10}$]$^+$, 53), 170 (35), 152 (8).

12-Azidomethyl-9,10-dihydro-12-hydroxy-9,10-propanoanthracene 122

122

$C_{18}H_{17}N_3O$ 291.35 g.mol^{-1}
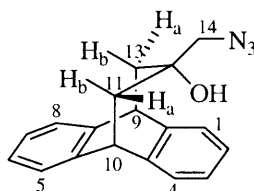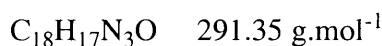
NaN_3 (297 mg, 4.2 mmol) was added as a single portion to a stirred solution of the epoxide **86** (104 mg, 0.42 mmol) in a mixture of MeOH (5 mL), CH_2Cl_2 (1 mL) and H_2O (1 mL). After addition of NH_4Cl (484 mg, 8.4 mmol) as a single portion, the resulting suspension was refluxed for 4 days. The solution was cooled to room temperature, extracted with CH_2Cl_2 (3 x 5 mL) and the combined organic layers were dried over Na_2SO_4, filtered and concentrated under reduced pressure. The crude product was purified by flash chromatography column (silica gel, gradient of elution 1:10 to 1:5 EtOAc/P.E. 40-60 °C) to yield the *title compound* **122** (99 mg, 81 %) as a white solid.

M.p. 115-118 °C (EtOAc); **HRMS**: found: [M+H]$^+$, 292.14357. $C_{18}H_{17}N_3O$ requires 292.14498; **IR** (CH_2Cl_2) v_{max} 3582 (s, OH), 3443 (br, OH), 3022 (m, H_{ar}), 2916 (s), 2854 (w), 2100 (s, N_3), 1475 (s), 1456 (s), 1298 (m, N_3), 1090 (s, OH), 1032 (s), 937 (m), 887 (w, OH), 768 (s), 737 (s), 598 (s), 532 (s) cm^{-1}; **^{1}H NMR** (300 MHz, $CDCl_3$) 7.39-7.36 (2H, m, H_1, H_4), 7.29-7.16 (6H, m, H_2, H_3, H_5, H_6, H_7, H_8), 4.16 (2H, dd, $^3J_{10,11b} = {}^3J_{9,13b} =$ 1.9 Hz, $^3J_{10,11a} = {}^3J_{9,13a} =$ 6.4 Hz, H_9, H_{10}), 2.77 (2H, s, CH_2N_3), 2.29 (2H, ddd, $^4J_{11a,13a} =$ 1.6 Hz, $^3J_{10,11a} = {}^3J_{9,13a} =$ 6.4 Hz, $^2J_{11a,11b} = {}^2J_{13a,13b} =$ 14.4 Hz, H_{11a}, H_{13a}), 1.92 (2H, dd, $^3J_{10,11b} = {}^3J_{9,13b} =$ 1.9 Hz, $^2J_{11a,11b} = {}^2J_{13a,13b} =$ 14.4 Hz, H_{11b}, H_{13b}); **^{13}C NMR** (75 MHz, $CDCl_3$) 143.6 (C_q), 141.6 (C_q), 127.1 (CH), 126.6 (CH), 126.4 (CH), 125.6 (CH), 75.1 (C_{12}), 62.4 (C_{14}), 44.3 (C_9, C_{10}), 42.1 (C_{11}, C_{13}); **EI-MS**, *m/z* (relative intensity) 291 ([M+H]$^+$, 13), 246 (21), 235 (100), 217 (22), 191 ([$C_{15}H_{11}$]$^+$, 37), 178 ([$C_{12}H_{10}$]$^+$, 91), 165 (6).

12-Formyl-9,10-dihydro-9,10-propanoanthracene 92

92

$C_{18}H_{16}O$ 248.32 g.mol^{-1}
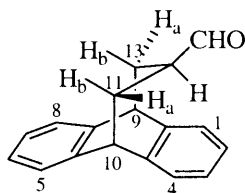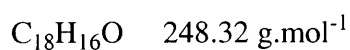
Triphenylphosphine (72 mg, 0.31 mmol) was added to a stirred solution of azide **122** (77 mg, 0.28 mmol) in THF (10 mL). The reaction was stirred at room temperature for 1 h then heated under reflux for 5 h. After cooling, the solvent was removed under reduced pressure and the residual oil dissolved in CH_2Cl_2 (30 mL). The solution was washed with aqueous copper sulphate solution (10% w/v, 15 mL), aqueous citric acid solution (10% w/v, 15 mL) and water (15 mL) before been extracted with CH_2Cl_2 (3 x 15 mL). The combined organic layers were then dried over Na_2SO_4, filtered and concentrated under reduced pressure. The crude mixture was purified by flash chromatography column (silica gel, 1:10 EtOAc/P.E. 40-60 °C) to afford the *title compound* **92** (57 mg, 74%) as a white solid.

The spectroscopic data obtained were identical to those previously described

12-Azidomethyl-9,10-dihydro-12-iodo-9,10-propanoanthracene 125

125

$C_{18}H_{16}IN_3$ 401.24 g.mol^{-1}
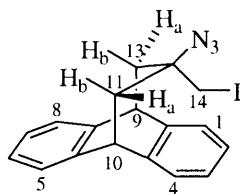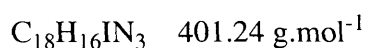
NaN_3 (280 mg, 4.3 mmol) was added as a single portion under a nitrogen atmosphere to ICl (1 M solution in CH_2Cl_2, 2 mL, 2 mmol) and the resulting suspension was stirred at room temperature for 1hr and then cooled to 0 °C. After addition of a solution of alkene **68** (232 mg, 1.0 mmol) in anhydrous CH_2Cl_2 (5 mL), the reaction mixture was warmed to room temperature and stirred for 2 days. The dark red solution was washed with an aqueous $Na_2S_2O_3$ solution (1 M, 10 mL) until the colour disappeared, extracted with CH_2Cl_2 (3 x 10 mL), dried over $MgSO_4$ and concentrated under reduced pressure. Flash column chromatography (silica gel, gradient of elution 1:50 to 1:6 EtOAc/P.E. 40-60 °C) gave the *title compound* **125** (281 mg, 70%) as a dark orange oil.

HRMS: found: $[M+H]^+$, 402.04767. $C_{18}H_{16}IN_3$ requires 402.04672; **IR** (CH_2Cl_2) v_{max} 3022 (m, H_{ar}), 2920 (s), 2854 (w), 2100 (s, N_3), 1581 (w), 1475 (s), 1456 (s), 1429 (w), 1199 (s), 1176 (s), 1107 (w),), 1055 (s), 1022 (s), 939 (w), 866 (w), 820 (s), 768 (s), 737 (s), 704 (s), 598 (s), 588 (s), 503 (s, C-I) cm^{-1}; ^{1}**H NMR** (400 MHz, $CDCl_3$) 7.42-7.40 (2H, m, H_1, H_4), 7.36-7.33 (2H, m, H_5, H_8), 7.30-7.25 (4H, m, H_2, H_3, H_6, H_7), 4.19 (2H, dd, $^3J_{10,11b} = {}^3J_{9,13b}$ = 1.8 Hz, $^3J_{10,11a} = {}^3J_{9,13a}$ = 6.2 Hz, H_9, H_{10}), 2.96 (2H, s, CH_2I), 2.35 (2H, ddd, $^4J_{11a,13a}$ = 1.8 Hz, $^3J_{10,11a} = {}^3J_{9,13a}$ = 6.2 Hz, $^2J_{11a,11b} = {}^2J_{13a,13b}$ = 14.8 Hz, H_{11a}, H_{13a}), 1.99 (2H, dd, $^3J_{10,11b} = {}^3J_{9,13b}$ = 1.8 Hz, $^2J_{11a,11b} = {}^2J_{13a,13b}$ = 14.8 Hz, H_{11b}, H_{13b}); ^{13}**C NMR** (100 MHz, $CDCl_3$) 143.3 (C_q), 140.3 (C_q), 128.4 (CH), 128.3 (CH), 126.0 (CH), 125.2 (CH), 62.5 (C_{12}), 44.0 (C_9, C_{10}), 38.2 (C_{11}, C_{13}), 19.7 (CH_2I); **EI-MS**, *m/z* (relative intensity) 323 (46), 266 ($[M+H]^+$, 56), 233 ($[M-MeOH+H]^+$, 100), 193 ($[C_{15}H_{12}+H]^+$, 61), 179 ($[C_{12}H_{10}+H]^+$, 55), 155 (51), 119 (51).

12,12-Aziridinyl-9,10-dihydro-9,10-propanoanthracene 121

121
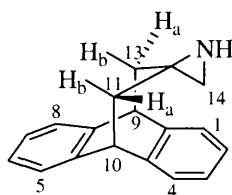
$C_{18}H_{17}N$ 247.33 g.mol^{-1}
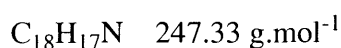
A suspension of LiAlH$_4$ (265 mg, 7 mmol) in anhydrous Et$_2$O (4 mL) was cooled to 0 °C under nitrogen atmosphere. A solution of the azide **125** (281 mg, 0.7 mmol) in anhydrous Et$_2$O (6mL) was added dropwise at 0 °C and the solution was stirred at room temperature overnight. The reaction mixture was quenched with aqueous potassium sodium tartrate solution (1 M, 20 mL) and extracted with Et$_2$O (3 x 10 mL). The combined organic layers were washed with brine (10 mL), dried over MgSO$_4$, filtered and concentrated under reduced pressure. Flash column chromatography (silica gel, gradient of elution 1:9:20:70 to 1:4:0:45 triethylamine/MeOH/P.E. 40-60 °C/EtOAc) afforded the *title compound* **121** (128 mg, 74%) as a light yellow solid.

M.p. 134-137 °C (EtOAc); **HRMS**: found: M$^+$, 247.13622. $C_{18}H_{17}N$ requires 247.13609; **IR** (CH$_2$Cl$_2$) ν_{max} 3653 (w), 3294 (s), 3020 (m), 2924 (s), 2851 (s), 1580 (w, NH), 1456 (s), 1475 (s), 1288 (w), 1173 (s), 1113 (m), 1034 (s), 1009 (s), 968 (s), 804 (s), 758 (m), 735 (s), 714 (s), 629 (w), 611 (w), 594 (s) cm^{-1}; **^{1}H NMR** (400 MHz, CDCl$_3$) 7.30-7.25 (4H, m, H$_1$, H$_4$, H$_5$, H$_8$), 7.19-7.16 (4H, m, H$_2$, H$_3$, H$_6$, H$_7$), 4.14 (2H, dd, $^3J_{10,11b}$ = $^3J_{9,13b}$ = 3.0 Hz, $^3J_{10,11a}$ = $^3J_{9,13a}$ = 5.2 Hz, H$_9$, H$_{10}$), 1.98 (2H, ddd, $^4J_{13b,14}$ = $^4J_{11b,14}$ = 1.2 Hz, $^3J_{10,11b}$ = $^3J_{9,13b}$ = 3.0 Hz, $^2J_{11a,11b}$ = $^2J_{13a,13b}$ = 13.2 Hz, H$_{11b}$, H$_{13b}$), 1.79 (2H, dd, $^3J_{10,11a}$ = $^3J_{9,13a}$ = 5.2 Hz, $^2J_{11a,11b}$ = $^2J_{13a,13b}$ = 13.2 Hz, H$_{11a}$, H$_{13a}$), 0.98 (2H, d, $^4J_{13b,14}$ = $^4J_{11b,14}$ = 1.2 Hz, H$_{14}$), 0.60 (1H, br, NH); **^{13}C NMR** (75 MHz, CDCl$_3$) 143.4 (C$_q$), 142.4 (C$_q$), 126.4 (CH), 126.3 (CH), 125.7 (CH), 125.6 (CH), 45.4 (C$_9$, C$_{10}$), 42.3 (C$_{11}$, C$_{13}$), 34.8 (C$_{12}$), 34.5 (C$_{14}$); **EI-MS**, *m/z* (relative intensity) 247 ([M]$^+$, 26), 230 (15), 229 (16), 215 (27), 202 (9), 191 ([C$_{15}$H$_{11}$]$^+$, 36), 178 ([C$_{12}$H$_{10}$]$^+$, 100), 165 (8), 149 (12); **Anal.** Found: C, 87.56; H, 6.86; N, 5.58. Calcd for C$_{18}$H$_{17}$N: C, 87.41; H, 6.93; N, 5.66.

9,10-Dihydro-12-methyl-9,10-prop-11-enoanthracene 95

9,10-dihydro-12,12-(N-chlorosulfonyl)oxoazetidinyl-9,10-propanoanthracene 126 and

9,10-dihydro-11,12-(N-chlorosulfonyl)oxoazetidinyl-12-methyl-9,10-propanoanthracene 127

95

$C_{18}H_{16}$ 232.32 g.mol^{-1}

126

$C_{19}H_{16}ClNO_3S$ 373.85 g.mol^{-1}

127

$C_{19}H_{16}ClNO_3S$ 373.85 g.mol^{-1}
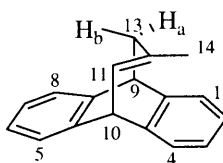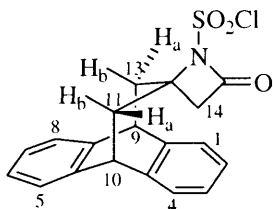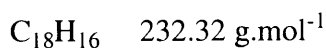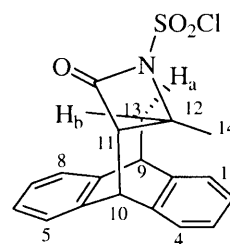
To a stirred solution of alkene **68** (148 mg, 0.64 mmol) in anhydrous CH_2Cl_2 (7 mL) chlorosulfonyl isocyanate (56 μL, 0.64 mmol) was added dropwise at 0 °C and the solution was stirred for 4 days. A mixture of Na_2SO_3 (9 mg, 0.07 mmol) and K_2CO_3 (185 mg, 1.4 mmol) in water (3 mL) was carefully added dropwise and stirred for 30 min. The mixture was diluted with water (10 mL) and the solution was extracted with CH_2Cl_2 (3 x 10 mL). The combined organic layers were washed with brine (10 mL), dried over Na_2SO_4 and concentrated under reduced pressure. Flash column chromatography (silica gel, gradient of elution 1:10 to 1:3.3 EtOAc/P.E. 40-60 °C) gave the *title compound* **95** and an inseparable mixture of the *title compounds* **126** and **127**. Crystallisation from EtOAc and P.E. 40-60° C afforded the *title compound* **126** (23.9 mg, 10%) as white square crystals. Concentration of the mother liquor under reduced pressure and crystallisation from EtOAc and P.E. 40-60° C provided the *title compound* **127** (81 mg, 36%) as white needles.

9,10-Dihydro-12-methyl-9,10-prop-11-enoanthracene 95

Spectroscopy data as obtained above

9,10-Dihydro-12,12-(N-chlorosulfonyl)oxoazetidinyl-9,10-propanoanthracene 126

M.p. 155-157 °C (EtOAc-P.E.); **HRMS** found: M^+, 373.05442. $C_{19}H_{16}ClNOS$ requires 373.05394; **IR** (CH_2Cl_2) v_{max} 2928 (w), 1817 (s, β-lactam), 1475 (s), 1458 (w), 1394 (s, SO_2Cl), 1184 (s, SO_2Cl), 1170 (s), 1096 (s, SO_2Cl), 1051 (w), 1032 (w), 899 (w), 771 (s), 762 (s), 715 (w), 660 (s), 577 (d, SO_2Cl), 552 (s) cm^{-1}; **^{1}H NMR** (300 MHz, $CDCl_3$) 7.35-7.29 (4H, m, H_1, H_4, H_5, H_8), 7.26-7.18 (4H, m, H_2, H_3, H_6, H_7), 4.27 (2H, dd, $^3J_{10,11b}$ = $^3J_{9,13b}$ = 0.9 Hz, $^3J_{10,11a}$ = $^3J_{9,13a}$ = 7.4 Hz, H_9, H_{10}), 2.64 (2H, ddd, $^4J_{11b,14}$ = $^4J_{13b,14}$ = 0.8 Hz, $^3J_{10,11b}$ = $^3J_{9,13b}$ = 0.9 Hz, $^2J_{11a,11b}$ = $^2J_{13a,13b}$ = 13.4 Hz, H_{11b}, H_{13b}), 2.51 (2H, ddd, $^4J_{11a,13a}$ = 1.9 Hz, $^3J_{10,11a}$ = $^3J_{9,13a}$ = 7.4 Hz, $^2J_{11a,11b}$ = $^2J_{13a,13b}$ = 13.4 Hz, H_{11a}, H_{13a}), 2.08 (2H, d, $^4J_{11b,14}$ = $^4J_{13b,14}$ = 0.8 Hz, H_{14}); **^{13}C NMR** (75 MHz, $CDCl_3$) 161.2 (C=O), 143.0 (C_q), 139.4 (C_q), 127.5 (CH), 127.1 (CH), 126.9 (CH), 125.5 (CH), 70.3 (C_{12}), 53.3 (C_{14}), 43.8 (C_9, C_{10}), 39.6 (C_{11}, C_{13}); **EI-MS**, m/z (relative intensity), 373 ($[M]^+$, 13), 232 ($[C_{18}H_{16}]^+$, 83), 217 (48), 191 ($[C_{15}H_{11}]^+$, 32), 178 ($[C_{12}H_{10}]^+$, 100); **Anal.** Found: C, 60.64; H, 4.28; N, 3.62. Calcd for $C_{19}H_{16}ClNO_3S$: C, 61.04; H, 4.31; N, 3.75.

9,10-Dihydro-11,12-(N-chlorosulfonyl)oxoazetidinyl-12-methyl-9,10-propanoanthracene 127

M.p. 148-151 °C (EtOAc); **HRMS**: found: M^+, 373.05442. $C_{19}H_{16}ClNO_3S$ requires 373.05394; **IR** $(CHCl_3)$ v_{max} 3055 (br, H_{ar}), 2932 (s), 2854 (w), 1809 (m, β-lactam), 1479 (s), 1456 (s), 1383 (s, SO_2Cl), 1200-1150 (m, SO_2Cl), 1097 (m, SO_2Cl), 1049 (s), 1034 (s), 987 (s), 953 (d), 931 (s), 829 (s), 700 (m), 634 (d, CONH), 571 (m, SO_2), 540 (s) cm^{-1}; **^{1}H NMR** (500 MHz, $CDCl_3$) 7.33-7.29 (4H, m, H_1, H_4, H_5, H_8), 7.26-7.21 (4H, m, H_2, H_3, H_6, H_7), 4.40 (1H, d, $^3J_{10,11}$ =5.0 Hz, H_{10}), 4.17 (1H, dd, $^3J_{9,13b}$ = 3.5 Hz, $^3J_{9,13a}$ = 4.2 Hz, H_9), 3.34 (1H, d, $^3J_{10,11}$ =5.0 Hz, H_{11}), 3.08 (1H, dd, $^3J_{9,13a}$ = 4.2 Hz, $^2J_{13a,13b}$ = 15.6 Hz, H_{13a}), 2.06 (1H, dd, $^3J_{9,13b}$ = 3.5 Hz, $^2J_{13a,13b}$ = 15.6 Hz, H_{13b}), 1.44 (3H, s, H_{14}); **^{13}C NMR** (125 MHz, $CDCl_3$) 162.9 (C=O), 141.4 (C_q), 140.0 (C_q), 137.8 (C_q), 135.5 (C_q), 128.0 (CH), 127.8 (CH), 127.7 (CH), 127.3 (CH), 127.2 (CH), 126.3 (CH), 126.2 (CH), 125.8 (CH), 70.4 (C_{12}), 60.9 (C_{13}), 44.5 (C_9), 43.8 (C_{10}), 37.3 (C_{11}), 31.7 (C_{14}); **EI-MS**,

m/z (relative intensity) 373 ($[M]^+$, 17), 232 ($[M\text{-}ClSO_2NCO]^+$, 75), 217 (66), 191 ($[C_{15}H_{11}]^+$, 100), 178 ($[C_{12}H_{10}]^+$, 48), 84 (34).

9,10-Dihydro-12-oxoazetidinyl-9,10-propanoanthracene 128,

9,10-dihydro-12,12-(*N*-chlorosulfonyl)oxoazetidinyl-9,10-propanoanthracene 126 and

9,10-Dihydro-12-((*N*-chlorosulfonyl)carbamoylmethyl)-9,10-propenoanthracene 129
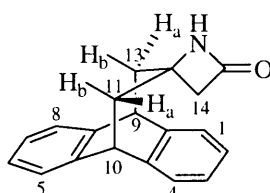
128

$C_{19}H_{17}NO$ 275.34 g.mol^{-1}

126
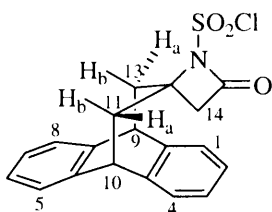
$C_{19}H_{16}ClNO_3S$ 373.85 g.mol^{-1}
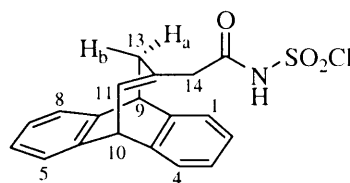
129

$C_{19}H_{16}ClNOS$ 373.85 g.mol^{-1}

Chlorosulfonyl isocyanate (220 µL, 2.5 mmol) kept 2 days over potassium carbonate in the fridge under nitrogen atmosphere, was added portionwise to a suspension of anhydrous Na_2CO_3 (0.35g) in anhydrous CH_2Cl_2 (13 mL) and the resulting mixture was cooled to 0 °C. A solution of alkene **68** (523 mg, 2.2 mmol) in anhydrous CH_2Cl_2 (13 mL) was added dropwise and the mixture was stirred at room temperature for 2 days under positive nitrogen pressure. The reaction was quenched by careful addition of a solution of Na_2SO_3 (40 mg, 0.3 mmol) and K_2CO_3 (830 mg, 6.0 mmol) in water (12 mL) and stirred for further 30 min. After dilution with water (30 mL) the resulting mixture was extracted with CH_2Cl_2 (3 x 15 mL). The combined organic layers were washed with brine (15 mL), dried over Na_2SO_4 and concentrated under reduced pressure. Flash column chromatography (silica gel, gradient of elution 1:10 to 5:1 EtOAc/P.E. 40-60 °C) gave an inseparable mixture of **126**

and **129** and then the *title compound* **128** (157 mg, 26%) as a white solid. Crystallisation of the first fraction from EtOAc and P.E provided **126** (321 mg, 39%) as a white solid and concentration of the mother liquor under reduced pressure afforded the *title compound* **129** (263 mg, 32%) as a white solid.

9,10-Dihydro-12-oxoazetidinyl-9,10-propanoanthracene 128

M.p. > 230 °C (decomp.) (EtOAc-P.E); **HRMS**: found: M^+, 275.13046. $C_{19}H_{17}NO$ requires 275.13101; **IR** (CH_2Cl_2) v_{max} 3333 (br, NH), 3219 (w), 2922 (s), 2851 (w), 1716 (br, β-lactam), 1473 (s), 1456 (w), 1433 (w, NH), 1367 (w), 1292 (w), 1267 (w), 1175 (w), 1113 (w), 1088 (s), 768 (s), 756 (w), 735 (s), 708 (w), 586 (s) cm^{-1}; ^{1}**H NMR** (500 MHz, CDCl$_3$) 7.31-7.29 (2H, m, H_1, H_4), 7.27-7.25 (2H, m, H_5, H_8), 7.20-7.18 (2H, m, H_2, H_3), 7.17-7.15 (2H, m, H_6, H_7), 4.73 (1H, br, NH), 4.14 (2H, dd, $^3J_{10,11b} = {}^3J_{9,13b} = 3.1$ Hz, $^3J_{10,11a} = {}^3J_{9,13a} = 5.1$ Hz, H_9, H_{10}), 2.22 (2H, s, H_{14}), 2.20 (2H, ddd, $^4J_{11a,13a} = 1.0$ Hz, $^3J_{10,11a} = {}^3J_{9,13a} = 5.1$ Hz, , $^2J_{11a,11b} = {}^2J_{13a,13b} = 13.9$ Hz, H_{11a}, H_{13a}), 2.15 (2H, dd, $^3J_{10,11b} = {}^3J_{9,13b} = 3.1$ Hz, $^2J_{11a,11b} = {}^2J_{13a,13b} = 13.9$ Hz, H_{11b}, H_{13b}); ^{13}**C NMR** (100 MHz, CDCl$_3$) 167.1 (C=O), 142.6 (C_q), 141.4 (C_q), 127.0 (CH), 126.7 (CH), 126.4 (CH), 125.8 (CH), 55.1 (C_{12}), 51.3 (C_{14}), 44.6 (C_9, C_{10}), 42.5 (C_{11}, C_{13}); **EI-MS**, *m/z* (relative intensity), 275 (M^+, 10), 232 (100), 217 (44), 192 ($C_{15}H_{12}{}^+$, 28), 191 ($C_{15}H_{11}{}^+$, 38), 178 ($C_{12}H_{10}{}^+$, 95); **Anal.** Found: C, 82.54; H, 6.23; N, 5.01. Calcd for $C_{19}H_{17}NO$: C, 82.88; H, 6.22; N, 5.09.

9,10-Dihydro-12,12-(*N*-chlorosulfonyl)oxoazetidinyl-9,10-propanoanthracene 126

The spectroscopic data obtained were identical to those previously described.

9,10-Dihydro-12-((*N*-chlorosulfonyl)carbamoylmethyl)-9,10-propenoanthracene 129

M.p. 201-204 °C; **HRMS**: found: M^+, 373.05416. $C_{19}H_{16}ClNOS$ requires 373.05394; **IR** (CH_2Cl_2) v_{max} 3400 (br, NH), 3043 (m, C=C), 3022 (m, H_{ar}), 2878 (m), 1475 (s), 1454 (s), 1421 (s), 1408 (s, SO_2Cl), 1174 (s), 1099 (w), 1032 (w), 928 (w), 866 (s), 826 (s), 779 (s), 764 (s), 741 (m), 764 (s), 714 (s), 600 (s), 548 (s) cm^{-1}; ^{1}**H NMR** (300 MHz, CDCl$_3$) 7.40-7.34 (2H, m, H_1, H_4) 7.27-7.22 (2H, m, H_5, H_8), 7.20-7.16 (4H, m, H_2, H_3, H_6, H_7), 6.46 (1H, ddd, $^4J_{11,14} = 1.6$ Hz, $^4J_{11,13a} = 1.9$ Hz, $^3J_{10,11} = 8.6$ Hz, H_{11}), 4.31 (1H, d, $^3J_{10,11} = 8.6$ Hz, H_{10}), 4.18 (1H, t, $^3J_{9,13} = 3.8$ Hz, H_9), 2.75 (2H, dd, $^4J_{13b,14} = 1.1$ Hz, $^4J_{11,14} = 1.6$ Hz,

H_{14}), 2.47 (2H, ddd, $^4J_{13b,14}$ = 1.1 Hz, $^4J_{11,13a}$ = 1.9 Hz, $^3J_{9,13}$ = 3.8 Hz, H_{13}); ^{13}**C NMR** (75 MHz, CDCl$_3$) 161.4 (C=O), 145.0 (C$_q$), 140.6 (C$_q$), 130.6 (C$_{11}$), 126.5 (CH), 126.3 (CH), 126.2 (CH), 125.2 (CH), 124.3 (CH), 116.9 (C$_{12}$), 45.5 (C$_{10}$), 45.3 (C$_9$), 36.5 (C$_{13}$), 26.6 (C$_{14}$); **EI-MS**, *m/z* (relative intensity), 373 ([M]$^+$, 28), 258 (81), 257 (71), 246 (90), 218 (87), 216 (97), 215 (91), 202 (91), 191 ([C$_{15}$H$_{11}$]$^+$, 95), 178 ([C$_{12}$H$_{10}$]$^+$, 100), 165 (31), 152 (25), 108 (32).

9,10-Dihydro-12,12-azetidinyl-9,10-propanoanthracene 130
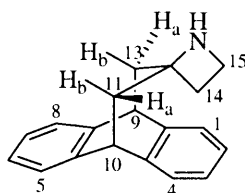
130

C$_{19}$H$_{19}$N   261.36 g.mol^{-1}

To a suspension of LiAlH$_4$ (23 mg, 3 mmol) in anhydrous Et$_2$O (4 mL) heated at reflux for 30 min was added dropwise a solution of the β-lactam **128** (83 mg, 0.3 mmol) in anhydrous CH$_2$Cl$_2$ (6 mL) and the resulting mixture was refluxed for 4 days. After cooling down to room temperature, the reaction mixture was quenched with an aqueous potassium sodium tartrate solution (20%, 20 mL) and extracted with CH$_2$Cl$_2$ (3 x 10 mL). The combined organic layers were washed with brine (10 mL), dried over Na$_2$SO$_4$, filtered and concentrated under reduced pressure. Crystallisation from benzene-hexane afforded the *title compound* **130** (59 mg, 76%) as a light yellow solid.

M.p. 213-217 °C (Benzene-Hexane); **HRMS**: found: (M+H)$^+$, 262.15907. C$_{19}$H$_{19}$N requires 262.15957; **IR** (CH$_2$Cl$_2$) v_{max} 3385 (br, NH), 2926 (br), 2446 (br), 1580 (s, NH), 1475 (s), 1456 (s), 1175 (s), 1113 (s), 1099 (s), 1030 (s), 939 (d), 768 (s), 735 (m), 702 (s), 613 (w), 588 (s), 463 (s) cm^{-1}; ^{1}**H NMR** (400 MHz, CDCl$_3$) 7.31-7.27 (2H, m, H$_1$, H$_4$) 7.27-7.23 (2H, m, H$_5$, H$_8$), 7.15-7.11 (2H, m, H$_2$, H$_3$), 7.10-7.06 (2H, m, H$_6$, H$_7$), 5.04 (1H, br, NH), 4.13 (2H, dd, $^3J_{10,11b}$ = $^3J_{9,13b}$ = 3.4 Hz, $^3J_{10,11a}$ = $^3J_{9,13a}$ = 4.8 Hz, H$_9$, H$_{10}$), 3.37 (2H, t, $^3J_{14,15}$ = 7.8 Hz, H$_{15}$), 2.41 (2H, dd, $^3J_{10,11a}$ = $^3J_{9,13a}$ = 4.8 Hz, $^2J_{11a,11b}$ = $^2J_{13a,13b}$ = 13.9 Hz,

H_{11a}, H_{13a}), 2.24 (2H, dd, $^3J_{10,11b} = {}^3J_{9,13b} = 3.4$ Hz, $^2J_{11a,11b} = {}^2J_{13a,13b} = 13.9$ Hz, H_{11b}, H_{13b}), 1.47 (2H, t, $^3J_{14,15} = 7.8$ Hz, H_{14}); ^{13}C NMR (100 MHz, CDCl$_3$) 142.5 (C$_q$), 141.6 (C$_q$), 126.4 (CH), 126.3 (CH), 125.9 (CH), 125.8 (CH), 66.5 (C$_{12}$), 44.1 (C$_9$, C$_{10}$), 43.1 (C$_{11}$, C$_{13}$), 40.8 (C$_{15}$), 34.3 (C$_{14}$); **CI(methane)-MS**, m/z (relative intensity) 261 ([M]$^+$, 31), 246 (7), 233 (100), 206 (19), 191 ([C$_{15}$H$_{11}$]$^+$, 22), 179 (58), 178 ([C$_{12}$H$_{10}$]$^+$, 79); **Anal.** Found: C, 87.12; H, 7.45; N, 5.43. Calcd for C$_{19}$H$_{19}$N: C, 87.31; H, 7.33; N, 5.36.

9,10-Dihydro-2-nitro-9,10-propanoanthracen-12-one 134 and 9,10-dihydro-2,6-dinitro-9,10-propanoanthracen-12-one 135

134
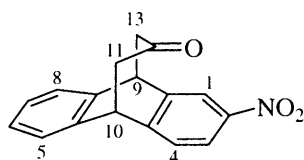
C$_{17}$H$_{13}$NO$_3$ 279.29 g.mol^{-1}
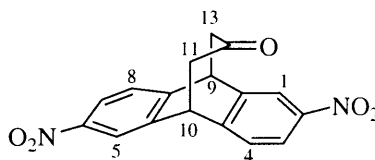
135

C$_{17}$H$_{12}$N$_2$O$_4$ 324.29 g.mol^{-1}

Fuming nitric acid (169 μL, 3.8 mmol) was added to a suspension of ketone **67** (351 mg, 1.5 mmol) in distilled acetic anhydride (3 mL) and CH$_2$Cl$_2$ (5 mL) at 0 °C. The solution was stirred at 3 °C for 24 h, warmed to room temperature, washed with saturated aqueous Na$_2$CO$_3$ solution (10 mL) and extracted with CH$_2$Cl$_2$ (3 x 5 mL). The combined organic layers were washed with brine (3 x 5 mL), dried over MgSO$_4$ and concentrated under reduced pressure. Flash column chromatography (silica gel, gradient of elution 1:20 to 1:3.3 EtOAc/P.E. 40-60 °C) provided the _title compounds_ **134** (30.5 mg, 8%) and **135** (26.5 mg, 6%) as light yellow square crystals.

9,10-Dihydro-2-nitro-9,10-propanoanthracen-12-one 134

M.p. 219-220 °C (EtOAc-P.E.); **HRMS** found: M$^+$, 279.09033 C$_{17}$H$_{13}$NO$_3$ requires 279.08954; **IR** (CH$_2$Cl$_2$) v_{max} 1693 (s, C=O), 1522 (s, NO$_2$), 1475 (w), 1460 (w), 1406 (w), 1340 (s, NO$_2$), 1163 (w), 1074 (w), 991 (s), 835 (w), 762 (w), 735 (w), 712 (w), 600 (w) cm^{-1}; ^{1}H NMR (500 MHz, CDCl$_3$) 8.22 (1H, dd, $^5J_{1,4} = 0.4$ Hz, $^4J_{1,3} = 2.3$ Hz, H$_1$), 8.10 (1H, dd, $^4J_{1,3} = 2.3$ Hz, $^3J_{3,4} = 8.2$ Hz, H$_3$), 7.50 (1H, dd, $^5J_{1,4} = 0.4$ Hz, $^3J_{3,4} = 8.2$ Hz, H$_4$), 7.36 (2H, m, H$_5$, H$_8$), 7.25 (2H, m, H$_6$, H$_7$), 4.39 (2H, m, H$_9$, H$_{10}$), 2.87 (4H, m, H$_{11}$, H$_{13}$);

^{13}C NMR (75 MHz, CDCl$_3$) 207.2 (C$_{12}$), 149.2 (C$_q$), 146.3 (C$_2$), 143.6 (C$_q$), 140.4 (C$_q$), 140.1 (C$_q$), 127.8 (CH), 126.9 (CH), 126.2 (CH), 122.6 (CH), 121.2 (CH), 50.7 (C$_{11}$, C$_{13}$), 43.5 (C$_9$, C$_{10}$); **EI-MS**, *m/z* (relative intensity), 279 ([M]$^+$, 100), 232 (75), 215 (25), 189 (82), 178 ([C$_{12}$H$_{10}$]$^+$, 28), 151 (12); **Anal.** Found: C, 72.90; H, 4.65; 4.97. Calcd for C$_{17}$H$_{13}$NO$_3$: C, 73.11; H, 4.69; N, 5.02.

9,10-dihydro-2,6-dinitro-9,10-propanoanthracen-12-one 135

M.p. 223 - 227 °C; **HRMS** found: M$^+$, 324.07505. C$_{17}$H$_{15}$N$_2$O$_4$ requires 324.07462; **IR** (CH$_2$Cl$_2$) ν_{max} 1699 (s, C=O), 1595 (w), 1526 (s, NO$_2$), 1421 (s), 1344 (d, NO$_2$), 1153 (d), 1128 (w), 1086 (w), 991 (w), 897 (H$_{ar}$), 739 (m) cm^{-1}; ^{1}H NMR (400 MHz, DMSO-d_6) 8.40 (2H, d, $^4J_{1,3}$ = $^4J_{5,7}$ = 2.4 Hz, H$_1$, H$_5$), 8.20 (2H, dd, $^4J_{1,3}$ = $^4J_{5,7}$ = 2.4 Hz, $^3J_{3,4}$ = $^3J_{7,8}$ = 8.3 Hz, H$_3$, H$_7$), 7.78 (2H, d, $^3J_{3,4}$ = $^3J_{7,8}$ = 8.3 Hz, H$_4$, H$_8$), 4.89 (2H, m, H$_9$, H$_{10}$), 2.91 (4H, m, H$_{11}$, H$_{13}$); ^{13}C NMR (100 MHz, DMSO-d_6) 212.1 (C$_{12}$), 154.8 (C$_B$, C$_D$), 151.8 (C$_2$, C$_6$), 148.1 (C$_A$, C$_C$), 132.9 (C$_4$, C$_8$), 127.8 (C$_3$, C$_7$), 126.5 (C$_1$, C$_5$), 55.0 (C$_{11}$, C$_{13}$), 47.1 (C$_9$ or C$_{10}$), 46.6 (C$_9$ or C$_{10}$),; **EI-MS**, *m/z* (relative intensity), 324 ([M]$^+$, 91), 308 (12), 307 (11), 294 (20), 277 (100), 251 (20), 231 (21), 202 (19), 189 (82), 176 (31), 163 (16); **Anal.** Found: C, 62.30; H, 3.66; N, 8.45. Calcd for C$_{17}$H$_{15}$N$_2$O$_4$: C, 62.96; H, 3.73; N, 8.64.

9,10-Dihydro-2-nitro-9,10-propanoanthracen-12-one 134

134

C$_{17}$H$_{13}$NO$_3$ 279.29 g.mol^{-1}
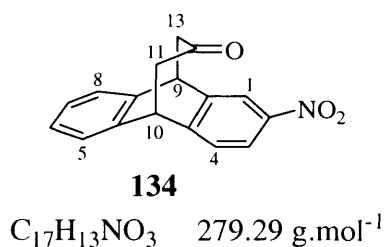
Cold fuming nitric acid (23 µL, 0.55 mmol) was added dropwise to freshly distilled acetic anhydride (80 µL) at 0 °C. The resulting solution was added to a stirred suspension of ketone **67** (117 mg, 0.5 mg) in a mixture of distilled MeNO$_2$ (1.0 mL), acetic anhydride (0.8 mL) and anhydrous CH$_2$Cl$_2$ (0.5 mL) at 0 °C. The solution was kept at this temperature with the use of a chiller unit for 24 h with stirring, then warmed to room temperature.

Water (10 mL) was added and the mixture was stirred vigorously for a further 3 h. The product was extracted with CH_2Cl_2 (3 x 5 mL) and the combined organic layers were washed with brine (3 x 5 mL), dried over Na_2SO_4 and concentrated under reduced pressure. The crude product was purified by flash column chromatography (silica gel, gradient of elution 1:10 to 1:5 EtOAc/P.E. 40-60 °C) to yield the *title compound* **134** (99 mg, 71%) as light yellow square crystals.

The spectroscopic data obtained were identical to those previously described

2-Amino-9,10-dihydro-9,10-propanoanthracen-12-one 138

138

$C_{17}H_{15}NO$ 249.31 g.mol^{-1}
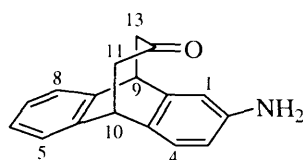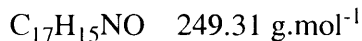
A mixture of $SnCl_2.2H_2O$ (770 mg, 3.4 mmol) in concentrated HCl (2.6 mL) was added dropwise over 15 min to a stirred solution of ketone **134** (280 mg, 1 mmol) in THF (10 mL). The stirring was maintained for 2 hrs before a further addition of $SnCl_2.2H_2O$ (770 mg, 3.4 mmol) in concentrated HCl (2.6 mL). After 2 h of stirring, the reaction was quenched with water (10 mL) and aqueous NaOH solution (2.5 M, 10 mL), filtered through celite and washed thoroughly with CH_2Cl_2. The solution was then extracted with CH_2Cl_2 (3 x 10 mL), dried over $MgSO_4$ and concentrated under reduced pressure. The crude product was purified by flash column chromatography (silica gel, gradient of elution 10:1 EtOAc/P.E. 40-60 °C to pure EtOAc) to yield to the *title compound* **138** (152 mg, 61%) as a light brown solid.

M.p. > 230 °C (decomp.); **HRMS** found: M$^+$, 249.11497. $C_{17}H_{15}NO$ requires 249.11536; **IR** (CH_2Cl_2) v_{max} 3426 (br, NH_2), 3348 (br, NH_2), 3022 (m, H_{ar}), 2844 (w), 1682 (s, C=O), 1620 (s, NH_2), 1499 (s), 1483 (s), 1456 (s), 1377 (s), 1263, (m), 1151 (s), 982 (w), 941(w),

870 (s), 818 (s), 744 (m), 687 (s), 587 (s), 561 (s) cm^{-1}; **^{1}H NMR** (400 MHz, CDCl$_3$) 7.32-7.30 (2H, m, H$_{ar}$), 7.22-7.19 (2H, m, H$_{ar}$), 7.12-7.10 (1H, d, $^3J_{3,4}$ = 7.9 Hz, H$_4$), 6.69 (1H, d, $^4J_{1,3}$ = 2.3 Hz, H$_1$), 6.51 (1H, dd, $^4J_{1,3}$ = 2.3 Hz, $^3J_{3,4}$ = 7.9 Hz, H$_3$), 4.12 (2H, m, H$_9$, H$_{10}$), 3.32 (2H, br, NH$_2$), 2.82 (4H, m, H$_{11}$, H$_{13}$); **^{13}C NMR** (100 MHz, CDCl$_3$) 209.9 (C$_{12}$), 145.3 (C$_2$), 142.9 (C$_q$), 142.5 (C$_q$), 141.7 (C$_q$), 131.7 (C$_q$), 126.9 (CH), 126.8 (CH), 125.9 (CH), 125.7 (CH), 113.3 (C$_1$ or C$_3$), 112.8 (C$_1$ or C$_3$), 51.3 (C$_{11}$ or C$_{13}$), 51.1 (C$_{11}$ or C$_{13}$), 43.6 (C$_9$ or C$_{10}$), 42.5 (C$_9$ or C$_{10}$); **EI-MS**, _m/z_ (relative intensity), 249 (M$^+$, 60), 206 ([C$_{15}$H$_{13}$N]$^+$, 100), 193 (15), 165 (9).

(±)-(9R,10S,12S)-2-Amino-9,10-dihydro-12-hydroxyl-12-methyl-9,10-propanoanthracene 139 and

(±)-(9R,10S,12R)-2-amino-9,10-dihydro-12-hydroxyl-12-methyl-9,10-propanoanthracene 140
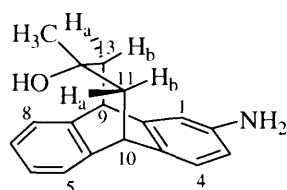
139

C$_{18}$H$_{19}$NO   265.35 g.mol^{-1}
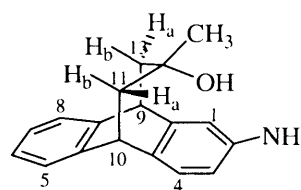
140

C$_{18}$H$_{19}$NO   265.35 g.mol^{-1}

Cerium (III) chloride heptahydrate (360 mg, 1.2 mmol) was ground in a mortar and placed in a three-necked flask fitted with a dropping funnel and a nitrogen inlet adaptor. The flask was evacuated (0.1 mmHg) and immersed in an oil bath at 140 °C without stirring for 1 h and then stirred for a further 1 h. The flask was cooled in an ice bath under nitrogen and anhydrous THF (2.6 mL) was added all at once with vigorous stirring. The ice bath was removed and the suspension was stirred overnight at room temperature. The flask was cooled to -78 °C under nitrogen and MeLi (1.6 M solution in Et$_2$O, 750 μL, 1.2 mmol) was added dropwise and the light yellow suspension was stirred for 1 hr. A solution of ketone **138** (50 mg, 0.2 mmol) in anhydrous THF (1.5 mL) was added dropwise and the reaction mixture was stirred for 2 h, then warmed up to 0 °C. The mixture was poured into an aqueous HCl solution (2M, 5 mL) and extracted with CH$_2$Cl$_2$ (3 x 2.5 mL). The combined

organic layers were washed with brine (2.5 mL), dried over $MgSO_4$ and concentrated under reduced pressure. Flash column chromatography (silica gel, 1:2 EtOAc/P.E. 40-60 °C) gave the _title compounds_ **139** (28 mg, 54%) and **140** (14 mg, 26%) as a brown oil.

(±)-(9R,10S,12S)-2-Amino-9,10-dihydro-12-hydroxyl-12-methyl-9,10-propanoanthracene 139

HRMS: found: M^+, 265.14600. $C_{18}H_{19}NO$ requires 265.14666; **IR** (CH_2Cl_2) v_{max} 3574 (s, OH), 3356 (br, NH_2 and OH), 3228 (w), 2928 (s, CH_3), 1689 (s, NH_2), 1620 (s, NH_2), 1481 (s), 1452 (s), 1375 (s, CH_3), 1278 (br, NH_2), 1227 (s), 1155 (s), 1107 (s), 1088 (s, OH), 1061 (s), 1031 (w), 964 (s), 878 (s, H_{ar}), 820 (s, H_{ar}), 737 (br), 702 (s), 673 (w), 592 (s, OH) cm^{-1}; **^{1}H NMR** (400 MHz, $CDCl_3$) 7.33 (2H, m, H_5, H_8), 7.21 (2H, m, H_6, H_7), 7.03 (1H, d, $^3J_{3,4}$ = 7.8 Hz, H_4), 6.63 (1H, d, $^4J_{1,3}$ = 2.3 Hz, H_1), 6.46 (1H, dd, $^4J_{1,3}$ = 2.3 Hz, $^3J_{3,4}$ = 7.8 Hz, H_3), 4.02 (1H, dd, $^3J_{10,11b}$ = 1.6 Hz, $^3J_{10,11a}$ = 6.9 Hz, H_{10}), 3.97 (1H, dd, $^3J_{9,13b}$ = 1.4 Hz, $^3J_{9,13a}$ = 6.6 Hz, H_9), 2.25 (1H, ddd, $^4J_{11a,13a}$ = 1.9 Hz, $^3J_{10,11a}$ = 6.9 Hz, $^2J_{11a,11b}$= 13.5 Hz, H_{11a}), 2.22 (1H, ddd, $^4J_{11a,13a}$ = 1.9 Hz, $^3J_{9,13a}$ = 6.6 Hz, $^2J_{13a,13b}$= 13.5 Hz, H_{13a}), 1.91 (1H, dd, $^3J_{9,13b}$ = 1.4 Hz, $^2J_{13a,13b}$= 13.5 Hz, H_{13b}), 1.87 (1H, dd, $^3J_{10,11b}$ = 1.6 Hz, $^2J_{11a,11b}$= 13.5 Hz, H_{11b}), 0.93 (3H, s, CH_3); **^{13}C NMR** (100 MHz, $CDCl_3$) 145.5 (C_q), 144.3 (C_q), 142.3 (C_q), 142.0 (C_q), 134.7 (C_2), 126.9 (CH), 126.8 (x 2, CH), 126.4 (CH), 126.2 (CH), 126.1 (CH), 125.9 (CH), 112.8 (C_1), 72.7 (C_{12}), 45.1 (C_{11} or C_{13}), 44.8 (C_9 or C_{10}), 44.2 (C_{11} or C_{13}), 43.7 (C_9 or C_{10}), 32.9 (CH_3); **EI-MS**, m/z (relative intensity), 265 ($[M]^+$, 86), 249 (22), 247 (32), 232 (29), 207 (99), 206 (100), 193 (86), 178 ($[C_{12}H_{10}]^+$, 21), 165 (39), 85 (63), 84 (97).

(±)-(9R,10S,12R)-2-amino-9,10-dihydro-12-hydroxyl-12-methyl-9,10-propanoanthracene 140

HRMS: found: M^+, 265.14626. $C_{18}H_{19}NO$ requires 265.14666; **IR** (CH_2Cl_2) v_{max} 3558 (s, OH), 3360 (br, NH_2 and OH), 3226 (br), 2928 (s, CH_3), 1620 (s, NH_2), 1481 (s), 1452 (s), 1377 (s, CH_3), 1278 (br, NH_2), 1227 (s), 1107 (s), 1088 (s, OH), 1061 (s), 972 (s), 881 (s, H_{ar}), 820 (s, H_{ar}), 737 (s), 702 (s), 673 (w), 590 (s, OH) cm^{-1}; **^{1}H NMR** (400 MHz, $CDCl_3$) 7.21 (2H, m, H_5, H_8), 7.15 (1H, d, $^3J_{3,4}$ = 7.9 Hz, H_4), 7.13 (2H, m, H_6, H_7), 6.74 (1H, d, $^4J_{1,3}$ = 2.3 Hz, H_1), 6.53 (1H, d, $^4J_{1,3}$ = 2.3 Hz, $^3J_{3,4}$ = 7.9 Hz, H_3), 3.99 (1H, dd, $^3J_{10,11b}$ = 1.3

Hz, $^3J_{10,11a}$ = 6.9 Hz, H$_{10}$), 3.95 (1H, dd, $^3J_{9,13b}$ = 1.3 Hz, $^3J_{9,13a}$ = 6.9 Hz, H$_9$), 2.26 (1H, ddd, $^4J_{11a,13a}$ = 2.1 Hz, $^3J_{10,11a}$ = 6.9 Hz, $^2J_{11a,11b}$ = 14.3 Hz, H$_{11a}$), 3.0 (2H, br, NH$_2$), 2.21 (1H, ddd, $^4J_{11a,13a}$ = 2.1 Hz, $^3J_{9,13a}$ = 6.9 Hz, $^2J_{13a,13b}$ = 14.3 Hz, H$_{13a}$), 1.86 (1H, dd, $^3J_{10,11b}$ = 1.3 Hz, $^2J_{11a,11b}$ = 14.3 Hz, H$_{11b}$) 1.84 (1H, dd, $^3J_{9,13b}$ = 1.3 Hz, $^2J_{13a,13b}$ = 14.3 Hz, H$_{13b}$), 0.93 (3H, s, CH$_3$); ^{13}**C NMR** (100 MHz, CDCl$_3$) 145.0 (C$_q$), 144.2 (C$_q$), 142.7 (C$_q$), 131.1 (C$_2$), 127.2 (CH), 126.2 (CH), 126.1 (CH), 125.2 (CH), 125.0 (CH), 114.0 (CH), 112.8 (CH), 72.8 (C$_{12}$), 45.2 (C$_9$ or C$_{10}$), 45.0 (C$_{11}$ or C$_{13}$), 44.6 (C$_{11}$ or C$_{13}$), 44.1 (C$_9$ or C$_{10}$), 32.7 (CH$_3$); **EI-MS**, *m/z* (relative intensity), 265 ([M]$^+$, 53), 247 (47), 232(25), 208 (100), 207 (100), 193 ([C$_{12}$H$_{12}$N]$^+$, 87), 165 (32).

CHAPTER 5

APPENDICES

Appendix 1 Dihedral angles φ and ψ measured from DFT minimised geometries of propanoanthracenes in the gas phase. Calculations involved full SCF calculations, vibrational mode and relaxed grid search. Only the energetically most stable rotamer is considered. Coupling constants $^3J_{10\text{-}11a}$ and $^3J_{10\text{-}11b}$ were calculated using Altona's equation.[232]

	X-down	Y-up	φ (°)	ψ (°)	$^3J_{10\text{-}11a}$ (Hz)	$^3J_{10\text{-}11b}$ (Hz)
77	OH	H	38	76	6.5	1.3
	H	OH	37	78	6.6	1.2
78	OH	CH₃	38	75	6.5	1.3
	CH₃	OH	38	74	6.5	1.4
79	OH	CH=CH₂	38	74	6.5	1.4
	CH=CH₂	OH	35	78	7.0	1.2
81	OH	C≡CH	38	76	6.5	1.3
	C≡CH	OH	38	76	6.5	1.3
83	OH	C≡N	38	76	6.6	1.3
	C≡N	OH	38	76	6.6	1.3
84	OCH₃	CH₃	35	78	7.0	1.2
	CH₃	OCH₃	39	74	6.4	1.4
85	OCH₃	C≡CH	31	80	7.6	1.1
	C≡CH	OCH₃	40	72	6.2	1.6
86	-O-	-CH₂-	36	79	6.8	1.1
	-CH₂-	-O-	36	79	6.8	1.1
87	-O-	-CH₂-	36	78	6.8	1.2
	-CH₂-	-O-	35	79	7.0	1.1
94	F	CH₃	37	77	6.7	1.2
	CH₃	F	37	76	6.6	1.3
96	F	H	37	78	6.7	1.2
	H	F	37	78	6.7	1.1
103	NH₂	CH₃	38	76	6.6	1.3
	CH₃	NH₂	38	75	6.5	1.4
116	NH₂	C≡N	37	76	6.6	1.3
	C≡N	NH₂	37	76	6.6	1.3
117	NH₂.HCl	CH₃	37	78	6.7	1.2
	CH₃	NH₂.HCl	38	75	6.6	1.3

118	NH$_2$.HCl	C≡N	36	78	6.8	1.2
	C≡N	NH$_2$.HCl	37	77	6.6	1.2
119	NH$_2$.MsOH	CH$_3$	37	78	6.7	1.2
	CH$_3$	NH$_2$.MsOH	38	75	6.6	1.3
120	NH$_2$.MsOH	C≡N	36	78	6.8	1.2
	C≡N	NH$_2$.MsOH	3.7	77	6.6	1.2
121	-NH-	-CH$_2$-	37	78	6.6	1.2
	-CH$_2$-	-NH-	35	80	7.0	1.1
128	-NH-	-CH$_2$-	39	76	6.4	1.3
	-CH$_2$-	-NH-	36	78	6.9	1.2
130	-NH-	-CH$_2$-	37	77	6.6	1.2
	-CH$_2$-	-NH-	35	78	7.0	1.1
139	OH	CH$_3$	38	75	6.5	1.3
	CH$_3$	OH	38	74	6.5	1.4
140	OH	CH$_3$	38	75	6.5	1.3
	CH$_3$	OH	38	74	6.5	1.4

Appendix 2   Distances between the substituent on the central bridge and the protons H_{11a} and H_{11b}, r_a and r_b respectively in both conformations, measured from MMX minimised geometries of propanoanthracenes in the gas phase and theoretical enhancement ratios $(r_a/r_b)^{-6}$. Observed enhancement ratio (η_A/η_B) by NOE experiments in solution, deuterated solvent and experimental temperature are indicated, and the preferential conformation is mentioned in bold type.

	X-down	Y-up	r_a (Å)	r_b (Å)	$(r_a/r_b)^{-6}$	(η_A/η_B)	solvent	Temp.
78	**OH**	**CH₃**	2.826	2.603	**0.61**	**0.59**	CDCl₃	298 K
	CH₃	OH	2.588	3.460	5.71			
79	**OH**	**CHCH₂**	3.285	3.539	**1.56**	**1.66**	CDCl₃	298 K
	CHCH₂	OH	3.000	3.999	5.60			
81	OH	C≡CH	4.542	4.181	0.61	1.53	C₆D₅CD₃	298 K
	C≡CH	OH	4.215	5.511	5.00			
87	-O-	-CH₂-	2.581	2.541	0.91	10.08	CDCl₃	298 K
	-CH₂-	**-O-**	2.363	3.685	**14.38**			
103	**NH₂**	**CH₃**	2.824	2.599	**0.61**	**0.62**	C₆D₅CD₃	298 K
	CH₃	NH₂	2.589	3.463	5.73			
117	**NH₃Cl**	**CH₃**	2.778	2.654	**0.76**	**0.54**	CDCl₃	298 K
	CH₃	NH₃Cl	2.598	3.460	5.58			
119	NH₃OMs	CH₃	2.778	2.654	0.76	4.15	CD₃OD	298 K
	CH₃	**NH₃OMs**	2.598	3.460	**5.58**			
128	-NH-	-CH₂-	2.621	2.545	0.84	10.75	CD₃OD	298 K
	-CH₂-	**-NH-**	2.373	3.705	**14.49**			
130	-NH-	-CH₂-	2.718	2.489	0.59	2.67	CD₃CN	263 K
	-CH₂-	-NH-	2.322	3.657	15.26			

Appendix 3 ^{1}H NMR spectra of the ether **84** in a CFCl$_3$:CD$_2$Cl$_2$ mixture 4:1 as a function of temperature
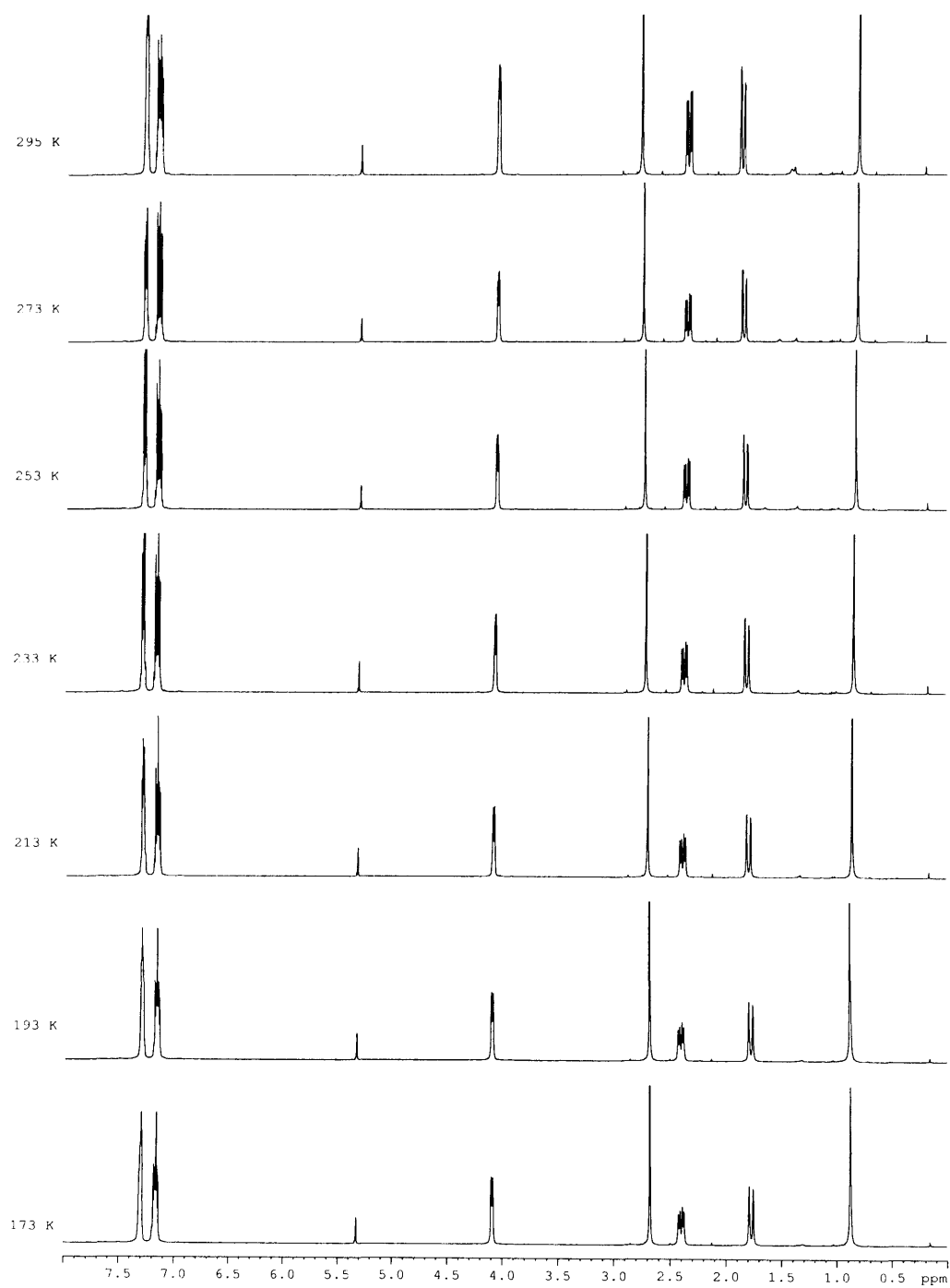
Enlargement of ^{1}H NMR spectra of the ether **84** in a $CFCl_3:CD_2Cl_2$ mixture 4:1 as a function of temperature
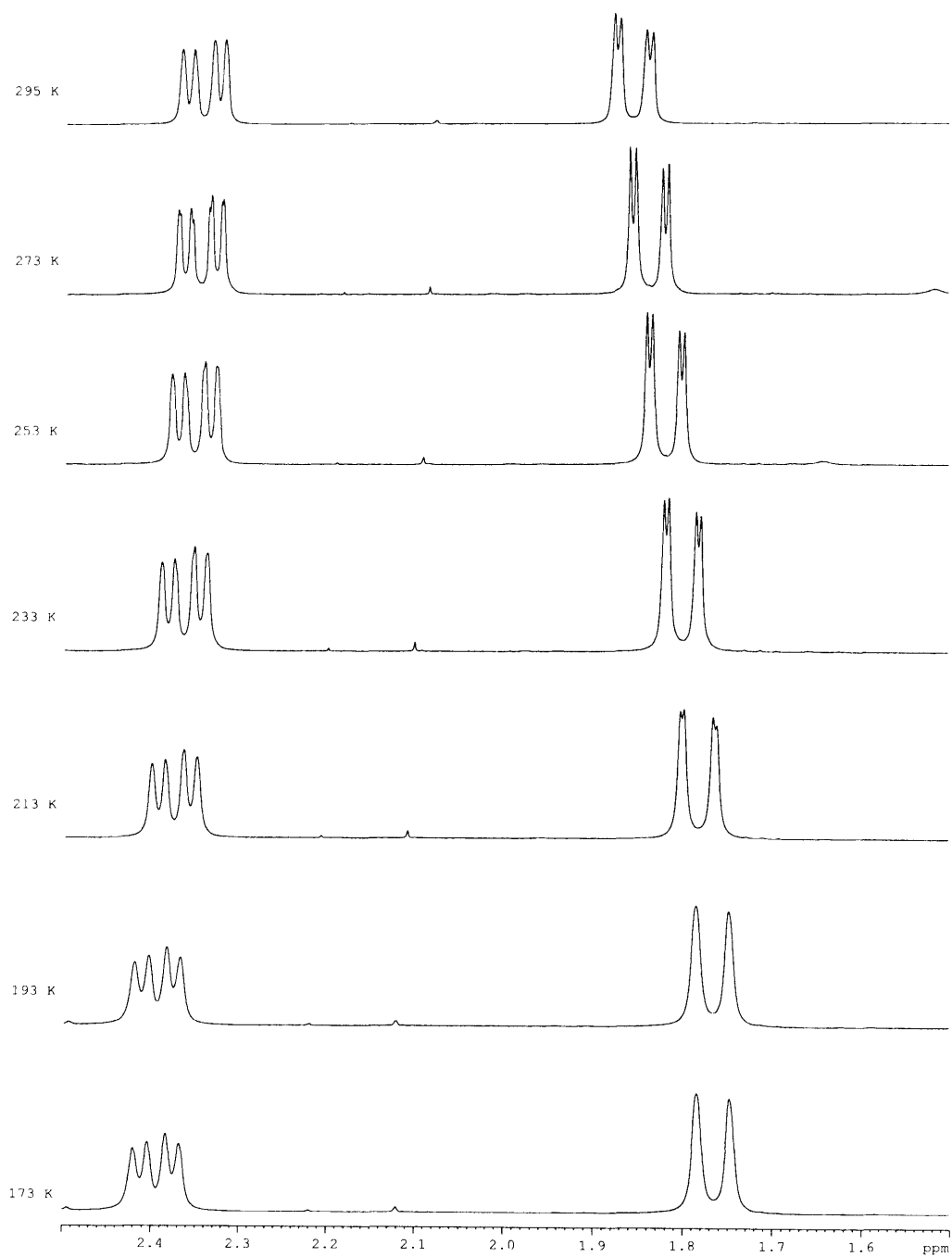
Appendix 4 ^{1}H NMR spectra of the propargylic alcohol **81** in a $CFCl_3:CD_2Cl_2$ mixture 4:1 as a function of temperature
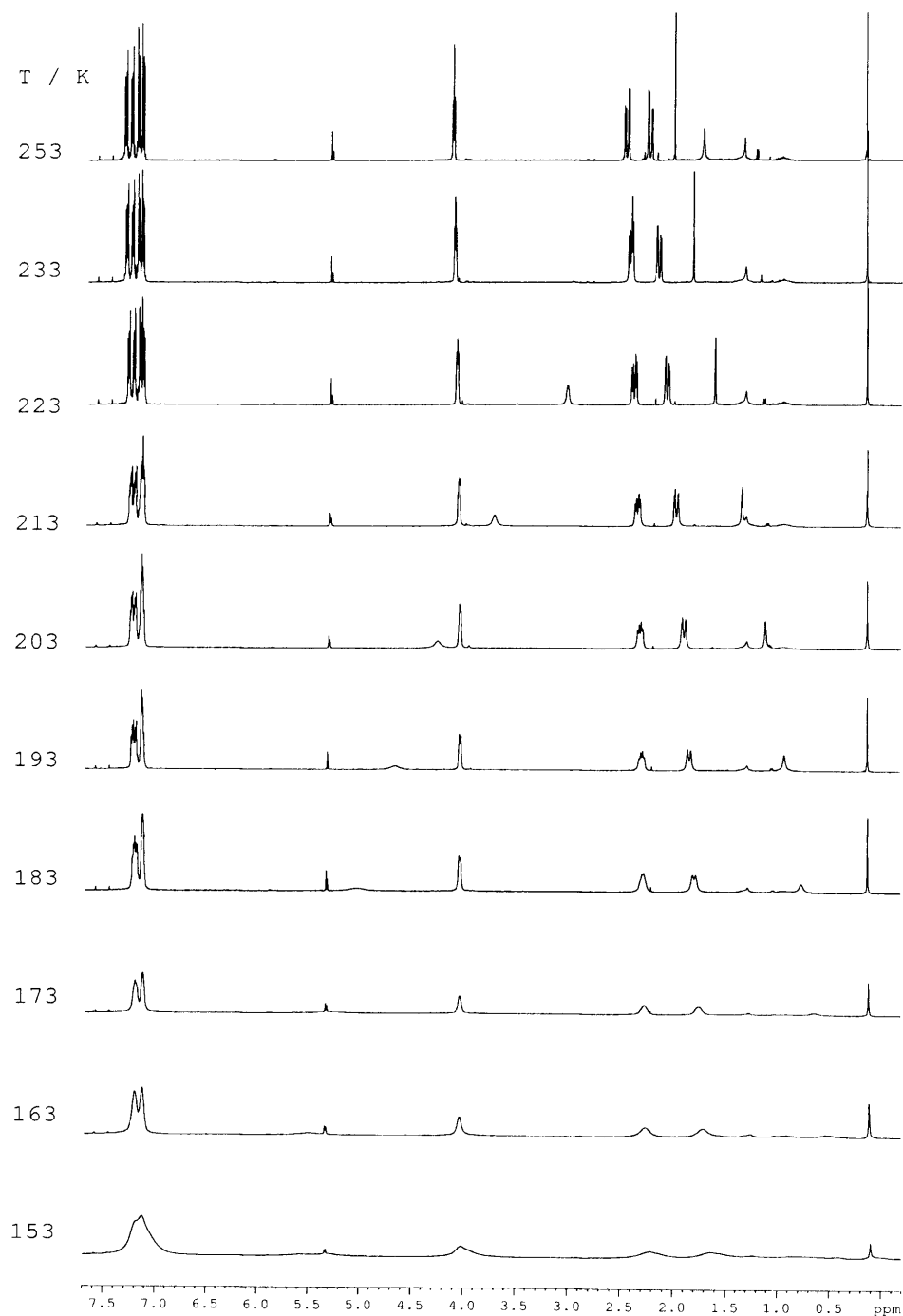
Appendix 5 ^{13}C chemical shifts of **116** in CDCl$_3$ solution and solid state
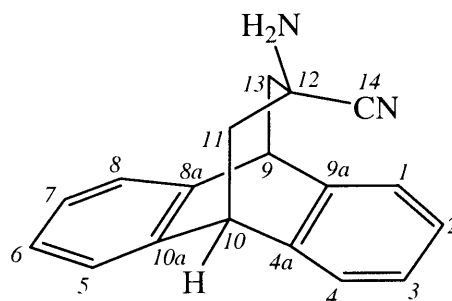
Carbon	**116** in CDCl$_3$	**116** in solid state
1,4	127.0	124-131
2,3	127.5	124-131
5,8	125.5	124-131
6,7	126.8	124-131
4a,9a	139.6	140.4 141.3
8a,10a	143.5	142.9 143.7
9,10	43.8	42.9 43.6
11,13	41.7	41.2 42.0
12	50.6	51.1 52.0
14	123.9	127.5[a] 127.9[a]

[a]Two peaks for the cyano carbon are due to the (^{13}C,^{14}N) residual dipolar coupling

Appendix 6   Dielectric constant ε, hydrogen bond acceptor parameter β for solvents used and population of the predominant conformer in different solvents at 298 K

	C_6D_{12}	CCl_4	$CDCl_3$	C_6D_6	$C_6D_5\text{-}CD_3$	CD_3CN	CD_3OD	C_5D_5N	DMSO-d_6
ε	2.0	2.2	4.7	2.3	2.4	35.7	32.6	12.3	46.8
β	0.3	0.6	0.8	2.2	2.2	4.7	5.8	7.0	8.9
77	93	93	95	95	-	97	100	98	100
78	93	95	93	89	88	74	51	52	50
79	92	-	90	89	-	-	62	-	55
81	66	61	52	52	62	70	82	82	78
83	69	-	74	76	79	93	96	-	95
84	66	68	69	67	-	69	67	67	67
85	76	75	74	73	-	67	71	-	68
86	-	-	50	74	77	40	37	-	35
87	-	-	89	93	-	87	-	-	-
94	77	83	95	87	-	97	88	-	93
96	99	-	92	95	-	-	96	-	87
103	78	78	78	73	74	70	75	68	59
116	-	-	96	95	-	100	100	-	100
121	74	73	68	73	-	71	69	-	73
128	59		66	51	-	77	86	-	100
130	61	61	61	65	67	68	60	72	82

	$CDCl_3$	$D_2O\text{:}H_2O$ 1:9	CD_3OD	DMSO-d_6
117	82	53	16	3
118	-	100	100	100
119	-	64	16	0
120	-	100	100	100

Appendix 7   Crystal structure and X-Ray data for **67**

Table A.1. Crystal data and structure refinement for **67**.

Chemical formula	$C_{17}H_{14}O$	
Formula weight	234.28	
Temperature	150(2) K	
Radiation, wavelength	MoKα, 0.71073 Å	
Crystal system, space group	monoclinic, $P2_1$	
Unit cell parameters	a = 8.4849(15) Å	$\alpha = 90°$
	b = 7.0537(12) Å	$\beta = 103.807(3)°$
	c = 10.2213(18) Å	$\gamma = 90°$
Cell volume	594.07(18) Å^3	
Z	2	
Calculated density	1.310 g/cm^3	
Absorption coefficient μ	0.080 mm^{-1}	
F(000)	248	
Crystal colour and size	colourless, 0.42 × 0.10 × 0.08 mm^3	
Data collection method	Bruker SMART APEX diffractometer ω rotation with narrow frames	
θ range for data collection	2.05 to 28.18°	
Index ranges	h −11 to 10, k −9 to 9, l −13 to 13	
Completeness to $\theta = 26.00°$	99.4 %	
Reflections collected	5176	
Independent reflections	2692 ($R_{int} = 0.0275$)	
Reflections with $F^2 > 2\sigma$	2388	
Absorption correction	semi-empirical from equivalents	
Min. and max. transmission	0.9673 and 0.9937	
Structure solution	direct methods	
Refinement method	Full-matrix least-squares on F^2	
Weighting parameters a, b	0.0816, 0.0421	
Data / restraints / parameters	2692 / 1 / 163	
Final R indices [$F^2 > 2\sigma$]	R1 = 0.0535, wR2 = 0.1314	
R indices (all data)	R1 = 0.0611, wR2 = 0.1361	
Goodness-of-fit on F^2	1.044	
Largest and mean shift/su	0.000 and 0.000	
Largest diff. peak and hole	0.269 and −0.179 e Å^{-3}	

Table A.2. Atomic coordinates and equivalent isotropic displacement parameters (Å^2) for **67**. U_{eq} is defined as one third of the trace of the orthogonalized U^{ij} tensor.

	x	y	z	U_{eq}
O(1)	0.0770(2)	1.0054(3)	0.1665(2)	0.0508(6)
C(1)	0.1658(3)	0.8684(3)	0.1910(2)	0.0260(5)
C(2)	0.1036(3)	0.6805(4)	0.1286(2)	0.0279(5)
C(3)	0.1809(2)	0.4970(3)	0.1992(2)	0.0236(5)
C(4)	0.3346(3)	0.8968(3)	0.2808(2)	0.0273(5)
C(5)	0.4207(3)	0.7206(3)	0.3555(2)	0.0224(5)
C(6)	0.3078(2)	0.6198(3)	0.4267(2)	0.0216(4)
C(7)	0.3167(3)	0.6374(3)	0.5632(2)	0.0250(5)
C(8)	0.2085(3)	0.5407(3)	0.6202(2)	0.0297(5)
C(9)	0.0908(3)	0.4251(4)	0.5421(3)	0.0321(6)
C(10)	0.0801(3)	0.4076(3)	0.4056(2)	0.0272(5)
C(11)	0.1876(2)	0.5055(3)	0.3472(2)	0.0222(4)
C(12)	0.3509(2)	0.4738(3)	0.1799(2)	0.0222(4)
C(13)	0.3878(3)	0.3462(3)	0.0879(2)	0.0258(5)
C(14)	0.5459(3)	0.3316(4)	0.0740(2)	0.0289(5)
C(15)	0.6653(3)	0.4435(3)	0.1515(2)	0.0286(5)
C(16)	0.6303(3)	0.5703(3)	0.2437(2)	0.0251(5)
C(17)	0.4720(2)	0.5850(3)	0.2588(2)	0.0212(4)

Table A.3. Bond lengths [Å] and angles [°] for **67**.

O(1)—C(1)	1.214(3)	C(1)—C(2)	1.511(3)
C(1)—C(4)	1.519(3)	C(2)—C(3)	1.549(3)
C(3)—C(11)	1.501(3)	C(3)—C(12)	1.510(3)
C(4)—C(5)	1.547(3)	C(5)—C(6)	1.512(3)
C(5)—C(17)	1.512(3)	C(6)—C(7)	1.385(3)
C(6)—C(11)	1.398(3)	C(7)—C(8)	1.380(3)
C(8)—C(9)	1.385(4)	C(9)—C(10)	1.382(4)
C(10)—C(11)	1.388(3)	C(12)—C(17)	1.388(3)
C(12)—C(13)	1.390(3)	C(13)—C(14)	1.386(3)
C(14)—C(15)	1.376(3)	C(15)—C(16)	1.382(3)
C(16)—C(17)	1.392(3)		

O(1)—C(1)—C(2)	118.3(2)	O(1)—C(1)—C(4)	118.0(2)
C(2)—C(1)—C(4)	123.69(19)	C(1)—C(2)—C(3)	118.06(18)
C(11)—C(3)—C(12)	109.13(16)	C(11)—C(3)—C(2)	110.21(18)
C(12)—C(3)—C(2)	109.93(18)	C(1)—C(4)—C(5)	117.29(18)
C(6)—C(5)—C(17)	109.35(17)	C(6)—C(5)—C(4)	109.68(17)
C(17)—C(5)—C(4)	111.17(18)	C(7)—C(6)—C(11)	119.62(19)
C(7)—C(6)—C(5)	123.69(19)	C(11)—C(6)—C(5)	116.68(18)
C(8)—C(7)—C(6)	120.0(2)	C(7)—C(8)—C(9)	120.6(2)
C(10)—C(9)—C(8)	120.0(2)	C(9)—C(10)—C(11)	119.9(2)
C(10)—C(11)—C(6)	119.99(19)	C(10)—C(11)—C(3)	122.9(2)
C(6)—C(11)—C(3)	117.15(18)	C(17)—C(12)—C(13)	120.2(2)
C(17)—C(12)—C(3)	117.44(19)	C(13)—C(12)—C(3)	122.34(19)
C(14)—C(13)—C(12)	119.8(2)	C(15)—C(14)—C(13)	119.7(2)
C(14)—C(15)—C(16)	121.0(2)	C(15)—C(16)—C(17)	119.6(2)
C(12)—C(17)—C(16)	119.6(2)	C(12)—C(17)—C(5)	116.65(17)
C(16)—C(17)—C(5)	123.77(18)		

Table A.4. Anisotropic displacement parameters (Å^2) for **67**. The anisotropic displacement factor exponent takes the form: $-2\pi^2[h^2a^{*2}U^{11} + ...+ 2hka^*b^*U^{12}]$

	U^{11}	U^{22}	U^{33}	U^{23}	U^{13}	U^{12}
O(1)	0.0480(11)	0.0312(11)	0.0621(13)	0.0042(10)	−0.0090(9)	0.0083(9)
C(1)	0.0299(11)	0.0203(11)	0.0265(11)	0.0062(9)	0.0041(9)	0.0010(9)
C(2)	0.0243(11)	0.0271(12)	0.0296(11)	0.0011(10)	0.0010(9)	−0.0010(9)
C(3)	0.0219(10)	0.0209(11)	0.0263(10)	−0.0018(9)	0.0022(8)	−0.0060(9)
C(4)	0.0311(12)	0.0166(11)	0.0338(12)	−0.0004(9)	0.0070(10)	−0.0041(9)
C(5)	0.0215(10)	0.0170(11)	0.0268(11)	−0.0019(9)	0.0021(9)	−0.0033(8)
C(6)	0.0208(10)	0.0165(10)	0.0263(11)	−0.0012(9)	0.0034(8)	0.0015(8)
C(7)	0.0274(11)	0.0182(11)	0.0283(11)	−0.0036(9)	0.0048(9)	0.0071(9)
C(8)	0.0342(12)	0.0265(13)	0.0312(12)	0.0029(10)	0.0133(10)	0.0117(10)
C(9)	0.0316(12)	0.0280(13)	0.0408(13)	0.0083(10)	0.0166(11)	0.0026(10)
C(10)	0.0257(11)	0.0228(12)	0.0337(12)	0.0006(10)	0.0079(9)	−0.0018(9)
C(11)	0.0221(10)	0.0175(10)	0.0267(10)	0.0001(9)	0.0051(8)	0.0015(9)
C(12)	0.0244(10)	0.0168(10)	0.0236(10)	0.0017(9)	0.0024(8)	−0.0023(9)
C(13)	0.0317(11)	0.0201(11)	0.0240(11)	−0.0024(8)	0.0036(9)	−0.0042(10)
C(14)	0.0371(12)	0.0240(12)	0.0278(12)	0.0018(10)	0.0122(10)	0.0018(10)
C(15)	0.0257(11)	0.0300(13)	0.0313(12)	0.0049(10)	0.0093(9)	0.0016(10)
C(16)	0.0253(10)	0.0201(11)	0.0285(11)	0.0035(9)	0.0038(9)	−0.0041(9)
C(17)	0.0225(10)	0.0159(10)	0.0242(11)	0.0017(8)	0.0035(8)	−0.0042(8)

Table A.5. Hydrogen coordinates and isotropic displacement parameters ($\mathring{A}^2$) for **67**.

	x	y	z	U
H(2A)	0.1177	0.6791	0.0352	0.034
H(2B)	−0.0144	0.6751	0.1228	0.034
H(3)	0.1137	0.3855	0.1588	0.028
H(4A)	0.3273	0.9938	0.3492	0.033
H(4B)	0.4045	0.9493	0.2248	0.033
H(5)	0.5193	0.7629	0.4240	0.027
H(7)	0.3972	0.7161	0.6176	0.030
H(8)	0.2147	0.5535	0.7139	0.036
H(9)	0.0176	0.3579	0.5824	0.039
H(10)	−0.0007	0.3286	0.3518	0.033
H(13)	0.3049	0.2693	0.0347	0.031
H(14)	0.5718	0.2446	0.0113	0.035
H(15)	0.7735	0.4335	0.1414	0.034
H(16)	0.7137	0.6469	0.2964	0.030

Table A.6. Torsion angles [°] for **67**.

O(1)–C(1)–C(2)–C(3)	-156.2(2)	C(4)–C(1)–C(2)–C(3)	25.0(3)
C(1)–C(2)–C(3)–C(11)	48.5(2)	C(1)–C(2)–C(3)–C(12)	-71.9(2)
O(1)–C(1)–C(4)–C(5)	157.0(2)	C(2)–C(1)–C(4)–C(5)	-24.2(3)
C(1)–C(4)–C(5)–C(6)	-49.8(3)	C(1)–C(4)–C(5)–C(17)	71.2(2)
C(17)–C(5)–C(6)–C(7)	137.3(2)	C(4)–C(5)–C(6)–C(7)	-100.6(2)
C(17)–C(5)–C(6)–C(11)	-43.7(2)	C(4)–C(5)–C(6)–C(11)	78.5(2)
C(11)–C(6)–C(7)–C(8)	0.8(3)	C(5)–C(6)–C(7)–C(8)	179.79(19)
C(6)–C(7)–C(8)–C(9)	0.2(3)	C(7)–C(8)–C(9)–C(10)	-0.7(4)
C(8)–C(9)–C(10)–C(11)	0.2(3)	C(9)–C(10)–C(11)–C(6)	0.8(3)
C(9)–C(10)–C(11)–C(3)	-178.5(2)	C(7)–C(6)–C(11)–C(10)	-1.3(3)
C(5)–C(6)–C(11)–C(10)	179.6(2)	C(7)–C(6)–C(11)–C(3)	178.1(2)
C(5)–C(6)–C(11)–C(3)	-1.0(3)	C(12)–C(3)–C(11)–C(10)	-136.0(2)
C(2)–C(3)–C(11)–C(10)	103.2(2)	C(12)–C(3)–C(11)–C(6)	44.6(3)
C(2)–C(3)–C(11)–C(6)	-76.2(2)	C(11)–C(3)–C(12)–C(17)	-43.9(3)
C(2)–C(3)–C(12)–C(17)	77.1(2)	C(11)–C(3)–C(12)–C(13)	135.7(2)
C(2)–C(3)–C(12)–C(13)	-103.3(2)	C(17)–C(12)–C(13)–C(14)	-0.7(3)
C(3)–C(12)–C(13)–C(14)	179.7(2)	C(12)–C(13)–C(14)–C(15)	0.0(3)
C(13)–C(14)–C(15)–C(16)	0.3(3)	C(14)–C(15)–C(16)–C(17)	0.1(3)
C(13)–C(12)–C(17)–C(16)	1.0(3)	C(3)–C(12)–C(17)–C(16)	-179.3(2)
C(13)–C(12)–C(17)–C(5)	179.6(2)	C(3)–C(12)–C(17)–C(5)	-0.7(3)
C(15)–C(16)–C(17)–C(12)	-0.8(3)	C(15)–C(16)–C(17)–C(5)	-179.3(2)
C(15)–C(16)–C(17)–C(5)	44.5(2)	C(4)–C(5)–C(17)–C(12)	-76.7(2)
C(6)–C(5)–C(17)–C(12)	-136.9(2)	C(4)–C(5)–C(17)–C(16)	101.8(2)
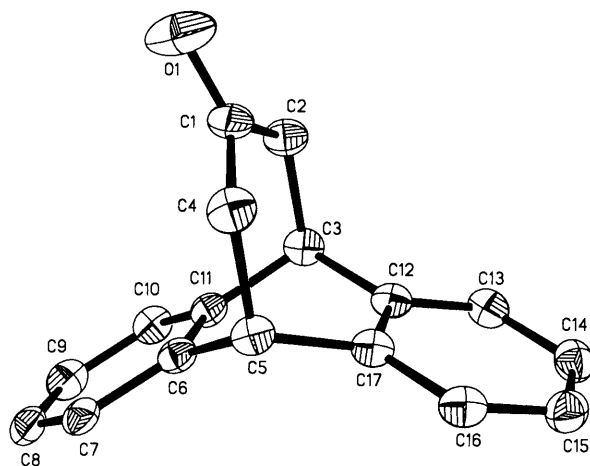
67

Scheme A.1

Appendix 8   Crystal structure and X-Ray data for **78**

Table B.1. Crystal data and structure refinement for **78**

Empirical formula	$C_{18}H_{18}O$
Formula weight	250.32
Temperature	120(2) K
Wavelength	0.71073 Å
Crystal system	Monoclinic
Space group	$P2_1/n$
Unit cell dimensions	$a = 10.1065(16)$ Å $\alpha = 90°$
	$b = 19.980(4)$ Å $\beta = 106.390(12)°$
	$c = 13.8550(19)$ Å $\gamma = 90°$
Volume	2684.1(8) Å^3
Z	8
Density (calculated)	1.239 Mg / m^3
Absorption coefficient	0.075 mm-1
_F(000)_	1072
Crystal	Rod; Colourless
Crystal size	$0.42 \times 0.10 \times 0.08$ mm^3
θ range for data collection	$4.90 - 27.48°$
Index ranges	$-13 \leq h \leq 13, -25 \leq k \leq 25, -17 \leq l \leq 17$
Reflections collected	36919
Independent reflections	36919 [$R_{int} = 0.0000$]
Completeness to $\theta = 27.48°$	99.2 %
Absorption correction	Semi–empirical from equivalents
Max. and min. transmission	0.9940 and 0.9693
Refinement method	Full-matrix least-squares on F^2
Data / restraints / parameters	36919 / 0 / 355
Goodness-of-fit on F^2	1.080
Final R indices [$F^2 > 2\sigma(F^2)$]	$R1 = 0.1072$, $wR2 = 0.2605$
R indices (all data)	$R1 = 0.1528$, $wR2 = 0.3138$
Extinction coefficient	0.006(2)
Largest diff. peak and hole	0.450 and -0.456 e Å-3

Table B.2. Atomic coordinates [× 10^4], equivalent isotropic displacement parameters [Å^2 × 10^3] and site occupancy factors. U_{eq} is defined as one third of the trace of the orthogonalized U^{ij} tensor.

Atom	x	y	z	U_{eq}	S.o.f.
C1	6436(2)	1022(1)	844(1)	21(1)	1
C2	7322(2)	466(1)	1444(1)	21(1)	1
C3	6795(2)	−42(1)	1902(1)	26(1)	1
C4	7674(2)	−534(1)	2438(2)	29(1)	1
C5	9060(2)	−518(1)	2505(1)	30(1)	1
C6	9592(2)	−10(1)	2047(1)	25(1)	1
C7	8724(2)	483(1)	1516(1)	21(1)	1
C8	9209(2)	1067(1)	999(1)	21(1)	1
C9	8232(2)	1128(1)	−47(1)	20(1)	1
C10	8648(2)	1188(1)	−916(1)	24(1)	1
C11	7679(2)	1245(1)	−1843(1)	26(1)	1
C12	6286(2)	1253(1)	−1912(1)	28(1)	1
C13	5863(2)	1192(1)	−1043(1)	23(1)	1
C14	6825(2)	1119(1)	−120(1)	20(1)	1
C15	6628(2)	1686(1)	1444(1)	24(1)	1
C16	8072(2)	1862(1)	2074(1)	24(1)	1
C17	9233(2)	1728(1)	1587(1)	25(1)	1
C18	8137(2)	2595(1)	2402(2)	33(1)	1
O1	8292(2)	1460(1)	2982(1)	29(1)	1
C21	3575(2)	605(1)	3224(1)	23(1)	1
C22	3228(2)	955(1)	2214(1)	21(1)	1
C23	2995(2)	624(1)	1301(1)	22(1)	1
C24	2695(2)	986(1)	410(1)	26(1)	1
C25	2645(2)	1675(1)	433(1)	27(1)	1
C26	2863(2)	2006(1)	1344(2)	26(1)	1
C27	3149(2)	1651(1)	2235(1)	22(1)	1
C28	3368(2)	1974(1)	3258(1)	24(1)	1
C29	2544(2)	1585(1)	3828(1)	24(1)	1
C30	1748(2)	1890(1)	4368(1)	31(1)	1
C31	1051(2)	1497(1)	4898(2)	37(1)	1
C32	1154(2)	811(1)	4884(2)	38(1)	1
C33	1944(2)	503(1)	4340(1)	30(1)	1
C34	2649(2)	888(1)	3813(1)	24(1)	1
C35	5126(2)	702(1)	3792(1)	26(1)	1
C36	5577(2)	1348(1)	4398(1)	25(1)	1
C37	4919(2)	1990(1)	3844(1)	26(1)	1
C38	5336(2)	1302(1)	5436(1)	28(1)	1
O21	7059(1)	1413(1)	4624(1)	37(1)	1

Table B.3. Bond lengths [Å] and angles [°].

C1–C14	1.508(2)	C1–C2	1.519(3)
C1–C15	1.548(2)	C1–H1	1.0000
C2–C3	1.380(3)	C2–C7	1.392(3)
C3–C4	1.392(3)	C3–H3	0.9500
C4–C5	1.378(3)	C4–H4	0.9500
C5–C6	1.384(3)	C5–H5	0.9500
C6–C7	1.384(3)	C6–H6	0.9500
C7–C8	1.521(3)	C8–C9	1.511(3)
C8–C17	1.550(3)	C8–H8	1.0000
C9–C10	1.387(2)	C9–C14	1.397(3)
C10–C11	1.383(3)	C10–H10	0.9500
C11–C12	1.385(3)	C11–H11	0.9500
C12–C13	1.391(3)	C12–H12	0.9500
C13–C14	1.379(3)	C13–H13	0.9500
C15–C16	1.515(3)	C15–H15A	0.9900
C15–H15B	0.9900	C16–O1	1.455(2)
C16–C18	1.530(3)	C16–C17	1.533(3)
C17–H17A	0.9900	C17–H17B	0.9900
C18–H18A	0.9800	C18–H18B	0.9800
C18–H18C	0.9800	O1–H1O	0.96(3)
C21–C22	1.514(3)	C21–C34	1.514(3)
C21–C35	1.555(3)	C21–H21	1.0000
C22–C23	1.388(2)	C22–C27	1.393(3)
C23–C24	1.389(3)	C23–H23	0.9500
C24–C25	1.379(3)	C24–H24	0.9500
C25–C26	1.387(3)	C25–H25	0.9500
C26–C27	1.382(3)	C26–H26	0.9500
C27–C28	1.516(2)	C28–C29	1.513(3)
C28–C37	1.549(3)	C28–H28	1.0000
C29–C30	1.385(3)	C29–C34	1.398(3)
C30–C31	1.396(3)	C30–H30	0.9500
C31–C32	1.375(3)	C31–H31	0.9500
C32–C33	1.386(3)	C32–H32	0.9500
C33–C34	1.388(3)	C33–H33	0.9500
C35–C36	1.536(3)	C35–H35A	0.9900
C35–H35B	0.9900	C36–O21	1.447(2)
C36–C38	1.527(3)	C36–C37	1.546(3)
C37–H37A	0.9900	C37–H37B	0.9900
C38–H38A	0.9800	C38–H38B	0.9800
C38–H38C	0.9800	O21–H21O	1.06(3)

C14–C1–C2	108.49(15)	C14–C1–C15	109.99(15)
C2–C1–C15	111.58(15)	C14–C1–H1	108.9
C2–C1–H1	108.9	C15–C1–H1	108.9
C3–C2–C7	120.11(18)	C3–C2–C1	122.98(18)
C7–C2–C1	116.91(16)	C2–C3–C4	119.59(19)
C2–C3–H3	120.2	C4–C3–H3	120.2
C5–C4–C3	120.25(19)	C5–C4–H4	119.9
C3–C4–H4	119.9	C4–C5–C6	120.28(19)
C4–C5–H5	119.9	C6–C5–H5	119.9
C7–C6–C5	119.75(19)	C7–C6–H6	120.1
C5–C6–H6	120.1	C6–C7–C2	120.02(18)
C6–C7–C8	123.78(17)	C2–C7–C8	116.20(17)
C9–C8–C7	107.70(15)	C9–C8–C17	110.17(15)
C7–C8–C17	111.40(14)	C9–C8–H8	109.2
C7–C8–H8	109.2	C17–C8–H8	109.2
C10–C9–C14	119.32(18)	C10–C9–C8	124.25(17)
C14–C9–C8	116.43(16)	C11–C10–C9	120.29(18)
C11–C10–H10	119.9	C9–C10–H10	119.9
C10–C11–C12	120.30(18)	C10–C11–H11	119.8
C12–C11–H11	119.8	C11–C12–C13	119.64(19)
C11–C12–H12	120.2	C13–C12–H12	120.2
C14–C13–C12	120.18(18)	C14–C13–H13	119.9
C12–C13–H13	119.9	C13–C14–C9	120.23(18)
C13–C14–C1	122.90(17)	C9–C14–C1	116.87(17)
C16–C15–C1	117.55(16)	C16–C15–H15A	107.9
C1–C15–H15A	107.9	C16–C15–H15B	107.9
C1–C15–H15B	107.9	H15A–C15–H15B	107.2
O1–C16–C15	104.91(15)	O1–C16–C18	106.75(15)
C15–C16–C18	110.29(16)	O1–C16–C17	109.59(15)
C15–C16–C17	116.03(15)	C18–C16–C17	108.84(16)
C16–C17–C8	118.65(15)	C16–C17–H17A	107.7
C8–C17–H17A	107.7	C16–C17–H17B	107.7
C8–C17–H17B	107.7	H17A–C17–H17B	107.1
C16–C18–H18A	109.5	C16–C18–H18B	109.5
H18A–C18–H18B	109.5	C16–C18–H18C	109.5
H18A–C18–H18C	109.5	H18B–C18–H18C	109.5
C16–O1–H1O	116.1(18)	C22–C21–C34	107.92(15)
C22–C21–C35	110.33(15)	C34–C21–C35	111.63(15)
C22–C21–H21	109.0	C34–C21–H21	109.0
C35–C21–H21	109.0	C23–C22–C27	119.91(17)
C23–C22–C21	123.87(17)	C27–C22–C21	116.22(16)
C22–C23–C24	120.01(18)	C22–C23–H23	120.0
C24–C23–H23	120.0	C25–C24–C23	120.00(18)
C25–C24–H24	120.0	C23–C24–H24	120.0

C24–C25–C26	120.05(18)	C24–C25–H25	120.0
C26–C25–H25	120.0	C27–C26–C25	120.44(19)
C27–C26–H26	119.8	C25–C26–H26	119.8
C26–C27–C22	119.58(18)	C26–C27–C28	123.69(17)
C22–C27–C28	116.72(17)	C29–C28–C27	108.22(15)
C29–C28–C37	111.27(16)	C27–C28–C37	111.01(15)
C29–C28–H28	108.8	C27–C28–H28	108.8
C37–C28–H28	108.8	C30–C29–C34	120.36(19)
C30–C29–C28	123.02(18)	C34–C29–C28	116.60(17)
C29–C30–C31	119.5(2)	C29–C30–H30	120.2
C31–C30–H30	120.2	C32–C31–C30	120.2(2)
C32–C31–H31	119.9	C30–C31–H31	119.9
C31–C32–C33	120.5(2)	C31–C32–H32	119.7
C33–C32–H32	119.7	C32–C33–C34	120.0(2)
C32–C33–H33	120.0	C34–C33–H33	120.0
C33–C34–C29	119.46(18)	C33–C34–C21	124.32(18)
C29–C34–C21	116.21(17)	C36–C35–C21	118.88(15)
C36–C35–H35A	107.6	C21–C35–H35A	107.6
C36–C35–H35B	107.6	C21–C35–H35B	107.6
H35A–C35–H35B	107.0	O21–C36–C38	103.42(15)
O21–C36–C35	108.82(15)	C38–C36–C35	111.24(16)
O21–C36–C37	107.85(16)	C38–C36–C37	110.93(16)
C35–C36–C37	113.95(15)	C36–C37–C28	118.15(16)
C36–C37–H37A	107.8	C28–C37–H37A	107.8
C36–C37–H37B	107.8	C28–C37–H37B	107.8
H37A–C37–H37B	107.1	C36–C38–H38A	109.5
C36–C38–H38B	109.5	H38A–C38–H38B	109.5
C36–C38–H38C	109.5	H38A–C38–H38C	109.5
H38B–C38–H38C	109.5	C36–O21–H21O	106.9(15)

Table B.4. Anisotropic displacement parameters [$\text{Å}^2 \times 10^3$] for **68**. The anisotropic displacement factor exponent takes the form: $-2\pi^2[h^2 a^{*2} U^{11} + \cdots + 2\, h\, k\, a^*\, b^*\, U^{12}]$.

Atom	U^{11}	U^{22}	U^{33}	U^{23}	U^{13}	U^{12}
C1	17(1)	20(1)	24(1)	−3(1)	5(1)	−2(1)
C2	22(1)	21(1)	22(1)	−5(1)	7(1)	−1(1)
C3	34(1)	21(1)	27(1)	−6(1)	13(1)	−5(1)
C4	41(1)	20(1)	29(1)	1(1)	14(1)	−4(1)
C5	37(1)	24(1)	25(1)	2(1)	6(1)	7(1)
C6	26(1)	26(1)	24(1)	−4(1)	7(1)	5(1)
C7	22(1)	22(1)	19(1)	−4(1)	4(1)	0(1)
C8	19(1)	22(1)	24(1)	−1(1)	9(1)	2(1)
C9	21(1)	14(1)	25(1)	−4(1)	7(1)	−1(1)
C10	29(1)	17(1)	29(1)	−2(1)	13(1)	−1(1)
C11	37(1)	21(1)	23(1)	−1(1)	13(1)	0(1)
C12	36(1)	20(1)	24(1)	−1(1)	2(1)	2(1)
C13	23(1)	18(1)	26(1)	−3(1)	3(1)	2(1)
C14	21(1)	12(1)	26(1)	−3(1)	7(1)	−2(1)
C15	26(1)	22(1)	27(1)	−1(1)	12(1)	1(1)
C16	27(1)	25(1)	21(1)	−2(1)	9(1)	−1(1)
C17	27(1)	24(1)	25(1)	−3(1)	9(1)	−6(1)
C18	42(1)	26(1)	33(1)	−7(1)	13(1)	−6(1)
O1	29(1)	34(1)	22(1)	1(1)	7(1)	−2(1)
C21	29(1)	16(1)	22(1)	−3(1)	5(1)	2(1)
C22	15(1)	25(1)	24(1)	−1(1)	5(1)	3(1)
C23	19(1)	21(1)	23(1)	−4(1)	5(1)	1(1)
C24	21(1)	37(1)	21(1)	−6(1)	6(1)	5(1)
C25	22(1)	36(1)	24(1)	6(1)	6(1)	6(1)
C26	22(1)	24(1)	31(1)	1(1)	7(1)	4(1)
C27	21(1)	23(1)	23(1)	−1(1)	7(1)	4(1)
C28	29(1)	16(1)	26(1)	−3(1)	9(1)	3(1)
C29	25(1)	25(1)	20(1)	−4(1)	2(1)	2(1)
C30	28(1)	38(1)	24(1)	−6(1)	4(1)	6(1)
C31	29(1)	58(2)	26(1)	−11(1)	11(1)	−3(1)
C32	36(1)	57(2)	25(1)	−3(1)	13(1)	−17(1)
C33	32(1)	36(1)	20(1)	−1(1)	3(1)	−8(1)
C34	24(1)	29(1)	17(1)	−2(1)	2(1)	−2(1)
C35	28(1)	26(1)	21(1)	−1(1)	4(1)	5(1)
C36	24(1)	29(1)	21(1)	−5(1)	3(1)	1(1)
C37	31(1)	25(1)	23(1)	−6(1)	6(1)	−3(1)
C38	37(1)	29(1)	17(1)	−2(1)	4(1)	3(1)
O21	22(1)	52(1)	34(1)	−6(1)	3(1)	−3(1)

Table B.5. Hydrogen coordinates [× 10^4] and isotropic displacement parameters [Å^2 × 10^3] for **68**.

Atom	x	y	z	U_{eq}	$S.o.f.$
H1	5445	886	677	25	1
H3	5838	−55	1851	31	1
H4	7316	−883	2758	35	1
H5	9654	−858	2868	36	1
H6	10549	1	2097	30	1
H8	10158	970	948	26	1
H10	9603	1190	−873	29	1
H11	7971	1278	−2436	31	1
H12	5622	1301	−2548	34	1
H13	4908	1200	−1087	28	1
H15A	6293	2055	961	29	1
H15B	6025	1671	1896	29	1
H17A	10118	1746	2126	30	1
H17B	9241	2103	1121	30	1
H18A	7419	2681	2737	50	1
H18B	7988	2884	1810	50	1
H18C	9044	2688	2869	50	1
H1O	9230(30)	1424(15)	3390(20)	87(11)	1
H21	3383	115	3112	28	1
H23	3040	149	1285	26	1
H24	2525	759	−216	32	1
H25	2461	1923	−175	33	1
H26	2815	2481	1356	31	1
H28	3013	2443	3162	28	1
H30	1676	2364	4377	37	1
H31	504	1703	5271	44	1
H32	681	545	5249	46	1
H33	2003	28	4328	36	1
H35A	5414	320	4259	31	1
H35B	5654	671	3290	31	1
H37A	5441	2114	3363	32	1
H37B	5057	2354	4347	32	1
H38A	5841	917	5799	42	1
H38B	4348	1246	5359	42	1
H38C	5664	1712	5814	42	1
H21O	7300(30)	1419(14)	3920(20)	73(9)	1

Table B.6. Hydrogen bonds [Å and °] for **68**

$D-H\cdots A$	$d(D-H)$	$d(H\cdots A)$	$d(D\cdots A)$	$\angle(DHA)$
O21–H21O$\cdots$O1	1.06(3)	1.86(3)	2.887(2)	161(2)
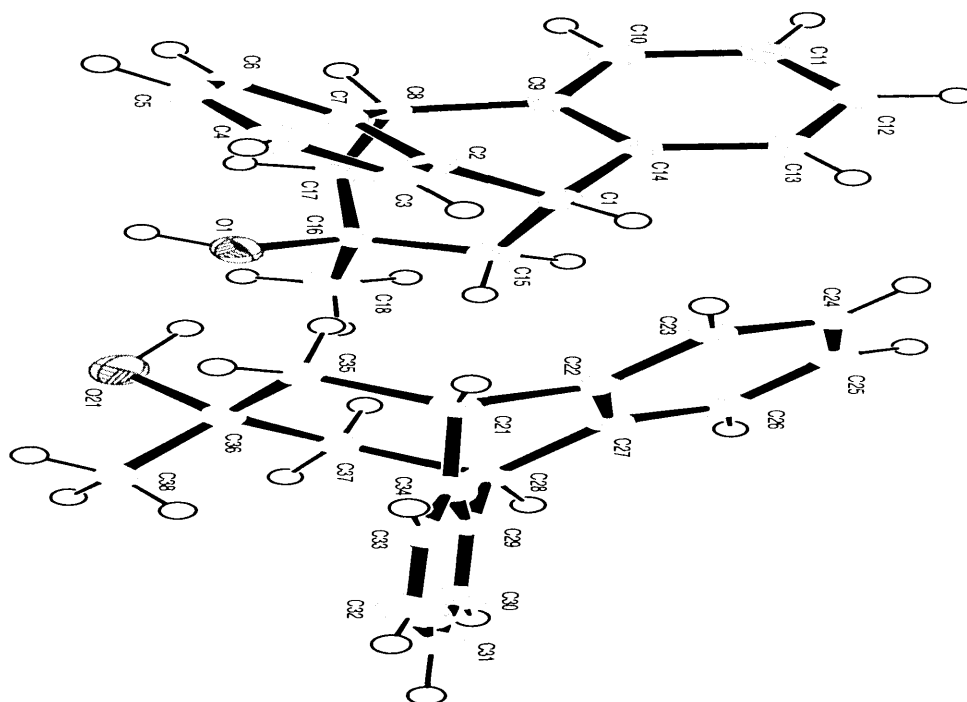
68

Scheme B.1

Appendix 9 Crystal structure and X-Ray data for **81**

Table C.1. Crystal data and structure refinement for **81**

Empirical formula	$C_{19}H_{15}O$
Formula weight	259.31
Temperature	120(2) K
Wavelength	0.71073 Å
Crystal system	Monoclinic
Space group	$C2/c$
Unit cell dimensions	$a = 17.668(4)$ Å $\qquad \alpha = 90°$
	$b = 7.3332(15)$ Å $\qquad \beta = 109.32(3)°$
	$c = 22.811(5)$ Å $\qquad \gamma = 90°$
Volume	2789.0(10) Å^3
Z	8
Density (calculated)	1.235 Mg / m^3
Absorption coefficient	0.075 mm-1
$F(000)$	1096
Crystal	Slab; colourless
Crystal size	$0.50 \times 0.50 \times 0.12$ mm^3
θ range for data collection	$3.36 - 27.50°$
Index ranges	$-22 \le h \le 22, -9 \le k \le 9, -29 \le l \le 29$
Reflections collected	14620
Independent reflections	3201 [$R_{int} = 0.0374$]
Completeness to $\theta = 27.50°$	99.5 %
Absorption correction	Semi−empirical from equivalents
Max. and min. transmission	0.9911 and 0.9636
Refinement method	Full-matrix least-squares on F^2
Data / restraints / parameters	3201 / 0 / 224
Goodness-of-fit on F^2	1.040
Final R indices [$F^2 > 2\sigma(F^2)$]	$R1 = 0.0609, wR2 = 0.1546$
R indices (all data)	$R1 = 0.0918, wR2 = 0.1786$
Extinction coefficient	0.0089(7)
Largest diff. peak and hole	0.416 and −0.252 e Å−3

Special details:
70:30 disorder about the bridgehead atom, omitted from figure for clarity. C7 = R, C11 = S for the pictured molecule, but centrosymmetric so the other enantiomer is generated in the crystal through the centre of symmetry

Table C.2. Atomic coordinates [× 10^4], equivalent isotropic displacement parameters [$Å^2$ × 10^3] and site occupancy factors. U_{eq} is defined as one third of the trace of the orthogonalized U^{ij} tensor.

Atom	x	y	z	U_{eq}	S.o.f.
C1	1030(1)	8011(1)	1582(1)	30(1)	1
C2	435(1)	8081(2)	1852(1)	34(1)	1
C3	−168(1)	9385(2)	1663(1)	42(1)	1
C4	−169(1)	10630(2)	1208(1)	42(1)	1
C5	430(1)	10582(2)	938(1)	37(1)	1
C6	1029(1)	9276(2)	1125(1)	31(1)	1
C7	1692(1)	6604(2)	1747(1)	33(1)	1
C8	1515(1)	5122(2)	1234(1)	49(1)	1
C10	1522(1)	7507(2)	382(1)	46(1)	1
C11	1695(1)	9113(2)	851(1)	35(1)	1
C9	1557(2)	5599(3)	639(1)	72(1)	0.631(6)
C12	1327(1)	4289(3)	132(1)	47(1)	0.682(5)
C13	912(1)	3312(3)	−280(1)	54(1)	0.698(2)
O1	2534(1)	5237(2)	740(1)	40(1)	0.7025(15)
C9'	1681(2)	5607(5)	609(1)	37(1)	0.369(6)
C12'	1300(5)	4227(9)	226(2)	95(2)	0.318(5)
C13'	1702(3)	3063(6)	−52(2)	49(1)	0.302(2)
O1'	516(2)	5770(5)	501(2)	65(1)	0.2975(15)
C14	2479(1)	7550(1)	1827(1)	33(1)	1
C15	3184(1)	7170(2)	2304(1)	39(1)	1
C16	3889(1)	8037(2)	2326(1)	44(1)	1
C17	3890(1)	9294(2)	1877(1)	45(1)	1
C18	3186(1)	9705(2)	1402(1)	41(1)	1
C19	2479(1)	8831(2)	1373(1)	35(1)	1

Table C.3. Bond lengths [Å] and angles [°] for **81**.

C1–C2	1.3832(16)	C1–C6	1.3945(15)
C1–C7	1.5117(15)	C2–C3	1.3891(16)
C2–H2	0.9500	C3–C4	1.3826(18)
C3–H3	0.9500	C4–C5	1.3879(18)
C4–H4	0.9500	C5–C6	1.3859(16)
C5–H5	0.9500	C6–C11	1.5098(16)
C7–C14	1.5093(15)	C7–C8	1.5525(16)
C7–H7	1.0000	C8–C9	1.426(3)
C8–C9'	1.587(4)	C8–H8A	0.9900
C8–H8B	0.9900	C10–C9'	1.481(4)
C10–C9	1.510(3)	C10–C11	1.5524(17)
C10–H10A	0.9900	C10–H10B	0.9900
C11–C19	1.5131(15)	C11–H11	1.0000
C9–C12	1.456(3)	C9–O1	1.685(4)
C12–C13	1.215(2)	O1–H1	0.8400
C9'–C12'	1.361(7)	C9'–O1'	1.994(5)
C12'–C13'	1.391(8)	O1'–H1'	0.8400
C14–C15	1.3853(15)	C14–C19	1.3983(15)
C15–C16	1.3838(17)	C15–H15	0.9500
C16–C17	1.3798(18)	C16–H16	0.9500
C17–C18	1.3840(16)	C17–H17	0.9500
C18–C19	1.3861(16)	C18–H18	0.9500

C2–C1–C6	119.60(10)	C2–C1–C7	123.63(9)
C6–C1–C7	116.76(10)	C1–C2–C3	120.34(10)
C1–C2–H2	119.8	C3–C2–H2	119.8
C4–C3–C2	119.83(11)	C4–C3–H3	120.1
C2–C3–H3	120.1	C3–C4–C5	120.30(11)
C3–C4–H4	119.9	C5–C4–H4	119.9
C6–C5–C4	119.78(11)	C6–C5–H5	120.1
C4–C5–H5	120.1	C5–C6–C1	120.15(11)
C5–C6–C11	123.19(10)	C1–C6–C11	116.65(9)
C14–C7–C1	108.79(9)	C14–C7–C8	111.14(10)
C1–C7–C8	110.04(8)	C14–C7–H7	108.9
C1–C7–H7	108.9	C8–C7–H7	108.9
C9–C8–C7	119.02(13)	C9–C8–C9'	7.3(2)
C7–C8–C9'	118.00(16)	C9–C8–H8A	107.7
C7–C8–H8A	107.6	C9'–C8–H8A	102.0
C9–C8–H8B	107.4	C7–C8–H8B	107.6
C9'–C8–H8B	113.9	H8A–C8–H8B	107.0
C9'–C10–C9	9.5(2)	C9'–C10–C11	120.07(15)
C9–C10–C11	117.48(12)	C9'–C10–H10A	113.7

C9–C10–H10A	107.7	C11–C10–H10A	107.9
C9'–C10–H10B	98.9	C9–C10–H10B	108.2
C11–C10–H10B	107.9	H10A–C10–H10B	107.2
C6–C11–C19	108.72(9)	C6–C11–C10	110.08(9)
C19–C11–C10	111.03(9)	C6–C11–H11	109.0
C19–C11–H11	109.0	C10–C11–H11	109.0
C8–C9–C12	120.4(2)	C8–C9–C10	126.0(2)
C12–C9–C10	109.71(17)	C8–C9–O1	101.84(17)
C12–C9–O1	90.4(2)	C10–C9–O1	96.2(2)
C13–C12–C9	160.4(3)	C12'–C9'–C10	118.6(3)
C12'–C9'–C8	102.1(4)	C10–C9'–C8	117.1(3)
C12'–C9'–O1'	72.2(4)	C10–C9'–O1'	80.3(2)
C8–C9'–O1'	68.56(19)	C9'–C12'–C13'	122.1(7)
C9'–O1'–H1'	109.4	C15–C14–C19	119.77(10)
C15–C14–C7	123.69(10)	C19–C14–C7	116.50(9)
C16–C15–C14	120.07(11)	C16–C15–H15	120.0
C14–C15–H15	120.0	C17–C16–C15	120.13(10)
C17–C16–H16	119.9	C15–C16–H16	119.9
C16–C17–C18	120.35(11)	C16–C17–H17	119.8
C18–C17–H17	119.8	C17–C18–C19	119.94(11)
C17–C18–H18	120.0	C19–C18–H18	120.0
C18–C19–C14	119.74(10)	C18–C19–C11	123.46(10)
C14–C19–C11	116.73(9)		

Table C.4. Anisotropic displacement parameters [$\text{Å}^2 \times 10^3$]. The anisotropic displacement factor exponent takes the form: $-2\pi^2[h^2 a^{*2} U^{11} + \cdots + 2\,h\,k\,a^*\,b^*\,U^{12}]$.

Atom	U^{11}	U^{22}	U^{33}	U^{23}	U^{13}	U^{12}
C1	37(1)	29(1)	27(1)	−6(1)	13(1)	−10(1)
C2	38(1)	40(1)	27(1)	−6(1)	14(1)	−13(1)
C3	34(1)	64(1)	29(1)	−7(1)	13(1)	−6(1)
C4	34(1)	55(1)	34(1)	−4(1)	7(1)	3(1)
C5	39(1)	41(1)	28(1)	0(1)	9(1)	−5(1)
C6	35(1)	31(1)	28(1)	−3(1)	12(1)	−8(1)
C7	49(1)	27(1)	31(1)	1(1)	23(1)	−5(1)
C8	86(1)	32(1)	45(1)	−6(1)	44(1)	−11(1)
C10	64(1)	46(1)	39(1)	2(1)	32(1)	−5(1)
C11	43(1)	30(1)	38(1)	7(1)	21(1)	−3(1)
C9	133(2)	35(1)	29(1)	−4(1)	1(1)	−11(1)
C12	82(1)	39(1)	37(1)	−12(1)	45(1)	−23(1)
C13	70(1)	59(1)	40(1)	−9(1)	28(1)	−16(1)
O1	41(1)	47(1)	35(1)	−1(1)	17(1)	3(1)
C9'	51(2)	45(2)	23(1)	2(1)	24(1)	−9(2)
C12'	213(5)	62(3)	35(2)	11(2)	77(2)	17(4)
C13'	65(2)	44(2)	45(2)	8(2)	28(2)	3(2)
O1'	31(1)	93(2)	65(2)	−32(2)	9(1)	−3(2)
C14	42(1)	25(1)	38(1)	2(1)	23(1)	2(1)
C15	49(1)	29(1)	43(1)	4(1)	23(1)	9(1)
C16	38(1)	43(1)	53(1)	−1(1)	16(1)	10(1)
C17	38(1)	40(1)	63(1)	−3(1)	25(1)	−2(1)
C18	43(1)	34(1)	55(1)	7(1)	27(1)	−1(1)
C19	40(1)	30(1)	42(1)	4(1)	22(1)	1(1)
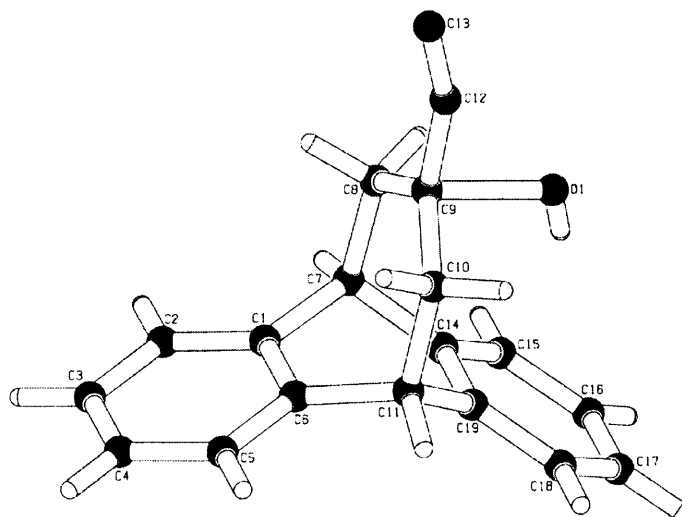
81

Scheme C.1

Appendix 10   Crystal structure and X-Ray data for **86**

Table D.1.   Crystal data and structure refinement for **86**

Chemical formula (moiety)	$C_{18}H_{16}O$
Chemical formula (total)	$C_{18}H_{16}O$
Formula weight	248.31
Temperature	120(2) K
Radiation, wavelength	synchrotron, 0.6751 Å
Crystal system, space group	monoclinic, $P2_1$
Unit cell parameters	a = 16.312(8) Å $\alpha = 90°$
	b = 7.247(3) Å $\beta = 90.243(7)°$
	c = 16.383(8) Å $\gamma = 90°$
Cell volume	1936.7(16) Å^3
Z	6
Calculated density	1.277 g/cm^3
Absorption coefficient μ	0.077 mm^{-1}
F(000)	792
Crystal colour and size	colourless, $0.20 \times 0.02 \times 0.02$ mm^3
Reflections for cell refinement	2391 (θ range 2.4 to 21.9°)
Data collection method	Bruker APEX2 CCD diffractometer thin-slice ω scans
θ range for data collection	2.4 to 20.8°
Index ranges	h −17 to 17, k −7 to 7, l −17 to 17
Completeness to $\theta = 20.8°$	99.2 %
Reflections collected	10797
Independent reflections	2577 ($R_{int} = 0.0736$)
Reflections with $F^2 > 2\sigma$	2262
Absorption correction	none
Structure solution	direct methods
Refinement method	Full-matrix least-squares on F^2
Weighting parameters a, b	0.1225, 1.4485
Data / restraints / parameters	2577 / 1 / 516
Final R indices [$F^2 > 2\sigma$]	R1 = 0.0678, wR2 = 0.1699
R indices (all data)	R1 = 0.0791, wR2 = 0.1837
Goodness-of-fit on F^2	1.054
Absolute structure parameter	0
Extinction coefficient	0.128(17)
Largest and mean shift/su	0.001 and 0.000
Largest diff. peak and hole	0.26 and −0.26 e Å^{-3}

Table D.2. Atomic coordinates and equivalent isotropic displacement parameters ($\mathring{A}^2$) for **86**. U_{eq} is defined as one third of the trace of the orthogonalized U^{ij} tensor.

	x	y	z	U_{eq}
O(1)	0.2663(6)	0.9843(11)	–0.1115(5)	0.049(2)
C(101)	0.2824(8)	0.7097(18)	0.0902(7)	0.048(3)
C(102)	0.2962(9)	0.8689(16)	0.0273(7)	0.050(3)
C(103)	0.2601(8)	0.8270(15)	–0.0566(7)	0.038(3)
C(104)	0.2789(8)	0.6450(16)	–0.0957(7)	0.044(3)
C(105)	0.2658(7)	0.4739(16)	–0.0412(7)	0.039(3)
C(106)	0.1871(8)	0.9277(19)	–0.0818(7)	0.052(3)
C(107)	0.3501(7)	0.5659(16)	0.0783(7)	0.037(3)
C(108)	0.4177(8)	0.5545(16)	0.1283(6)	0.041(3)
C(109)	0.4786(8)	0.4231(19)	0.1130(7)	0.048(3)
C(110)	0.4690(8)	0.3007(18)	0.0490(7)	0.049(3)
C(111)	0.4019(8)	0.3104(17)	–0.0005(7)	0.043(3)
C(112)	0.3387(7)	0.4424(16)	0.0128(7)	0.039(3)
C(113)	0.1979(8)	0.6242(17)	0.0756(7)	0.042(3)
C(114)	0.1308(8)	0.6622(19)	0.1232(7)	0.048(4)
C(115)	0.0551(9)	0.5853(17)	0.1065(8)	0.054(4)
C(116)	0.0469(9)	0.466(2)	0.0425(8)	0.053(4)
C(117)	0.1138(7)	0.4263(16)	–0.0050(7)	0.042(3)
C(118)	0.1891(8)	0.5023(16)	0.0107(7)	0.046(3)
O(2)	0.2015(5)	0.9311(11)	0.6209(5)	0.044(2)
C(201)	0.4142(8)	0.7102(15)	0.5802(7)	0.040(3)
C(202)	0.3452(7)	0.8655(14)	0.5844(7)	0.035(3)
C(203)	0.2624(7)	0.7889(15)	0.6068(7)	0.039(3)
C(204)	0.2265(8)	0.6229(16)	0.5592(7)	0.041(3)
C(205)	0.2902(7)	0.4606(15)	0.5543(7)	0.037(3)
C(206)	0.2306(7)	0.8205(19)	0.6899(7)	0.044(3)
C(207)	0.4118(7)	0.6206(16)	0.4965(7)	0.037(3)
C(208)	0.4638(7)	0.6679(17)	0.4364(7)	0.041(3)
C(209)	0.4558(7)	0.5841(16)	0.3591(7)	0.041(3)
C(210)	0.3930(7)	0.4576(17)	0.3475(7)	0.040(3)
C(211)	0.3399(7)	0.4092(17)	0.4071(7)	0.039(3)
C(212)	0.3469(8)	0.4927(15)	0.4836(7)	0.043(3)
C(213)	0.4004(7)	0.5707(17)	0.6462(7)	0.038(3)
C(214)	0.4451(7)	0.5692(18)	0.7174(7)	0.039(3)
C(215)	0.4284(7)	0.4336(18)	0.7754(7)	0.043(3)
C(216)	0.3656(7)	0.3069(18)	0.7627(7)	0.044(3)
C(217)	0.3205(7)	0.3101(16)	0.6905(7)	0.037(3)
C(218)	0.3373(7)	0.4393(16)	0.6319(7)	0.042(3)
O(3)	0.0551(5)	0.4208(12)	0.4558(5)	0.046(2)
C(301)	0.1272(7)	–0.0497(16)	0.3717(7)	0.042(3)
C(302)	0.1207(8)	0.1159(15)	0.4318(8)	0.042(3)

C(303)	0.0731(7)	0.2756(15)	0.3973(7)	0.037(3)
C(304)	0.0961(9)	0.3500(18)	0.3144(7)	0.048(3)
C(305)	0.1032(8)	0.1977(17)	0.2476(8)	0.046(3)
C(306)	−0.0109(8)	0.3032(19)	0.4265(9)	0.053(3)
C(307)	0.1989(7)	−0.0145(15)	0.3152(6)	0.036(3)
C(308)	0.2767(8)	−0.0909(16)	0.3271(7)	0.040(3)
C(309)	0.3423(7)	−0.0433(18)	0.2772(7)	0.043(3)
C(310)	0.3305(8)	0.0818(19)	0.2147(7)	0.047(3)
C(311)	0.2517(8)	0.1604(17)	0.2034(7)	0.043(3)
C(312)	0.1879(8)	0.1125(16)	0.2532(7)	0.039(3)
C(313)	0.0483(7)	−0.0682(16)	0.3239(7)	0.041(3)
C(314)	−0.0108(7)	−0.2032(16)	0.3410(7)	0.042(3)
C(315)	−0.0831(8)	−0.2138(19)	0.2949(7)	0.047(3)
C(316)	−0.0950(8)	−0.0867(18)	0.2318(8)	0.052(3)
C(317)	−0.0350(8)	0.0427(16)	0.2151(8)	0.046(3)
C(318)	0.0367(7)	0.0536(18)	0.2590(7)	0.044(3)

Table D.3. Bond lengths [Å] and angles [°] for **86**.

O(1)–C(103)	1.456(13)	O(1)–C(106)	1.442(15)
C(101)–H(101)	1.000	C(101)–C(102)	1.565(17)
C(101)–C(107)	1.531(17)	C(101)–C(113)	1.529(18)
C(102)–H(10A)	0.990	C(102)–H(10B)	0.990
C(102)–C(103)	1.524(16)	C(103)–C(104)	1.498(17)
C(103)–C(106)	1.455(17)	C(104)–H(10C)	0.990
C(104)–H(10D)	0.990	C(104)–C(105)	1.544(17)
C(105)–H(105)	1.000	C(105)–C(112)	1.496(16)
C(105)–C(118)	1.530(18)	C(106)–H(10E)	0.990
C(106)–H(10F)	0.990	C(107)–C(108)	1.374(16)
C(107)–C(112)	1.408(16)	C(108)–H(108)	0.950
C(108)–C(109)	1.399(18)	C(109)–H(109)	0.950
C(109)–C(110)	1.381(18)	C(110)–H(110)	0.950
C(110)–C(111)	1.361(16)	C(111)–H(111)	0.950
C(111)–C(112)	1.425(17)	C(113)–C(114)	1.376(18)
C(113)–C(118)	1.389(16)	C(114)–H(114)	0.950
C(114)–C(115)	1.381(18)	C(115)–H(115)	0.950
C(115)–C(116)	1.366(18)	C(116)–H(116)	0.950
C(116)–C(117)	1.373(17)	C(117)–H(117)	0.950
C(117)–C(118)	1.369(16)	O(2)–C(203)	1.451(13)
O(2)–C(206)	1.463(14)	C(201)–H(201)	1.000
C(201)–C(202)	1.593(16)	C(201)–C(207)	1.517(16)
C(201)–C(213)	1.499(16)	C(202)–H(20A)	0.990
C(202)–H(20B)	0.990	C(202)–C(203)	1.507(16)
C(203)–C(204)	1.547(16)	C(203)–C(206)	1.478(16)
C(204)–H(20C)	0.990	C(204)–H(20D)	0.990
C(204)–C(205)	1.571(16)	C(205)–H(205)	1.000
C(205)–C(212)	1.504(17)	C(205)–C(218)	1.491(16)
C(206)–H(20E)	0.990	C(206)–H(20F)	0.990
C(207)–C(208)	1.346(17)	C(207)–C(212)	1.422(17)
C(208)–H(208)	0.950	C(208)–C(209)	1.409(16)
C(209)–H(209)	0.950	C(209)–C(210)	1.386(17)
C(210)–H(210)	0.950	C(210)–C(211)	1.355(17)
C(211)–H(211)	0.950	C(211)–C(212)	1.395(16)
C(213)–C(214)	1.373(16)	C(213)–C(218)	1.421(16)
C(214)–H(214)	0.950	C(214)–C(215)	1.395(17)
C(215)–H(215)	0.950	C(215)–C(216)	1.391(17)
C(216)–H(216)	0.950	C(216)–C(217)	1.391(15)
C(217)–H(217)	0.950	C(217)–C(218)	1.369(16)
O(3)–C(303)	1.455(14)	O(3)–C(306)	1.453(15)
C(301)–H(301)	1.000	C(301)–C(302)	1.556(16)
C(301)–C(307)	1.517(17)	C(301)–C(313)	1.509(17)
C(302)–H(30A)	0.990	C(302)–H(30B)	0.990
C(302)–C(303)	1.503(16)	C(303)–C(304)	1.510(16)

C(303)–C(306)	1.466(18)		C(304)–H(30C)	0.990
C(304)–H(30D)	0.990		C(304)–C(305)	1.559(18)
C(305)–H(305)	1.000		C(305)–C(312)	1.515(18)
C(305)–C(318)	1.517(18)		C(306)–H(30E)	0.990
C(306)–H(30F)	0.990		C(307)–C(308)	1.397(16)
C(307)–C(312)	1.381(16)		C(308)–H(308)	0.950
C(308)–C(309)	1.392(17)		C(309)–H(309)	0.950
C(309)–C(310)	1.381(17)		C(310)–H(310)	0.950
C(310)–C(311)	1.417(17)		C(311)–H(311)	0.950
C(311)–C(312)	1.371(18)		C(313)–C(314)	1.402(17)
C(313)–C(318)	1.395(17)		C(314)–H(314)	0.950
C(314)–C(315)	1.399(16)		C(315)–H(315)	0.950
C(315)–C(316)	1.398(17)		C(316)–H(316)	0.950
C(316)–C(317)	1.384(17)		C(317)–H(317)	0.950
C(317)–C(318)	1.372(18)			

C(103)–O(1)–C(106)	60.3(8)		H(101)–C(101)–C(102)	109.6
H(101)–C(101)–C(107)	109.6		H(101)–C(101)–C(113)	109.6
C(102)–C(101)–C(107)	108.2(10)		C(102)–C(101)–C(113)	109.1(10)
C(107)–C(101)–C(113)	110.8(10)		C(101)–C(102)–H(10A)	109.0
C(101)–C(102)–H(10B)	109.0		C(101)–C(102)–C(103)	113.0(10)
H(10A)–C(102)–H(10B)	107.8		H(10A)–C(102)–C(103)	109.0
H(10B)–C(102)–C(103)	109.0		O(1)–C(103)–C(102)	111.9(9)
O(1)–C(103)–C(104)	114.2(9)		O(1)–C(103)–C(106)	59.4(7)
C(102)–C(103)–C(104)	118.8(10)		C(102)–C(103)–C(106)	117.9(11)
C(104)–C(103)–C(106)	119.3(10)		C(103)–C(104)–H(10C)	108.4
C(103)–C(104)–H(10D)	108.4		C(103)–C(104)–C(105)	115.5(9)
H(10C)–C(104)–H(10D)	107.5		H(10C)–C(104)–C(105)	108.4
H(10D)–C(104)–C(105)	108.4		C(104)–C(105)–H(105)	109.0
C(104)–C(105)–C(112)	110.7(10)		C(104)–C(105)–C(118)	109.2(10)
H(105)–C(105)–C(112)	109.0		H(105)–C(105)–C(118)	109.0
C(112)–C(105)–C(118)	110.0(9)		O(1)–C(106)–C(103)	60.3(8)
O(1)–C(106)–H(10E)	117.7		O(1)–C(106)–H(10F)	117.7
C(103)–C(106)–H(10E)	117.7		C(103)–C(106)–H(10F)	117.7
H(10E)–C(106)–H(10F)	114.9		C(101)–C(107)–C(108)	122.9(10)
C(101)–C(107)–C(112)	115.9(10)		C(108)–C(107)–C(112)	121.3(11)
C(107)–C(108)–H(108)	119.9		C(107)–C(108)–C(109)	120.2(10)
H(108)–C(108)–C(109)	119.9		C(108)–C(109)–H(109)	120.2
C(108)–C(109)–C(110)	119.7(11)		H(109)–C(109)–C(110)	120.2
C(109)–C(110)–H(110)	119.8		C(109)–C(110)–C(111)	120.5(13)
H(110)–C(110)–C(111)	119.8		C(110)–C(111)–H(111)	119.2
C(110)–C(111)–C(112)	121.6(12)		H(111)–C(111)–C(112)	119.2
C(105)–C(112)–C(107)	117.1(11)		C(105)–C(112)–C(111)	125.9(10)
C(107)–C(112)–C(111)	116.7(10)		C(101)–C(113)–C(114)	123.3(11)
C(101)–C(113)–C(118)	117.9(11)		C(114)–C(113)–C(118)	118.7(12)
C(113)–C(114)–H(114)	119.3		C(113)–C(114)–C(115)	121.3(12)

H(114)–C(114)–C(115)	119.3	C(114)–C(115)–H(115)	120.2
C(114)–C(115)–C(116)	119.5(13)	H(115)–C(115)–C(116)	120.2
C(115)–C(116)–H(116)	120.3	C(115)–C(116)–C(117)	119.4(13)
H(116)–C(116)–C(117)	120.3	C(116)–C(117)–H(117)	119.2
C(116)–C(117)–C(118)	121.6(11)	H(117)–C(117)–C(118)	119.2
C(105)–C(118)–C(113)	115.3(11)	C(105)–C(118)–C(117)	125.3(10)
C(113)–C(118)–C(117)	119.3(12)	C(203)–O(2)–C(206)	61.0(7)
H(201)–C(201)–C(202)	109.0	H(201)–C(201)–C(207)	109.0
H(201)–C(201)–C(213)	109.0	C(202)–C(201)–C(207)	109.09(9)
C(202)–C(201)–C(213)	109.7(10)	C(207)–C(201)–C(213)	111.19(9)
C(201)–C(202)–H(20A)	109.1	C(201)–C(202)–H(20B)	109.1
C(201)–C(202)–C(203)	112.6(9)	H(20A)–C(202)–H(20B)	107.8
H(20A)–C(202)–C(203)	109.1	H(20B)–C(202)–C(203)	109.1
O(2)–C(203)–C(202)	113.1(9)	O(2)–C(203)–C(204)	112.0(9)
O(2)–C(203)–C(206)	59.9(7)	C(202)–C(203)–C(204)	120.1(10)
C(202)–C(203)–C(206)	119.1(10)	C(204)–C(203)–C(206)	116.8(11)
C(203)–C(204)–H(20C)	109.4	C(203)–C(204)–H(20D)	109.4
C(203)–C(204)–C(205)	111.1(9)	H(20C)–C(204)–H(20D)	108.0
H(20C)–C(204)–C(205)	109.4	H(20D)–C(204)–C(205)	109.4
C(204)–C(205)–H(205)	108.2	C(204)–C(205)–C(212)	109.4(9)
C(204)–C(205)–C(218)	111.8(9)	H(205)–C(205)–C(212)	108.2
H(205)–C(205)–C(218)	108.2	C(212)–C(205)–C(218)	110.9(10)
O(2)–C(206)–C(203)	59.1(7)	O(2)–C(206)–H(20E)	117.9
O(2)–C(206)–H(20F)	117.9	C(203)–C(206)–H(20E)	117.9
C(203)–C(206)–H(20F)	117.9	H(20E)–C(206)–H(20F)	115.0
C(201)–C(207)–C(208)	122.5(11)	C(201)–C(207)–C(212)	115.5(11)
C(208)–C(207)–C(212)	121.8(11)	C(207)–C(208)–H(208)	120.3
C(207)–C(208)–C(209)	119.4(12)	H(208)–C(208)–C(209)	120.3
C(208)–C(209)–H(209)	120.9	C(208)–C(209)–C(210)	118.3(11)
H(209)–C(209)–C(210)	120.9	C(209)–C(210)–H(210)	118.4
C(209)–C(210)–C(211)	123.1(10)	H(210)–C(210)–C(211)	118.4
C(210)–C(211)–H(211)	120.5	C(210)–C(211)–C(212)	118.9(11)
H(211)–C(211)–C(212)	120.5	C(205)–C(212)–C(207)	116.5(10)
C(205)–C(212)–C(211)	125.1(11)	C(207)–C(212)–C(211)	118.4(11)
C(201)–C(213)–C(214)	122.5(11)	C(201)–C(213)–C(218)	116.4(10)
C(214)–C(213)–C(218)	121.1(11)	C(213)–C(214)–H(214)	120.7
C(213)–C(214)–C(215)	118.7(11)	H(214)–C(214)–C(215)	120.7
C(214)–C(215)–H(215)	119.7	C(214)–C(215)–C(216)	120.6(10)
H(215)–C(215)–C(216)	119.7	C(215)–C(216)–H(216)	119.9
C(215)–C(216)–C(217)	120.2(12)	H(216)–C(216)–C(217)	119.9
C(216)–C(217)–H(217)	120.0	C(216)–C(217)–C(218)	120.0(11)
H(217)–C(217)–C(218)	120.0	C(205)–C(218)–C(213)	116.2(10)
C(205)–C(218)–C(217)	124.3(10)	C(213)–C(218)–C(217)	119.3(10)
C(303)–O(3)–C(306)	60.6(8)	H(301)–C(301)–C(302)	109.4
H(301)–C(301)–C(307)	109.4	H(301)–C(301)–C(313)	109.4
C(302)–C(301)–C(307)	108.2(9)	C(302)–C(301)–C(313)	109.6(10)

Angle	Value	Angle	Value
C(307)—C(301)—C(313)	110.9(9)	C(301)—C(302)—H(30A)	109.0
C(301)—C(302)—H(30B)	109.0	C(301)—C(302)—C(303)	113.1(9)
H(30A)—C(302)—H(30B)	107.8	H(30A)—C(302)—C(303)	109.0
H(30B)—C(302)—C(303)	109.0	O(3)—C(303)—C(302)	114.5(9)
O(3)—C(303)—C(304)	112.7(9)	O(3)—C(303)—C(306)	59.7(7)
C(302)—C(303)—C(304)	118.9(11)	C(302)—C(303)—C(306)	117.6(11)
C(304)—C(303)—C(306)	118.8(11)	C(303)—C(304)—H(30C)	108.9
C(303)—C(304)—H(30D)	108.9	C(303)—C(304)—C(305)	113.4(10)
H(30C)—C(304)—H(30D)	107.7	H(30C)—C(304)—C(305)	108.9
H(30D)—C(304)—C(305)	108.9	C(304)—C(305)—H(305)	108.9
C(304)—C(305)—C(312)	108.4(10)	C(304)—C(305)—C(318)	110.2(10)
H(305)—C(305)—C(312)	108.9	H(305)—C(305)—C(318)	108.9
C(312)—C(305)—C(318)	111.3(10)	O(3)—C(306)—C(303)	59.8(8)
O(3)—C(306)—H(30E)	117.8	O(3)—C(306)—H(30F)	117.8
C(303)—C(306)—H(30E)	117.8	C(303)—C(306)—H(30F)	117.8
H(30E)—C(306)—H(30F)	114.9	C(301)—C(307)—C(308)	123.4(10)
C(301)—C(307)—C(312)	117.5(11)	C(308)—C(307)—C(312)	118.8(11)
C(307)—C(308)—H(308)	119.4	C(307)—C(308)—C(309)	121.3(10)
H(308)—C(308)—C(309)	119.4	C(308)—C(309)—H(309)	120.2
C(308)—C(309)—C(310)	119.6(11)	H(309)—C(309)—C(310)	120.2
C(309)—C(310)—H(310)	120.5	C(309)—C(310)—C(311)	118.9(12)
H(310)—C(310)—C(311)	120.5	C(310)—C(311)—H(311)	119.6
C(310)—C(311)—C(312)	120.8(11)	H(311)—C(311)—C(312)	119.6
C(305)—C(312)—C(307)	115.6(12)	C(305)—C(312)—C(311)	123.7(11)
C(307)—C(312)—C(311)	120.6(12)	C(301)—C(313)—C(314)	123.0(10)
C(301)—C(313)—C(318)	116.8(11)	C(314)—C(313)—C(318)	120.2(11)
C(313)—C(314)—H(314)	119.7	C(313)—C(314)—C(315)	120.6(12)
H(314)—C(314)—C(315)	119.7	C(314)—C(315)—H(315)	120.8
C(314)—C(315)—C(316)	118.5(13)	H(315)—C(315)—C(316)	120.8
C(315)—C(316)—H(316)	120.1	C(315)—C(316)—C(317)	119.8(11)
H(316)—C(316)—C(317)	120.1	C(316)—C(317)—H(317)	118.7
C(316)—C(317)—C(318)	122.5(11)	H(317)—C(317)—C(318)	118.7
C(305)—C(318)—C(313)	115.8(10)	C(305)—C(318)—C(317)	125.7(11)
C(313)—C(318)—C(317)	118.4(12)		

Table D.4.   Anisotropic displacement parameters (Å^2) for **86**.   The anisotropic displacement factor exponent takes the form: $-2\pi^2[h^2a^{*2}U^{11} + ...+ 2hka^*b^*U^{12}]$

	U^{11}	U^{22}	U^{33}	U^{23}	U^{13}	U^{12}
O(1)	0.079(6)	0.019(4)	0.049(5)	0.001(4)	0.008(4)	−0.007(4)
C(101)	0.075(9)	0.030(7)	0.037(7)	0.000(6)	0.002(6)	−0.003(7)
C(102)	0.079(10)	0.016(6)	0.054(8)	−0.005(6)	−0.002(7)	−0.010(6)
C(103)	0.063(8)	0.012(6)	0.039(6)	0.012(6)	−0.010(5)	−0.001(6)
C(104)	0.061(8)	0.029(6)	0.041(7)	−0.009(6)	−0.007(6)	0.000(6)
C(105)	0.062(8)	0.020(6)	0.035(6)	−0.003(5)	0.006(6)	−0.004(6)
C(106)	0.066(9)	0.042(8)	0.047(7)	0.006(7)	0.003(6)	−0.007(8)
C(107)	0.050(7)	0.020(6)	0.042(7)	−0.003(6)	−0.010(6)	−0.008(6)
C(108)	0.072(8)	0.020(7)	0.030(6)	−0.004(5)	0.000(6)	−0.015(7)
C(109)	0.060(8)	0.043(8)	0.041(7)	0.004(7)	−0.012(6)	−0.013(8)
C(110)	0.062(8)	0.030(7)	0.055(8)	0.012(7)	−0.013(6)	−0.012(7)
C(111)	0.065(8)	0.025(6)	0.040(7)	0.001(6)	0.002(6)	0.003(7)
C(112)	0.062(8)	0.015(6)	0.041(6)	0.000(6)	0.006(5)	−0.013(6)
C(113)	0.053(8)	0.024(7)	0.049(7)	0.010(6)	0.000(6)	−0.004(6)
C(114)	0.076(10)	0.023(7)	0.044(7)	0.003(6)	−0.021(7)	0.013(7)
C(115)	0.085(11)	0.025(8)	0.054(8)	0.016(7)	0.007(7)	0.015(8)
C(116)	0.068(9)	0.030(8)	0.060(8)	−0.001(7)	−0.003(7)	−0.008(7)
C(117)	0.062(8)	0.024(7)	0.040(6)	−0.013(6)	−0.006(6)	−0.005(7)
C(118)	0.079(9)	0.020(6)	0.040(7)	−0.009(6)	−0.023(6)	0.006(7)
O(2)	0.058(5)	0.022(4)	0.052(5)	−0.008(4)	−0.011(4)	0.008(4)
C(201)	0.051(7)	0.020(6)	0.050(7)	0.003(6)	−0.019(6)	−0.004(6)
C(202)	0.049(7)	0.009(5)	0.047(7)	0.002(5)	−0.007(6)	0.000(5)
C(203)	0.055(7)	0.017(6)	0.046(7)	0.000(6)	0.001(6)	0.001(6)
C(204)	0.059(8)	0.024(7)	0.039(7)	−0.006(6)	−0.006(5)	0.002(6)
C(205)	0.047(7)	0.011(5)	0.053(7)	−0.007(6)	−0.015(5)	0.000(5)
C(206)	0.054(7)	0.037(7)	0.041(7)	−0.002(6)	−0.009(6)	0.006(7)
C(207)	0.050(7)	0.022(6)	0.040(7)	−0.005(5)	−0.005(6)	0.001(6)
C(208)	0.049(7)	0.024(6)	0.049(7)	0.007(6)	−0.014(6)	0.001(6)
C(209)	0.059(8)	0.026(7)	0.036(6)	−0.002(6)	−0.012(5)	0.009(6)
C(210)	0.060(7)	0.023(7)	0.038(6)	−0.014(6)	−0.020(6)	0.008(6)
C(211)	0.051(7)	0.029(7)	0.038(6)	−0.009(6)	−0.001(6)	0.003(7)
C(212)	0.061(8)	0.014(6)	0.053(7)	−0.003(6)	−0.007(6)	0.008(6)
C(213)	0.046(7)	0.028(6)	0.042(7)	0.001(6)	0.004(6)	0.001(6)
C(214)	0.040(7)	0.034(7)	0.042(7)	−0.007(6)	−0.016(5)	0.007(6)
C(215)	0.051(7)	0.030(7)	0.047(7)	−0.001(6)	−0.015(5)	0.007(7)
C(216)	0.051(7)	0.031(7)	0.049(7)	0.005(6)	−0.003(6)	0.008(7)
C(217)	0.050(7)	0.020(6)	0.043(6)	−0.007(6)	−0.008(5)	0.000(6)
C(218)	0.056(7)	0.020(6)	0.050(7)	−0.008(6)	−0.006(6)	−0.001(6)
O(3)	0.063(5)	0.032(5)	0.044(4)	−0.006(4)	−0.009(4)	−0.003(5)

C(301)	0.067(8)	0.022(6)	0.038(6)	0.000(6)	−0.010(6)	−0.006(7)
C(302)	0.050(7)	0.019(7)	0.057(7)	0.000(6)	−0.007(6)	−0.004(6)
C(303)	0.059(8)	0.014(6)	0.037(6)	−0.004(5)	0.005(5)	−0.001(6)
C(304)	0.067(8)	0.023(6)	0.053(8)	0.007(6)	−0.002(6)	−0.001(6)
C(305)	0.073(9)	0.023(7)	0.043(7)	0.003(6)	−0.002(6)	0.000(6)
C(306)	0.068(9)	0.027(7)	0.064(8)	−0.010(7)	−0.007(7)	0.006(7)
C(307)	0.054(7)	0.014(5)	0.039(6)	0.003(5)	−0.020(5)	0.009(6)
C(308)	0.073(9)	0.013(6)	0.033(6)	−0.006(5)	−0.021(6)	0.007(7)
C(309)	0.050(7)	0.031(7)	0.048(7)	0.001(6)	−0.010(6)	0.000(6)
C(310)	0.063(8)	0.031(7)	0.047(7)	−0.006(7)	−0.011(6)	0.003(7)
C(311)	0.070(9)	0.021(6)	0.038(7)	0.000(6)	−0.007(6)	−0.007(7)
C(312)	0.064(8)	0.019(7)	0.035(6)	−0.011(6)	−0.013(6)	0.004(6)
C(313)	0.072(8)	0.016(6)	0.035(6)	0.005(6)	0.006(5)	0.007(7)
C(314)	0.061(8)	0.021(7)	0.044(7)	−0.009(6)	−0.007(6)	0.006(7)
C(315)	0.067(8)	0.029(7)	0.045(7)	0.000(6)	−0.010(6)	0.006(7)
C(316)	0.056(8)	0.044(8)	0.055(8)	−0.010(7)	−0.018(6)	0.012(8)
C(317)	0.059(8)	0.028(7)	0.051(7)	0.007(6)	−0.013(6)	0.007(7)
C(318)	0.054(8)	0.034(7)	0.045(7)	−0.010(6)	−0.005(6)	0.004(6)

Table D.5. Hydrogen coordinates and isotropic displacement parameters ($\mathring{A}^2$) for **86**.

	x	y	z	U
H(101)	0.2855	0.7603	0.1469	0.057
H(10A)	0.2710	0.9834	0.0485	0.060
H(10B)	0.3558	0.8913	0.0217	0.060
H(10C)	0.3367	0.6464	−0.1138	0.053
H(10D)	0.2441	0.6319	−0.1451	0.053
H(105)	0.2577	0.3632	−0.0767	0.047
H(10E)	0.1493	0.8668	−0.1208	0.062
H(10F)	0.1601	1.0072	−0.0408	0.062
H(108)	0.4232	0.6360	0.1734	0.049
H(109)	0.5263	0.4180	0.1464	0.058
H(110)	0.5095	0.2091	0.0395	0.059
H(111)	0.3972	0.2270	−0.0451	0.052
H(114)	0.1366	0.7429	0.1686	0.057
H(115)	0.0091	0.6153	0.1393	0.065
H(116)	−0.0047	0.4104	0.0310	0.063
H(117)	0.1077	0.3442	−0.0498	0.050
H(201)	0.4691	0.7690	0.5885	0.048
H(20A)	0.3615	0.9593	0.6253	0.042
H(20B)	0.3412	0.9275	0.5307	0.042
H(20C)	0.2113	0.6625	0.5034	0.049
H(20D)	0.1762	0.5791	0.5868	0.049
H(205)	0.2594	0.3435	0.5440	0.045
H(20E)	0.1928	0.7273	0.7129	0.053
H(20F)	0.2673	0.8804	0.7302	0.053
H(208)	0.5054	0.7570	0.4459	0.049
H(209)	0.4924	0.6135	0.3161	0.049
H(210)	0.3870	0.4023	0.2953	0.048
H(211)	0.2984	0.3198	0.3971	0.047
H(214)	0.4866	0.6587	0.7269	0.046
H(215)	0.4602	0.4278	0.8241	0.051
H(216)	0.3534	0.2180	0.8035	0.052
H(217)	0.2780	0.2225	0.6817	0.045
H(301)	0.1373	−0.1656	0.4033	0.051
H(30A)	0.0938	0.0736	0.4825	0.050
H(30B)	0.1766	0.1583	0.4462	0.050
H(30C)	0.1492	0.4153	0.3189	0.057
H(30D)	0.0543	0.4411	0.2970	0.057
H(305)	0.0964	0.2559	0.1926	0.056
H(30E)	−0.0512	0.3576	0.3881	0.064
H(30F)	−0.0336	0.2107	0.4647	0.064
H(308)	0.2850	−0.1771	0.3700	0.048
H(309)	0.3948	−0.0966	0.2861	0.051

H(310)	0.3745	0.1147	0.1798	0.056
H(311)	0.2431	0.2473	0.1608	0.052
H(314)	−0.0017	−0.2882	0.3842	0.050
H(315)	−0.1232	−0.3052	0.3063	0.056
H(316)	−0.1441	−0.0892	0.2005	0.062
H(317)	−0.0437	0.1272	0.1716	0.056

Table D.6. Torsion angles [°] for **86**.

C(107)–C(101)–C(102)–C(103)	83.6(13)	C(113)–C(101)–C(102)–C(103)	-37.0(14)
C(106)–O(1)–C(103)–C(102)	-110.4(12)	C(106)–O(1)–C(103)–C(104)	110.9(11)
C(101)–C(102)–C(103)–O(1)	174.1(11)	C(101)–C(102)–C(103)–C(104)	-49.3(16)
C(101)–C(102)–C(103)–C(106)	108.2(13)	O(1)–C(103)–C(104)–C(105)	-175.1(11)
C(102)–C(103)–C(104)–C(105)	49.3(15)	C(106)–C(103)–C(104)–C(105)	-107.9(13)
C(103)–C(104)–C(105)–C(112)	-82.7(13)	C(103)–C(104)–C(105)–C(118)	38.5(14)
C(102)–C(103)–C(106)–O(1)	100.2(11)	C(104)–C(103)–C(106)–O(1)	-102.4(11)
C(102)–C(101)–C(107)–C(108)	100.9(13)	C(102)–C(101)–C(107)–C(112)	-79.9(13)
C(113)–C(101)–C(107)–C(108)	-139.5(11)	C(113)–C(101)–C(107)–C(112)	39.7(14)
C(101)–C(107)–C(108)–C(109)	-178.3(11)	C(112)–C(107)–C(108)–C(109)	2.5(18)
C(107)–C(108)–C(109)–C(110)	-2.2(17)	C(108)–C(109)–C(110)–C(111)	1.8(18)
C(109)–C(110)–C(111)–C(112)	-1.6(18)	C(101)–C(107)–C(112)–C(105)	4.5(15)
C(101)–C(107)–C(112)–C(111)	178.5(10)	C(108)–C(107)–C(112)–C(105)	-176.3(10)
C(108)–C(107)–C(112)–C(111)	-2.2(17)	C(110)–C(111)–C(112)–C(105)	175.2(11)
C(110)–C(111)–C(112)–C(107)	1.8(17)	C(104)–C(105)–C(112)–C(107)	72.7(13)
C(104)–C(105)–C(112)–C(111)	-100.8(13)	C(118)–C(105)–C(112)–C(107)	-48.1(13)
C(118)–C(105)–C(112)–C(111)	138.4(11)	C(102)–C(101)–C(113)–C(114)	-102.0(14)
C(102)–C(101)–C(113)–C(118)	78.0(13)	C(107)–C(101)–C(113)–C(114)	139.0(12)
C(107)–C(101)–C(113)–C(118)	-41.0(14)	C(101)–C(113)–C(114)–C(115)	178.4(11)
C(118)–C(113)–C(114)–C(115)	-1.6(18)	C(113)–C(114)–C(115)–C(116)	1.5(18)
C(114)–C(115)–C(116)–C(117)	-1.0(18)	C(115)–C(116)–C(117)–C(118)	0.7(19)
C(116)–C(117)–C(118)–C(105)	-176.8(12)	C(116)–C(117)–C(118)–C(113)	-0.8(18)
C(101)–C(113)–C(118)–C(105)	-2.3(15)	C(101)–C(113)–C(118)–C(117)	-178.7(11)
C(114)–C(113)–C(118)–C(105)	177.6(11)	C(114)–C(113)–C(118)–C(117)	1.2(17)
C(104)–C(105)–C(118)–C(113)	-74.9(12)	C(104)–C(105)–C(118)–C(117)	101.3(13)
C(112)–C(105)–C(118)–C(113)	46.8(13)	C(112)–C(105)–C(118)–C(117)	-137.0(12)
C(207)–C(201)–C(202)–C(203)	84.5(12)	C(213)–C(201)–C(202)–C(203)	-37.3(12)
C(206)–O(2)–C(203)–C(202)	-111.3(11)	C(206)–O(2)–C(203)–C(204)	109.1(11)
C(201)–C(202)–C(203)–O(2)	172.6(9)	C(201)–C(202)–C(203)–C(204)	-51.4(13)
C(201)–C(202)–C(203)–C(206)	105.3(12)	O(2)–C(203)–C(204)–C(205)	-172.8(8)
C(202)–C(203)–C(204)–C(205)	50.8(13)	C(206)–C(203)–C(204)–C(205)	-106.5(12)
C(203)–C(204)–C(205)–C(212)	-84.4(12)	C(203)–C(204)–C(205)–C(218)	38.8(13)
C(202)–C(203)–C(206)–O(2)	101.4(10)	C(204)–C(203)–C(206)–O(2)	-101.1(11)
C(202)–C(201)–C(207)–C(208)	98.9(13)	C(202)–C(201)–C(207)–C(212)	-76.5(12)
C(213)–C(201)–C(207)–C(208)	-140.1(12)	C(213)–C(201)–C(207)–C(212)	44.5(14)
C(201)–C(207)–C(208)–C(209)	-177.4(10)	C(212)–C(207)–C(208)–C(209)	-2.3(18)
C(207)–C(208)–C(209)–C(210)	1.3(16)	C(208)–C(209)–C(210)–C(211)	-0.9(16)
C(209)–C(210)–C(211)–C(212)	1.4(18)	C(210)–C(211)–C(212)–C(205)	176.8(11)
C(210)–C(211)–C(212)–C(207)	-2.3(16)	C(201)–C(207)–C(212)–C(205)	-0.9(14)
C(201)–C(207)–C(212)–C(211)	178.3(10)	C(208)–C(207)–C(212)–C(205)	-176.4(12)
C(208)–C(207)–C(212)–C(211)	2.8(17)	C(204)–C(205)–C(212)–C(207)	79.6(12)
C(204)–C(205)–C(212)–C(211)	-99.5(12)	C(218)–C(205)–C(212)–C(207)	-44.2(13)
C(218)–C(205)–C(212)–C(211)	136.7(11)	C(202)–C(201)–C(213)–C(214)	-101.7(13)
C(202)–C(201)–C(213)–C(218)	77.6(12)	C(207)–C(201)–C(213)–C(214)	137.8(12)
C(207)–C(201)–C(213)–C(218)	-43.0(15)	C(201)–C(213)–C(214)–C(215)	-179.7(11)
C(218)–C(213)–C(214)–C(215)	1.0(17)	C(213)–C(214)–C(215)–C(216)	-2.4(17)
C(214)–C(215)–C(216)–C(217)	2.3(18)	C(215)–C(216)–C(217)–C(218)	-0.7(18)
C(216)–C(217)–C(218)–C(213)	-176.9(11)	C(216)–C(217)–C(218)–C(213)	-0.7(16)
C(201)–C(213)–C(218)–C(205)	-2.3(15)	C(201)–C(213)–C(218)–C(217)	-178.8(10)
C(214)–C(213)–C(218)–C(205)	177.0(11)	C(214)–C(213)–C(218)–C(217)	0.5(17)
C(204)–C(205)–C(218)–C(213)	-76.4(12)	C(204)–C(205)–C(218)–C(217)	99.9(13)

C(212)—C(205)—C(218)—C(213)	46.0(13)	C(212)—C(205)—C(218)—C(217)	-137.7(11)
C(307)—C(301)—C(302)—C(303)	84.5(12)	C(313)—C(301)—C(302)—C(303)	-36.5(13)
C(306)—O(3)—C(303)—C(302)	-108.9(12)	C(306)—O(3)—C(303)—C(304)	111.1(13)
C(301)—C(302)—C(303)—O(3)	171.1(9)	C(301)—C(302)—C(303)—C(304)	-51.5(14)
C(301)—C(302)—C(303)—C(306)	104.0(13)	O(3)—C(303)—C(304)—C(305)	-171.7(10)
C(302)—C(303)—C(304)—C(305)	50.2(16)	C(306)—C(303)—C(304)—C(305)	-104.9(13)
C(303)—C(304)—C(305)—C(312)	-83.7(14)	C(303)—C(304)—C(305)—C(318)	38.4(15)
C(302)—C(303)—C(306)—O(3)	103.6(11)	C(304)—C(303)—C(306)—O(3)	-100.9(11)
C(302)—C(301)—C(307)—C(308)	98.0(12)	C(302)—C(301)—C(307)—C(312)	-76.1(12)
C(313)—C(301)—C(307)—C(308)	-141.8(11)	C(313)—C(301)—C(307)—C(312)	44.1(13)
C(301)—C(307)—C(308)—C(309)	-174.9(11)	C(312)—C(307)—C(308)—C(309)	-0.9(16)
C(307)—C(308)—C(309)—C(310)	0.0(17)	C(308)—C(309)—C(310)—C(311)	0.7(17)
C(309)—C(310)—C(311)—C(312)	-0.5(18)	C(310)—C(311)—C(312)—C(305)	176.8(11)
C(310)—C(311)—C(312)—C(307)	-0.4(17)	C(301)—C(307)—C(312)—C(305)	-2.0(15)
C(301)—C(307)—C(312)—C(311)	175.5(11)	C(308)—C(307)—C(312)—C(305)	-176.4(10)
C(308)—C(307)—C(312)—C(311)	1.1(16)	C(304)—C(305)—C(312)—C(307)	78.5(12)
C(304)—C(305)—C(312)—C(311)	-98.9(13)	C(318)—C(305)—C(312)—C(307)	-42.9(14)
C(318)—C(305)—C(312)—C(311)	139.7(11)	C(302)—C(301)—C(313)—C(314)	-103.2(12)
C(302)—C(301)—C(313)—C(318)	78.6(13)	C(307)—C(301)—C(313)—C(314)	137.4(11)
C(307)—C(301)—C(313)—C(318)	-40.7(14)	C(301)—C(313)—C(314)—C(315)	179.8(11)
C(318)—C(313)—C(314)—C(315)	-2.1(17)	C(313)—C(314)—C(315)—C(316)	-0.1(17)
C(314)—C(315)—C(316)—C(317)	1.5(18)	C(315)—C(316)—C(317)—C(318)	-0.7(19)
C(316)—C(317)—C(318)—C(305)	-176.4(11)	C(316)—C(317)—C(318)—C(313)	-1.5(18)
C(301)—C(313)—C(318)—C(305)	-3.5(16)	C(301)—C(313)—C(318)—C(317)	-178.9(11)
C(314)—C(313)—C(318)—C(305)	178.2(10)	C(314)—C(313)—C(318)—C(317)	2.8(17)
C(304)—C(305)—C(318)—C(313)	-74.4(13)	C(304)—C(305)—C(318)—C(317)	100.6(14)
C(312)—C(305)—C(318)—C(313)	46.0(15)	C(312)—C(305)—C(318)—C(317)	-139.0(12)
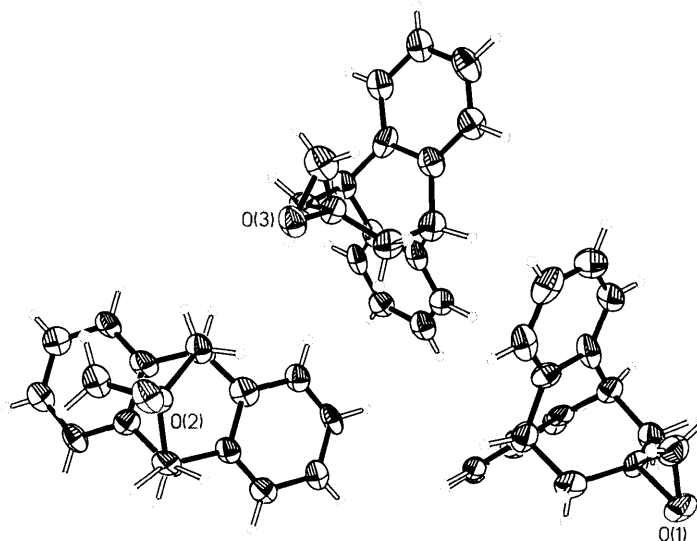
The three molecules in the asymmetric unit, with 50% probability displacement ellipsoids. One of the molecules, showing the disposition of the three-membered ring. All three molecules have a similar arrangement.

86

Scheme D.1
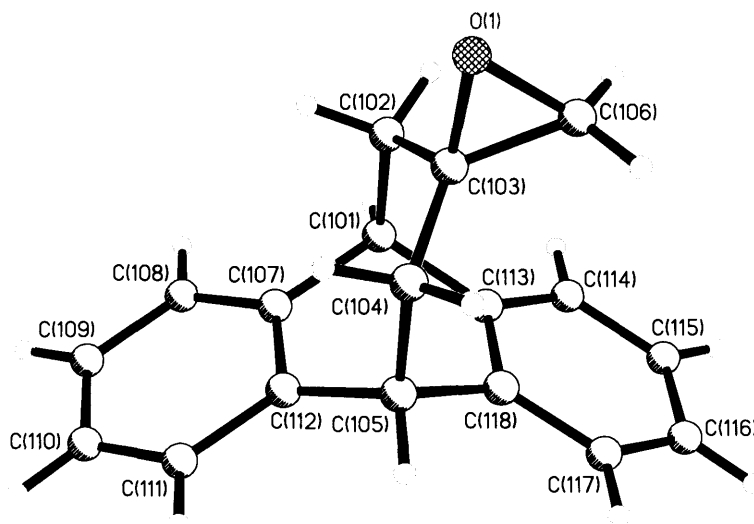
Appendix 11 Crystal structure and X-Ray data for **116**

Table E.1. Crystal data and structure refinement for **116**.

Chemical formula	$C_{18}H_{16}N_2$
Formula weight	260.33
Temperature	293(2) K
Radiation, wavelength	MoKα, 0.71073 Å
Crystal system, space group	monoclinic, P2$_1$/c
Unit cell parameters	a = 13.8169(18) Å α = 90°
	b = 11.8799(15) Å β = 100.271(2)°
	c = 8.5789(11) Å γ = 90°
Cell volume	1385.6(3) Å^3
Z	4
Calculated density	1.248 g/cm^3
Absorption coefficient μ	0.074 mm^{-1}
F(000)	552
Crystal colour and size	colourless, 0.34 × 0.30 × 0.09 mm^3
Data collection method	Bruker SMART APEX diffractometer
	ω rotation with narrow frames
θ range for data collection	1.50 to 28.32°
Index ranges	h −17 to 18, k −15 to 15, l −11 to 11
Completeness to θ = 26.00°	100.0 %
Reflections collected	12052
Independent reflections	3318 (R$_{int}$ = 0.0325)
Reflections with F^2>2σ	2412
Absorption correction	semi-empirical from equivalents
Min. and max. transmission	0.9753 and 0.9934
Structure solution	direct methods
Refinement method	Full-matrix least-squares on F^2
Weighting parameters a, b	0.0685, 0.2468
Data / restraints / parameters	3318 / 0 / 189
Final R indices [F^2>2σ]	R1 = 0.0594, wR2 = 0.1391
R indices (all data)	R1 = 0.0847, wR2 = 0.1536
Goodness-of-fit on F^2	1.038
Largest and mean shift/su	0.000 and 0.000
Largest diff. peak and hole	0.229 and −0.165 e Å^{-3}

Table E.2. Atomic coordinates and equivalent isotropic displacement parameters ($\mathring{A}^2$) for **116**. U_{eq} is defined as one third of the trace of the orthogonalized U^{ij} tensor.

	x	y	z	U_{eq}
N(1)	0.31821(17)	0.3225(2)	0.5809(3)	0.0728(6)
N(2)	0.45773(12)	0.37057(15)	0.3058(2)	0.0629(5)
C(1)	0.30283(12)	0.59834(14)	0.2434(2)	0.0411(4)
C(2)	0.38276(14)	0.65311(16)	0.2014(2)	0.0494(5)
C(3)	0.41334(16)	0.62624(18)	0.0611(2)	0.0585(5)
C(4)	0.36305(16)	0.5477(2)	−0.0382(2)	0.0621(6)
C(5)	0.28187(15)	0.49364(18)	0.0011(2)	0.552(5)
C(6)	0.25163(12)	0.51748(15)	0.14342(19)	0.0425(4)
C(7)	0.26875(12)	0.61729(15)	0.3991(2)	0.0440(4)
C(8)	0.15785(13)	0.62316(15)	0.3723(2)	0.0455(4)
C(9)	0.10652(16)	0.70077(17)	0.4470(3)	0.0608(5)
C(10)	0.00491(17)	0.6961(2)	0.4237(3)	0.0709(6)
C(11)	−0.04540(16)	0.6161(2)	0.3269(3)	0.0702(7)
C(12)	0.00530(14)	0.53908(19)	0.2513(3)	0.0610(5)
C(13)	0.10726(13)	0.54221(15)	0.2738(2)	0.0459(4)
C(14)	0.16940(12)	0.45725(15)	0.2042(2)	0.0458(4)
C(15)	0.21067(13)	0.36917(15)	0.3318(2)	0.0481(4)
C(16)	0.30533(13)	0.40244(16)	0.4467(2)	0.0466(4)
C(17)	0.30562(13)	0.52145(16)	0.5161(2)	0.0475(4)
C(18)	0.39068(13)	0.38916(15)	0.3624(2)	0.0476(4)

Table E.3. Bond lengths [Å] and angles [°] for **116.**

N(1)–C(16)	1.478(2)	N(2)–C(18)	1.141(2)
C(1)–C(2)	1.384(2)	C(1)–C(6)	1.394(2)
C(1)–C(7)	1.510(2)	C(2)–C(3)	1.382(3)
C(3)–C(4)	1.366(3)	C(4)–C(5)	1.385(3)
C(5)–C(6)	1.388(2)	C(6)–C(14)	1.512(3)
C(7)–C(8)	1.510(2)	C(7)–C(17)	1.543(3)
C(8)–C(13)	1.384(3)	C(8)–C(9)	1.388(3)
C(9)–C(10)	1.383(3)	C(10)–C(11)	1.367(3)
C(11)–C(12)	1.383(3)	C(12)–C(13)	1.388(3)
C(13)–C(14)	1.515(2)	C(14)–C(15)	1.548(3)
C(15)–C(16)	1.542(3)	C(16)–C(18)	1.498(3)
C(16)–C(17)	1.534(3)		
C(2)–C(1)–C(6)	120.31(16)	C(2)–C(1)–C(7)	123.33(16)
C(6)–C(1)–C(7)	116.31(15)	C(3)–C(2)–C(1)	120.02(19)
C(4)–C(3)–C(2)	120.00(19)	C(3)–C(4)–C(5)	120.59(18)
C(4)–C(5)–C(6)	120.19(19)	C(5)–C(6)–C(1)	118.86(17)
C(5)–C(6)–C(14)	124.70(17)	C(1)–C(6)–C(14)	116.36(14)
C(8)–C(7)–C(1)	109.87(14)	C(8)–C(7)–C(17)	109.98(14)
C(1)–C(7)–C(17)	110.28(14)	C(13)–C(8)–C(9)	119.96(18)
C(13)–C(8)–C(7)	116.69(15)	C(9)–C(8)–C(7)	123.26(17)
C(10)–C(9)–C(8)	119.7(2)	C(11)–C(10)–C(9)	120.6(2)
C(10)–C(11)–C(12)	120.0(2)	C(11)–C(12)–C(13)	120.2(2)
C(8)–C(13)–C(12)	119.56(18)	C(8)–C(13)–C(14)	116.32(15)
C(12)–C(13)–C(14)	124.03(17)	C(6)–C(14)–C(13)	109.52(15)
C(6)–C(14)–C(15)	111.05(14)	C(13)–C(14)–C(15)	109.54(15)
C(16)–C(15)–C(14)	116.25(14)	N(1)–C(16)–C(18)	108.22(15)
N(1)–C(16)–C(17)	107.36(17)	C(18)–C(16)–C(17)	109.69(15)
N(1)–C(16)–C(15)	107.68(16)	C(18)–C(16)–C(15)	108.36(15)
C(17)–C(16)–C(15)	115.31(15)	C(16)–C(17)–C(7)	116.74(14)
N(2)–C(18)–C(16)	173.91(19)		

Table E.4. Anisotropic displacement parameters (Å^2) for **116**. The anisotropic displacement factor exponent takes the form: $-2\pi^2[h^2a^{*2}U^{11} + ...+ 2hka^*b^*U^{12}]$

	U^{11}	U^{22}	U^{33}	U^{23}	U^{13}	U^{12}
N(1)	0.0706(14)	0.0799(16)	0.0704(13)	0.0321(12)	0.0194(11)	0.0077(12)
N(2)	0.0478(10)	0.0673(12)	0.0760(12)	0.0017(9)	0.0172(9)	0.0092(8)
C(1)	0.0429(9)	0.0387(9)	0.0419(9)	0.0015(7)	0.0081(7)	0.0016(7)
C(2)	0.0502(10)	0.0449(10)	0.0553(11)	0.0042(8)	0.0153(9)	−0.0039(8)
C(3)	0.0581(12)	0.0641(13)	0.0571(12)	0.0170(10)	0.0206(10)	0.0032(10)
C(4)	0.0670(13)	0.0839(15)	0.0393(10)	0.0103(10)	0.0198(9)	0.0154(12)
C(5)	0.0600(12)	0.0662(13)	0.0372(9)	−0.0051(9)	0.0022(8)	0.0073(10)
C(6)	0.0420(9)	0.0467(10)	0.0374(9)	−0.0011(7)	0.0031(7)	0.0048(8)
C(7)	0.0448(10)	0.0429(9)	0.0458(10)	−0.0128(7)	0.0123(8)	−0.0104(7)
C(8)	0.0476(10)	0.0424(10)	0.0490(10)	−0.0011(8)	0.0153(8)	0.0005(8)
C(9)	0.0686(13)	0.0477(11)	0.0720(14)	−0.0059(10)	0.0280(11)	0.0049(10)
C(10)	0.0679(14)	0.0637(14)	0.0897(16)	0.0081(13)	0.0371(13)	0.0227(12)
C(11)	0.0449(11)	0.0818(16)	0.0856(17)	0.0163(13)	0.0165(11)	0.0174(11)
C(12)	0.0407(10)	0.0719(14)	0.0682(13)	0.0025(11)	0.0038(9)	0.0029(9)
C(13)	0.0400(9)	0.0476(10)	0.0493(10)	0.0007(8)	0.0061(8)	0.0023(8)
C(14)	0.0388(9)	0.0494(10)	0.0464(10)	−0.0130(8)	0.0002(7)	−0.0054(8)
C(15)	0.0430(10)	0.0409(9)	0.0625(11)	−0.0043(8)	0.0151(8)	−0.0071(8)
C(16)	0.0415(9)	0.0539(11)	0.0458(10)	0.0103(8)	0.0117(8)	0.0011(8)
C(17)	0.0418(9)	0.0665(12)	0.0340(8)	−0.0059(8)	0.0066(7)	−0.0066(8)
C(18)	0.0406(10)	0.0475(10)	0.0540(11)	0.0064(8)	0.0068(8)	0.0020(8)

Table E.5. Hydrogen coordinates and isotropic displacement parameters (Å^2) for **116**.

	x	y	z	U
H(1N)	0.326(2)	0.253(3)	0.542(4)	0.114(12)
H(2N)	0.375(2)	0.344(2)	0.649(3)	0.087(9)
H(2A)	0.4159	0.7080	0.2676	0.059
H(3A)	0.4681	0.6616	0.0343	0.070
H(4A)	0.3835	0.5305	−0.1330	0.075
H(5A)	0.2475	0.4412	−0.0681	0.066
H(7A)	0.2957	0.6888	0.4445	0.053
H(9A)	0.1403	0.7557	0.5125	0.073
H(10A)	−0.0295	0.7479	0.4742	0.085
H(11A)	−0.1137	0.6135	0.3121	0.084
H(12A)	−0.0290	0.4850	0.1850	0.073
H(14A)	0.1280	0.4187	0.1155	0.055
H(15A)	0.1601	0.3528	0.3938	0.058
H(15B)	0.2235	0.3002	0.2785	0.058
H(17A)	0.3723	0.5391	0.5672	0.057
H(17B)	0.2653	0.5208	0.5979	0.057

Table E.6. Torsion angles [°] for **116**.

C(6)–C(1)–C(2)–C(3)	–1.2(3)	C(7)–C(1)–C(2)–C(3)	175.95(17)
C(1)–C(2)–C(3)–C(4)	1.7(3)	C(2)–C(3)–C(4)–C(5)	–0.6(3)
C(3)–C(4)–C(5)–C(6)	–1.0(3)	C(4)–C(5)–C(6)–C(1)	1.5(3)
C(4)–C(5)–C(6)–C(14)	–174.95(18)	C(2)–C(1)–C(6)–C(5)	–0.4(3)
C(7)–C(1)–C(6)–C(5)	–177.77(16)	C(2)–C(1)–C(6)–C(14)	176.35(16)
C(7)–C(1)–C(6)–C(14)	–1.0(2)	C(2)–C(1)–C(7)–C(8)	138.35(17)
C(6)–C(1)–C(7)–C(8)	–44.4(2)	C(2)–C(1)–C(7)–C(17)	–100.27(19)
C(6)–C(1)–C(7)–C(17)	76.99(18)	C(1)–C(7)–C(8)–C(13)	45.1(2)
C(17)–C(7)–C(8)–C(13)	–76.43(19)	C(1)–C(7)–C(8)–C(9)	–138.26(18)
C(17)–C(7)–C(8)–C(9)	100.2(2)	C(13)–C(8)–C(9)–C(10)	0.5(3)
C(7)–C(8)–C(9)–C(10)	–175.95(19)	C(8)–C(9)–C(10)–C(11)	–0.3(3)
C(9)–C(10)–C(11)–C(12)	–0.1(3)	C(10)–C(11)–C(12)–C(13)	0.4(3)
C(9)–C(8)–C(13)–C(12)	–0.3(3)	C(7)–C(8)–C(13)–C(12)	176.44(17)
C(9)–C(8)–C(13)–C(14)	–176.87(17)	C(7)–C(8)–C(13)–C(14)	–0.2(2)
C(11)–C(12)–C(13)–C(8)	–0.2(3)	C(11)–C(12)–C(13)–C(14)	176.12(19)
C(5)–C(6)–C(14)–C(13)	–137.68(18)	C(1)–C(6)–C(14)–C(13)	45.8(2)
C(5)–C(6)–C(14)–C(15)	101.2(2)	C(1)–C(6)–C(14)–C(15)	–75.35(19)
C(8)–C(13)–C(14)–C(6)	–45.2(2)	C(12)–C(13)–C(14)–C(6)	138.39(19)
C(8)–C(13)–C(14)–C(15)	76.83(19)	C(12)–C(13)–C(14)–C(15)	–99.6(2)
C(6)–C(14)–C(15)–C(16)	37.6(2)	C(13)–C(14)–C(15)–C(16)	–83.53(18)
C(14)–C(15)–C(16)–N(1)	165.88(16)	C(14)–C(15)–C(16)–C(18)	–77.28(19)
C(14)–C(15)–C(16)–C(17)	46.1(2)	N(1)–C(16)–C(17)–C(7)	–165.77(15)
C(18)–C(16)–C(17)–C(7)	76.85(19)	C(15)–C(16)–C(17)–C(7)	–45.8(2)
C(8)–C(7)–C(17)–C(16)	82.97(18)	C(1)–C(7)–C(17)–C(16)	–38.3(2)
N(1)–C(16)–C(18)–N(2)	12(2)	C(17)–C(16)–C(18)–N(2)	128.5(19)
C(15)–C(16)–C(18)–N(2)	–104.9(19)		
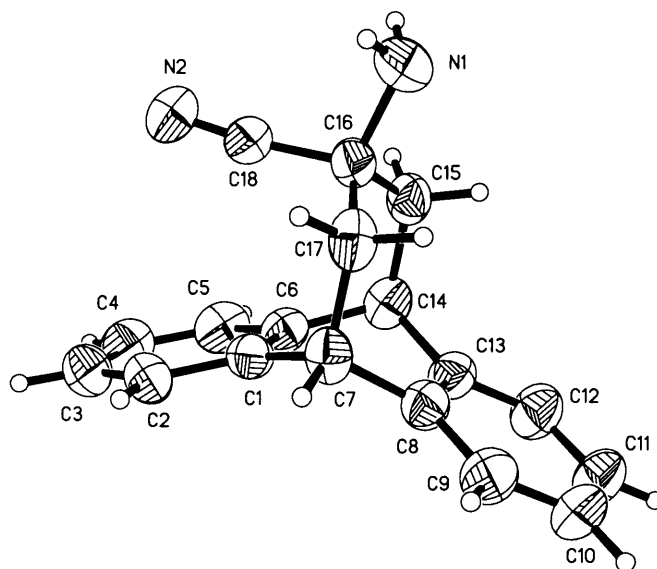
116

Scheme E.1

CHAPTER 6

REFERENCES

1   (a) S. K. Burley, G. A. Petsko, _Science_, **1985**, _229_, 23; (b) S. K. Burley, G. A. Petsko, _Adv. Protein Chem._, **1988**, _39_, 125; (c) H. –J. Schneider, _Angew. Chem. Int. Ed. Engl._, **1991**, _30_, 1417; (d) C. A. Hunter, _Chem. Soc. Rev._, **1994**, 101; (e) M. C. T. Fyfe, J. F. Stoddart, _Acc. Chem. Res._, **1997**, _30_, 393.

2   (a) J. Vrbancich, G. L. D. Ritchie, _J. Chem. Soc., Faraday Trans._ 2, **1980**, _76_, 648; (b) J. Pawliszyn, M. M. Szczesniak, S. Scheiner, _J. Phys. Chem_, **1984**, _88_, 1726.

3   (a) K. C. Janda, C. Hemminger, J. S. Winn, S. E. Novick, S. J. Harris, W. Klemperer, _J. Chem. Phys._, **1975**, _63_, 1419; (b) J. M. Steed, T. A. Dixon, W. Klemperer, _J. Chem. Phys._, **1979**, _70_, 4940.

4   C. A. Hunter, J. K. M. Sanders, J. Am. Chem. Soc., **1990**, 112, 5525.

5   (a) G. Karlström, P. Linse, A. Wallqvist, B. Jönsson, _J. Am. Chem. Soc._, **1983**, _105_, 3777; (b) S. K. Burley, G. A. Petsko, _J; Am. Chem. Soc._, **1986**, _108_, 7995; (c) S. L. Price, A. J. Stone, _J. Chem. Phys._, **1987**, _86_, 2859; (d) W; L; Jorgenson, D. L. Severance, _J. Am. Chem. Soc._, **1990**, _112_, 4768.

6   (a) P. Hobza, H. L. Selzle, E. W. Schlag, _J. Am. Chem. Soc._, **1994**, _116_, 3500; (b) P. Hobza, H. L. Selzle, E. W. Schlag, _Chem. Rev._, **1994**, _94_, 1767.

7   E. G. Cox, W. J. Cruickshank, J. A. S. Smith, _Proc. R. Soc. London Ser. A_, **1958**, _247_, 1.

8   R. Laatikainen, J. Ratilainen, R. Sebastian, H. Santa, _J. Am. Chem. Soc._, **1995**, _117_, 11006.

9   J. Singh, J. M. Thorton, _FEBS Letters_, **1985**, _191_, 1.

10   G. B. McGaughey, M. Gagné, A. K. Rappé, _J. Biol. Chem._, **1998**, _25_, 15458.

11   (a) R. Bhattacharyya, U. Samanta, P. Chakrabarti, _Protein Eng._, **2002**, _15_, 91; (b) R. Chelli, F. L. Gervasio, P. Procacci, V. Schettino, _J. Am. Chem. Soc._, **2002**, _124_, 6133.

12   S. M. Butterfield, P. R. Patel, M. L. Waters, _J. Am. Chem. Soc._, **2002**, _124_, 9751.

13   A. G. W. Leslie, S. Arnott, R. Chandrasekaran, R. L. Ratliff, _J. Mol. Biol._, **1980**, _143_, 49.

14   C. A. Hunter, _Phil. Trans. R. Soc. Lond. A_, **1993**, _345_, 77.

15   (a) H. Kurebayashi, T. Haino, S. Usui, Y. Fukazawa, _Tetrahedron_, **2001**, _57_, 8667; (b) Y. Yoshitake, J. Misaka, K. Setoguchi, M. Abe, T. Kawaji, M. Eto, K. Harano, _J. Chem. Soc., Perkin Trans._ 2, **2002**, 1611: (c) G. Grossmann, M. J. Potrzebowski, S. Olejniczak, N. E. Ziolkowska, G. D. Bujacz, W. Ciesielski, W. Prezdo, V. Nazarov, V. Golovsko, _New. J. Chem._, **2003**, _27_, 1095.

16   For reviews on aromatic interactions: (a) W. B. Jennings, B. M. Farrell, J. F. Malone, _Acc. Chem. Res._, **2001**, _34_, 885; (b) C. A. Hunter, K. R. Lawson, J. Perkins, C. J. Urch, _J. Chem. Soc., Perkin Trans._ 2, **2001**, 651; (c) E. A. Meyer, R. K. Castellano, F. Diederich, _Angew. Chem., Int. Ed._, **2003**, _42_, 1210.

17   (a) F. Cozzi, M. Cinquini, R. Annuziata, T. Dwyer, J. S. Siegel, _J. Am. Chem. Soc._, **1992**, _114_, 5729; (b) F. Cozzi, M. Cinquini, R. Annuziata, J. S. Siegel, _J. Am. Chem. Soc._, **1993**, _115_, 5330; (c) F. Cozzi, F. Ponzini, R. Annunziata, M. Cinquini, J. S. Siegel, _Angew. Chem. Int. Ed. Engl._, **1995**, _34_, 1019.

18   N. J. Heaton, P. Bello, B. Herradon, A. DelCampo, J. Jimenez-Barbero, _J. Am. Chem. Soc._, **1998**, _120_, 9632.

19   T.A. Hamor, W. B. Jennings, L. D. Proctor, M. S. Tolley, D. R. Boyd, T. Mullan, _J. Chem. Soc., Perkin Trans._ 2, **1990**, 25.

20   D. R. Boyd, T. A. Evans, W. B. Jennings, J. F. Malone, W. O. O'Sullivan, A. Smith, _J. Chem. Soc. Chem. Comm._, **1996**, 2269.

21   S. Paliwal, S. Geib, C. S. Wilcox, _J. Am. Chem. Soc._, **1994**, _116_, 4497.

22   E. Kim, S. Paliwal, C. S. Wilcox, _J. Am. Chem. Soc._, **1998**, _120_, 11192.

23   (a) T. Ren, Y. Jin, K. S. Kim, D. H. Kim, _J. Biomol. Struct. Dyn._, **1997**, _15_, 401; (b) K. Nakamura, K. N. Houk, _Org. Lett._, **1999**, _1_, 2049; (c) J. Ribas, E. Cubero, F. J. Luque, M. Orozco, _J. Org. Chem._, **2002**, _67_, 7057.

24   H. -J. Schneider, _Angew. Chem. Int. Ed. Engl._, **1991**, _30_, 1417.

25   S. B. Ferguson, F. Diederich, _Angew. Chem. Int. Ed. Engl._, **1986**, _25_, 1127.

26   F. Diederich, _Angew. Chem., Int. Ed. Engl._, **1988**, 27, 362 and references therein.

27   J. Rebek Jr., _Angew. Chem., Int. Ed. Engl._, **1990**, _29_, 245.

28   (a) S. C. Zimmerman, C. M. VanZyl, _J. Am. Chem. Soc._, **1987**, _109_, 7894; (b) S. C. Zimmerman, C. M. VanZyl, G. S. Hamilton, _J. Am. Chem. Soc._, **1989**, _11_, 1373.

29   (a) M. Kamieth, F. –G. Klärner, F. Diederich, _Angew. Chem., Int. Ed. Engl._, **1998**, _37_, 3303; (b) F. –G. Klärner, U. Burkert, M. Kamieth, R. Boese, J. Benet-Buchholz, _Chem. Eur. J._, **1999**, _5_, 1700;

(c) F. –G. Klärner, B. Kahlert, R. Boese, D. Bläser, A. Juris, F. Marchioni, *Chem. Eur. J.*, **2005**, *11*, 3363.

30   F. –G. Klärner, B. Kahlert, *Acc. Chem. Res.*, **2003**, *36*, 919.

31   (a) C. A. Schalley, R. K. Castellano, M. S. Brody, D. M. Rudkevich, G. Siuzdak, J. Rebek Jr., *J. Am. Chem. Soc.*, **1999**, *121*, 4568; (b) C. Zonta, S. Cossu, O. De Lucchi, *Eur. J. Org. Chem.*, **2000**, 1965; (c) S. Kubik, R. Goddard, *Eur. J. Org. Chem.*, **2001**, 311.

32   (a) A. P. Bisson, F. J. Carver, C. A. Hunter, J. P. Waltho, *J. Am. Chem. Soc.*, **1994**, *116*, 10292; (b) H. Adams, F. J. Carver, C. A. Hunter, J. C. Morales, E. M. Seward, *Angew. Chem., Int. Ed. Engl.*, **1996**, *35*, 1542; (c) H. Adams, K. D. M. Harris, G. A. Hembury, C. A. Hunter, D. Livingstone, J. F. McCabe, *J. Chem. Soc. Chem. Comm*, **1996**, 2531; (d) F. J. Carver, C. A. Hunter, E. M. Seward, *J. Chem. Soc. Chem. Comm.*, **1998**, 775 (e) A. P. Bisson, F. J. Carver, D. S. Eggleston, R. C. Haltiwanger, C. A. Hunter, D. L. Livingstone, J. F. McCabe, C. Rotger, A. E. Rowan, *J. Am. Chem. Soc.*, **2000**, *122*, 8856; (f) H. Adams, C. A. Hunter, K. R. Lawson, J. Perkins, S. E. Spey, C. J. Urch, J. M. Sanderson, *Chem. Eur. J.*, **2001**, *7*, 4863.

33   A. G. Martinez, J. O. Barcina, A.D. Cerezo, *Chem. Eur. J.*, **2001**, *7*, 1171.

34   H. Adams, C. A. Hunter, K. R. Lawson, J. Perkins, S. E. Spey, C. J. Urch, J. M. Sanderson, *Chem. Eur. J.*, **2001**, *7*, 4854.

35   (a) D. B. Smithrud, E. M. Sanford, I. Chao, S. B. Ferguson, D. R. Carcanague, J. D. Evanseck, K. N. Houk, F. Diederich, *Pure & Appl. Chem.*, **1990**, *62*, 2227; (b) D. B. Smithrud, F. Diederich, *J. Am. Chem. Soc.*, **1990**, *112*, 339 and reference therein.

36   M. Nishio, *Tetrahedron*, **1995**, *51*, 8665.

37   (a) A comprehensive literature list of CH/π hydrogen bonds is available on the website: http://www.tim.hi-ho.ne.jp/dionisio; (b) M. Nishio, M. Hirota, *Tetrahedron*, **1989**, *45*, 7201; (c) M. Nishio, M. Hirota, Y. Umezawa, *The CH/π Interaction. Evidence, Nature, and Consequences*; Wiley-VCH: New-York, **1998**; (d) M. Nishio, *CrystEngComm.*, **2004**, *6*, 130.

38   T. Steiner, *Angew. Chem., Int. Ed. Engl.*, **2002**, *41*, 48.

39   Y. Umezawa, M. Nishio, *Bioorg. Med. Chem.*, **1998**, *6*, 2507.

40   H. Suezawa, T. Yoshida, Y. Umezawa, S. Tsuboyama, M. Nishio, *Eur. J. Inorg. Chem.*, **2002**, 3148.

41   S. Tsuzuki, K. Honda, T. Uchimaru, M. Mikami, K. Tanabe, *J. Am. Chem. Soc.*, **2000**, *122*, 3746.

42   O. Takahashi, Y. Kohno, S. Iwasaki, K. Saito, M. Iwaoka, S. Tomoda, Y. Umezawa, S. Tsuboyama, M. Nishio, *Bull. Chem. Soc. Jpn.*, **2001**, *74*, 2421.

43   H. Suezama, T. Hashimoto, K. Tsuchinaga, T. Yoshida, T. Yuzuri, K. Sakakibara, M. Hirota, M. Nishio, *J. Chem. Soc., Perkin Trans. 2*, **2000**, 1243.

44   Y. Umezawa, S. Tsuboyama, H. Takahashi, J. Uzawa, M. Nishio, *Bioorg. Med. Chem.*, **1999**, *7*, 2021.

45   Y. Umezawa, S. Tsuboyama, H. Takahashi, J. Uzawa, M. Nishio, *Tetrahedron*, **1999**, *55*, 10047 and references therein

46   (a) Y. Kodama, K. Nishihata, M. Nishio, Y. Iitaka, *J. Chem. Soc., Perkin Trans. 2*, **1976**, 1490; (b) M. Hirota, Y. Takahashi, M. Nishio, K. Nishihata, *Bull. Chem. Soc. Jpn.*, **1978**, *51*, 2358.

47   R. Ehama, A. Yokoo, M. Tsushima, T. Yuzuri, H. Suezawa, M. Hirota, *Bull. Chem. Soc. Jpn.*, **1993**, *66*, 814.

48   M. Hirota, K. Sakaibara, H. Suezawa, T. Yuzuri, E. Ankai, M. Nishio, *J. Phys. Org. Chem.*, **2000**, *13*, 620.

49   (a) O. Takahashi, Y. Kohno, Y. Gondoh, K. Saito, M. Nishio, *Bull. Chem. Soc. Jpn.*, **2003**, *76*, 369; (b) O. Takahashi, Y. Kohno, K. Saito, M. Nishio, *Chem. Eur. J.*, **2003**, *9*, 756.

50   (a) P. Chakrabarti, U. Samanta, *J. Mol. Biol.*, **1995**, *251*, 9; (b) M. Brandl, M. S. Weiss, A. Jabs, J. Sühnel, R. Hilgenfeld, *J. Mol. Biol.*, **2001**, *307*, 357.

51   A. Frontera, C. Garau, D. Quinonero, P. Ballester, A. Costa, P. M. Deya, *Org. Lett.*, **2003**, *5*, 1135.

52   S. Re, S. Nagase, *Chem. Comm.*, **2004**, 658.

53   H. Takahashi, S. Tsuboyama, Y. Umezawa, K. Honda, M. Nishio, *Tetrahedron*, **2000**, *56*, 6185.

54   K. Kobayashi, Y. Asakawa, Y. Kikuchi, H. Toi, Y. Aoyama, *J. Am. Chem. Soc.*, **1993**, *115*, 2648.

55   N. Jaiboon, N. Chaichit, B. Pipoosananakaton, T. Tuntulani, M. Sukwattanasinitt, *J. Chem. Cryst.*, **2000**, *30*, 717.

56   (a) Y. Shimohigashi, T. Nose, Y. Yamauchi, I. Maeda, *Biopolymers*, **1999**, *51*, 9; (b) Y. Umezawa, M. Nishio, *Bioorg. Med. Chem.*, **2000**, *8*, 2643 and references therein; (c) V. Spiwok, P. Lipovova, T.

Skalova; E. Buchtelova, J. Hasek, B. Kralova, *Carbohydrate Research*, **2004**, *339*, 2275; (d) C. D. Tatko, M. L . Waters, *J. Am. Chem. Soc.*, **2004**, *126*, 2028.

57   N. K. Vyas, M. N. Vyas, F. A. Quiocho, *Science*, **1988**, *242*, 1290.

58   O. Rusin, K. Lang, V. Kral, *Chem. Eur. J.*, **2002**, *8*, 655.

59   H. –C. Weiss, R. Boese, H. L. Smith, M. M. Harley, *Chem. Comm.*, **1997**, 1703.

60   A. Fujii, S. Morita, M. Miyazaki, T. Ebata, N. Mikami, *J. Phys. Chem. A*, **2004**, *108*, 2652.

61   (a) J. A. Tucker, K. N. Houk, B. M. Trost, *J. Am. Chem. Soc.*, **1990**, *112*, 5465; (b) S. Mataka, J. Ma, T. Thiemann, J. M. Rudzinski, H. Tsuzuki, T. Sawada, M. Tashiro, *Tetrahedron*, **1997**, *53*, 885; (c) G. Ujaque, P. S. Lee, K. N. Houk, M. F. Hentemann, S. J. Danishefsky, *Chem. Eur. J.*, **2002**, *8*, 3423.

62   A. V. Malkov, A. Mariani, K. N. MacDougall, P. Kocovsky, *Org. Lett.*, **2004**, *6*, 2253.

63   Y. Kobayashi, T. Kurasawa, K. Kinbara, K. Saigo, *J. Org. Chem.*, **2004**, *69*, 7436.

64   M. Nishio, *Tetrahedron*, **2005**, *61*, 6923 and references therein.

65   T. Yamato, A. Miyazawa, M. Tashiro, *J. Chem. Soc., Perkin Trans. 1*, **1993**, 3127.

66   O. Takahashi, K. Saito, Y. Kohno, H. Suezawa, S. Ishihara, M. Nishio, *New J. Chem.*, **2004**, *28*, 355.

67   O. Takahashi, Y. Gondoh, K. Saito, Y. Kohno, H. Suezawa, T. Yoshida, S. Ishihara, M. Nishio, *New J. Chem.*, **2003**, *27*, 1639.

68   G. Toth, K. E. Köver, R. F. Murphy, S. Lovas, *J. Phys. Chem. B*, **2004**, *108*, 9287.

69   (a) G. A. Jeffrey, W. Saenger, *Hydrogen Bonding in Biologiccal Structures*, Springer, Berlin, **1991**; (b) G. A. Jeffrey, *An Introduction to Hydrogen Bonding*, Oxford University Press, Oxford, **1997**; (c) G. R. Desiraju, T. Steiner, *The Weak Hydrogen Bond in Structural Chemistry and Biology*, Oxford University Press, Oxford, **1999**.

70   A. Wlodawer, J. Walter, R. Huber, L. Sjölin, *J. Mol. Biol.*, **1984**, *180*, 301 and references therein.

71   T. Steiner, G. Koellner, *J. Mol. Biol.*, **2001**, *305*, 535 and references therein.

72   M. F. Perutz, G. Fermi, D. J. Abraham, C. Poyart, E. Bursaux, *J. Am. Chem. Soc.*, **1986**, *108*, 1064.

73   (a) M. Levitt, M. F. Perutz, *J. Mol. Biol.*, **1988**, *201*, 751; (b) M. F. Perutz, *Phil. Trans. R. Soc. A*, **1993**, *345*, 105.

74   T. Steiner, A. M. M. Schreurs, J. A. Kanters, J. Kroon, *Acta Crystallogr. Sect. D*, **1998**, *54*, 25.

75   J. L. Atwood, F. Hamada, K. D. Robinson, G. W. Orr, R. L. Vincent, *Nature*, **1991**, *349*, 683.

76   B. Brutschy, *Chem. Rev.*, **2000**, *100*, 3891.

77   S. Suzuki, P. G. Green, R. E. Bumgarner, S. Dasgupta, W. A. Goddard III, G. A. Blake, *Science*, **1992**, *257*, 942.

78   D. A. Rodham, S. Suzuki, R. D. Suenram, F. J. Lovas, D. Dasgupta, W. A. Goddard III, G. A. Blake, *Nature*, **1993**, *362*, 735

79   S. Tsuzuki, K. Honda, T. Uchimaru, M. Mikami, K. Tanabe, *J. Am. Chem. Soc.*, **2000**, *122*, 11450.

80   J. F. Malone, C. M. Murray, M. H. Charlton, R. Docherty, A. J. Lavery, *J. Chem. Soc., Faraday Trans.*, **1997**, *93*, 3429.

81   A. Courty, M. Mons, I. Dimicoli, F. Piuzzi, M. –P. Gaigeot, V. Brenner, P. de Pujo, P. Millié, *J. Phys. Chem. A*, **1998**, *102*, 6590.

82   G. Duan, V. H. Smith Jr., D. F. Weaver, *J. Phys. Chem. A*, **2000**, *104*, 4521.

83   G. Columberg, A. Bauder, *J. Chem. Phys.*, **1997**, *106*, 504.

84   (a) P. Hobza, Z. Havlas, *Chem. Rev.*, **2000**, *100*, 4253; (b) K. Hermansson, *J. Phys. Chem. A*, **2002**, *106*, 4695.

85   F. H. Allen, V. J. Hoy, J. A. K. Howard, V. R. Thalladi, G. R. Desiraju, C. C. Wilson, G. J. McIntyre, *J. Am. Chem. Soc.*, **1997**, *119*, 3477.

86   M. C. Etter, *J. Phys. Chem.*, **1991**, *95*, 4601.

87   (a) H. S. Rzepa, M. L. Webb, A. M. Z. Slawin, D. J. Williams, *J. Chem. Soc., Chem. Comm.*, **1991**, 765.
      See also: (b) H. S. Rzepa, M. L. Webb, *J. Chem. Soc. Perkin Trans. 2*, **1994**, 703; (c) M. L. Webb, H. S. Rzepa, *Chirality*, **1994**, *6*, 245.

88   A. M. Sweeting, L. Rheingold, *J. Phys. Chem.*, **1988**, *92*, 5648.

89   (a) C. A. Hunter, *J. Am. Chem. Soc.*, **1992**, *114*, 5303; (b) H. Adams, F. J. Carver, C. A. Hunter, N. J. Osborne, *Chem. Comm.* **1996**, 2529.

90   C. Allot, H. Adams, P. L. Bernad Jr, C. A. Hunter, C. Rotger, J. A. Thomas, *Chem. Comm.*, **1998**, 2449.

91   O. Takahashi, K. Saito, Y. Kohno, H. Suezawa, S. Ishihara, M. Nishio, *Eur. J. Org. Chem.*, **2004**, 2398.

92   D. H. Wertz, N. L. Allinger, *Tetrahedron*, **1974**, *30*, 1579.

93   J. C. Ma, D. A. Dougherty, *Chem. Rev.*, **1997**, *97*, 1303 and references therein.

94   (a) J. P. Gallivan, D. A. Dougherty, *Proc. Natl. Acad. Sci. USA*, **1999**, *96*, 9459; (b) C. D. Andrew, S. Bhattacharjee, N. Kokkoni, J. D. Hirst, G. R. Jones, A. J. Doig, *J. Am. Chem. Soc.*, **2002**, *124*, 12706.

95   E. V. Pletneva, A. T. Laederach, D. B. Fulton, N. M. Kostic, *J. Am. Chem. Soc.*, **2001**, *123*, 6232.

96   C. A. Olson, Z. S. Shi, N. R. Kallenbach, *J. Am. Chem. Soc.*, **2001**, *123*, 6451.

97   S. Z. Shi, C. A. Olson, N. R. Kallenbach, *J. Am. Chem. Soc.*, **2002**, *124*, 3284.

98   (a) J. Fernandez-Recio, A. Vazquez, C. Civera, P. Sevilla, J. Sancho, *J. Mol. Biol.*, **1997**, *267*, 184; (b) M. L. Waters, *Biopolymers*, **2004**, *76*, 435.

99   L. K. Tsou, C. D. Tatko, M. L. Waters, *J. Am. Chem. Soc.*, **2002**, *124*, 14917.

100   (a) C. Chipot, B. Maigret, D. A. Pearlman, P. A. Kollman, *J. Am. Chem. Soc.*, **1996**, *118*, 2998; (b) J. P. Gallivan, D. A. Dougherty, *J. Am. Chem. Soc.*, **2000**, *122*, 870.

101   T. J. Shepodd, M. A. Petti, D. A. Dougherty, *J. Am. Chem. Soc.*, **1988**, *110*, 1983.

102   M. Haridas, B. F. Anderson, E. N. Baker, *Acta Crystallogr Sect. D.*, **1995**, *D51*, 629.

103   A. M. de Vos, M. Ultsch, A. A. Kossiakoff, *Science*, **1992**, *255*, 306.

104   W. Somers, M. Ultsch, A. A. Kossiakoff, *Nature*, **1994**, *372*, 478.

105   K. M. Amstrong, R. Fairman, R. L. Baldwin, *J. Mol. Biol.*, **1993**, *230*, 284.

106   T. P. Burghardt, N. Juranic, S. Macura, K. Ajtai, *Biopolymers*, **2002**, *63*, 261.

107   Z. Shi, C. A. Olson, A. J. Bell Jr., N. R. Kallenbach, *Biopolymers*, **2001**, *60*, 366

108   (a) C. D. Tatko, M. L. Waters, *Protein Science*, **2003**, *12*, 2443; (b) S. E. Kiehna, M. L. Waters, *Protein Science*, **2003**, *12*, 2657.

109   N. S. Scrutton, A. R. C. Raine, *Biochem. J.*, **1996**, *319*, 1.

110   K. Brejc, W. J. van Dijk, R. V. Klaassen, M. Schuurmans, J. van der Oost, A. B. Smit, T. K. Sixma, *Nature*, **2001**, *411*, 269.

111   (a) D. A. Dougherty, *Science*, **1996**, *271*, 163; (b) W. Zhong, J. P. Gallivan, Y. Zhang, L. Li, H. A. Lester, D. A. Dougherty, *Proc. Natl. Acad. Sci. USA*, **1998**, *95*, 12088.

112   J. Sunner, K. Nishizawa, P. Kebarle, *J. Phys. Chem.*, **1981**, *85*, 1814.

113   (a) C. A. Deakyne, M. Meot-Ner (Mautner), *J. Am. Chem. Soc.*, **1985**, *107*, 469; (b) M. Meot-Ner (Mautner), C. A. Deakyne, *J. Am. Chem. Soc.*, **1985**, *107*, 474.

114   (a) K. S. Kim, J. Y. Lee, S. J. Lee, T. -K. Ha, D. H. Kim, *J. Am. Chem. Soc.*, **1994**, *116*, 7399; (b) J. Y. Lee, S. J. Lee, H. S. Choi, S. J. Cho, K. S. Kim, T. -K. Ha, *Phys. Lett.*, **1995**, *232*, 67.

115   (a)S. Mecozzi, A. P. West Jr., D. A. Dougherty, *J. Am. Chem. Soc.*, **1996**, *118*, 2307; (b) E. Cubero, F. J. Luque, M. Orozco, *Proc. Natl. Acad. Sci. USA*, **1998**, *95*, 5976.

116   M. A. Montes-Moran, J. A. Menendez, E. Fuente, D. Suarez, *J. Phys. Chem. B*, **1998**, *102*, 5595.

117   E. S. Stoyanov, S. P. Hoffmann, K. -C. Kim, F. S. Tham, C. A. Reed, *J. Am. Chem. Soc.*, **2005**, *127*, 7664.

118   D. A. Stauffer, D. A. Dougherty, *Tetrahedron Lett.*, **1988**, *29*, 6039.

119   P. C. Kearney, L. S. Mizoue, R. A. Kumpf, J. E. Forman, A. McCurdy, D. A. Dougherty, *J. Am. Chem. Soc.*, **1993**, *115*, 9907.

120   D. A. Dougherty, D. A. Stauffer, *Science*, **1990**, *250*, 1558.

121   H. -J. Schneider, F. Werner, T. Blatter, *J. Phys. Org. Chem.*, **1993**, *6*, 590.

122   A. W. Schwabacher, S. Zhang, W. Davy, *J. Am. Chem. Soc.*, **1993**, *115*, 6995.

123   (a) P. Lhotak, S. Shinkai, *J. Phys. Org. Chem.*, **1997**, *10*, 273; (b) A. Arduini, A. Casnati, A. Pochini, R. Ungaro, *Curr. Opin. Chem. Biol.*, **1997**, *1*, 467.

124   (a) K. Araki, H. Shimizu, S. Shinkai, *Chem. Lett.*, **1993**, 205; (b) A. Ikeda, S. Shinkai, *J. Am. Chem. Soc.*, **1994**, *116*, 3102; (c) F. Inokuchi, Y. Miyahara, T. Inazu, S. Shinkai, *Angew. Chem. Int. Ed. Engl.*, **1995**, *34*, 1364.

125   S. E. Thompson, D. B. Smithrud, *J. Am. Chem. Soc.*, **2002**, *124*, 442.

126   K. Schärer, M. Morgenthaler, R. Paulini, U. Obst-Sander, D. W. Banner, D. Schlatter, J. Benz, M. Stihle, F. Diederich, *Angew. Chem. Int. Ed. Engl.*, **2005**, *44*, 4400.

127   M. L. Paddock, K. H. Weber, C. Chang, M. Y. Okamura, *Biochemistry*, **2005**, *44*, 9619.

128   T. Grawe, T. Schrader, P. Finocchiaro, G. Consiglio, S. Failla, *Org. Lett.* **2001**, *3*, 1597.

129   M. Herm, O. Molt, T. Schrader, *Angew. Chem. Int. Ed. Engl.*, **2001**, *40*, 3148.

168   A. Steinreiber, H. Hellström, S. F. Mayer, V. A. Orru, K. Faber, *Synlett*, **2001**, *1*, 111.

169   P. Moussou, A. Archelas, R. Furstoss, *Tetrahedron*, **1998**, *54*, 1563.

170   (a) B. E. Smart, *J. Fluorine Chem.*, **2001**, *109*, 3. (b) F. M. D. Ismail, *J. Fluorine Chem.*, **2002**, *118*, 27. (c) J. D. Dunitz, *ChemBioChem*, **2004**, *5*, 614. (d) M. Shimizu, T. Hiyama, *Angew. Chem. Int. Ed.*, **2005**, *44*, 214 and references therein.

171   E. M. Hancock, A. C. Cope, *J. Am. Chem. Soc.*, **1944**, *66*, 1738.

172   A. M. Gaber, G. A. Hunter, H. McNab, *J. Chem. Soc. Perkin Trans 1*, **2002**, 548-554.

173   Coutts et al., *Can. J. Chem.*, **1978**, *56*, 3056.

174   A. Hassner, C. Heathcock, *J. Org. Chem.*, **1965**, *30*, 1748.

175   (a) F. A. Davis, S. Lee, H. Zhang, D. L. Fanelli, *J. Org. Chem.*, **2000**, *65*, 8704; (b) G. K. S. Prakash, M. Mandal, G. A. Olah, *Org. Lett.*, **2001**, *3*, 2847; (c) G. Borg, M. Chino, J. A. Ellman, *Tet. Lett.*, **2001**, *42*, 1433; (d) G. K. S. Prakash, M. Mandal, G. A. Olah, *Angew. Chem. Int. Ed.*, **2001**, *40*, 589; (e) D. A. Cogan, G. Liu, J. Ellman, *Tetrahedron*, **1999**, *5*, 8883; (f) J. P. MacMahon, J. A. Ellman, *Org. Lett.*, **2004**, *6*, 1645.

176   G. Liu, D. A. Cogan, T. D. Owens, T. P. Tang, J. A. Ellman, *J. Org. Chem.*, **1999**, *64*, 1278.

177   (a) L. I. Krimen, D. J. Cota, *Org. Reactions, Ed Wiley, vol. 17*, pp. 213; (b) J. J. Ritter, J. Kalish, *J. Am. Chem. Soc.*, **1948**, *70*, 4045; (c) J. J. Ritter, J. Kalish, *J. Am. Chem. Soc.*, **1948**, *70*, 4048.

178   A. Jirgensons, V. Kauss, I. Kalvinsh, M. R. Gold, *Synthesis*, **2000**, *12*, 1709.

179   A. Burger, S. E. Zimmerman, *J. Med. Chem.*, **1966**, *9*, 469.

180   A. DalPozzo, M. Ni, L. Muzi, A. Caporale, R. De Castiglione, B. Kaptein, Q. B. Broxterman, F. Fromaggio, *J. Org. Chem.*, **1978**, *43*, 4, 555.

181   S. SWaminathan, K. V. Narayanan, *Chem. Rev.*, **1971**, *71*, 429.

182   R. R. Tykwinsky, F. Diederich, V. Gramlich, P. Seiler, *Helv. Chim. Acta*, **1996**, *79*, 634.

183   H. C. J. Ottenheijm, R. Plate, J. H. Noordik, J. D. M. Herscheid, *J. Org. Chem.*, **1982**, *47*, 2147.

184   L. H. Sternbach, E. Reeder; O. Keller, W. Metlesics, *J. Org. Chem.*, **1961**, *26*, 4488.

185   (a)R. Greven, P. Jütten, H.-D. Scharf, *J. Org. Chem.*, **1993**, *58*, 3742. (b) R. Greven, P. Jütten, H.-D. Scharf, *Carbohyd. Res.*, **1995**, *275*, 83.

186   (a) A. Von Marxer, M. Horvath, *Helv. Chim. Acta*, **1964**, *47*, 1101; (b) T. Kolasa, S. K. Sharma, M. J. Miller, *Tetrahedron*, **1988**, *44*, 5431; (c) J. A. Marco, M. Carda, J. Murga, S. Rodriguez, E. Falomir, M. Oliva, *Tet. Asym.*, **1998**, *9*, 1679.

187   S. Franco, F. L. Merchan, P. Merino, T. Tejero, *Synth. Comm.*, **1995**, *25*, 2275.

188   (a) P. Merino, S. Franco, J. M. Gascon, F. L. Merchan, T. Tejero, *Tet. Asym.*, **1997**, *8*, 3489; (b) Z. Y. Chang, R. M. Coates, *J. Org. Chem.*, **1990**, *55*, 3475.

189   S. Pinet, S. U. Pandya, P. Y. Chavant, A. Ayling, Y. Vallee, *Org. Lett.*, **2002**, *4*, 1463.

190   P. Merino, S. Franco, F. L. Merchan, T. Tejero, *J. Org. Chem.*, **1998**, *63*, 5627.

191   J. Micova, B. Steiner, M. Koos, V. Langer, M. Durik, D. Gyepesova, L. Smrcok, *Carbohyd. Res.*, **2002**, *337*, 8, 663.

192   (a) P. Lakshminarasimhan, R. B. Sunoj, J. Chandrasekhar, V. Ramamurthy, *J. Am. Chem. Soc.*, **2000**, *122*, 4815; (b) S. Yamada, C. Morita, *J. Am. Chem. Soc.*, **2002**, *124*, 8184.

193   H. Shao, Q. Zhu, M. Goodman, *J. Org. Chem.*, **1995**, *60*, 790.

194   B. G. M. Burgaud, D. C. Horwell, A. Padova, M. C. Pritchard, *Tetrahedron*, **1996**, *52*, 13035.

195   C. Najera, J. M. Sansano, *Tetrahedron*, **1991**, *47*, 5193.

196   (a) R. S. Atkinson, B. D. Judkins, *J. Chem. Soc Perkin Trans. 1*, **1981**, 2615; (b) T. C. Jenkins, M. A. Naylor, P. O'Neill, M. D. Threadgrill, S. Cole, I. J. Stratford, G. E. Adams, E. M. Fielden, M. J. Suto, M. A. Stier, *J. Med. Chem.*, **1990**, *33*, 2603.

197   (a) D. A. Evans, M. M. Faul, M. T. Bilodeau, *J. Org. Chem.*, **1991**, *56*, 6744; (b) D. A. Evans, M. M. Faul, M. T. Bilodeau, *J. Am. Chem. Soc.*, **1994**, *116*, 2742; (c) D. Tanner, *Angew. Chem. Int. Ed. Engl.*, **1994**, *33*, 599.

198   (a) F. W. Fowler, A. Hassner, L. A. Levy, *J. Am. Chem. Soc.*, **1967**, *89*, 2077; (b) A. Hassner, G. J. Matthews, F. W. Fowler, *J. Am. Chem. Soc.*, **1969**, *91*, 5046; (c) E. J. Parish, W. D. Nes, *Synth. Comm.*, **1988**, *18*, 221.

199   (a) M. M. Campbell, N. Abbas, M. Sainsbury, *Tetrahedron*, **1985**, *41*, 5637; (b) J. S. Brimacombe, M. S. Saeed, T. J. R. Weakley, *J. Chem. Soc. Perkin Trans. 1*, **1980**, 2061.

200   R. C. Cambie, J. L. Jurlina, P. S. Rutledge, P. D. Woodgate, *J. Chem. Soc. Perkin Trans. 1*, **1982**, 315.

201   For reviews on chlorosulfonyl isocyanate: (a) R. Graf, _Angew. Chem. Int. Ed. Engl._, **1968**, _7_, 172; (b)
       E. J. Moriconi, W. C. Meyer, _J. Org. Chem._, **1971**, _36_, 2841; (c) J. K. Rasmussen, A. Hassner, _Chem._
       Rev., **1976**, _76_, 389; (d) D. N. Dhar, K. S. K. Murthy, _Synthesis_, **1986**, 437.

202   (a) T. Durst, J. O'Sullivan, _J. Org. Chem._, **1970**, _35_, 2043; (b) A. Hassner, N. Wiegland, _J. Org._
       Chem., **1986**, _51_, 3652.

203   E. Forro, F. Fülöp, _Tet. Asym._, **2001**, _12_, 2351.

204   C. Palomo, M. Oiarbide, S. Bindi, _J. Org. Chem._, **1998**, _63_, 2469.

205   Z. Kaluza, W. Abramski, C. Belzecki, J. Grodner, D. Mostowicz, R. Urbanski, M. Chmielewski,
       Synlett, **1994**, 539.

206   R. Graf, _Org. Synth._, **1966**, _46_, 51.

207   F. J. Waller, A. G. M. Barrett, D. C. Braddock, D. Ramprasad, _Chem. Comm._, **1997**, 613.

208   T. Ohwada, I. Okamoto, N. Haga, K. Shudo, _J. Org. Chem._, **1994**, _59_, 3975.

209   J.E. Baldwin, A.G. Swanson, J. K. Cha, J. A. Murphy, _Tetrahedron_, **1986**, _42_, 14, 3943.

210   B. Masci, _Tetrahedron_, **1989**, _45_, 2719.

211   J. P. Springer, _J. Org. Chem._, **1982**, _47_, 4329.

212   H. Günther, _NMR Spectroscopy. Basic Principles, Concepts, and Applications in Chemistry._ 2nd
       Edition, Wiley, **1995**, pp. 344

213   D. Neuhaus, M.P. Williamson. _The Nuclear Overhauser Effect in Structural and Conformational_
       Analysis, 2nd Edition, Wiley-VCH, **2000**.

214   R. Dutler, A. Rauk, T. S. Sorensen, _J. Am. Chem. Soc._, **1987**, _109_, 3224.

215   F. H. Allen, J. A. K. Howard, V. J. Hoy, G. R. Desiraju, D. S. Reddy, C. C. Wilson, _J. Am. Chem._
       Soc., **1996**, _118_, 4081.

216   G. R. Desiraju, _J. Chem. Soc. Dalton Trans._, **2000**, 3745.

217   R. S. Morgan, C. E. Tatsch, R. H. Gushard, J. M. McAdon, P. K. Warme, _Int. J. Peptide Protein Res._,
       1978, _11_, 209.

218   C. A. Hunter, _Angew. Chem. Int. Ed._, **2004**, _43_, 5310.

219   G. L. Cantrell, R. Filler, _J. Fluorine Chem._, **1985**, _29_, 417.

220   I. Okamoto, T. Ohwada, K. Shudo, _J. Org. Chem._, **1996**, _61_, 3155.

221   H. Adams, J. -L. Jimenez Blanco, G. Chessari, C. A. Hunter, C. M. R. Low, J. M. Sanderson, J. G.
       Vinter, _Chem. Eur. J._, **2001**, _7_, 3494.

222   (a) G. K. S. Prakash, R. Krishnamurti, G. A. Olah, _J. Am. Chem. Soc._, **1989**, _111_, 393; (b) J. -C.
       Blazejewski, E. Anselmi, M. P. Wilmshurst, _Tet. Lett._, **1999**, _40_, 5475; (c) D. Saleur, J. -P. Bouillon,
       C. Portella, _J. Org. Chem._, **2001**, _66_, 4543.

223   Y. Chang, C. Chai, _Tet. Lett._, **2005**, _46_, 3161.

224   S. J. Opella, M. H. Frey, _J. Am. Chem. Soc._, **1979**, _101_, 5854.

225   L. B. Alemany, D. M. Grant, T. D. Alger, R. J. Pugmire, _J. Am. Chem. Soc._, **1983**, _105_, 6697.

226   M.F. Schlecht, _Molecular Modeling on the PC._ Wiley-VCH, New York, **1998**.

227   Gaussian 03, Revision B.05, M. J. Frisch, G. W. Trucks, H. B. Schlegel, G. E. Scuseria, M. A. Robb,
       J. R. Cheeseman, J. A. Montgomery, Jr., T. Vreven, K. N. Kudin, J. C. Burant, J. M. Millam, S. S.
       Iyengar, J. Tomasi, V. Barone, B. Mennucci, M. Cossi, G. Scalmani, N. Rega, G. A. Petersson, H.
       Nakatsuji, M. Hada, M. Ehara, K. Toyota, R. Fukuda, J. Hasegawa, M. Ishida, T. Nakajima, Y.
       Honda, O. Kitao, H. Nakai, M. Klene, X. Li, J. E. Knox, H. P. Hratchian, J. B. Cross, V. Bakken, C.
       Adamo, J. Jaramillo, R. Gomperts, R. E. Stratmann, O. Yazyev, A. J. Austin, R. Cammi, C. Pomelli, J.
       W. Ochterski, P. Y. Ayala, K. Morokuma, G. A. Voth, P. Salvador, J. J. Dannenberg, V. G.
       Zakrzewski, S. Dapprich, A. D. Daniels, M. C. Strain, O. Farkas, D. K. Malick, A. D. Rabuck, K.
       Raghavachari, J. B. Foresman, J. V. Ortiz, Q. Cui, A. G. Baboul, S. Clifford, J. Cioslowski, B. B.
       Stefanov, G. Liu, A. Liashenko, P. Piskorz, I. Komaromi, R. L. Martin, D. J. Fox, T. Keith, M. A. Al-
       Laham, C. Y. Peng, A. Nanayakkara, M. Challacombe, P. M. W. Gill, B. Johnson, W. Chen, M. W.
       Wong, C. Gonzalez, and J. A. Pople, Gaussian, Inc., Wallingford CT, **2004**.

228   M. W. Wong, _Chem. Phys. Lett._, **1996**, _256_, 391.

229   M. Mons, E. G. Robertson, J. P. Simons. _J. Phys. Chem. A_, **2000**, _104_, 1430.

230   K. Ishihara, Q. Gao, H. Yamamoto, _J. Org. Chem._, **1993**, _58_, 6917.

231   A. El-Wareth, A. O. Sarhan, H. M. R. Hoffmann, _Chem. Ber._, **1994**, _127_, 1755.

232   C. A. G. Haaasnoot, F. A. A. M. DeLeeuw, C. Altona, _Tetrahedron_, **1980**, _36_, 2783.

130   S. Rensing, T. Schrader, *Org. Lett.*, **2002**, *4*, 2161.

131   (a) A. P. Bisson, V. M. Lynch, M. -K. C. Monahan, E. V. Anslyn, *Angew. Chem. Int. Ed. Engl.*, **1997**, *36*, 2340; (b) H. S. Choi, S. B. Suh, S. J. Cho, K. S. Kim, *Proc. Natl. Acad. Sci. USA*, **1998**, *95*, 12094; (c) K. S. Oh, C. -W. Lee, H. S. Choi, S. J. Lee, K. S. Kim, *Org. Lett.*, **2000**, *2*, 2679; (d) S.Yun, Y. -O. Kim, D. Kim, H. G. Kim, H. Ihm, J. K. Kim, C. -W. Lee, W. J. Lee, J. Yoon, K. S. Oh, J. Yoon, S. -M. Park, K. S. Kim, *Org. Lett.*, **2003**, *5*, 471.

132   L. Garel, B. Lozach, J. -P. Dutasta, A. Collet, *J. Am. Chem. Soc.*, **1993**, *115*, 11652.

133   (a) S. Roelens, R. Torriti, *J. Am. Chem. Soc.*, **1998**, *120*, 12443; (b) S. Bartoli, G. De Nicola, S. Roelens, *J. Org. Chem.*, **2003**, *68*, 8149.

134   C. A. Ilioudis, M. J. Bearpark, J. W. Steed, *New J. Chem.*, **2005**, *29*, 64.

135   (a) R. Arnecke, V. Böhmer, R. Cacciapaglia, A. Dalla Cort, L. Mandolini, *Tetrahedron*, **1997**, *53*, 4901; (b) V. Dvornikovs, D. B. Smithrud, *J. Org. Chem.*, **2002**, *67*, 2160.

136   M. Lämsa, J. Huuskonen, K. Rissanen, J. Pursiainen, *Chem. Eur. J.*, **1998**, *4*, 1.

137   S. Kubik, R. Goddard, *Eur. J. Org. Chem.*, **2001**, 311.

138   (a) R.arnecke, V. Böhmer, R. Cacciapaglia, A. Dalla Cort, L. Mandolini, *Tetrahedron*, **1997**, *53*, 4901; (b) K. -S. Jeong, K. -M. Hahn, Y. L. Cho, *Tetrahedon Lett.*, **1998**, *39*, 3779; (c) K. Araki, H. Hayashida, *Tetrahedron Lett.*, **2000**, *41*, 1209.

139   M. Nic, PhD Thesis, *University of London*, **1995**.

140   H. M. R. Hoffmann and Usama Karama, *Chem. Ber.*, **1992**, *125*, 2803.

141   H. Kim, H. M. R. Hoffmann, *Eur. J. Org. Chem*, **2000**, 2195.

142   E. J. Corey, T. P. Loh, *J. Am. Chem. Soc.*, **1991**, *113*, 8966.

143   B. B. Snider, *J. Org. Chem.*, **1973**, *38*, 3961.

144   F. Weiss and R. Rusch, *Bull. Soc. Chim. Fr.*, **1964**, 550.

145   (a) A. de la Hoz, A. Diaz-Ortis, A. Moreno, F. Langa, *Eur. J. Org. Chem.*, **2000**, *22*, 3659; (b) P. Lidstrom, J. Tierney, B. Wathey, J. Westman, *Tetrahedron*, **2001**, *57*, 9225.

146   P. N. Confalone, D. L. Confalone, *J. Org. Chem.*, **1980**, *45*, 1470.

147   K. Munefumi, W. Yoshifumi, K. Youichi, S. Junji, Y. Kenjiro, K. Hideyuki, K. Naoaki, K. Hideo, A. Shinichiro, I. Fumiyoshi, *J. Med. Chem.*, **1989**, *32*, 1326-1334.

148   (a) K. Takai, Y. Hotta, K. Oshima, H. Nozaki, *Bull. Chem. Soc. Jpn.*, **1980**, *53*, 1698; (b) J. Hibino, T. Okazoe, K. Takai, H. Nozaki, *Tet. Lett.*, **1985**, *26*, 5579.

149   L. Lombardo, *Tet. Lett.*, **1982**, *23*, 4293.

150   R. J. Rawson, I. T. Harrison, *J. Org. Chem.*, **1970**, *35*, 2057.

151   E. C. Friedrich, S. E. Lunetta, E. J. Lewis, *J. Org. Chem.*, **1989**, *54*, 2388.

152   E. C. Friedrich, J. M. Domek, R. Y. Pong, *J. Org. Chem.*, **1985**, *50*, 4640.

153   A. G. Myers, P. S. Dragovich, E. Y. Kuo, *J. Am. Chem. Soc.*, **1992**, *114*, 9369.

154   T. Imamoto, *Comprehensive Organic Synthesis. Selectivity, Strategy and Efficiency in Modern Organic Chemistry. Volume 1: Additions to C-X p-bonds. Part I*; Trost, B. M.; Fleming I.; Schreiber, S. L.; *Edition. Pergamon Press. Oxford*, **1991**, pp. 231.

155   T. Imamoto, Y. Sugiura, N. Takiyama, *Tet. Lett.*, **1984**, *25*, 4233.

156   T. J. Mason, M. J. Harrison, J. A. Hall, G. Dan Sargent, *J. Am. Chem. Soc.*, **1973**, *95*, 1849.

157   T. Imamoto, T. Kusumoto, Y. Tawarayama, Y. Sugiura, T. Mita, Y. Hatanaka, and M. Yokoyama, *J. Org. Chem.*, **1984**, *49*, 21, 3904.

158   Hsing-Jang Liu, Kah-Shan Shia, Xiao Shang, Bing-Yan Zhu, *Tetrahedron*, **1999**, *55*, 3803.

159   Yanfang Wang, Jincui Li, Yulin Wu, Yaozeng Huang, , Lilan Shi and Jianhua Yang, *Tet. Lett.*, **1987**, *27*, *38*, 4583.

160   P. Magnus, R. Carter, M. Davies, J. Elliott, T. Pitterna, *Tetrahedron*, **1996**, 52, *18*, 6283.

161   A. A. Cordi, I. Berque-Bestel, T. Persigand, J. -M. Lacoste, A. Newman-Tancredi, V. Audinot, M. J. Millan, *J. Med. Chem.*, **2001**, *44*, 787.

162   T. W. Greene, P. G. M. Wuts, *Protective Groups in Organic Synthesis, Third Edition, Edition Wiley Interscience*, **1999**, pp. 658 and references therein.

163   M. B. Andrus, E. L. Meredith, B. B. V. Soma Sekhar, *Org. Lett.*, **2001**, *03*, 02, 259.

164   T. Lange, J-D. van Loon, R. R. Tykwinski, M. Schreiber, F. Diederich, *Synthesis*, **1996**, *4*, 537.

165   K. Okuma, Y. Tanaka, S. Kaji, H. Ohta, *J. Org. Chem.*, **1983**, *48*, 5133.

166   L.A. Paquette, F.J. Montgomery, T.Z. Wang, J. Org. Chem., **1995**, 60, 24, 7857.

167   A. Steinreiber, I. Ospiran, S. F. Mayer, V. A. Orru, K. Faber, *Eur. J. Org. Chem.*, **2000**, *22*, 3703

201   For reviews on chlorosulfonyl isocyanate: (a) R. Graf, *Angew. Chem. Int. Ed. Engl.*, **1968**, *7*, 172; (b) E. J. Moriconi, W. C. Meyer, *J. Org. Chem.*, **1971**, *36*, 2841; (c) J. K. Rasmussen, A. Hassner, *Chem. Rev.*, **1976**, *76*, 389; (d) D. N. Dhar, K. S. K. Murthy, *Synthesis*, **1986**, 437.

202   (a) T. Durst, J. O'Sullivan, *J. Org. Chem.*, **1970**, *35*, 2043; (b) A. Hassner, N. Wiegland, *J. Org. Chem.*, **1986**, *51*, 3652.

203   E. Forro, F. Fülöp, *Tet. Asym.*, **2001**, *12*, 2351.

204   C. Palomo, M. Oiarbide, S. Bindi, *J. Org. Chem.*, **1998**, *63*, 2469.

205   Z. Kaluza, W. Abramski, C. Belzecki, J. Grodner, D. Mostowicz, R. Urbanski, M. Chmielewski, *Synlett*, **1994**, 539.

206   R. Graf, *Org. Synth.*, **1966**, *46*, 51.

207   F. J. Waller, A. G. M. Barrett, D. C. Braddock, D. Ramprasad, *Chem. Comm.*, **1997**, 613.

208   T. Ohwada, I. Okamoto, N. Haga, K. Shudo, *J. Org. Chem.*, **1994**, *59*, 3975.

209   J.E. Baldwin, A.G. Swanson, J. K. Cha, J. A. Murphy, *Tetrahedron*, **1986**, *42*, 14, 3943.

210   B. Masci, *Tetrahedron*, **1989**, *45*, 2719.

211   J. P. Springer, *J. Org. Chem.*, **1982**, *47*, 4329.

212   H. Günther, *NMR Spectroscopy. Basic Principles, Concepts, and Applications in Chemistry. 2nd Edition, Wiley*, **1995**, pp. 344

213   D. Neuhaus, M.P. Williamson. *The Nuclear Overhauser Effect in Structural and Conformational Analysis, 2nd Edition, Wiley-VCH*, **2000**.

214   R. Dutler, A. Rauk, T. S. Sorensen, *J. Am. Chem. Soc.*, **1987**, *109*, 3224.

215   F. H. Allen, J. A. K. Howard, V. J. Hoy, G. R. Desiraju, D. S. Reddy, C. C. Wilson, *J. Am. Chem. Soc.*, **1996**, *118*, 4081.

216   G. R. Desiraju, *J. Chem. Soc. Dalton Trans.*, **2000**, 3745.

217   R. S. Morgan, C. E. Tatsch, R. H. Gushard, J. M. McAdon, P. K. Warme, *Int. J. Peptide Protein Res.*, **1978**, *11*, 209.

218   C. A. Hunter, *Angew. Chem. Int. Ed.*, **2004**, *43*, 5310.

219   G. L. Cantrell, R. Filler, *J. Fluorine Chem.*, **1985**, *29*, 417.

220   I. Okamoto, T. Ohwada, K. Shudo, *J. Org. Chem.*, **1996**, *61*, 3155.

221   H. Adams, J. -L. Jimenez Blanco, G. Chessari, C. A. Hunter, C. M. R. Low, J. M. Sanderson, J. G. Vinter, *Chem. Eur. J.*, **2001**, *7*, 3494.

222   (a) G. K. S. Prakash, R. Krishnamurti, G. A. Olah, *J. Am. Chem. Soc.*, **1989**, *111*, 393; (b) J. -C. Blazejewski, E. Anselmi, M. P. Wilmshurst, *Tet. Lett.*, **1999**, *40*, 5475; (c) D. Saleur, J. -P. Bouillon, C. Portella, *J. Org. Chem.*, **2001**, *66*, 4543.

223   Y. Chang, C. Chai, *Tet. Lett.*, **2005**, *46*, 3161.

224   S. J. Opella, M. H. Frey, *J. Am. Chem. Soc.*, **1979**, *101*, 5854.

225   L. B. Alemany, D. M. Grant, T. D. Alger, R. J. Pugmire, *J. Am. Chem. Soc.*, **1983**, *105*, 6697.

226   M.F. Schlecht, *Molecular Modeling on the PC*. Wiley-VCH, New York, **1998**.

227   Gaussian 03, Revision B.05, M. J. Frisch, G. W. Trucks, H. B. Schlegel, G. E. Scuseria, M. A. Robb, J. R. Cheeseman, J. A. Montgomery, Jr., T. Vreven, K. N. Kudin, J. C. Burant, J. M. Millam, S. S. Iyengar, J. Tomasi, V. Barone, B. Mennucci, M. Cossi, G. Scalmani, N. Rega, G. A. Petersson, H. Nakatsuji, M. Hada, M. Ehara, K. Toyota, R. Fukuda, J. Hasegawa, M. Ishida, T. Nakajima, Y. Honda, O. Kitao, H. Nakai, M. Klene, X. Li, J. E. Knox, H. P. Hratchian, J. B. Cross, V. Bakken, C. Adamo, J. Jaramillo, R. Gomperts, R. E. Stratmann, O. Yazyev, A. J. Austin, R. Cammi, C. Pomelli, J. W. Ochterski, P. Y. Ayala, K. Morokuma, G. A. Voth, P. Salvador, J. J. Dannenberg, V. G. Zakrzewski, S. Dapprich, A. D. Daniels, M. C. Strain, O. Farkas, D. K. Malick, A. D. Rabuck, K. Raghavachari, J. B. Foresman, J. V. Ortiz, Q. Cui, A. G. Baboul, S. Clifford, J. Cioslowski, B. B. Stefanov, G. Liu, A. Liashenko, P. Piskorz, I. Komaromi, R. L. Martin, D. J. Fox, T. Keith, M. A. Al-Laham, C. Y. Peng, A. Nanayakkara, M. Challacombe, P. M. W. Gill, B. Johnson, W. Chen, M. W. Wong, C. Gonzalez, and J. A. Pople, Gaussian, Inc., Wallingford CT, **2004**.

228   M. W. Wong, *Chem. Phys. Lett.*, **1996**, *256*, 391.

229   M. Mons, E. G. Robertson, J. P. Simons. *J. Phys. Chem. A*, **2000**, *104*, 1430.

230   K. Ishihara, Q. Gao, H. Yamamoto, *J. Org. Chem.*, **1993**, *58*, 6917.

231   A. El-Wareth, A. O. Sarhan, H. M. R. Hoffmann, *Chem. Ber.*, **1994**, *127*, 1755.

232   C. A. G. Haaasnoot, F. A. A. M. DeLeeuw, C. Altona, *Tetrahedron*, **1980**, *36*, 2783.